Nuclear Energy Research Initiative

2008

Annual Report

Disclaimer

Printed with soy ink on recycled paper.

Foreword

The Nuclear Energy Research Initiative (NERI) supports research that addresses long-term barriers to maintaining and expanding nuclear generation of electricity in this country. The current NERI projects are closely linked to the principal research programs sponsored by the Department of Energy's Office of Nuclear Energy (DOE-NE): the Generation IV Nuclear Energy Systems Initiative (Generation IV), the Advanced Fuel Cycle Initiative (AFCI), and the Nuclear Hydrogen Initiative (NHI). With its focus on applied nuclear energy research, NERI has been realizing its goal of both developing advanced nuclear energy systems and providing state-of-the-art research concerning nuclear science and technology.

Since its inception in fiscal year (FY) 1999, NERI has helped to maintain and improve the nuclear research infrastructure in this country by encouraging, preserving, and advancing nuclear science and technology research and development (R&D). To further this mission, NE decided to refocus NERI in FY 2004 to exclusively fund research led solely by the Nation's universities, with national laboratories and industry partners providing valuable contributions as collaborators. In FY 2008, NE further advanced this undertaking, restructuring the current NERI program to create the new NE University Programs (NEUP). NEUP, which will take the place of the NERI program, has two primary objectives: to better integrate university research with technical programs, and to further the quality of nuclear science and engineering education. Strong university involvement is particularly important to promote and maintain a robust nuclear science and engineering infrastructure to meet future technical challenges.

The *Nuclear Energy Research Initiative 2008 Annual Report* summarizes the progress of the 25 projects initiated in FY 2006, the 22 projects initiated in FY 2007, and the 11 FY 2007 NERI Consortia research projects. Summaries of projects initiated in FY 1999 through FY 2005 can be found in previous NERI annual reports. This report disseminates the results of NERI-sponsored research to the R&D community to spur yet more innovation, assuring a bright future for nuclear energy in the United States and the world.

R. Shane Johnson
Acting Assistant Secretary for Nuclear Energy
U.S. Department of Energy

Table of Contents

NUCLEAR ENERGY RESEARCH INITIATIVE

1.0 Overview and Program History

The Nuclear Energy Research Initiative (NERI)

The Nuclear Energy Reserach Initiative (NERI) is a national, research-oriented initiative managed and funded by the Department of Energy, Office of Nuclear Energy (DOE-NE). The purpose is to sponsor university-led research and development (R&D) that addresses the principal barriers related to the growth of nuclear energy in the United States. The initiative has helped DOE foster innovative ideas in NE's primary research programs: advanced nuclear energy systems, hydrogen production from nuclear power, and advanced nuclear fuels and fuel cycles. In addition to responding to the Nation's need for current nuclear energy research to advance the development of nuclear energy technology, NERI is helping to preserve the Nation's nuclear science and engineering infrastructure—enabling the United States to maintain a competitive position in the nuclear energy arena at home and abroad. NERI goals and objectives are summarized in the graphic on the following page.

NERI Development

DOE created NERI in fiscal year (FY) 1999 in response to recommendations provided by the President's Committee of Advisors on Science and Technology. The importance of nuclear power to the Nation's future energy supply requires that DOE apply its unique resources, specialized expertise, and national leadership to address all potential barriers to maintaining and expanding its use.

Additional information on the NERI program, including previous annual reports, is available at the NERI website: http://nuclear.energy.gov/neri/neNERIresearch.html.

NERI 2008 Annual Report

This *Nuclear Energy Research Initiative 2008 Annual Report* serves to inform interested parties of progress made in NERI on a programmatic level, as well as research progress made on individual NERI projects. Following is an overview of each section:

- Section 2 discusses the impact NERI has had on U.S. university nuclear programs.

- Section 3 describes the new Nuclear Energy University Programs (NEUP), explaining the overall purpose and structure.

- Section 4 highlights the major accomplishments of the NERI program.

- Section 5 presents progress reports for each of the 47 FY 2006 and FY 2007 projects, as well as for each of the 11 FY 2007 NERI Consortia (NERI-C) projects.

Projects are organized by their primary research area: the Generation IV Nuclear Energy Systems Initiative (Generation IV), the Advanced Fuel Cycle Initiative (AFCI), and the Nuclear Hydrogen Initiative (NHI). Numbering is designated by the FY in which the award was made. At the end of the document, there is an index of NERI projects grouped by FY and sequentially ordered by project number.

VISION
To maintain a viable nuclear
energy option to help meet the
Nation's future energy needs

GOALS/OBJECTIVES
Address potential technical and scientific obstacles
Advance the state of U.S. nuclear technology
Promote and maintain a nuclear infrastructure

SCOPE OF PROGRAM

Advanced Nuclear Energy Systems   Advanced Nuclear Fuels/Fuel Cycles

Hydrogen Production from Nuclear Power

R&D PRIORITIES

Advanced reactors, systems, and components	Advanced fuels
Alternative energy conversion cycles	Transmutation science and engineering
Design and evaluation methods	Fuel cycle systems analysis
Advanced structural materials	Thermochemical cycles
SNF separations technologies	High-temperature electrolysis

Reactor-hydrogen production process interface

IMPLEMENTATION STRATEGY

Competitive peer-reviewed R&D selection process   Individually managed projects

Collaborative research efforts   Continuous DOE oversight

RESULTS

U.S. nuclear leadership	Innovative technologies
Nuclear infrastructure development	Advances in nuclear engineering
Nuclear public awareness	Worldwide partnerships

NUCLEAR ENERGY RESEARCH INITIATIVE

2.0 NERI and U.S. Universities: Advancing the Goals of Nuclear R&D Programs

Focus on Universities

One of NERI's long-term goals is to maintain the country's leading position in nuclear energy research by improving the nuclear science and engineering infrastructure. In order to achieve this long-range goal, NERI is focused on cultivating research partnerships with universities across the United States. This helps educational institutions remain at the forefront of science education and research, advances the important work of existing nuclear R&D programs, and serves as training for the next generation of nuclear scientists who will carry on the groundbreaking work being performed at national laboratories, universities, and private corporations. Funding creative research ideas at the Nation's universities and colleges serves another purpose as well: it helps solve important issues that the private sector is unable to fund alone owing to the high-risk nature of the research and/or the extended period before a return on investment is realized.

Participants in NERI's initial planning workshop recommended that NERI be viewed as a "seed program" where new nuclear-related technological and scientific concepts could be investigated. Based on this philosophy, NERI has provided universities and colleges with a competitive, peer-reviewed research program that allows faculty and students an opportunity to conduct innovative research in nuclear engineering and related areas. Of the 186 projects awarded through FY 2008, 88 percent involved U.S. colleges and universities as lead investigators or collaborators. To date, a total of 64 national universities and colleges have participated in NERI projects.

NERI has provided U.S. universities and colleges with the opportunity to work closely with industry and DOE national laboratories and has introduced these researchers to other nuclear energy-related government programs. In addition to research related to Generation IV, AFCI, and NHI programs, NERI's activities are coordinated with other relevant DOE energy research programs in the Office of Science, the Office of Energy Efficiency and Renewable Energy, and the U.S. Nuclear Regulatory Commission. Furthermore, DOE leverages NERI program resources by encouraging no-cost collaboration with international research organizations and nuclear technology agencies. In this way, universities are also given the opportunity to gain experience with international research interests and capabilities.

Student Participation

One great success of NERI and other DOE programs is that nuclear-related educational opportunities at the universities have significantly increased. Universities have benefited from increased research dollars, which have served as incentives for new student recruitment. This involvement has revitalized student interest in nuclear engineering. In FY 1998, only 500 students enrolled in U.S. universities were seeking degrees in nuclear engineering. According to a survey performed for DOE in March 2009 by the Oak Ridge Institute for Science and Education, over 2,500 students—more than 1,300 undergraduates and more than 1,200 graduate/doctoral students—were enrolled in nuclear engineering programs in FY 2008.

Approximately 685 undergraduate, graduate, and doctorate students have participated in NERI projects since the program's inception. Figure 1 shows how student participation has changed with time. In addition, numerous post-doctoral fellows at universities have been involved in NERI research projects. In FY 2008 alone, 86 undergraduate, 146 graduate, and 102 doctoral students participated in NERI R&D.
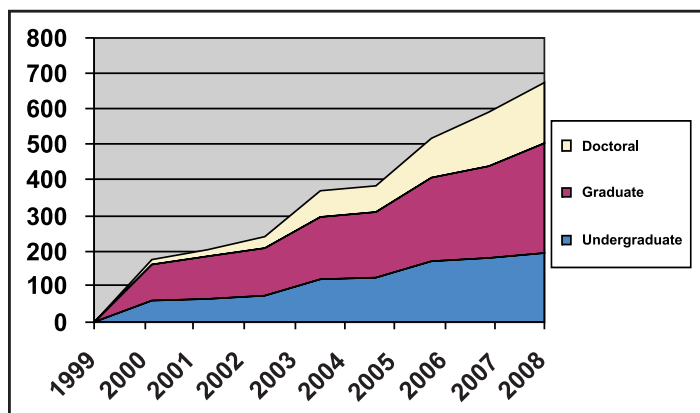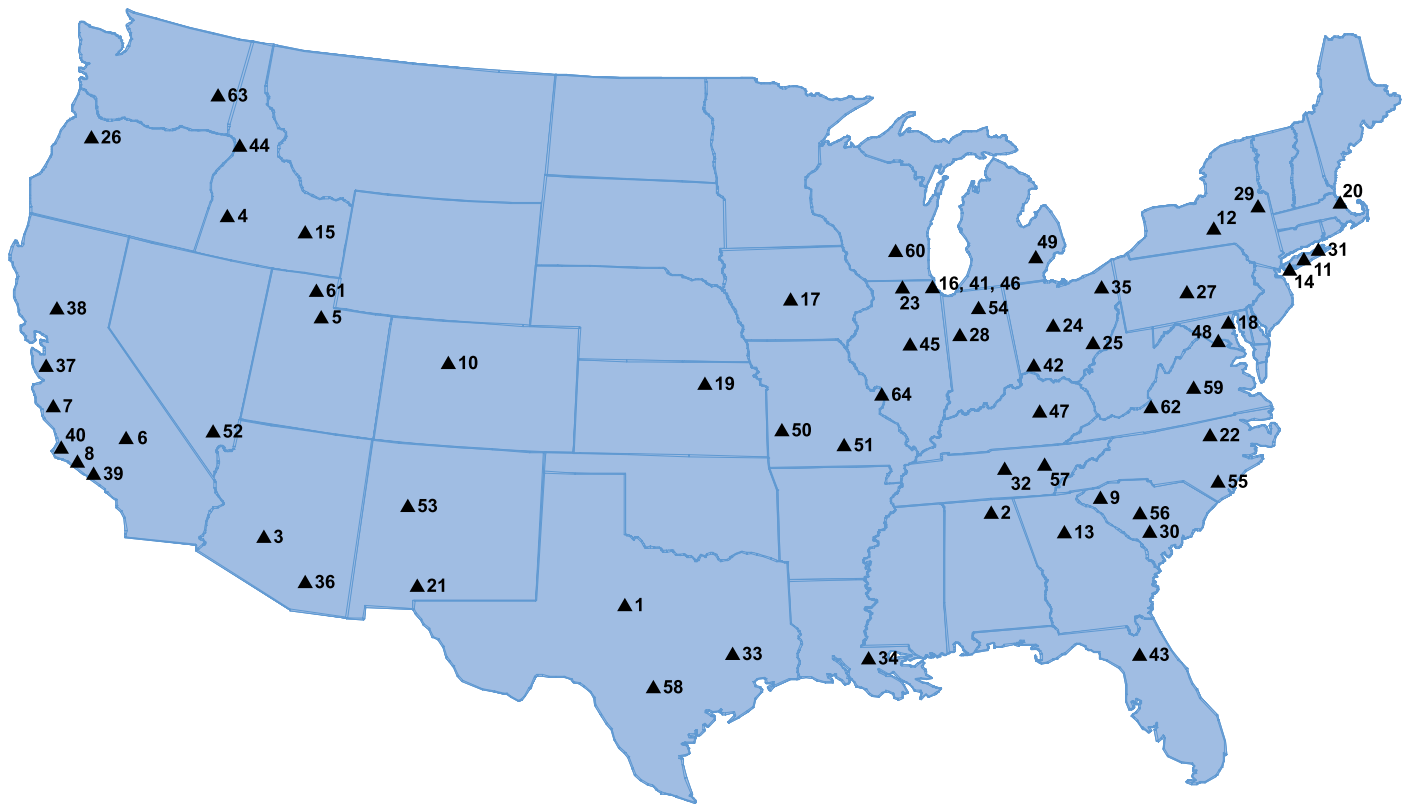

Figure 1. Cumulative NERI Student Participation Profile - FY 1999 through FY 2008.

Over the past few years, graduates of these programs have had higher-than-normal grade point averages, showing that these programs are training highly qualified individuals who will sustain the future growth of the nuclear power industry. Figure 2 provides a map and complete listing of the 64 universities and colleges that have participated in NERI since the program's inception.

UNIVERSITY KEY

#	University
1	Abilene Christian University
2	Alabama A&M University
3	Arizona State University
4	Boise State University
5	Brigham Young University
6	California Institute of Technology
7	California Polytechnic State University
8	California State University, Northridge
9	Clemson University
10	Colorado School of Mines
11	Columbia University
12	Cornell University
13	Georgia Institute of Technology
14	Hunter College (CUNY)
15	Idaho State University
16	Illinois Institute of Technology
17	Iowa State University
18	Johns Hopkins University
19	Kansas State University
20	Massachusetts Institute of Technology
21	New Mexico State University
22	North Carolina State University
23	Northwestern University
24	Ohio State University
25	Ohio University
26	Oregon State University
27	Pennsylvania State University
28	Purdue University
29	Rensselaer Polytechnic University
30	South Carolina State University
31	State University of New York, Stony Brook
32	Tennessee Technological University
33	Texas A&M University
34	Tulane University
35	University of Akron
36	University of Arizona
37	University of California, Berkeley
38	University of California, Davis
39	University of California, Los Angeles
40	University of California, Santa Barbara
41	University of Chicago
42	University of Cincinnati
43	University of Florida
44	University of Idaho
45	University of Illinois, Urbana-Champaign
46	University of Illinois, Chicago
47	University of Kentucky
48	University of Maryland, College Park
49	University of Michigan
50	University of Missouri, Columbia
51	University of Missouri, Rolla
52	University of Nevada, Las Vegas
53	University of New Mexico
54	University of Notre Dame
55	University of North Carolina, Wilmington
56	University of South Carolina
57	University of Tennessee
58	University of Texas, Austin
59	University of Virginia
60	University of Wisconsin
61	Utah State University
62	Virginia Polytechnic Institute and State University
63	Washington State University
64	Washington University in St. Louis

Figure 2. Locations of universities and colleges participating in NERI projects.

Nuclear Energy Research Initiative

3.0 The New Nuclear Energy University Programs

A rebirth of interest in nuclear energy is under way in the United States and across the world, driven by concern to secure safe energy supplies and to mitigate consequences of global climate change. Not only government but also private industry and U.S. academic institutions have made substantial investments to support expansion of nuclear power.

Recent research activities, however, have not been fully integrated to achieve optimal benefits. In FY 2009, NE addressed this need by restructuring the NERI program to create the new NE University Programs (NEUP). Through NEUP, NE will better integrate university research with technical programs, producing outcomes relevant to the Nation's interests. NEUP's objectives include the following:

- Addressing technical nuclear energy R&D challenges
- Maintaining the Nation's global leadership position in nuclear energy R&D
- Advancing the state of U.S. nuclear science and technology
- Enhancing the Nation's nuclear science and engineering infrastructure to prepare the nuclear industry for future expansion

To realize its mission, NEUP addresses a significant challenge in the nuclear industry: meeting its human capital, educational, and research needs. Acquiring a well-trained workforce is crucial to the development and operation of existing and proposed nuclear plants, yet the United States is beginning to experience significant shortfalls with regard to its science and engineering labor force. Approximately one quarter of active U.S. scientists and engineers are nearing retirement age, and—despite NERI's successes discussed in the previous section—student enrollments are still lower than needed to replace the current workforce, let alone support a nuclear renaissance.

NEUP emphasizes enhancing the quality of nuclear science and engineering education, cultivating and expanding the trained workforce that supports expansion of U.S. nuclear power. Following are NE's goals for the U.S. education system:

- Attracting the brightest and best students to nuclear professions
- Integrating R&D efforts of national laboratories, industry, and universities in the revitalization of nuclear education
- Facilitating transfer of knowledge from the current aging nuclear workforce to the next generation of nuclear workers, including technicians, engineers, and scientists

As with NERI, NEUP projects will correlate with current DOE-NE-sponsored programs referenced in this annual report: Generation IV, AFCI, and NHI. In addition, DOE-NE is supporting two new initiatives: the Light Water Reactor Sustainability program, which develops knowledge to predict changes in a nuclear power plant environment over time; and the Plutonium-238 Development program, which seeks to produce plutonium-238 domestically for use in radioisotope power systems. Through NEUP, DOE-NE will also sponsor investigator-initiated research that furthers the principal R&D missions.

The Center for Advanced Energy Studies (CAES) Nuclear Energy University Programs Office will provide NEUP with administrative support, ensuring the university program's successful implementation. CAES will facilitate technical integration of NE university programs with NE R&D programs. The office will undertake such activities as administering proposal processes, implementing review and selection processes, and hosting reviews of university R&D. The figure on the following page illustrates the new NEUP integrated approach.

CAES will support university R&D and infrastructure development, promoting accountable relationships between universities, technology integration offices (TIOs), and technology development offices (TDOs). For example, the R&D process will begin each year with a workshop: NE program managers, TIOs, TDOs, and stakeholders from the university and industrial communities will meet to determine research needs of NE programs. The workshop ensures alignment between NE research programs and university R&D programs, enables program-relevant production, and enhances quality and availability of nuclear engineering and science professionals.
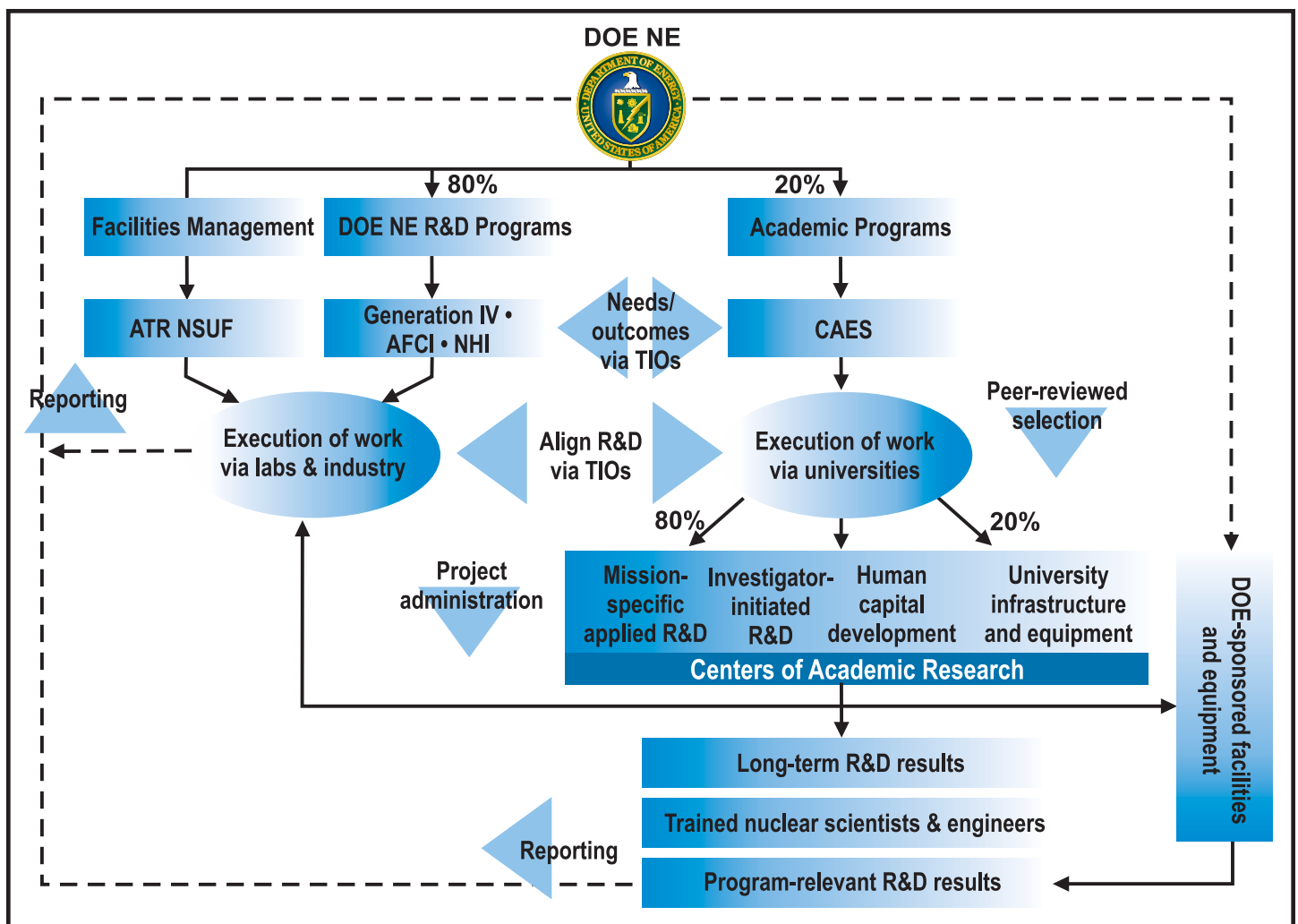
Figure 3. Illustration of the new NEUP approach to the technical integration of NE university programs with NE R&D programs.

To support NEUP's efforts toward human capital and infrastructure development, solicitations will be made for scholarship and fellowship programs, as well as for support of nuclear science and engineering infrastructure needs of colleges and universities. CAES will work to place select scholarship and fellowship recipients within the national laboratory system as interns and as full-time employees.

The center will also promote the program's communications and outreach. Effective communication fosters stakeholder trust, augments integration and collaboration, serves as a catalyst for accomplishing NEUP objectives, and provides national visibility of NEUP accomplishments.

NEUP's outreach plan will help build awareness in the industry and the Nation. The university program contributes to a larger effort to strengthen U.S. education and research; recently enacted legislation, the America COMPETES Act, invests in innovative education to improve U.S. competitiveness in the global economy. The United States has historically been a leader in nuclear technology—an increasingly important element in addressing today's changing energy needs. With government, industry, and universities playing significant roles in realizing nuclear power's potential, NE's new program will play a vital role in meeting the demand created by a burgeoning nuclear renaissance.

NUCLEAR ENERGY RESEARCH INITIATIVE

4.0 NERI R&D Accomplishments

The NERI program has provided funding to universities across the United States, supporting projects directly relevant to DOE nuclear research. In fact, national laboratories and industry collaborate with the universities, emphasizing intersecting aims and applicable results. The program has successfully attracted academic researchers in various fields related to the nuclear industry—which, in turn, has attracted new students to those fields of study (described in Section 2). As a result, the country is closer to the goal of promoting our nuclear infrastructure through an educated workforce.

This widespread response to DOE funding also moves the United States forward on the path to finding better ways to address obstacles in the use of nuclear energy, thus expanding its role in our energy arsenal and maintaining the U.S. position as an industry leader. Several projects have already contributed to industry knowledge. Other projects are ongoing and address a wide range of subjects from reactor design to new fuel sources to waste reduction—all in support of DOE programs and objectives. This section provides an overview of NERI's recent contributions, a summary of the program's success as a focus for relevant research, information about funding, and a list of NERI participants.

Generation IV. NERI-funded projects have made significant contributions to developing new reactor systems that achieve high burnup using transmutation and recycled fuel. U.S. Generation IV designs are currently focused on the very high-temperature reactor (VHTR), the design of choice for the Next Generation Nuclear Plant (NGNP), and six of the current sixteen Generation IV projects are conducting research that contributes primarily to the NGNP's development. These projects include improving methods of design, analysis, and construction, as well as studying radiation effects that would influence safety.

Research has focused on not only specific reactors but also concepts that could apply to more than one Generation IV design type. Current projects include three that focus on improving design and evaluation methods, such as one that seeks to understand and manage uncertainties in simulation software used to model the nuclear cores of Generation IV reactors. Seven Generation IV project teams are examining materials that could be used in advanced reactors.

AFCI. Over the years, NERI-funded researchers have provided findings that bolster development of advanced fuel systems and fuel technologies for both existing and Generation IV nuclear systems. Improving the safety and cost-effectiveness of the fuel cycle (e.g., through waste component separation, recycling, or waste reduction) is part of the program mission.

Of the 33 current AFCI projects, over half of them address advanced fuels and fuel separations directly. Examples include a project team researching solvent extraction schemes to isolate cesium (Cs) and strontium (Sr) from used nuclear fuel, as well as examining fabrication and characterization of ceramic forms for Cs and Sr isotopes; three projects working toward separating transuranic elements and safeguarding the process; and one group comparing two means of recycling actinides—using fast burner reactors versus using inert matrix fuel in light water reactors—with a focus on economics and proliferation resistance.

Six projects are using advanced modeling and simulation techniques to provide data for evaluating nuclear systems with unprecedented accuracy. Another six teams are contributing toward safe design and construction of fast burner reactors, which provide advantages for fuel usage. Project objectives include a design that transmutes legacy waste and operates in a sustainable closed cycle, an optimized thermocouple design for high temperatures and long durations, an analysis of materials for reactor construction, and risk-informed design and evaluation tools.

NHI. The United States has not yet achieved economic, commercial-scale production of hydrogen using nuclear energy. NERI projects provide much-needed research in this area. Nine current projects are contributing to developing technologies to produce hydrogen with heat and/or electricity from next-generation nuclear energy systems at costs that are competitive with other transportation fuels. Several of these project teams are examining different aspects of thermochemical cycles. Other research areas include solid oxide electrolyzer cells, heat transfer, and models that simulate hydrogen production options.

Section 5 provides summaries of all ongoing NERI projects, including their objectives and findings.

Project Awards

FY 2008 began the transition from NERI to NEUP (Section 3), which will begin soliciting new projects in FY 2009. Although some research projects were awarded to universities through the Global Nuclear Energy Partnership, no new NERI projects were awarded.

DOE awarded 22 projects in FY 2007; recipients included 20 U.S. universities, 5 national laboratories, 2 U.S. businesses, and 1 international laboratory collaborator. This represents an $11.4 million Federal government commitment to nuclear R&D during the three-year lifetime of these projects. With each university contributing an additional 20 percent cost-share, the total funds directed toward nuclear R&D increased to $14.4 million.

Also in FY 2007, DOE awarded eleven NERI projects involving consortia (NERI-C). NERI-C brought NERI to the next level, providing greater funding for larger-scale projects that involved a minimum of three cooperating organizations—always led by a university. These eleven projects furthered DOE's mission to generate crossover between organizations, generate new academic interest, and set advanced research goals. These eleven projects comprise a total of $30.7 million for the three-year period. Funding was distributed among 38 U.S. universities, 7 national laboratories, and 1 U.S. business.

In FY 2006, 25 projects were initiated in support of the R&D programs, as well as an additional 35 projects in FY 2005. The total investment in these projects over their three-year term is $32.1 million, distributed among 37 U.S. universities, 7 national laboratories, and 4 corporations. In addition, one university, one laboratory, and three corporations are participating on a strictly cost-share basis. Two foreign educational institutions participate but are ineligible for U.S. funding.

These successes follow an initial history of successful project recruitment. DOE's NERI program released its first solicitation in FY 1999, receiving 308 R&D proposals and making 46 awards. The total cost of these 46 research projects for the three-year period was approximately $52 million. Similar progress was made from FY 2000 to FY 2002, with an additional 47 NERI projects awarded. The total cost of these research projects for the three-year period was approximately $58 million, shared among 20 U.S. universities, 10 national laboratories, 18 private businesses, and 7 foreign R&D organizations.

No new NERI projects were awarded in FY 2003 or FY 2004. Projects awarded from FY 1999 to FY 2005 are now complete, so this annual report does not include specifics of their achievements. Information about completed projects can be obtained from previous annual reports.

Funding

On-going NERI projects are funded directly by of the Generation IV, AFCI, and NHI programs. Figures 4, 5, and 6 illustrate the funding distributions since FY 2005.
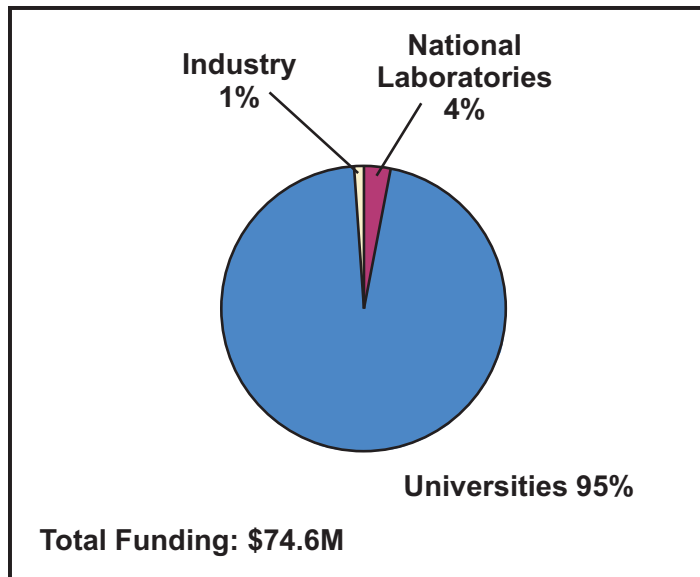

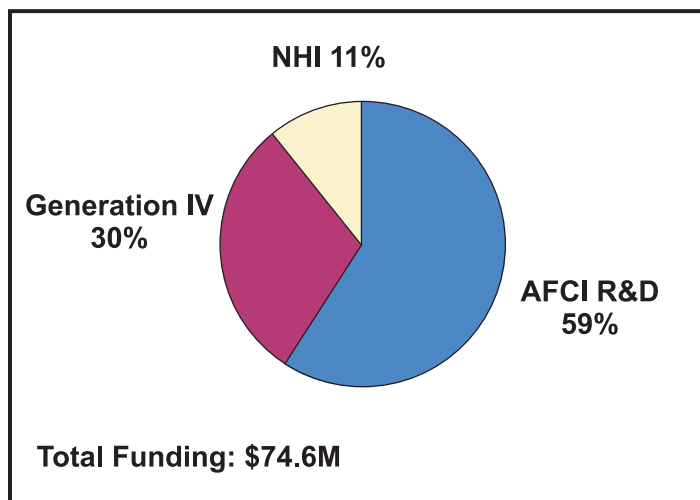Figure 4. Distribution of NERI research funds by recipient from FY 2005 to FY 2008.

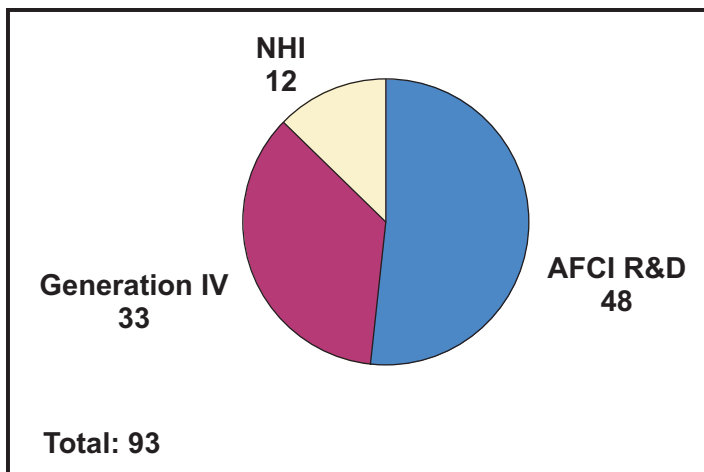Figure 5. Distribution of NERI research funds by R&D program area from FY 2005 to FY 2008.

Figure 6. Distribution of FY 2005 thorugh FY 2008 NERI projects by R&D program area.

Figure 7. Distribution of FY 1999 through FY 2004 NERI projects by R&D area.

In previous years NERI funding was provided by Congress as a separate budget line item in the Energy and Water Development Appropriations Act. The U.S. government invested over $118 million to fund NERI research projects during the first six years of the NERI program. Figure 7 illustrates the cumulative number of research projects awarded through FY 2004 in each of the four original R&D areas, while Figure 8 shows the distribution of this funding among national laboratories, U.S. universities, and industry.

DOE does not fund foreign participants as part of the NERI program. Their participation has been supported by the foreign organizations interested in the research being conducted. Although the PIs are responsible for soliciting such support, foreign participation in NERI projects is contingent upon DOE approval.
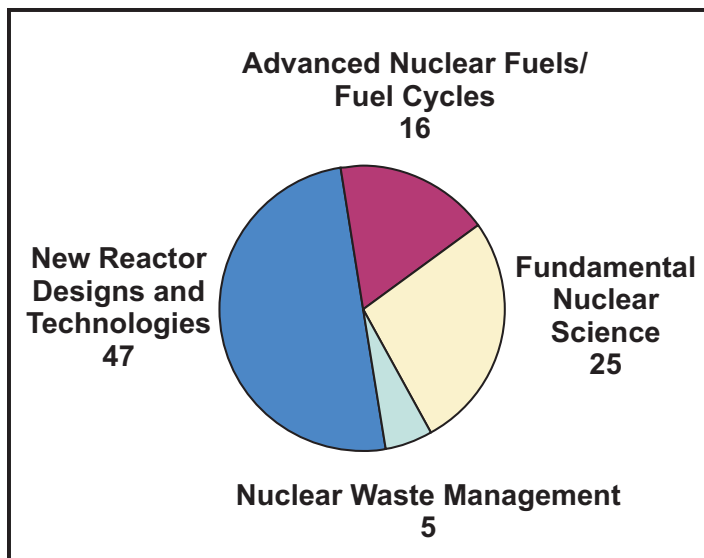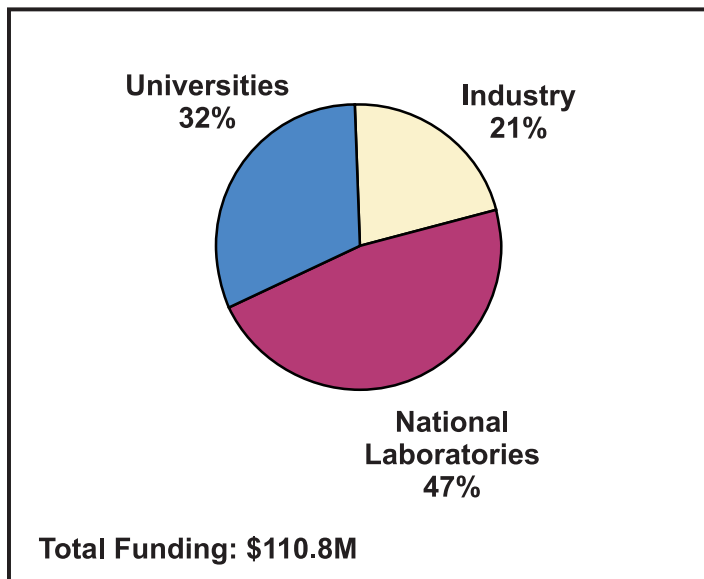

Figure 8. Distribution of NERI research funds by recipient from FY 1999 to FY 2004.

NERI Participants

NERI research participants in 2008 included 51 U.S. universities, 10 national laboratories, 6 private businesses, and 1 foreign organization. The participating organizations are provided below.

U.S. Universities

Abilene Christian University

Alabama A&M University

Boise State University

Brigham Young University

California Institute of Technology

California Polytechnic State University

California State University, Northridge

Colorado School of Mines

Columbia University

Cornell University

Georgia Institute of Technology

Hunter College (CUNY)

Idaho State University

Kansas State University

Massachusetts Institute of Technology

North Carolina State University

Northwestern University

Ohio State University

Ohio University

Oregon State University

Pennsylvania State University

Purdue University

Rensselaer Polytechnic Institute

South Carolina State University

State University of New York, Stony Brook

Tennessee Technological University

Texas A&M University

Tulane University

University of California, Berkeley

University of California, Davis

University of California, Los Angeles

University of California, Santa Barbara

University of Chicago

University of Cincinnati

University of Florida

University of Idaho

University of Illinois, Chicago

University of Illinois, Urbana-Champaign

University of Michigan

University of Missouri, Columbia

University of Missouri, Rolla

University of Nevada, Las Vegas

University of New Mexico

University of North Carolina, Wilmington

University of South Carolina

University of Tennessee

University of Texas, Austin

University of Wisconsin, Madison

Virginia Polytechnic Institute and State University

Washington State University

Washington University in St. Louis

U.S. DOE National Laboratories

Argonne National Laboratory

Brookhaven National Laboratory

Idaho National Laboratory

Lawrence Berkeley National Laboratory

Lawrence Livermore National Laboratory

Los Alamos National Laboratory

Oak Ridge National Laboratory

Pacific Northwest National Laboratory

Sandia National Laboratories

Savannah River National Laboratory

Industrial Organizations

Eltron Research, Inc.

General Atomics

Stress Engineering Services, Inc.

Studsvik of America

TransWare Enterprises, Inc.

Westinghouse Electric Company LLC

International Collaborators

Commissariat à l'énergie atomique (France)

NUCLEAR ENERGY RESEARCH INITIATIVE

5.0   Project Summaries and Abstracts

5.1   Generation IV Nuclear Energy Systems Initiative

There are 16 NERI projects currently being performed under the Generation IV Nuclear Energy Systems Initiative. Six of these projects were awarded in FY 2006, eight projects in FY 2007, and two NERI-C projects in FY 2007.

Generation IV nuclear energy systems are being developed to achieve high burnup using transmutation and recycled fuel, allowing for efficient use of domestic uranium resources and minimizing radioactive waste. Advances in safety and physical protection will guard against possible acts of terror or diversion of nuclear materials, helping to ensure public confidence in nuclear technology.

Current U.S. efforts are focused on SFR and VHTR technologies; in FY 2009, newly awarded Generation IV reactor projects will support these systems. Foreign collaborators are leading research on the other reactor systems under GIF. The MSR is not currently a national research focus, although the concept shares many research areas with the NGNP. Direct U.S. support of the GFR, LFR, and SCWR will continue through the completion of ongoing research projects.

During FY 2008, researchers worked on projects spanning most of the Generation IV program elements. In the area of advanced gas-cooled reactor fuel development, they are developing online failure monitoring and improving analytical techniques. Design and evaluation projects focus on improving modeling capabilities, neutronic analysis, thermal-hydraulic/heat transfer analysis, model uncertainty evaluations, and risk assessment techniques. Energy conversion projects target nuclear heat transport and supercritical CO_2 systems. Materials evaluations continue to occupy a large percentage of the Generation IV program, with studies on radiation behavior, improvement of corrosion resistance, development of advanced ceramics and metal alloys, and improvement of analytical modeling capabilities. Research is being conducted specific to reactor technologies; studies involve lead and lead-bismuth corrosion for the LFR, thermal-hydraulic modeling and materials evaluation for the SCWR, and design analysis methods and materials development for the VHTR. Section 7.2 discusses projects related to the SFR, as they are currently funded under AFCI.

Under the two FY 2007 NERI-C projects related to the Generation IV program, NERI research efforts focus on NGNP and crosscutting materials-related activities. These projects involve the VHTR and structural materials.

For more information about Generation IV, refer to this website: http://nuclear.energy.gov/genIV/neGenIV1.html.

A summary of each project being performed under this initiative follows.

NUCLEAR ENERGY RESEARCH INITIATIVE

Directory of Generation IV Nuclear Energy Systems Initiative Project Summaries and Abstracts

NUCLEAR ENERGY RESEARCH INITIATIVE

Ab Initio-Based Modeling of Radiation Effects in Multi-Component Alloys

PI: Dane Morgan, University of Wisconsin-Madison

Collaborators: None

Project Number: 06-006

Program Area: Generation IV

Project Start Date: March 2006

Project End Date: March 2010

Research Objectives

The objective of this project is to develop a highly accurate thermokinetic model for austenitic stainless steels based on fundamental quantum mechanical calculations. The model will incorporate the true temperature- and composition-dependence of the diffusion constants and provide missing information on interstitial motion.

In order to establish the critical data and computer programs to build the model, researchers will pursue the following specific tasks:

- Perform initial *ab initio* calculations of atomic-scale properties of pure elements and alloys
- Develop iron-chromium-nickel (Fe-Cr-Ni) radiation-induced segregation (RIS) simulation and validation/refinement based on semi-analytic expressions for diffusion constants
- Develop Fe-Cr-Ni RIS simulation methods based on Monte-Carlo techniques
- Perform validation/refinement by comparing analytical results to experiments
- Extend calculations and simulations to a preliminary ferritic Fe-Cr model

Research Progress

Over the past fiscal year, research has focused on the dilute X concentration limits for Ni-X alloys (X = Cr or Fe). The following is a synopsis of the progress made for these systems.

Multifrequency Models. Researchers have completed a full derivation of how vibrational, electronic, and magnetic excitations can be included, along with T=0

energies, in constructing a multifrequency model for diffusion of dilute solute in an fcc host. The resulting model has been parameterized with *ab initio* energetics and used to predict the tracer diffusion constants for Cr and Fe in Ni. The results are valuable for both constraining the diffusion constant values and for identifying the true temperature dependence of the parameters. For example, the tracer diffusion constant for Cr in Ni is typically written in the Arrhenius form $D_0 e^{-\beta Q}$, where D_0 is the assumed constant. However, as shown in Figure 1, D_0 can change dramatically due to a temperature dependency that is difficult to determine without *ab initio* parameterization.

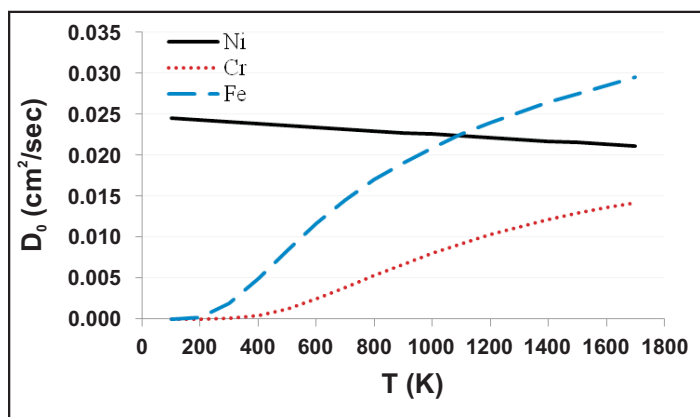Figure 1. Temperature dependence of the *ab initio* prefactor, D_0, for vacancy tracer diffusion.

Kinetic Monte Carlo. Researchers have worked with the University of Michigan to develop a flexible kinetic Monte Carlo (kMC) code to simulate diffusion of concentrated multicomponent systems. Although focused on the dilute case, they have developed the code to the extent that concentrated alloy simulations are possible.

Initial studies of diffusion constants versus concentration assessed how well dilute diffusion models might perform in more concentrated alloys. Figure 2 shows the ratio of approximate solute chemical diffusion constants to their dilute values based on kMC simulations for a variety of hopping rates (Γ), solute-vacancy binding (BE), and solute-solute interactions (BB). Surprisingly, the results show that the diffusion constants generally change by less than a factor of 2.5 for solute compositions up to 50 percent. This suggests that dilute tracer diffusion constants provide valuable insight into the more concentrated alloy, although in some cases the dilute values can change dramatically with composition.

Rate Equation Modeling. The kinetic parameters from multifrequency models and kMC will be used in rate equations to model RIS. The research team has formulated the complete set of equations, including all cross terms, implied by the basic flux relations $J = -L\nabla\mu$. They have written a code to time evolve the flux equations (in cooperation with the Commissariat à l'énergie atomique) and introduced the *ab initio*-derived Onsager coefficients (L) into the program. The initial results for RIS in Ni-18Cr are shown in Figure 3, where the code predicts Cr enrichment over long time periods. The result is opposite to the trends seen experimentally, an error due to limitations of the dilute model for predicting diffusion constants for interstitials. This limitation is being removed through the addition of concentration effects. The reduced RIS expected at higher temperatures is clearly reproduced in changing from 473 K to 873 K.

Planned Activities

Over the next fiscal year, researchers will continue their efforts to refine the semi-analytic model for diffusion constants and to develop an RIS model based on the values. This will be based on approximations of dilute solution in the Ni host and/or non-interacting solid solution models.

Researchers will also develop models for the more concentrated alloy. This will involve some simple modifications of the dilute model, such as adding an interstitial trapping term, and the continued development of kMC codes and cluster expansions of the on-lattice and hopping energetics.
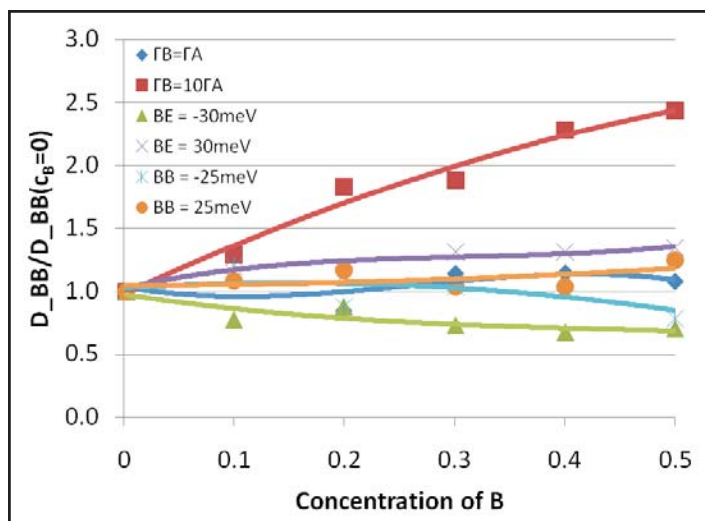
Figure 2. Chemical diffusion coefficient ratios versus solute concentration. T=800 K.
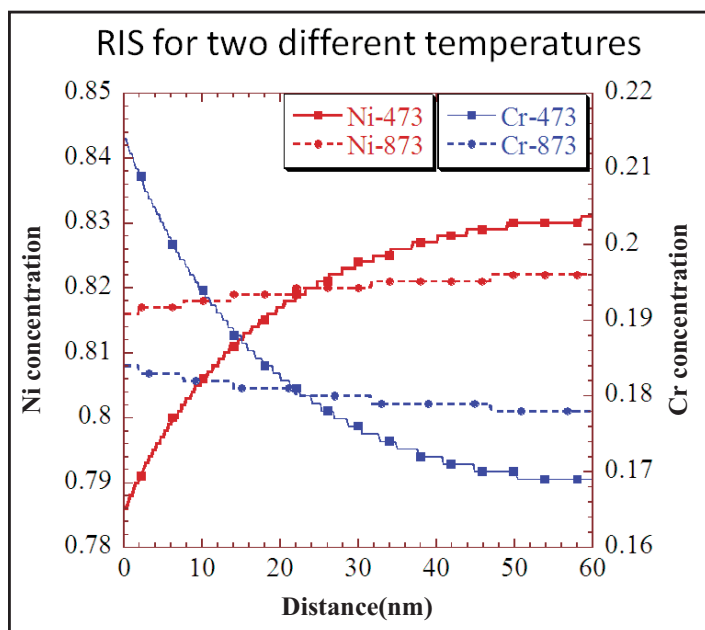
Figure 3. Preliminary RIS results for Ni-18 Cr using dilute alloy model at 473 K and 873 K to demonstrate the code.

Through the remainder of the project, researchers will obtain full and accurate cluster expansions, complete the kMC codes, and combine them to derive improved diffusion constants. The temperature- and composition-dependent diffusion constants will be used with the rate equation code to study RIS in the Ni-Fe-Cr alloy.

Finally, researchers will further refine the models through comparison to RIS experiments, using the results to explore the effects of RIS on voids through void growth modeling. If time permits, researchers will extend their approach to Fe-Cr ferritic model systems.

NUCLEAR ENERGY RESEARCH INITIATIVE

Managing Model Data Uncertainties in Simulator Predictions for Generation IV Systems via Optimum Experimental Design

PI: Paul J. Turinsky and Hany S. Abdel-Khalik, North Carolina State University (NC State)

Collaborators: Argonne National Laboratory (ANL), Idaho National Laboratory (INL)

Project Number: 06-046

Program Area: Generation IV

Project Start Date: March 2006

Project End Date: March 2009

Research Objectives

The objective of this project is to understand and manage uncertainties in simulation software used to model the nuclear core of proposed Generation IV reactors that are caused by uncertainties in the software data itself. Researchers will optimize experiments by determining and quantifying the uncertainties of key design attributes, using INL's Zero Power Physics Reactor (ZPPR) facility as a test basis to reduce model data uncertainties. The team will then complete a pseudo-ZPPR experiment for the optimum design via simulation to determine observable values and will use these values to obtain adapted nuclear data.

The goal of this project is to produce the following methodologies and results, each of which has merit as a stand-alone method or can be used collectively to optimize experimental design:

- A methodology to determine covariance matrices for responses of a complex engineering system and an experimental system

- A methodology to interpret experimental system results via adaptive simulation

- A methodology to optimize the experimental configuration most economically appropriate for reducing the uncertainties of the complex engineering system

- A covariance matrix originating from nuclear data uncertainties for the key design attributes of a Generation IV nuclear core

- Optimum experimental system properties for a ZPPR experimental facility, which are most appropriate for reducing uncertainties of key design attributes of a Generation IV nuclear core

Research Progress

A study was completed on integral parameter sensitivity, uncertainty, and representativity of a fast critical experiment with regard to a Generation IV fast recycle reactor concept. All nuclear reactor designs rely on basic nuclear data, which are obtained by evaluating experimental data from benchmark experiments designed to provide information about basic nuclear data and reactor operation, such as reaction cross sections. In the United States between the 1950s and 1990s, scientists performed many reactor physics and criticality benchmark experiments to provide information on the physics of operating fast reactors similar to those proposed under Generation IV. The split-table, fast critical ZPPR at INL was one of the test reactors operated during this time period.

Since nuclear reactor designs are sensitive to the basic nuclear data provided for calculations, designers must allow margin for the uncertainty in that data in order to license, build, and operate the reactors. A better understanding of sensitivity and uncertainty in the nuclear data, and perhaps further evaluation of some data, can reduce margin requirements and save money. Any good design draws upon data from an accurate experiment that is representative of the design being considered.

This work analyzes and compares various integral parameters of the advanced burner test reactor (ABTR) design concept, published by ANL in 2006, to an established benchmark, ZPPR 15 Assembly B (ZPPR-15B). The research team conducted sensitivity and uncertainty

analyses for integral parameters on both reactors using the efficient subspace method (ESM) developed at NC State. They then compared the reactors using the representativity factor method to determine if ZPPR-15B physics adequately represents ABTR physics. Finally, they modified the ZPPR-15B computational model to include several drawers of transuranic (TRU) targets to simulate an experiment to provide additional data on minor actinide behavior in a fast reactor environment.

Since the sensitivity and uncertainty analyses are first-order based, the first step is to confirm that the model in question behaves linearly over the range of perturbations to be introduced. If the model is approximately linear over the range of possible perturbations, then higher order terms are negligible and ESM can be reliably used.

For the ANL REBUS core simulator code, the model Ω is judged to behave linearly if the following condition is satisfied:

$$\left| \Omega\left(\overline{\sigma}_0 + \sum_{i=1}^{n} a_i \delta \overline{\sigma}_i\right) - \Omega\left(\overline{\sigma}_0\right) - \sum_{i=1}^{n} a_i \delta \overline{y}_i \right| < \varepsilon$$

where $\overline{\sigma}_0$ is the input cross sections, $\overline{y}_0$ is the calculated observables, the subscript "0" denotes the unperturbed values, and ε is the prescribed numerical error tolerance limit.

After confirming the model is linear, researchers developed calculations for the representativity factor, defined as the following:

$$r_{RE} = \frac{\left(\overline{S}_R^T \overline{\overline{C}}_\sigma \overline{S}_E\right)}{\sqrt{\left(\overline{S}_R^T \overline{\overline{C}}_\sigma \overline{S}_R\right)\left(\overline{S}_E^T \overline{\overline{C}}_\sigma \overline{S}_E\right)}}$$

where $\overline{\overline{C}}_\sigma$ denotes the cross-section covariance matrix, and $\overline{S}_R$ and $\overline{S}_E$ are the sensitivity vectors of an integral parameter, b_x, to n input data for a reactor design and an experiment, respectively.

$$\overline{S}_R = \begin{vmatrix} S_{R1} \\ S_{R2} \\ \vdots \\ S_{Rn} \end{vmatrix} \text{ and } \overline{S}_E = \begin{vmatrix} S_{E1} \\ S_{E2} \\ \vdots \\ S_{En} \end{vmatrix}, \text{ where } S_{x,i} = \frac{\partial b_x}{\partial \sigma_i} \cdot \frac{\sigma_i}{b_x}$$

The optimal experiment for a reactor design is one in which r_{RE} is as close to one as possible, which means $\overline{S}_R$ and $\overline{S}_E$ are as similar as possible.

When more than one parameter is of interest, researchers can extend the representativity factor to a matrix $\overline{\overline{R}}_{RE}$, whose diagonals are the r_{RE} for each parameter:

$$\overline{\overline{R}}_{RE} = \left[\left(\overline{S}_R^T \overline{\overline{C}}_\sigma \overline{S}_R\right)^{-1}\left(\overline{S}_R^T \overline{\overline{C}}_\sigma \overline{S}_E\right) \times \left(\overline{S}_E^T \overline{\overline{C}}_\sigma \overline{S}_E\right)^{-1}\left(\overline{S}_E^T \overline{\overline{C}}_\sigma \overline{S}_R\right)\right]^{1/2}$$

For the ideal experiment for a design concept, $\overline{\overline{R}}_{RE}$ would be as close as possible to the identity matrix. Once the representativity is available, the posterior covariance matrix $\overline{\overline{C}}_R^{(P)}$ can be calculated in terms of the representativity matrix as:

$$\overline{\overline{C}}_R^{(P)} = \overline{\overline{C}}_R^{(0)}\left(\overline{\overline{I}} - \overline{\overline{R}}_{RE}^2\left[\overline{\overline{I}} - \left(\overline{S}_E^T \overline{\overline{C}}_\sigma \overline{S}_R\right)^{-1} \overline{\overline{C}}_E\left(\overline{S}_E^{-1} \overline{S}_R\right)\right]^{-1}\right)$$

$$\overline{\overline{C}}_R^{(P)} = \overline{\overline{C}}_R^{(0)}\left(\overline{\overline{I}} - \overline{\overline{R}}_{RE}^2\left[\overline{\overline{I}} + \overline{\overline{E}}\right]^{-1}\right)$$

where $\overline{\overline{C}}_R^{(0)}$ and $\overline{\overline{C}}_E$ represent the prior covariance for the reactor design and the experimental uncertainties, respectively. The posterior covariance matrix $\overline{\overline{C}}_R^{(P)}$ denotes the parameters' uncertainties if the experiment were to be conducted and the results used to adapt the input data. The experimental errors term, $\overline{\overline{E}}$, will limit the uncertainty reduction of using the representativity matrix for adaption, except in the case of a "perfect" experiment where $\overline{\overline{C}}_E = 0$, which was assumed for the following results.

To evaluate the above equations, singular value decomposition is utilized where inverse matrix operations appear to address ill-conditioned matrices. Note that the sensitivity matrices introduced are never explicitly determined, with the action of the sensitivity matrices on the cross-section covariance matrix directly evaluated using the ESM.

Table 1 shows the cross section-induced relative uncertainty for all three reactors (in percent standard deviation) on the parameters of conversion ratio and k-effective, as well as U-238 capture and Pu-239 fission reaction rates at a representative inner core node.

	Relative Uncertainty (% st. dev.)		
	ABTR	ZPPR 15B	ZPPR w/TRU
k-effective	0.8036	0.861	0.8662
conversion ratio	2.1002	2.0328	2.0222
U-238 capture, inner core	2.2657	1.9488	1.9761
Pu-239 fission, inner core	0.6563	0.8018	0.8167

Table 1. Uncertainties for integral parameters and major reaction rates.

Reaction rate uncertainties are low due to the well-known cross sections. Analysis of the sensitivity profiles for each reactor showed that these reaction rates were most sensitive to cross sections with larger uncertainties that affected the flux spectrum rather than their own cross-section uncertainty. The uncertainties on k-effective and conversion ratio, which are defined by reaction rates, are also shown to be low. Table 2 presents uncertainties on fission reaction rates of Am-241, Am-243, and Cm-244 for each reactor at a representative test node. These reaction rates are important for destroying minor actinides in a burner reactor. These reaction rates show much larger uncertainty due primarily to the large uncertainty of their own cross sections, rather than effects of the flux spectrum.

	Relative Uncertainty (% st. dev.)		
	ABTR	ZPPR 15B	ZPPR w/ TRU
Am-241 fission	8.3395	N/A	8.2533
Am-243 fission	6.2976	N/A	6.4149
Cm-244 fission	40.2892	N/A	40.5837

Table 2. Uncertainties for minor actinide fission rates.

The two ZPPR variations, benchmark and TRU modification, were compared to ABTR for representativity. Table 3 shows the representativity for each reactor to ABTR for k-effective, U-238 capture rate, and Pu-239 fission rate. Table 4 shows the representativity for each reactor to ABTR for the minor actinide fission rates mentioned above.

	Representativity to ABTR	
	ZPPR 15B	ZPPR w/ TRU
k-effective	0.9122	0.9204
U-238 capture, inner core	0.9616	0.9625
Pu-239 fission, inner core	0.5339	0.5429

Table 3. Representativity for integral parameters and major reaction rates.

	Representativity to ABTR	
	ZPPR 15B	ZPPR w/ TRU
Am-241 fission	N/A	0.9939
Am-243 fission	N/A	0.9869
Cm-244 fission	N/A	0.9992

Table 4. Representativity for minor actinide fission rates.

The representativity of the minor actinide fissions is high because their sensitivities are dominated by the contributions of their own cross-section uncertainty, which are basic data that are independent of reactor design. The representativity for U-238 capture, as well as k-effective, is also relatively high, indicating that ZPPR physics for these parameters is similar to ABTR. The Pu-239 fission rates are lower than the other representativities, likely because Pu-239's cross section is so well known that the uncertainty on the reaction rate comes mostly from cross sections affecting the flux spectrum, which are different for each reactor.

Planned Activities

The research team will evaluate the posterior covariance matrix for ABTR using a regularization methodology. They need to obtain the cost of margin for the ABTR and the cost to conduct experiments at ZPPR; if the information is not available, the team will develop an acceptable approximation. With the cost information, they will formulate and solve an optimization problem, trading off the cost of performing ZPPR experiments with the cost savings due to the resulting reduced margins for ABTR. The solution to this optimization problem will yield the optimum experimental design.

NUCLEAR ENERGY RESEARCH INITIATIVE

Uncertainty Quantification in the Reliability and Risk Assessment of Generation IV Reactors

PI: Karen Vierow, Texas A&M University (TAMU)

Collaborators: Ohio State University (OSU)

Project Number: 06-057

Program Area: Generation IV

Project Start Date: March 2006

Project End Date: March 2009

Research Objectives

The goal of this project is to develop practical approaches and tools for dynamic reliability and risk assessment techniques that can be used to augment the uncertainty quantification process in probabilistic risk assessment (PRA) methods for Generation IV reactors. The objectives are to 1) develop practical approaches and computationally efficient software to test event tree completeness, 2) integrate a reactor safety code with PRA, and 3) assess and propagate plant state uncertainties in the PRA analysis.

This project involves generating a dynamic event tree (DET) tool and assessing and quantifying uncertainty propagation. In the first phase, researchers will modify current software for DET generation, link it to a best-estimate computer code such as MELCOR, and identify modeling uncertainties via the Phenomena Identification and Ranking Table technique. They will then test the integrated software package on select, high-risk initiating events. In the second phase, the team will improve the computational efficiency by coupling the DET generation software with sampling software developed by Sandia National Laboratories. Finally, they will test this new software on select initiating events.

Research Progress

Five operating regimes are postulated for design basis accidents (DBAs):

1) Pressurized loss of forced circulation (P-LOFC)

2) Depressurized loss of forced circulation (D-LOFC)

3) D-LOFC with air ingress

4) P-LOFC with anticipated transient without scram (ATWS)

5) D-LOFC with ATWS

Important phenomena for an LOFC event include flow reversal and accompanying low heat removal rates at no-flow conditions.

Regarding severe accidents in the pebble bed modular reactor (PBMR), an LOFC such as pressurized conduction cooldown is a key event because potentially harmful amounts of air and/or water may ingress into the core depending on assumptions. Important phenomena include the following:

- Conduction cooldown

- Complicated helium recirculation patterns

- Graphite oxidation

- Characterization of fission product transport through primary circuit

For the current project, researchers have selected a pressurized LOFC event in which the reactor has been scrammed. Both DBA and severe accident analysis capabilities can be investigated. The MELCOR code with the PBMR input deck is capable of simulating decay heat generation and decay heat removal via the graphite reflectors. Uncertainties in this analysis need to be resolved for any of the current analysis tools, rendering the depressurized LOFC analysis a good demonstration problem.

The Figures of Merit for this event have been identified in the International Atomic Energy Agency TECDOC-1198 as the following:

- Integrated heat loss from the reactor that exceeds the decay heat production under hypothetical accident conditions

- Peak core temperature below the demonstrated fuel degradation temperature (1,600°C)

- Oxygen concentrations in high-temperature regions of the core (>1,000°C) that are not sufficient to induce graphite oxidation

- Reactor vessel temperatures

Researchers tested the MELCOR model of the PBMR for steady state operation under a variety of parametric conditions. They varied parameters to observe the effect on calculation results. As an example, the convective heat transfer coefficient from the fuel spheres to the coolant is a key parameter that was shown to affect the fuel temperatures and determine whether safety limits were violated.

Several extensions were made to the MELCOR input deck for the selected event, and a decay heat model was added to the PBMR deck.

During an event where forced convection is lost, cooling of the pebble bed core is accomplished passively using natural circulation and conduction, causing system pressure to fall from 7.0 MPa to 4.5 MPa and the wall temperature to increase from 300°C to 350°C. Helium flow in the core will reverse in direction and travel upward, back down through the reactor pressure vessel area surrounding the core, and exit the vessel. Therefore, the MELCOR model of the PBMR core previously developed was modified to allow for the mitigation of heat during the P-LOFC event. This has been accomplished by changing the periphery heat structures in the original PBMR model into control volumes and heat structures representing the reflectors, core bypass, reactor shroud, helium inlet to the core (the "riser"), the vessel wall, and containment atmosphere, as shown in Figure 1.
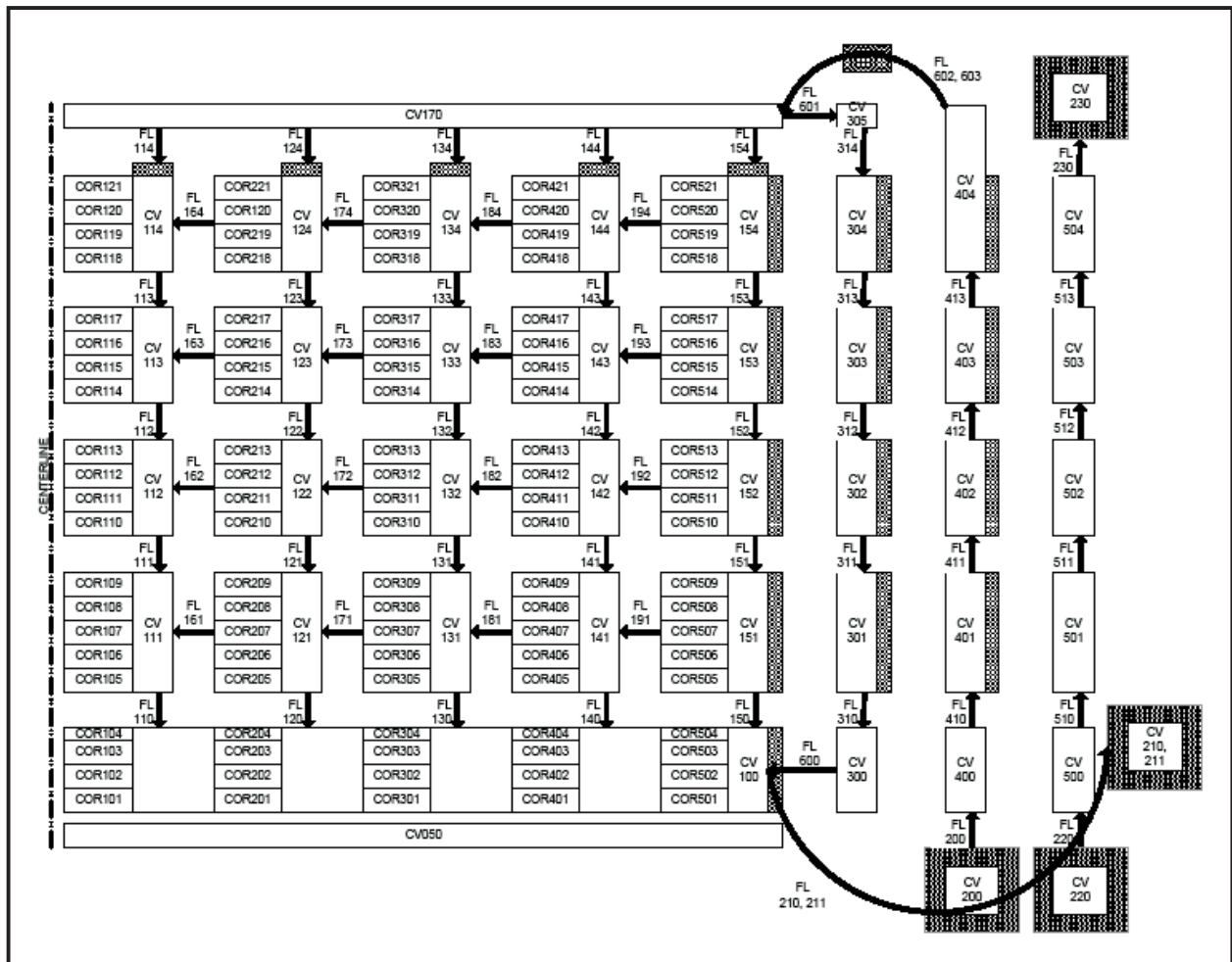

Figure 1. MELCOR Nodalization of PBMR for P-LOFC.

Helium is generated in a "time-independent" volume (i.e., temperature and pressure are constant and helium removal from the volume does not change the conditions of the volume) and moves through the system at a specified flow rate of 129 kg/s due to a velocity source. The coolant rises until it reaches the inlet plenum, then descends through reactor and bypass, using conservation equations to determine the split of the flow. All of this helium then flows into a mass and energy "sink volume." The containment is modeled using a source of nitrogen (the predominant component of air); heat transfer occurs between the reactor and containment air via heat structures representing the reactor pressure vessel wall.

In order to correctly represent the flow during the P-LOFC event, researchers included additional features in the PBMR model. Core power is maintained at 268 MWt for the beginning of the calculation. CV200 is set initially as a time-independent volume. This means that the temperature and pressure of the volume is constant, and helium removal from the volume does not change the conditions of the volume. FL602 controls the mass flow rate at the beginning of the calculation by specifying a velocity of the coolant through the flow path by using the density of the helium. FL210 connects to CV210 for the initial phase of the calculation to allow the specified pressure condition to be constant at the outlet. To run the transient, the core power level will switch to that of time-dependent decay heat. CV200 switches to a time-dependent volume, meaning that the temperature and pressure in the volume calculate dynamically, and a sink in the volume is activated. The flow area in FL602 switches from 100 percent to 0 percent, preventing flow from being forced into the system. FL603 switches open in order to allow MELCOR to calculate the flow rate via natural circulation. FL210 closes to prevent the pressure condition of CV210 from influencing the system, and FL211 opens to connect the pressure condition specified in CV211 to drive part of the flow. Therefore, the event can be modeled in MELCOR using several modifications to the input deck.

A computational infrastructure has been developed outside this NERI project that supports the generation of multiple DETs on a distributed computing architecture composed of a heterogeneous collection of computational and storage nodes. The DET generation is managed by a driver, called Analysis of Dynamic Accident Progression Trees (ADAPT), that 1) determines when branching is to occur, 2) initiates multiple restarts of system code analyses, 3) determines the probabilities of scenarios, 4) determines when a scenario can be terminated, and 5) combines similar scenarios to reduce the scope of the analysis.

There have been several advancements in the development of ADAPT. First, the researchers linked the ADAPT code to the MELCOR severe accident analysis code in the first year of the project. However, since ADAPT has been designed with a simulator agnostic infrastructure, the team also recently linked the RELAP5-3D thermal hydraulic analysis code to ADAPT to accommodate other PBMR models. In addition, they have made several improvements to the graphical user interface for ADAPT by adding more advanced features for downloading data from the compute cluster where severe accident simulations are performed, as well as allowing for more experiment execution control. The graphical user interface now allows the user to upload and launch experiments. Finally, a user's manual and developer's guide has been developed for the graphical user interface to aid future users and developers of the software.

The computational infrastructure software was completed at OSU, and initial testing was performed at TAMU. In the second year of the project, the ADAPT-MELCOR system was successfully run on TAMU's machines.

Planned Activities

Following is a synopsis of the tasks the team plans to conduct over the next period:

- Complete determination of key modeling uncertainties

- Generate uncertainty input for the PBMR input deck

- Model key uncertainties for a representative Generation IV plant through best estimate code input

- Link the computational infrastructure with the input deck

- Test the software integration, to consist of validation and verification exercises

- Prepare documentation for the user's manual

- Quantify modeling uncertainties for a reference Generation IV reactor

- Discuss software coupling with best estimate codes other than the demonstration code

NUCLEAR ENERGY RESEARCH INITIATIVE

An Advanced Neutronic Analysis Toolkit with In-Line Monte Carlo Capability for VHTR Analysis

PI: William R. Martin, University of Michigan

Collaborators: Studsvik of America; Idaho National Laboratory; Los Alamos National Laboratory; General Atomics; Oak Ridge National Laboratory; TransWare Enterprises, Inc.

Project Number: 06-068

Program Area: Generation IV

Project Start Date: March 2006

Project End Date: March 2009

Research Objectives

The goal of this project is to augment a conventional lattice physics code to allow the analysis of very high-temperature reactor (VHTR) configurations with TRISO particle fuel. This project will establish "proof-of-principle" by combining the capability of the MCNP5 Monte Carlo code with the CPM-3 code. CPM-3 is a lattice physics code based on the method-of-characteristics (MOC) and the collision probability (CP) method. Conventional MOC-CP lattice codes such as CPM-3 cannot analyze TRISO fuel because the integration paths cannot resolve the fuel particles. The final package will inherit the substantial downstream capabilities of a production MOC-CP code such as cross-section generation for global nodal analysis and depletion, systematic preparation of cross-section sets for accident analysis, and efficient fuel cycle analyses and assessment of alternative fuel management schemes. The final product will be a validated neutronics methodology for VHTR design and analysis, including cross-section generation, global reactor analysis, depletion, and fuel management.

The primary objectives are listed below:

- To develop a methodology and demonstrate "proof-of-principle" to combine a collision probability code (CPM-3) and MCNP5 to allow the analysis of VHTR configurations

- To apply the coupled CPM-3/MCNP5 methodology to a deep burn configuration and assess its capability to treat low-lying resonances of plutonium isotopes and to adapt the methodology as needed to handle these important resonances

- To demonstrate the capability of using the methodology with a production lattice physics code other than CPM-3

- To verify and validate the coupled CPM-3/MCNP5 methodology for a nominal VHTR full core configuration with temperature feedback as well as startup/operational data from Fort St. Vrain

- To assess the applicability of the coupled methodology to analyze pebble bed configurations

Research Progress

The research team has made significant progress toward meeting project goals during this past year. The key task has been successfully demonstrating that resonance cross sections from MCNP5 can be used within CPM-3 to allow CPM-3 to be used for the analysis of VHTR configurations, including an explicit treatment of the TRISO particle fuel. Moreover, this can be done with a simpler, more efficient, and more effective approach than originally proposed. A brief summary of the key accomplishments is given below.

CPM-3/MCNP5 Coupling Methodology. The original approach involved the concurrent execution of MCNP5 and CPM-3 using a Fortran-90 interface that communicated information from one code to the other during the simulation of a specific configuration. The improved approach defines a "double heterogeneity factor" (DHF) that, when multiplied by the MOC-CP code's prediction of the microscopic resonance cross section, yields a cross section that is properly shielded for the presence of the particle fuel. There will be an array of DHFs that has length equal to the number of resonance groups times the number of resonance isotopes.

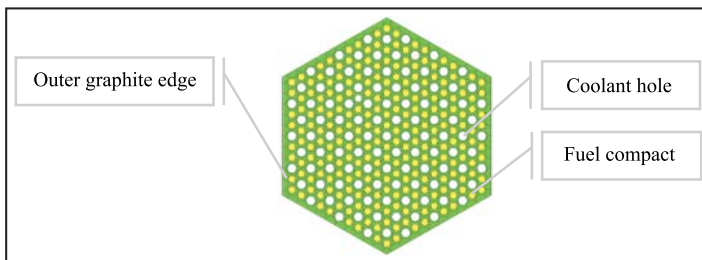***Numerical Results for VHTR Fuel Assembly.*** The VHTR fuel assembly is shown in Figure 1.

Figure 1. VHTR fuel assembly.

The outer graphite edge of the assembly was modeled explicitly with CPM-3 by modeling portions of two adjacent fuel assemblies with reflecting boundary conditions on each face of the rectangular assembly, as depicted in Figure 2.
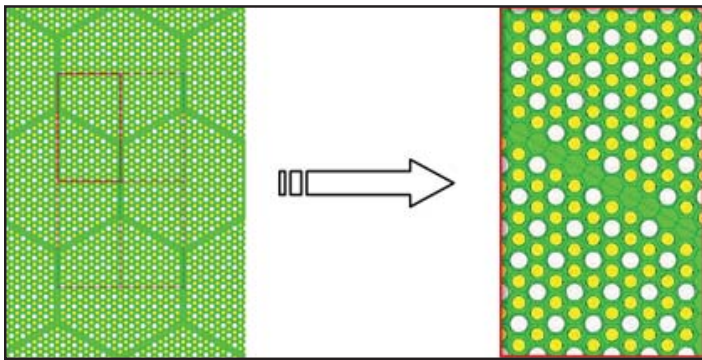

Figure 2. Modeling a VHTR fuel assembly with CPM-3.

The configuration shown on the right side of Figure 2 was analyzed by MCNP5 in two ways: modeling the fuel compact regions 1) with heterogeneous fuel (resolving the microspheres) and 2) with homogeneous fuel. Similarly, the configuration in Figure 2 was analyzed by CPM-3 with DHFs (heterogeneous fuel) and without DHFs (homogeneous fuel). In addition, the CPM-3 calculation was performed with our original approach, using MCNP5-generated resonance cross sections. The results for these five cases are shown in Table 1.

The new approach (with DHFs) agrees to within 0.07 percent of the MCNP5 benchmark result and yields essentially the same results as the original approach (with MCNP5 cross sections). However, there are substantial advantages with the new approach, including far simpler coding, easier implementation, and more flexible methodology that accounts for spatial dependence of the Dancoff factors.

Planned Activities

The following activities will be accomplished during the next period of the project:

1) Work with Studsvik-Scandpower to couple MCNP5 with HELIOS using DHFs computed consistent with the HELIOS library group structure

2) Set up a validation test problem (e.g., Fort St. Vrain) with the assistance of General Atomics, and perform an MCNP5 benchmark calculation for this problem

3) Set up and run a nominal full-core VHTR benchmark case with temperature feedback and depletion, and analyze this case with MCNP5 and the coupling methodology with DHFs. The team will account for temperature feedback using RELAP5/Athena. In addition, they will model gamma heat deposition due to fission and capture gammas to determine core and reflector heating distributions. The benchmark Monte-Carlo analysis will include temperature feedback and depletion and will be performed with heterogeneous and homogeneous TRISO fuel. These calculations will allow researchers to predict the space-dependent DHFs throughout the core and as a function of depletion.

Case	k_∞	% difference
MCNP5 – heterogeneous fuel (reference)	1.4980	-
CPM-3 – with MCNP5 cross sections	1.4974	0.04
CPM-3 – with MCNP5 DHFs	1.4990	0.07
MCNP5 – homogeneous fuel	1.4322	4.4
CPM-3 original – homogeneous fuel	1.4409	3.8

Table 1. Comparison of MCNP5 and CPM-3 calculations for a VHTR fuel assembly.

NUCLEAR ENERGY RESEARCH INITIATIVE

Improving Corrosion Behavior in Supercritical Water Reactor, Lead Fast Reactor, and Very High-Temperature Reactor Materials by Formation of a Stable Oxide

PI: Arthur T. Motta, Pennsylvania State University

Collaborators: Westinghouse Electric Company, Los Alamos National Laboratory (LANL), University of Wisconsin, University of Michigan

Project Number: 06-100

Program Area: Generation IV

Project Start Date: March 2006

Project End Date: March 2009

Research Objectives

This project is designed to establish a technical basis for corrosion protection of candidate materials for three different types of reactors: the supercritical water reactor (SCWR), the lead fast reactor (LFR), and the very high-temperature reactor (VHTR). The materials to be studied include ferritic-martensitic steels, austenitic alloys, and Ni-based alloys. In order to understand the mechanisms associated with corrosion behavior in these materials, researchers will conduct a systematic study on the nature of protective films formed during corrosion tests in simulated reactor environments. The overall objective is to understand why certain alloys exhibit better corrosion behavior than others by examining the oxide microstructure. Alloys that resist corrosion develop a protective oxide layer that limits the access of corrosive species to the underlying metal, leading to stable oxide growth. The alloy chemistry and microstructure determine the differences between a protective and a non-protective oxide. Very small changes in microstructure can significantly affect corrosion rate.

oxide layers using scanning electron microscopy (SEM) and synchrotron radiation fluorescence and diffraction. In most cases, researchers observed a three-layer structure with an outer layer containing only Fe_3O_4; an inner layer containing a mixture of $FeCr_2O_4$, Fe_3O_4, and a small quantity of Cr_2O_3; and a diffusion layer containing a mixture of base metal grains and oxide precipitates in the form of $FeCr_2O_4$ and Cr_2O_3. The dependence of the oxide microstructure with the exposure time was especially of interest with the appearance of the Cr_2O_3 ribbon on the 9Cr oxide dispersion strengthened (ODS) 600°C sample. The evolution with exposure time of 9Cr ODS 600°C is shown in Figure 1.

Research Progress

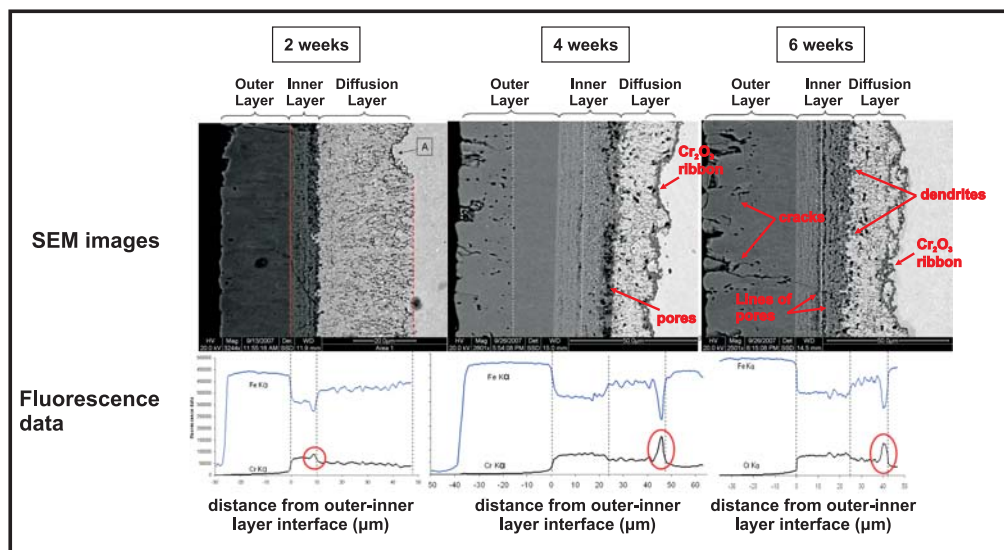During this year, the team continued characterizing the

Figure 1. Evolution with exposure time of the oxide structure of 9Cr ODS 600°C. The fluorescence data is plotted below the SEM images.

Another sample that was analyzed using the same techniques is the Generation III ferritic-martensitic alloy, HCM12A. This alloy contains approximately 11 weight percent (wt%) of chromium and does not contain any ODS particles like 9Cr ODS, but rather exhibits ferritic-martensitic laths. Even though both alloys exhibit a different base metal microstructure, they show similar oxidation behavior with a three-layer structure containing Fe_3O_4 in the outer oxide, a mixture of $FeCr_2O_4$ and Fe_3O_4 in the inner oxide, and a diffusion layer containing a mixture of oxide precipitates ($FeCr_2O_4$ and Cr_2O_3) and Fe bcc metal grains. The oxidation of HCM12A stands out from that of 9Cr ODS by the correlation observed between the base metal microstructure and the oxide precipitates formed in the diffusion layer. The oxide precipitates form in the direction of the ferritic-martensitic laths and seem to be forming at the lath boundaries. Figure 2 displays two SEM images of HCM12A exposed to 600°C supercritical water for two weeks where the influence of the base metal microstructure on the oxide precipitation can be observed.

Researchers continue to study alloys oxidized in flowing lead-bismuth eutectic and have chosen five alloys for final analysis, which are listed below in Table 1.

Alloy #3 and T91 have comparable amounts of Cr (8 percent to 9 percent), whereas the HT-9 alloys all contain about 12 wt%. Also, three HT-9 samples from the same stock were run—two in the delta loop and one in the IPPE loop to give a comparison of the oxidation at higher temperatures for longer times. Finally, one of the HT-9 samples oxidized in the Delta loop was annealed before
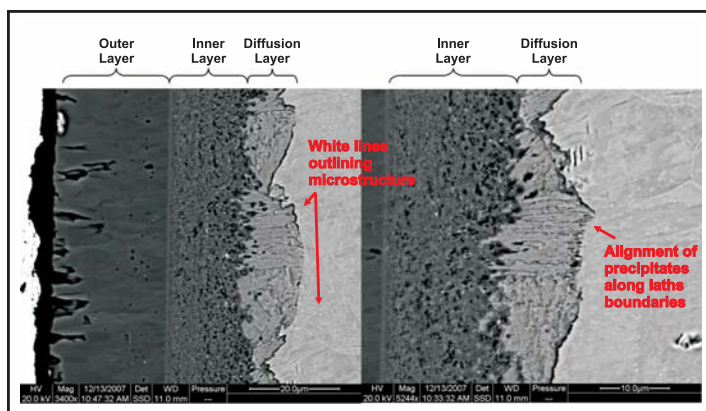

Figure 2. SEM images showing the influence of the base metal microstructure on the oxide precipitation of the oxide layers formed after a two-week exposure to supercritical water at 600°C.

corrosion, giving a basis on which to compare a heat-treated sample to an untreated one. Comparisons between these samples are currently being developed.

The T91 sample's micro x-ray fluorescence and diffraction results are shown in Figure 3. It can be seen that T91 forms a dense inner layer and a porous outer oxide layer. The first half of the outer oxide displays bright "spots" indicating the presence of heavier elements which were discovered through an energy dispersive spectrometer to be lead and bismuth. Below the SEM image in Figure 3 is the fluorescence data. In the inner oxide, the iron content decreases and chromium content increases, suggesting a combination of iron, chromium, and oxygen phases. Just before the inner oxide/outer oxide interface, there is a distinct section of chromium enrichment and iron depletion. The outer oxide contains almost no chromium and very

Alloy Name	Corrosion Loop	Corrosion Temp	Corrosion Time	Alloying Elements (wt%)								
				Fe	Cr	C	Ni	Mo	Si	Mn	W	V
HT-9 Delta	Delta (LANL)	500°C	666 h	84.5	12	0.2	0.5	1	0.4	0.6	0.5	0.3
HT-9 Annl	Delta (LANL)	500°C	666 h	84.5	12	0.2	0.5	1	0.4	0.6	0.5	0.3
HT-9 IPPE	IPPE	550°C	3000 h	84.5	12	0.2	0.5	1	0.4	0.6	0.5	0.3
T91	Delta (LANL)	500°C	666 h	89.4	8.3	0.1	0.2	1	0.4	0.4	–	0.2
Alloy #3	Delta (LANL)	500°C	666 h	91	9							

Table 1. Studied alloy corrosion conditions and major alloying elements.
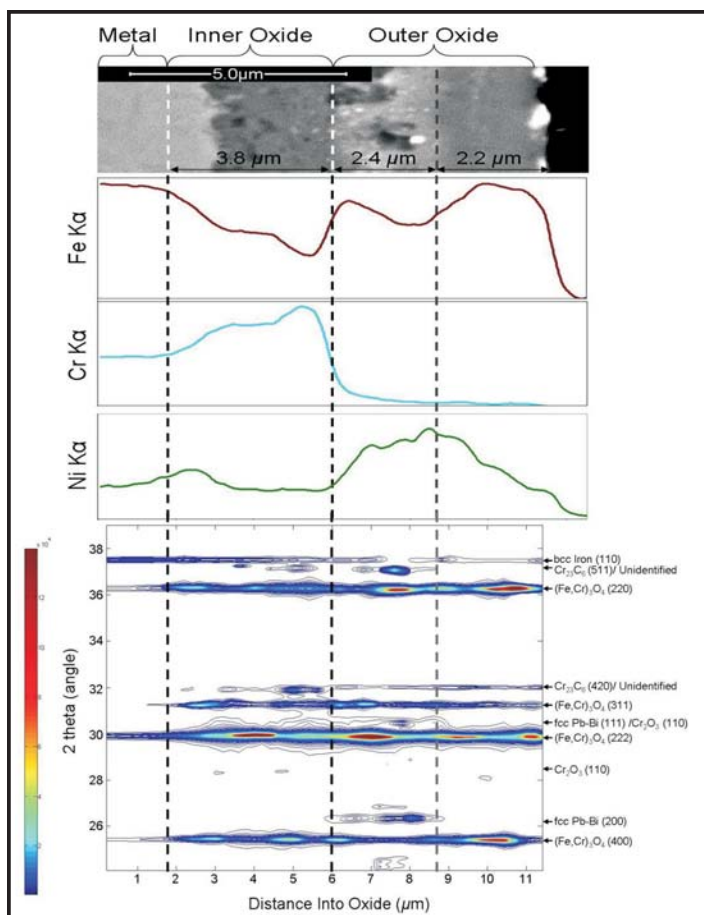
Figure 3. SEM image of T91 with corresponding x-ray fluorescence information and contour plot of phases found using x-ray diffraction.

high levels of iron. Also, nickel is enriched in the outer oxide. Previous researchers have seen that lead-bismuth eutectic tends to leach nickel out of metal structures.

The diffraction information at the bottom of Figure 3 is a contour plot of the fitted data where the intensity of the peaks is shown using the color bar on the left. The metal section of this sample contains peaks for both bcc Fe as well as magnetite Fe_3O_4 peaks. The magnetite peaks in the metal region are probably a result of the unevenness of the metal-oxide interface due to the tendency for the metals to oxidize preferentially along the lath of its grain boundaries. These magnetite peaks increase in the inner oxide and are accompanied by very small spinel ($FeCr_2O_4$) peaks.

Planned Activities

For the remainder of the project, the research team plans to conduct a few final examinations at the microbeam synchrotron radiation diffraction facility. Researchers will focus on obtaining additional synchrotron radiation diffraction and fluorescence data and analyzing the oxide layers using transmission electron microscopy (TEM). TEM analysis of HCM12A will try to elucidate how the base metal microstructure influences the oxide precipitation and whether there is segregation of certain elements at the lath boundaries.

NUCLEAR ENERGY RESEARCH INITIATIVE

Multi-Scale Modeling of the Deformation of Advanced Ferritic Steels for Generation IV Nuclear Energy Systems

PI: Nasr M. Ghoniem, University of California-Los Angeles

Collaborators: California State University-Northridge

Project Number: 06-109

Program Area: Generation IV

Project Start Date: March 2006

Project End Date: March 2009

Research Objectives

The objective of this project is to develop a multi-scale modeling framework to assist in developing radiation-resistant steels with improved mechanical properties for high-temperature applications in Generation IV reactors. In this project, researchers will develop a hybrid *ab initio/* continuum model to describe the core of dislocations in iron (Fe), since empirical interatomic potentials are not accurate and do not allow studies on the effects of local chemical changes in alloys. The model will facilitate studies of dislocation core structures in steels, without *ad hoc* assumptions of interatomic forces. The model will be applied to determine the core structure of screw dislocations in Fe, as well as the interaction between dislocations and oxide and carbide precipitates, because they control the ductility and high-temperature strength of steels. Researchers will develop dislocation dynamics models to simulate the mechanical properties of radiation-damaged steels as a function of the neutron dose. They will also develop single dislocation interaction with nano-voids, precipitates, and self-interstitial atom (SIA) clusters during irradiation. The team will use this information in a comprehensive rate theory model of radiation damage and in-reactor deformation to predict in-reactor deformation, with full microstructure information linked with the deformation field.

Research Progress

Ab Initio Modeling of Dislocation-Precipitate Interaction. One of the primary reasons Fe-based alloys harden is the presence of precipitates in the Fe matrix induced by neutron irradiation. Cu precipitates interact with dislocations in α-Fe, changing the mobility and/or dislocation core structure, thus inducing embrittlement of α-Fe. *Ab initio* simulations are necessary to reveal the underlying mechanism for the interaction between the Cu precipitates and the screw dislocation in α-Fe. The results indicate that the dislocation core cannot be localized at the precipitate-matrix interface; the dislocation core spontaneously returns to the center of the precipitate. In addition, the team found for the first time that the precipitate size has a large effect on the dislocation core polarization, which may affect mobility. Spherical Cu precipitates larger than 2.0 nm have a polarized dislocation core, whereas the core is un-polarized for precipitates smaller than 1.3 nm, similar to the un-polarized core in α-Fe. Figure 1 provides snapshots of the dislocation core at 2 ps, 12 ps, and 14 ps for the 2.3 nm Cu precipitate and at 4.5 ps for the 1.0 nm Cu precipitate.

Core Structure of Self-Interstitial Clusters in Copper and Iron. The research team developed a new computational method to analyze the core structure of dislocations and self-interstitial loops in bcc Fe and fcc copper, combining quantum mechanical determination of crystal lattice slip resistance with continuum mechanics for the elastic field. The method was based on the Peierls-Nabarro (PN) model and input of atomistic information prepared by separate *ab initio* calculations. The core structure of dislocations can also be simulated by the classical molecular dynamics (MD) method. However, the reliability of the classical MD simulation result strongly depends on the accuracy of the interatomic potential, which is either empirically or semi-empirically developed by fitting an equation to available experimental and *ab initio* calculation results. To determine the atomic arrangements in the dislocation cores using the hybrid method, the team
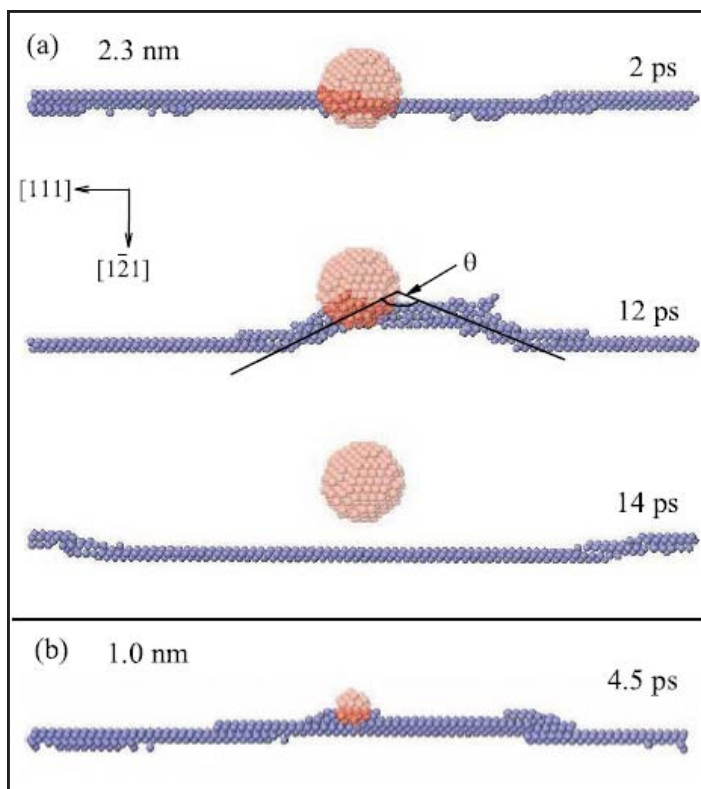
Figure 1. (a) Snapshots of the dislocation core at 2 ps, 12 ps, and 14 ps for the 2.3 nm Cu precipitate; (b) snapshot at 4.5 ps for the 1.0 nm Cu precipitate.

developed a new method that enables the calculation of displacements of atoms based on the elasticity of the infinitesimal dislocations, as well as the construction of atomic arrangements of the dislocation core.

Dislocation Interaction with SIA Clusters and Radiation Hardening. SIA clusters have a significant influence on damage evolution and the mechanical properties of irradiated materials. Researchers performed kinetic Monte Carlo (kMC) computer simulations to determine the kinetics of SIA cluster "clouds" in the vicinity of edge dislocations. The simulations included the elastic interactions between SIA clusters and between clusters and dislocations. Researchers presented the results of the kMC simulations, which describe the formation of clouds of SIA clusters in the presence of internal elastic fields during neutron irradiation of bcc Fe and the corresponding evolution kinetics. They studied the size and spatial distribution of SIA clusters in the cloud region for a variety of neutron displacement damage dose levels. The main features of the investigations included the following: 1) determination of the kinetics and spatial extent of defect clouds near static dislocations, 2) assessment of the influence of localized patches of SIA clouds on the pinning-depinning motion of dislocations in irradiated materials, 3) demonstration of the conditions for the formation of self-organized SIA raft patterns as a result of the interaction between mobile dislocations and glissile SIA clusters, and 4) estimation of the radiation hardening effects of SIA clusters. Researchers conducted a study of the collective dynamics of thousands of SIA clusters, driven in their motion by their own interactions and by their interactions with moving dislocations, to demonstrate some of the conditions for the emergence of a self-organized pattern of SIA cluster rafts. The study showed that the critical stress to unlock trapped dislocations from SIA cluster clouds is in reasonable agreement with experimental observations.

Crystal Plasticity Modeling of Localized Deformation. The objective of this research is to develop an understanding of the mechanical behavior and dislocation microstructure evolution of single and polycrystals and to delineate the physical and mechanical origins of spatially localized plastic deformation in irradiated materials. The team developed a rate-independent crystal plasticity model to incorporate micromechanics, crystallinity, and microstructure into a continuum description of finite strain plasticity. They employed a comprehensive dislocation density model based on rate theory to determine the strain hardening behavior within each plastic slip system for the fcc crystal structure. They coupled the finite strain effects and the kinematics of crystal plasticity with the dislocation-density based model via the hardening matrix in crystal plasticity. Researchers applied the material models they developed to study single and polycrystal deformation behavior of copper. They also developed interfaces between the ABAQUS user's subroutine Umat and the ABAQUS main code to allow further extension of the current method. Simulations carried out for polycrystals clearly illustrated the heterogeneous nature of plastic strain and the corresponding spatial heterogeneity of the mobile dislocation density. The origins of the spatial heterogeneities were essentially geometric as a result of constraints on grain rotation (finite strain effects) and geometric softening due to plastic unloading of neighboring crystals.

Planned Activities

Ab Initio Modeling

- Continue the development of formalism and codes for a PN model for bcc materials and the effect of impurities on the core structure

- Continue the development of a hybrid *ab initio* approach for the Cu-Fe interface and Cu precipitates

- Continue the development of the concurrent multi-scale approach

- Study the formation of kinks on screw dislocations in Fe

Dislocation Dynamics Modeling

- Continue dislocation dynamics simulations of the collective motion of large numbers (over several thousand) of SIA clusters and moving dislocations to investigate SIA cluster patterns in irradiated Fe

Constitutive and Crystal Plasticity Modeling

- Continue the development of a rate theory model for dislocation populations in irradiated Fe

- Include spatial gradient effects in the rate theory model of dislocation populations

- Continue the development of a crystal plasticity framework that includes dislocation populations in the finite element method solutions

- Develop applications of the crystal plasticity model to polycrystalline material deformation

NUCLEAR ENERGY RESEARCH INITIATIVE

An Advanced Integrated Diffusion/Transport Method for the Design, Analysis, and Optimization of Very High-Temperature Reactors

PI: Farzad Rahnema, Georgia Institute of Technology

Collaborators: Idaho National Laboratory

Project Number: 07-003

Program Area: Generation IV

Project Start Date: July 2007

Project End Date: July 2010

Research Objectives

The main objective of this research is to develop an integrated diffusion/transport (IDT) method to substantially improve accuracy of nodal diffusion methods for design and analysis of very high-temperature reactors (VHTRs). Owing to the presence of control rods in the reflector regions of the pebble-bed reactor (PBR), traditional nodal diffusion methods will not accurately model these regions, within which diffusion theory breaks down in the vicinity of high neutron absorption and steep flux gradients. The proposed IDT method will use a local transport solver based on a new incident flux response expansion method in the controlled nodes. Diffusion theory will be used in the rest of the core. This approach will improve the accuracy of the core solution by generating transport solutions of controlled nodes while maintaining computational efficiency by using diffusion solutions in nodes where such a treatment is sufficient. The transport method will initially be developed and coupled to the reformulated 3-D nodal diffusion model in the PEBBED code for PBR core design and fuel-cycle analysis.

This method will also be extended to the prismatic VHTR. The research team expects the new method to accurately capture transport effects in highly heterogeneous regions with steep flux gradients. The calculations of these nodes with transport theory will avoid errors associated with spatial homogenization commonly used in diffusion methods in reactor core simulators.

Research Progress

During the project's first year, the team developed a 2-D cylindrical transport method to generate response functions for non-multiplying regions (inner and outer reflectors). In addition, the team conducted consistency checks on a 2-D pebble bed modular reactor (PBMR) benchmark. The following describes this research in more detail.

Development of the 2-D(r,θ) Response Function-Based Transport Method. The aim of this task is to develop a 2-D cylindrical transport method to generate response functions, in terms of exiting partial currents and surface-averaged and node-averaged scalar fluxes, for non-multiplying regions such as inner and outer reflectors to couple with the diffusion method used in the fuel region.

To generate response functions for a coarse mesh, researchers must approximate the mesh boundaries' neutron phase space distributions; an approximation is necessary since the whole core solution is not known *a priori*. To this end, the team has developed a set of new expansion functions for an arbitrary 2-D cylindrical surface. The new expansion functions are a tensor product of Legendre polynomials $P_n(\chi)$ and Chebyshev polynomials $U_n(\chi)$ of the second kind:

$$f_{ijkl}\left(\vec{r},\hat{\Omega},E\right)=P_i\left(\vec{r}\right)U_j\left(\cos\theta\right)P_k\left(\cos\varphi\right)P_l\left(E\right)$$

where i, j, k, and l are expansion orders in spatial, polar angle, azimuthal angle, and energy variables, respectively. Chebyshev polynomials $U_n(\mu)$ have the recurrence relation given below:

$$U_0\left(\mu\right)=1$$
$$U_1\left(\mu\right)=2\mu$$
$$U_{n+1}\left(\mu\right)=2\mu U_n\left(\mu\right)-U_{n-1}\left(\mu\right) \text{ for } n\geq1$$

The new expansion functions also avoid the singularity introduced by the conventional Legendre polynomial expansion since the lowest-order expansion function

represents an isotropic flux. These new expansion functions serve as a boundary condition imposed on an inner/outer coarse mesh to generate response functions for coupling with diffusion solutions in fuel regions.

Development of the 2-D(r,θ) RMNB Diffusion Method. The goal of this task is to include transport treatment in selected nodes of a diffusion nodal code. The targeted nodes are non-multiplying regions in a PBR reflector with control rods or voids in the control rods' locations. Transport effects are captured through use of response functions. The response functions can be manipulated in such a way that they form a set of equations that can easily be incorporated into the nodal diffusion code.

In this approach, the outward current average nodal-scalar-flux and edge-scalar-flux values are formulated in terms of response functions, and the edge currents are expressed in terms of the outward- and inward-facing currents. The edge-current equations and the outward-current response function formulation are algebraically manipulated to obtain expressions for the nodal inward-facing currents. These nodal inward-facing current relations are then substituted into the response function formulation of the average scalar flux to obtain the nodal response balance equation. Next, the response function-formulated edge-scalar-flux values are set equal to the edge-scalar-flux values of designated transport nodes or the edge-scalar-flux values multiplied by a discontinuity factor of designated diffusion nodes. This results in a continuous flux interface equation that has currents as the unknowns. The inward currents obtained from the nodal balance equation are substituted into the flux interface expression. For an interface between a transport node and a diffusion node, edge currents obtained from the balance equation are substituted into the flux interface expression.

The equations for constructing the linear system in the direct coarse-mesh finite difference (CMFD) form requires considering triplets of nodes in all possible combinations of diffusion and transport nodes in each direction (r, theta, and z). The equations for all directions and for all possible combinations of adjacent nodes (e.g., diffusion-transport-diffusion) have been analytically derived. The resulting expressions for the coefficients of the overall flux-coupling matrix have also been obtained.

Implementation of the 2-D(r,θ) Response Function-Based Transport Method and Preliminary Tests. The research team implemented the previously developed 2-D(r,θ) incident flux expansion method into the MCNP code. They used the new set of expansion functions

to sample the initial position (r,θ), energy (E), and direction (Ω) of incoming neutrons. The team tallied expansion coefficients of quantities of interest, such as outgoing partial currents and average fluxes, as a response function corresponding to a unit incoming flux imposed on the mesh boundaries.

Figure 1 shows a 2-D PBMR400 benchmark problem that was used to do a consistency check. The benchmark consists of an inner reflector region with a diameter of 2 meters (m), an annular fuel region of 0.85 m thickness, and a 0.5 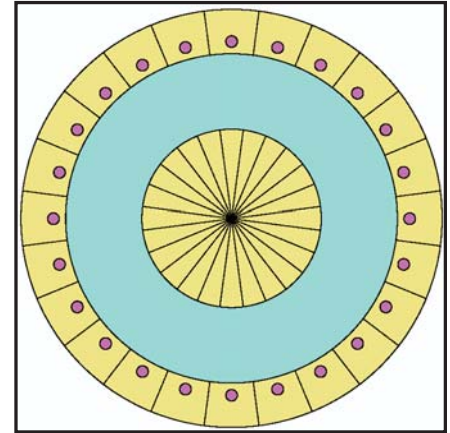m-thick controlled outer-reflector region. Twenty-four control rods, each 13 cm in diameter, have centers positioned on the circumference of a 3.974-m-diameter ring.

Figure 1. Geometric configuration of a 2-D PBMR400 PBR consisting of an inner reflector, an annular fuel region, and a controlled outer reflector.

To check accuracy of these response functions, the research team compared the superposition of the response functions with the reference results directly computed by the MCNP simulations. Figure 2 illustrates the relative difference between the two solutions for the outer-reflector coarse mesh. The agreement between the two solutions is excellent. These results indicate that the response function-based transport method can reproduce solutions to the same accuracy as MCNP reference calculations.
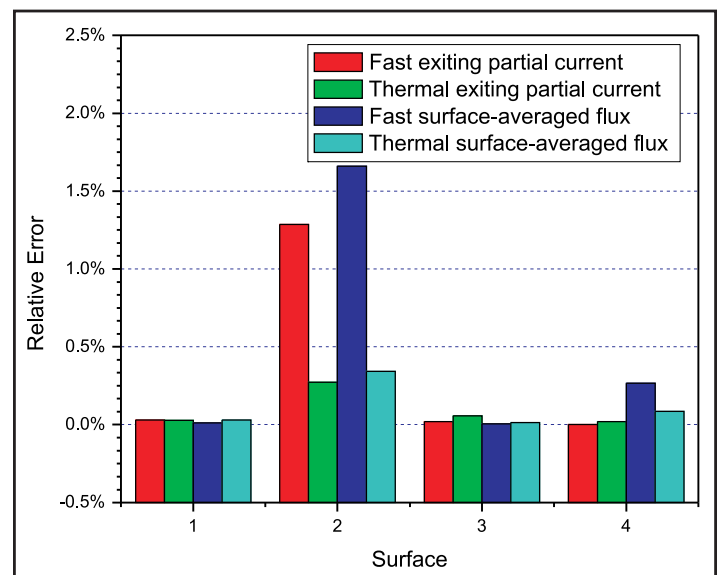

Figure 2. Relative difference between the superposition-based response functions and reference solutions for the outer-reflector coarse mesh.

Planned Activities

For the upcoming year, the research team plans to complete the following activities:

- Develop a new set of expansion functions that are suitable to couple with diffusion approximations in 3-D cylindrical geometry (Task 2.1)

- Develop a 3-D(r,θ) response-matrix nodal balance diffusion method (Task 2.2)

- Integrate results of Tasks 2.1 and 2.2 into the PEBBED code (Task 2.3)

- Test the product of Task 2.3 on a 3-D PBR benchmark problem

NUCLEAR ENERGY RESEARCH INITIATIVE

Implications of Graphite Radiation Damage on the Neutronic, Operational, and Safety Aspects of Very High-Temperature Reactors

PI: Ayman I. Hawari, North Carolina State University (NCSU)

Collaborators: Idaho National Laboratory, Oak Ridge National Laboratory

Project Number: 07-011

Program Area: Generation IV

Project Start Date: June 2007

Project End Date: May 2010

Project Description

This project entails experimental and computational investigations to study radiation effects of graphite in very high-temperature reactors (VHTRs). Researchers will use molecular dynamic and *ab initio* molecular static calculations to 1) simulate radiation damage in graphite under various irradiation and temperature conditions, 2) generate thermal neutron scattering cross sections for damaged graphite, and 3) examine the resulting microstructure to identify damage formations that may produce the Wigner effect.

In both the prismatic and pebble-bed VHTR designs, the graphite moderator is expected to reach exposure levels of 10^{21} to 10^{22} n/cm^2 over the lifetime of the reactor, resulting in damage to the graphite structure. Studies of irradiated graphite show changes in thermal conductivity and heat capacity at fluences less than 10^{21} n/cm^2. These properties depend on the behavior of atomic vibrations (phonons) in the graphite solid. Certain alterations in phonon behavior would produce changes in these properties, and such alterations are likely to impact thermal neutron scattering, with implications for the VHTR's neutronic and safety behavior. Another important phenomenon pertains to published data showing that a high-temperature (greater than 1,200°C) Wigner-like effect may exist in graphite. If confirmed, this effect would have direct implications on the safety behavior of VHTRs.

Research Progress

During the first year, work focused on studying the structure of unirradiated reactor-grade graphite using neutron-diffraction techniques. Using the neutron powder diffractometer system, the research team took measurements on reactor-grade graphite samples (density = 1.65 ± 0.05 g/cm^3) at the NCSU PULSTAR reactor. The team developed a computer code capable of performing Rietveld analysis on reactor-grade graphite neutron powder diffraction patterns. However, to improve the ability of the code to analyze the structure of reactor-grade graphite more faithfully, the team had to perform several experimental and computational improvements. These included adding a diffractometer zero correction as a refinable parameter. In addition, the team performed experimental adjustments to ensure accuracy of the diffractometer's angular settings during a measurement. The adjustments resulted in correcting for differences in the intersection location of the Debye-Scherrer scattering cones in the diffraction system's various detectors.

Researchers investigated two reactor-grade graphite specimens. Each specimen was cut from the same block of reactor-grade graphite, but from locations that were perpendicular to each other. Figure 1 shows results of the refinement program's application to the measured diffraction patterns. The reduced χ^2 is 1.7 for Specimen #1 and 1.6 for Specimen #2.

Computationally, work focused on developing the methodology for utilizing classical molecular dynamics (MD) techniques to derive the thermal neutron scattering law in structures that are representative of unirradiated and irradiated graphite. In this case, the analysis is based on using statistical correlation functions, which serve as a link between fundamental microscopic variables and
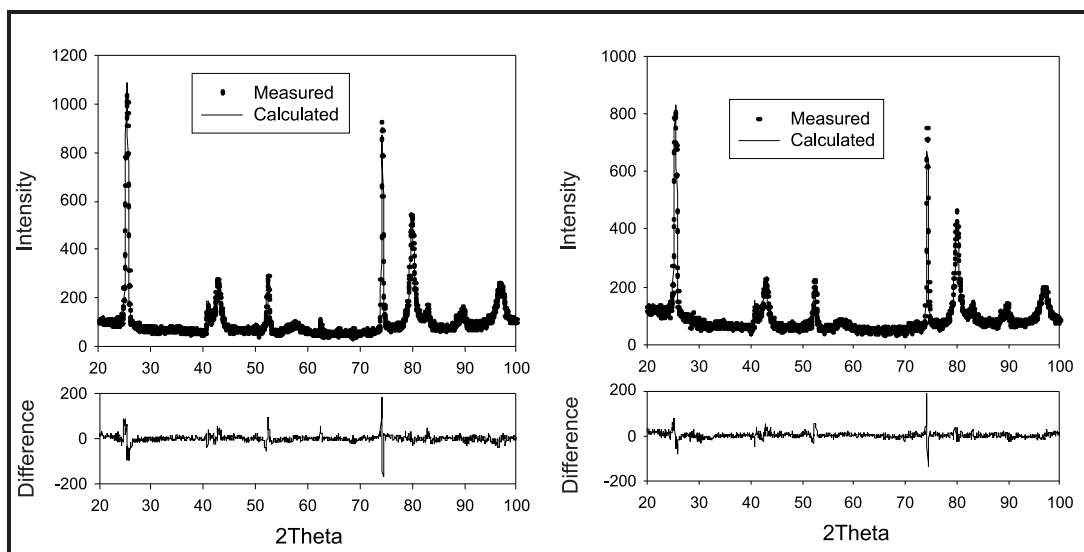
Figure 1. Reactor-grade graphite diffraction patterns for Specimen #1 (left) and Specimen #2 (right). The diffraction patterns are measured using the neutron powder diffractometer at the NCSU PULSTAR reactor. The calculated patterns were fitted to the measured patterns using a Rietveld-like approach.

measurable material properties. The relevant correlation function in scattering law calculations is the dynamic pair correlation function, which the equation below provides:

$$G(\vec{r},\tau) = \lim_{t \to \infty} \frac{1}{Nt} \int \int \rho(\vec{r}',t) \rho(\vec{r}'+\vec{r},t+\tau) d\vec{r}' dt \quad (1)$$

where N is the number of atoms and $\vec{r}$ is the position vector. The particle density operator, $\rho(\vec{r},t)$, is defined as the following:

$$\rho(\vec{r},t) = \sum_j \delta\{\vec{r} - \vec{R}_j(t)\} \quad (2)$$

in which $\vec{R}_j(t)$ is the position vector of atom j at time t. Qualitatively stated, $G(\vec{r},\tau)$ is proportional to the probability of finding an atom at position $\vec{r}$ following a time delay τ, given that an atom was initially at the origin $\vec{r} = 0$. Discretizing Equation (1) and introducing Equation (2) results in the following equation:

$$G(\vec{r},\tau) = \frac{1}{NM} \sum_{k=1}^{M} \sum_{i,j} \delta\{\vec{r} + \vec{R}_i(t_k) - \vec{R}_j(t_k + \tau)\} \quad (3)$$

which is directly calculable from the standard output of an MD simulation.

The utility of $G(\vec{r},\tau)$ in thermal neutron scattering calculations lies in its 2-D Fourier transform:

$$S(\vec{Q},w) = \frac{1}{2\pi h} \int_{-\infty}^{\infty} \int_{-\infty}^{\infty} G(\vec{r},\tau) e^{i(\vec{Q}\cdot\vec{r} - w\tau)} d\vec{r} d\tau \quad (4)$$

where the scattering law, $S(\vec{Q},\omega)$, may be broken up into two components:

$$S(\vec{Q},\omega) = S_s(\vec{Q},\omega) + S_d(\vec{Q},\omega) \quad (5)$$

in which S_s and S_d are the self and distinct terms, respectively. The self term (associated with incoherent effects) arises from the $i = j$ portion of the summation of Equation (3), while the distinct term (associated with coherent effects) arises from all $i \neq j$ terms. In this nomenclature, the differential scattering cross section can be expressed succinctly as the following:

$$\frac{d^2\sigma}{d\Omega dE} = \frac{1}{4\pi} \frac{k'}{k} \left(\sigma_{coh} S(\vec{Q},\omega) + \sigma_{incoh} S_s(\vec{Q},\omega) \right), \quad (6)$$

where k and k' represent the magnitudes of the wave vectors of the incident and scattered neutron, respectively; σ_{coh} is the bound atom coherent scattering cross section; σ_{incoh} is the bound atom incoherent scattering cross section; and $\vec{Q} = \vec{k} - \vec{k}'$.

The $G(\vec{r},\tau)$ method for calculating the double differential cross section requires only the time-dependent atomic positions and is applicable to any system, at any temperature, and with any degree of lattice imperfection (e.g., due to radiation damage). This method is ideally suited to atomistic simulation techniques, such as classical MD, to the extent that the interatomic potential energy function is reliable.

Using the formulation presented above, NCSU used their MD code to examine the self correlation function, $G_s(\vec{r},\tau)$, of a room-temperature graphite system with and without the presence of induced radiation damage. In the latter case, the damage was generated through a sequence of five 1-keV cascades initiated at randomized locations within

a 33,000-atom supercell. Figure 2 shows the results. The time-dependence of $G_s(\bar{r},\tau)$ is manifested as oscillatory perturbations in the displayed values, but such fluctuations were found to be insignificant on the scale shown.

Formulae employed in standard codes (e.g., NJOY) for computing the thermal scattering cross section are
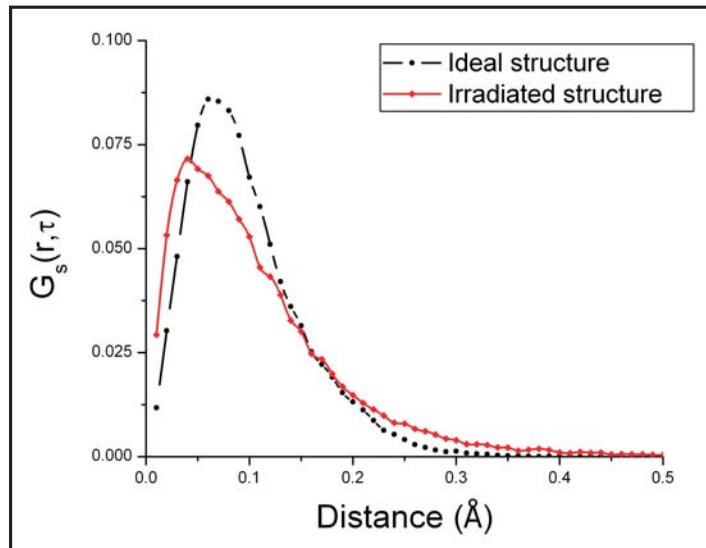

Figure 2. Impact of irradiation on the self part of the graphite pair correlation function.

predicated on a Gaussian form of $G_s(\bar{r},\tau)$ (this is termed the "Gaussian approximation"). Figure 2 shows clearly that, although the Gaussian approximation appears reasonable for the ideal graphite structure, the existence of defects in the irradiated structure brings about a departure from Gaussian behavior. The research team expects this departure to become more severe as the radiation dose of the graphite increases.

Planned Activities

Over the next year of this project, the research team will perform further studies of the structural aspects of reactor-grade graphite using neutron scattering techniques. In addition, team members will explore measurements of the dynamical properties of unirradiated and irradiated graphite samples. The computational work will continue to establish an MD-based approach for generating thermal neutron scattering cross sections for reactor-grade graphite. The team will focus on including the distinct component of the pair correlation function, $G_d(\bar{r},\tau)$, as well as evaluation of the thermal neutron scattering cross section in damaged graphite.

NUCLEAR ENERGY RESEARCH INITIATIVE

Advancing the Fundamental Understanding and Scale-Up of TRISO Fuel Coaters via Advanced Measurement and Computational Techniques

PI: Muthanna Al-Dahhan, Washington University

Collaborators: None

Project Number: 07-017

Program Area: Generation IV

Project Start Date: September 2007

Project End Date: August 2010

Research Objectives

The overall research objectives of this project are to 1) advance fundamental understanding of the hydrodynamics TRISO fuel coaters by systematically investigating the effect of design and operating variables, 2) evaluate the reported dimensionless groups as scaling factors, and 3) establish a reliable scale-up methodology for TRISO fuel particle spouted bed coaters based on hydrodynamics similarity via advanced measurement and computational techniques. Researchers will develop an on-line, non-invasive measurement technique based on gamma-ray densitometry (i.e., nuclear gauge densitometry [NGD]) that can be installed for coater process monitoring to ensure proper performance and operation and to facilitate the developed scale-up methodology.

To achieve these objectives, the research team will use the following research tools:

- Optical probes for solids and gas holdups and solids velocity distribution measurements

- Gamma ray computed tomography (CT) for measuring the solids and gas holdup cross-sectional distribution along the spouted bed height, spouted diameter, and fountain height

- Radioactive particle tracking (RPT) technique for measuring the 3-D flow patterns and field, solids velocity, turbulent parameters, circulation time, and other related quantities

- Gas dynamics measurement technique

- Pressure transducers

The team will then use the knowledge obtained as benchmark data to evaluate the computational fluid dynamics models and their closures to facilitate the developed scale-up methodology, to identify conditions for hydrodynamics similarity, and to further investigate and optimize the process performance of TRISO coaters.

Research Progress

The following progress has been made since the last report. The research team:

- Constructed the spouted bed coater with a 6" i.d., 3' height, and 60° base angle with 10 ports along its height for the optical probe and pressure transducer measurements

- Constructed a smaller (3" i.d.) spouted bed coater with a 3' height and 60° base angle with 10 ports along its height for the optical probe and pressure transducer measurements

- Constructed blank spouted bed columns of 3" i.d. and 6" i.d., without any ports, for the CT and RPT measurements

- Conducted experiments on the 6" i.d. spouted bed column with a ½" optical probe to obtain radial solid holdup profile at six axial positions and six radial positions for each cross section at inlet gas velocity of Ug=1.09 m/s (Figure 1)

- Designed a new, smaller probe with ⅛" diameter tubing and performed experiments with this new system; the new probe was necessary owing to unsatisfactory results obtained with the ½" optical probe due to the probe's size (Figure 2)

- Prepared and initiated gamma-ray CT measurements (Figure 3)

The research team also compared preliminary results of the CT and the optical probe (Figure 5). A CT scan obtained higher solid hold-up values, but the trend of the solid hold-up distribution was the same for both techniques. The column wall's metal ports could account for the difference in results; the ports caused higher attenuation of gamma rays, thus effecting higher solid hold-up values. Constructing new blank spouted bed units, which were designed specifically for the CT and RPT measurements, corrects the problem. Work on these units is in progress.

Figure 1. Spouted bed of 6" i.d. with ½" optical probe.

Figure 2. The old ½" optical probe (on the left), and the new ⅛" optical probe (on the right).
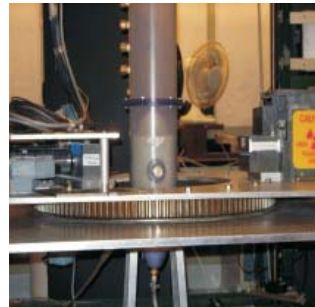
Figure 3. CT measurements on the spouted bed reactor (6" i.d.).
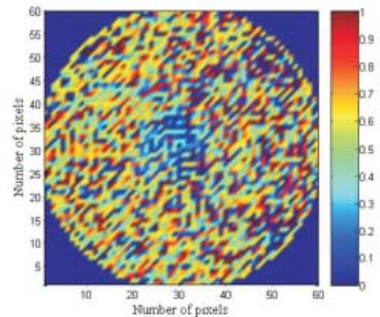
Figure 4. Time averaged cross-sectional solids hold-up distribution (CT scan).
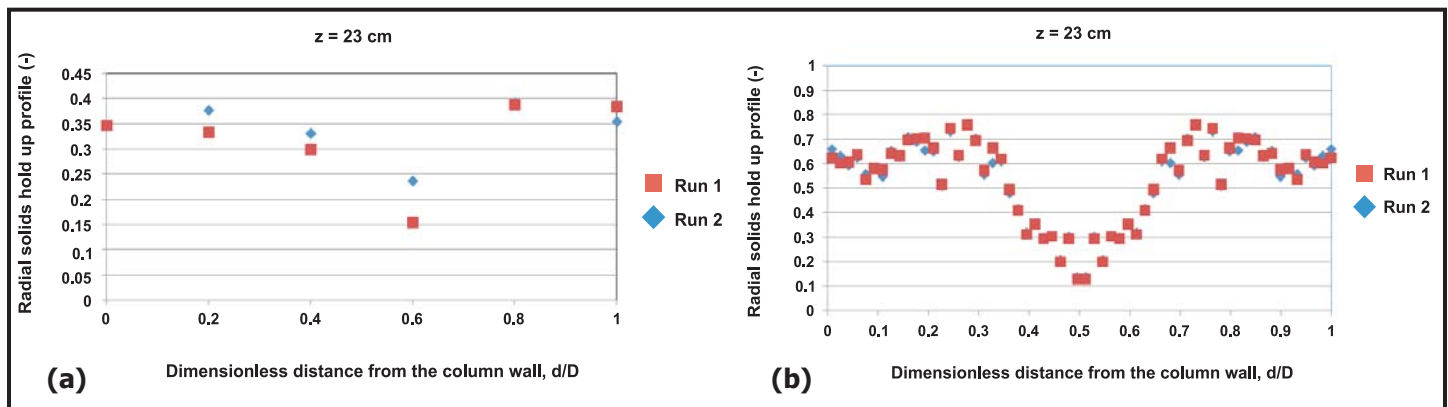
Figure 5. Radial solids hold-up profiles obtained by the optical probe method (⅛" diameter tubing): (a) and CT; (b) at the level z=23 cm from the distributor and gas velocity U_g=1.09 m/s.

Planned Activities

The following are planned activities for the coming year:

- Continue the experiments with the optical probe system and CT to evaluate reported dimensionless groups as scaling factors

- Assess the pressure transducer measurements and evaluate regime transition from obtained data

- Develop the NGD for flow regime transition by applying it first on a fluidized bed and then on a spouted bed

- Acquire an advanced optical probe technique that can simultaneously measure not only solids and gas holdups but also solids velocity for a wide range of solid particle sizes

NUCLEAR ENERGY RESEARCH INITIATIVE

Fission Product Transport in TRISO-Coated Particle Fuels:
Multi-Scale Modeling and Experiment

PI: Izabela A. Szlufarska, University of Wisconsin-Madison

Collaborators: None

Project Number: 07-018

Program Area: Generation IV

Project Start Date: June 2007

Project End Date: June 2010

Research Objectives

The objective of this project is to develop a multiscale computational model of fission product transport through TRISO coatings. The model will build on the strength of massively parallel molecular dynamics (MD) simulations to provide a full atomistic picture of silicon carbide (SiC) microstructural features (for example, grain boundaries [GBs]); the research will apply quantum mechanical approaches to determine highly accurate diffusion barriers in these structures, as well as continuum-level theories to determine diffusion rates in macroscopic samples. Experiments will provide input for simulated microstructures (for example, information about typical GB textures) and validation of modeling predictions. The research team will employ the developed model to determine fast diffusion mechanisms of Ag through SiC coating.

Research Progress

In the last year, research focused on generating realistic GB structures of SiC through MD simulations, on fitting an empirical force field for interactions of Ag with SiC, and on *ab initio* calculations of defect energetics and diffusion coefficients through bulk SiC.

Grain-Boundary Models. The first step in MD simulations was to generate realistic models of GBs typically observed in experimental structures. Based on GB type distribution obtained in electron backscatter diffraction (EBSD) experiments, the research team determined that Σ3, Σ9, and Σ27 GBs are the most frequent special GB types in β-SiC.

Using in-house codes, the team generated a number of special GBs, including Σ3, Σ5, Σ9, and Σ27, as well as a number of high-energy GBs. The structures generated in the simulations were compared against the team's own *ab initio* calculations and against structural data available in the literature. The team determined that Tersoff potential is the most suitable for representing SiC GBs, and researchers found a very good agreement between their own atomic configurations and those found in literature (see Figure 1 for a comparison of a triple junction as generated in the team's code and as published in literature). Researchers will use these GB models to determine diffusion coefficients of Ag and to establish whether GB diffusion can account for the excessive release of Ag from TRISO-coated particle fuels.
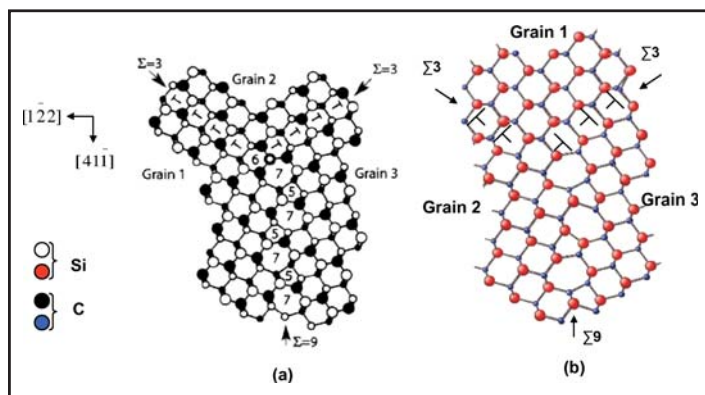

Figure 1. Atomistic models of a triple junction GB: (a) triple junction structure with zigzag Σ9 generated in tight binding calculations from Reference [1]; (b) triple junction generated by in-house Voronoi construction code.

Defect Energetics. Researchers have completed their study of neutral defects in SiC and Ag impurities in SiC. The results will form the foundation for modeling of bulk transport. Table 1 summarizes the most stable defects.

Reference States	Energy/Atom (eV)
Bulk Si (diamond structure)	-5.44
Bulk C (graphite structure)	-9.20
Bulk Ag (fcc structure)	-2.83
Defects	**ΔE_f (eV)**
V_{Si}	7.62
V_C	4.64
Ag_{Si}	6.51
Ag_C	7.58
Ag_I	9.74

Table 1. Defect formation energies for Ag in SiC.

Based on a simple thermokinetic model, these defect energies can be used to estimate an upper bound on the thermally activated bulk diffusivity. Table 2 shows the predicted values and compares them to experimental values estimated from Ag integral release measurements and collected in Reference [2]. The calculated upper-bound values of D are significantly lower than those observed from the experiments and show a much larger activation energy (calculation gives an activation energy of 4.64 eV compared to about 2.1 eV from the experimental data). The high activation energy and low diffusion constant are due to the high vacancy formation energy and correspondingly low concentration of vacancies predicted for the SiC material at equilibrium.

A related calculation for interstitials shows that, owing to their large formation energy, they are also unlikely to transport enough Ag to be consistent with experimental Ag release. The basic energy results and thermodynamic analysis suggest that simple interstitial or vacancy mediated diffusion of Ag through nonirradiated bulk SiC at thermal equilibrium is insufficient to explain the observed transport of Ag in SiC TRISO fuels. Therefore, other aspects of the diffusion most likely need to be included. Possibilities include different energetics from charged Ag defects, radiation-induced defects (e.g., much higher vacancy concentrations), additional Ag hopping mechanisms (e.g., kick-out mechanisms or GB diffusion), or diffusion through pores or cracks. Researchers are presently extending their study to include some of these additional effects.

Temp (K)	D_{expt} (m²/s) [2]	D_{calc} (m²/s)
1,000	2.8E-20	4.0E-30
1,200	1.7E-18	3.1E-26
1,400	3.3E-17	1.9E-23
1,600	3.0E-16	2.3E-21
1,800	1.7E-15	9.8E-20
2,000	6.7E-15	2.0E-18

Table 2. Predicted upper bound for thermal vacancy mediate Ag diffusion constant and an experimental Ag diffusion constant. The large difference shows that radiation effects or alternative diffusion mechanisms to the one identified here are likely to play a role.

Experimental Analysis of SiC. The researchers have completely characterized the CVD β-SiC microstructure obtained from Rohm and Hass using x-ray diffraction (XRD), Raman spectroscopy, energy dispersive spectroscopy (EDS), and EBSD techniques. XRD analysis shows the material is β-SiC with patterns taken from both the SiC's plan view (perpendicular to growth direction) and cross section (along growth direction), as shown in Figure 2. The patterns match the standard pattern of β-SiC [ICDD 29-1129]; the shoulder observed on the plan view sample is assumed to be an artifact of a high-stacking fault density. Raman analysis showed dominant peaks at 796 cm⁻¹ and 970 cm⁻¹ corresponding to β-SiC and no detectable free Si. Microstructural information obtained from EBSD analysis provided data on phase, GB distribution, texture, and grain size. Table 3 shows the results, comparing them with the SiC layer from TRISO particles fabricated by Oak Ridge National Laboratory (ORNL). The comparison shows that the different SiCs have similar textures and are predominantly
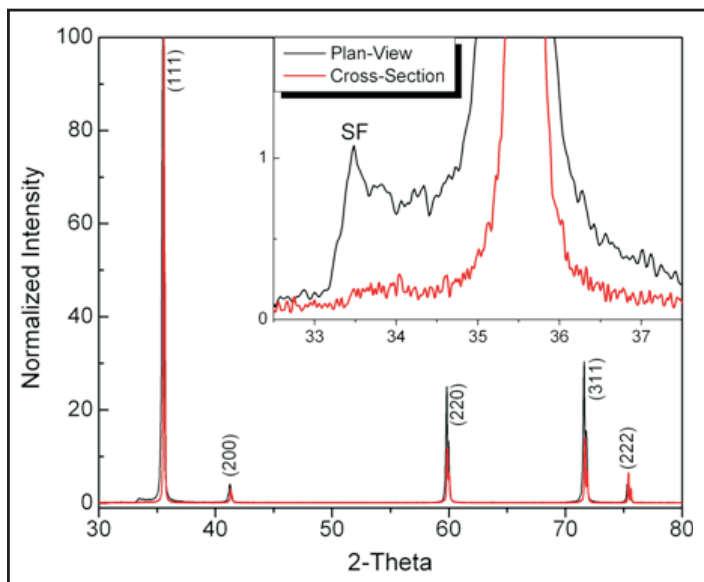

Figure 2. XRD pattern of plan view and cross section of as-received SiC from Rohm and Haas.

β-SiC. The differences in grain size and shape in this work will allow for investigation along various microstructures, and the significant fraction of Low-Σ CSLBs will allow for investigation of more CSL GBs.

SiC	ORNL	This Work
Phase (Predominate)	β-phase	
Grain Size (avg.)	1.3 μm	3.5 -8.4 μm
Grain Shape (avg.)	0.69	0.49-0.68
Σ1 Boundaries	High (>30%)	Low (<~10%)
Low-Σ CSLB	Low (~10%)	Median (>30%)
General Boundaries	High (>50%)	
Texture	Near <111> Texture	
Impurities (free Si of C)	?	No Detectable

Table 3. Microstructural comparison of ORNL TRISO SiC layer and as-received SiC from Rohm and Haas.

Diffusion Couple Construction and Analysis.
Researchers have validated design for the Ag/SiC diffusion couples and completed successful 1,000-hour heat treatments at 800°C and 1,200°C for diffusion couples of Ag/SiC and Ag+10 wt%Si/SiC. Because of volatility of the molybdenum diffusion couple canisters and temperature limits of SiO_2 sealing tubes, the heat treatments at 1,200°C+ required a new furnace set-up. An atmosphere-controlled furnace was purchased from MTI and modified in-house. The new diffusion couples are brought to temperature in flowing UHP Ar with the Mo canisters wrapped in a Ta foil getter. The results show no oxidation of the Mo.

Analysis of the 800°C diffusion couples shows no discernable Ag penetration using EDS techniques on a lose-electrons oxidation 1530 field emission scanning electron microscope at 20 keV. The issues with this technique stem from the high detection limits and large excitation volume (approximately 1 μm³) compared to the GBs' small volume. Thus, researchers have pursued transmission electron microscopy (TEM) analysis of the diffusion couples. TEM sample preparation is under way to create samples with specific CSL GBs along the Ag/SiC interface by using EBSD in conjunction with a focused ion beam, as Figure 3 illustrates.

Planned Activities

Future activities will focus on using MD simulations to study diffusion of Ag through SiC. Researchers are in the process of developing a force field that describes Ag interactions with SiC. Once they have validated this force field, the researchers will employ it to determine diffusion coefficients in GBs most frequently occurring in SiC. In the meantime, a simplified Lennard-Jones potential is being used to determine the dependence of diffusion coefficients on the size of the atoms diffusing through GBs.

The research team is performing *ab initio* calculations for charged defects to assess the possibility that Ag forms a non-neutral defect. The team will then determine hopping barriers for bulk and simple GB structures from *ab initio* and for more complex GB structures from molecular dynamics. A kinetic Monte Carlo code is being developed for studying long-time diffusion based on the hopping barriers. The team will discretize continuum-level diffusion equations with parameters determined
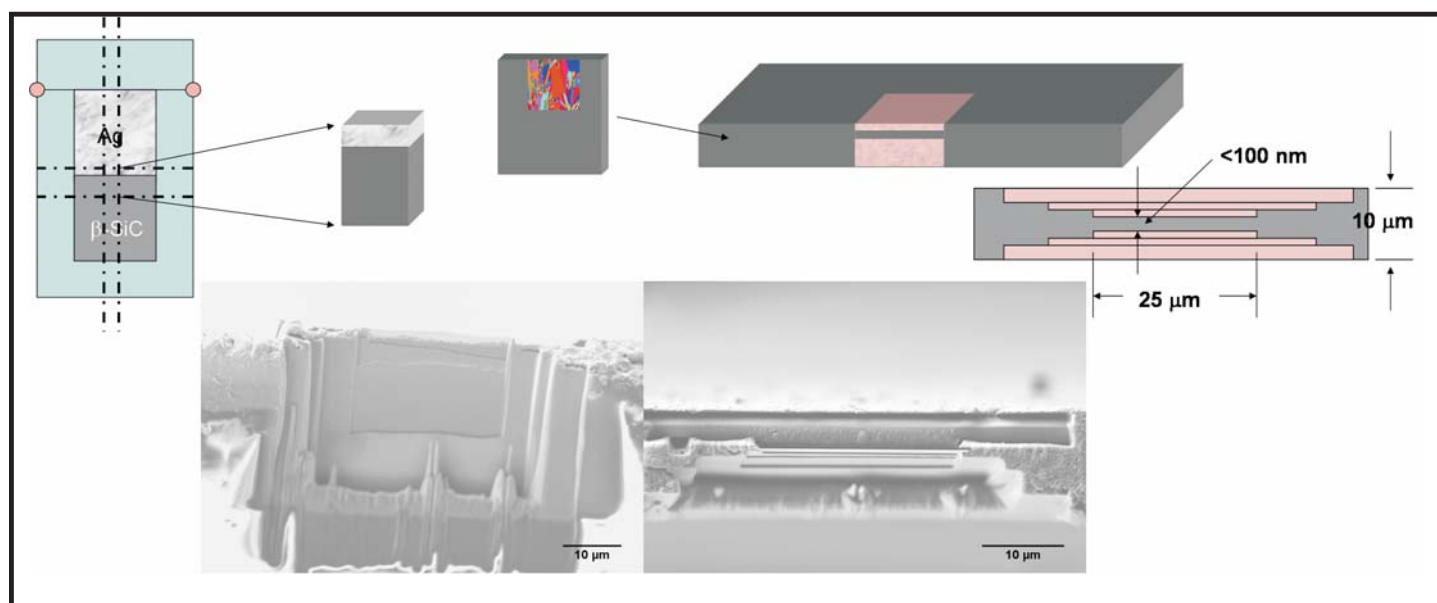

Figure 3. Schematic of selective CSL TEM sample preparation.

from atomistic simulations, then solve those equations for experimental SiC microstructures in order to determine Ag concentration profiles and integral release rates through SiC coatings.

References:

[1]   K. Tanaka and M. Kohyama, *Atomic Structure Analysis of Σ= 3, 9 and 27 Boundary, and Multiple Junctions in β-SiC.* JEOL News, 2003. 38(2): pp. 8-10.

[2]   Gerczak, T., Tan, L., Allen, T.R., Khalil, S., Shrader, D., Liu, Y., Heim, A., Morgan, D., and Szlufarska, I., *Experimental and Simulation Insight on the Transport of Silver Fission Product In SiC*, 4th International Topical Meeting on High Temperature Reactor Technology, Washington D.C., September 28, 2008, HTR2008-58131.

[3]   V.V. Pujar and J.D. Cawley, "Computer Simulations of Diffraction Effects Due to Stacking Faults in β-SiC: I, Simulation Results," Journal of American Ceramic Society, 80, pp. 1653-1662, 1997.

[4]   L. Tan, T.R. Allen, J.D. Hunn, and J.H. Miller, "EBSD for Microstructure and Property Characterization of the SiC-coating in TRISO Fuel Particles," Journal of Nuclear Materials, 372, pp. 400-404, 2008.

NUCLEAR ENERGY RESEARCH INITIATIVE

Emissivity of Candidate Materials for Very High-Temperature Reactor Applications:
Role of Oxidation and Surface Modification Treatments

PI: Kumar Sridharan, University of Wisconsin-Madison

Collaborators: None

Project Number: 07-020

Program Area: Generation IV

Project Start Date: April 2007

Project End Date: March 2010

Research Objectives

The objectives of this project are to 1) evaluate emissivities of candidate materials for the reactor pressure vessel (RPV) and internal components of the very high-temperature reactor (VHTR) in air and helium environments from 300°C to 900°C; 2) study the effects of emerging and commercial surface treatments on emissivity after exposure in air and helium environments at elevated temperatures; 3) develop a comprehensive understanding of the relationships between emissivity, oxide characteristics, and surface treatments by characterizing surface oxides that form on untreated and surface-modified alloys after elevated temperature exposure; and 4) develop an integral separate-effects emissivity database for potential candidate materials and surface modification treatments.

Thermal radiation from the outer surface will partially cool the RPV and the VHTR's internal components. With an unexpected increase in temperature, thermal radiation becomes a significant mode of heat dissipation because of its fourth-power temperature dependence, according to the Stefan-Boltzmann equation. Oxidation will inevitably occur at these higher temperatures, so material emissivity is clearly intricately related to chemical, physical, and mechanical characteristics of the oxide scales that form on the surface, including their chemical composition, grain morphology, topography, and porosity. The growing field of surface modification provides opportunities for achieving high emissivities at high temperatures by changing topography and grain orientation or inducing controlled surface compositional changes.

Research Progress

The construction of a state-of-the-art emissivity measurement system is nearly complete. The system will measure spectral emissivity for various candidate materials in air and VHTR purity helium at elevated temperatures. The design consists of a sample test chamber for sample heating, an optics column consisting of a periscope system to guide the radiant heat to a Fourier transform infrared (FTIR), and a gas chromatography system for measuring inlet and outlet gas compositions (see Figure 1).

The sample test chamber consists of a cylindrical block of monolithic silicon carbide 8" in diameter and 8" in height. Eight holes or cavities that are 0.25" in diameter have been machined circumferentially in this block, with seven of these holes measuring 0.25" in depth to house material test samples for emissivity evaluation, and an eighth hole measuring 1.5" in depth to serve as the black-body reference. By selecting a material with high emissivity and using geometrical considerations to further enhance the emissivity, researchers will ensure that this cavity closely approaches the desired emissivity value of close-to-unity. An axial central hole through the block about 0.25" in diameter will be used for introducing air or VHTR-grade helium. Additionally, thermocouple inlet holes have been provided from the outside surface of the block to just below (approximately 0.5") each of the seven sample cavities and the black-body cavity to allow for accurate real-time determination of sample and black-body temperatures. Two semi-cylindrical heaters at 1,600 watts, 240 volts, surround the silicon carbide block, which is capable of
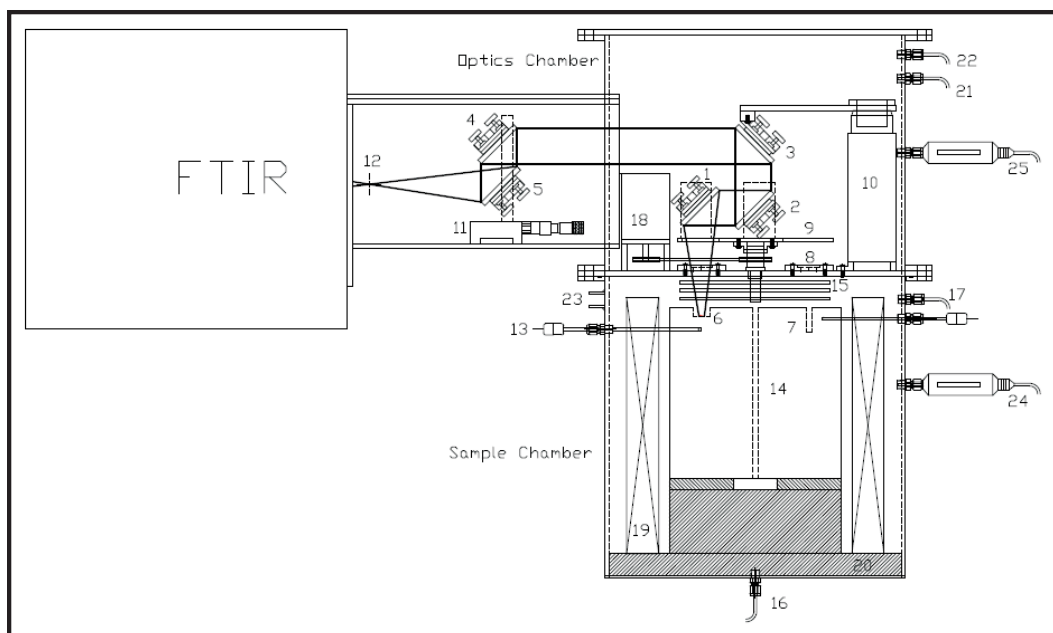
Figure 1. Schematic illustration of the High-Temperature Spectral Emissivity Measurement System. (1, 5) collimating mirrors, (2, 3, 4) flat mirrors, (6) test samples, (7) black body, (8) aperture and calcium fluoride window, (9) optical plate and rod assembly, (10) vertical optical adjustment, (11) optical stage and post assembly, (12) FTIR focus point, (13) thermocouples, (14) silicon carbide block, (15) ceramic radiation shields, (16) test gas inlet, (17) test gas outlet, (18) stepper motor, (19) radiation heaters, (20) alumina insulation, (21) cover gas inlet, (22) cover gas outlet, (23) 240V power in, (24) sample chamber pressure transducer, (25) optical chamber pressure transducer.

furnace holding the sample/isothermal block will be operated in conjunction with a gas chromatograph, which will allow for assessment of inlet and outlet gas compositions. This is particularly important in experiments in both air and VHTR helium, which will react with the sample surface. A comparison of the inlet and outlet gas compositions will enable the research team to achieve the broader goals of correlating emissivity with materials corrosion, in conjunction with separate materials characterization work.

The team has conducted preliminary testing of the high-temperature spectral emissivity measurement system on materials of well-documented emissivities in order to benchmark the system's accuracy. Figure 2 shows an example of these measurements: pure tantalum metal, tested at 500°C in an air environment. Due to the oxidation in an air environment, emissivity increased. The data from these measurements compare reasonably well with other data from literature, including data from the National Physical Laboratory, located in the UK.

maintaining a constant temperature over 1,100°C. Swage-lok© compression fitting fills all heating chamber inlets or fittings, maintaining a stable test atmosphere. To best maintain an isothermal environment, high-temperature ceramic insulation fills the bottom and sides of the can.

Two 6" diameter aluminum-oxide top covers sequester the radiant heat in the furnace experimental system. A shutter system will allow researchers to selectively expose any one given sample at a time for emissivity measurements. A periscope guides radiation to an FTIR spectrometer through a CaF_2 window, which will be used to measure emissivity values in the temperature range of 300°C to 900°C in the infrared through ultraviolet spectral range. The FTIR is a state-of-the-art system (Bruker Optics Vertex-70 FTIR), procured specifically for this research. Unique features of this system include gold-coated internal optics, KBr Beamsplitter, Mercury Cadmium Telluride liquid N_2-cooled detector, and a spectral range of approximately 1 micron to 25 microns. The FTIR will automatically scan over the entire spectrum with a high-resolution response to even weak signals and will allow for measurements over a wide range of temperatures and wavelengths. The
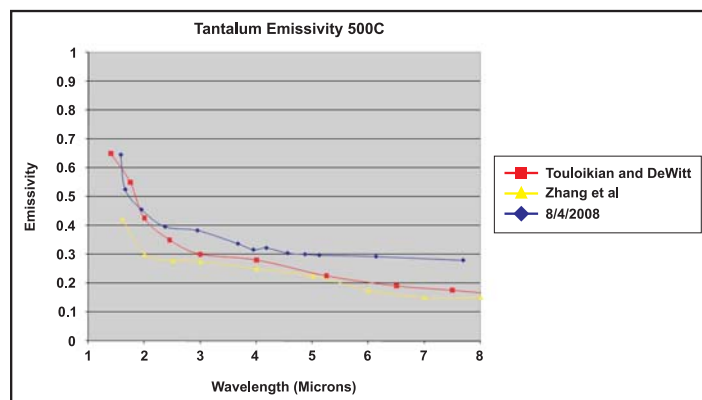

Figure 2. Preliminary spectral emissivity data (dark blue) acquired for pure tantalum in ambient air at 500°C.

Using the electro discharge machining technique, the team sectioned samples of all test alloys to a size of 0.5" x 0.5" and 1 mm in thickness (alloys include ferritic steels, T91, SA508, and T22, as well as austenitic alloys Incoloy 800H, Haynes 230, Inconel 617, and 304 stainless steel). The samples have been engraved on one side with a numeric code designation to allow for ready sample identification after high-temperature exposures. Samples of all alloys have been polished to a mirror-like finish by grinding with progressively finer grits of silicon carbide paper, using 1-micron diamond paste for final polishing. The samples will be placed in cavities in the silicon carbide block, as shown in Figure 3.

Figure 3. Top view of the silicon carbide block with samples inserted into the seven sample cavities with the black-body cavity at the six o'clock position.

Although researchers will perform sample spectral emissivity measurements *in situ*, the team has initiated experiments on air oxidation of samples at 850°C for 250 hours, acquiring information about composition and topography of the oxide layers that form on various alloys. Figure 4 shows the surface morphology of the oxide layer that formed on Haynes 230 alloy and the corresponding energy-dispersive-spectrometer (EDS) compositional analysis of this oxide, after this high-temperature exposure. These oxidized samples will also be tested for spectral emissivity.

Diamond-like carbon (DLC) coatings have been deposited on SA 508 ferritic stainless steel and 316 austenitic stainless steel samples using the plasma immersion ion implantation and deposition process. For DLC deposition, researchers first sputter-cleaned the samples for about 10 minutes using an argon plasma at a -5kV voltage bias. Following this, the team used a methane plasma to implant carbon ions into the samples' surfaces at -20kV to a dose of 3×10^{17} ions/cm^2. Finally, the DLC coating was deposited using an acetylene plasma and energy of -5kV. Previous studies have shown the carbon implantation step to enhance adhesion of the DLC coatings.

After DLC coating, the team used an optical profilometer (Zygo New View) to determine the coating's thickness. Figure 5 shows the results, which indicate the film thickness to be about 500 nm and the surface roughness to be about 160 nm (root mean square roughness).
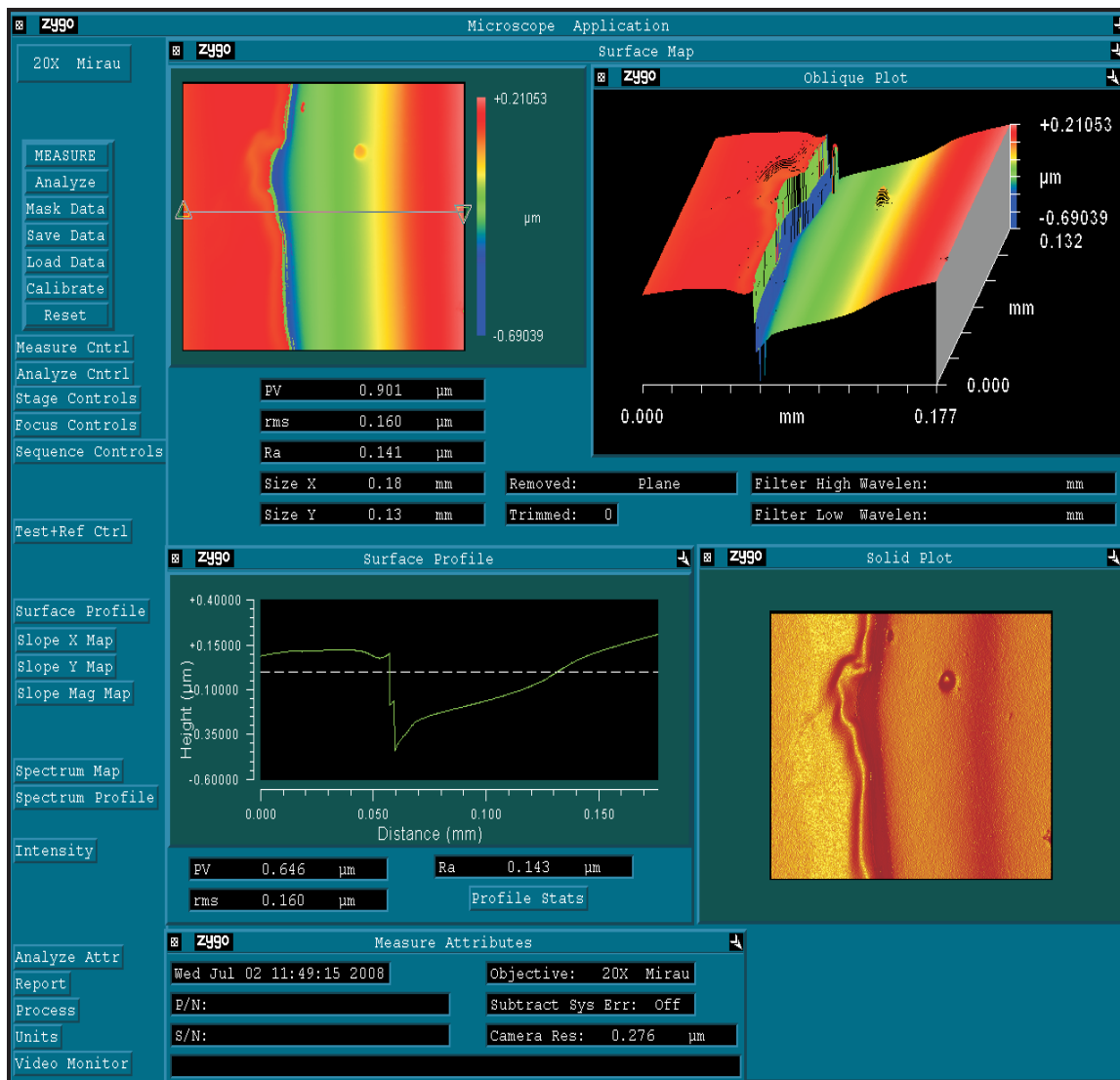

Figure 4. (a) Scanning electron microscopy (SEM) surface image of Haynes 230 alloy exposed to a temperature of 850°C for 250 hours in air and (b) corresponding EDS compositional analysis of the surface oxide.
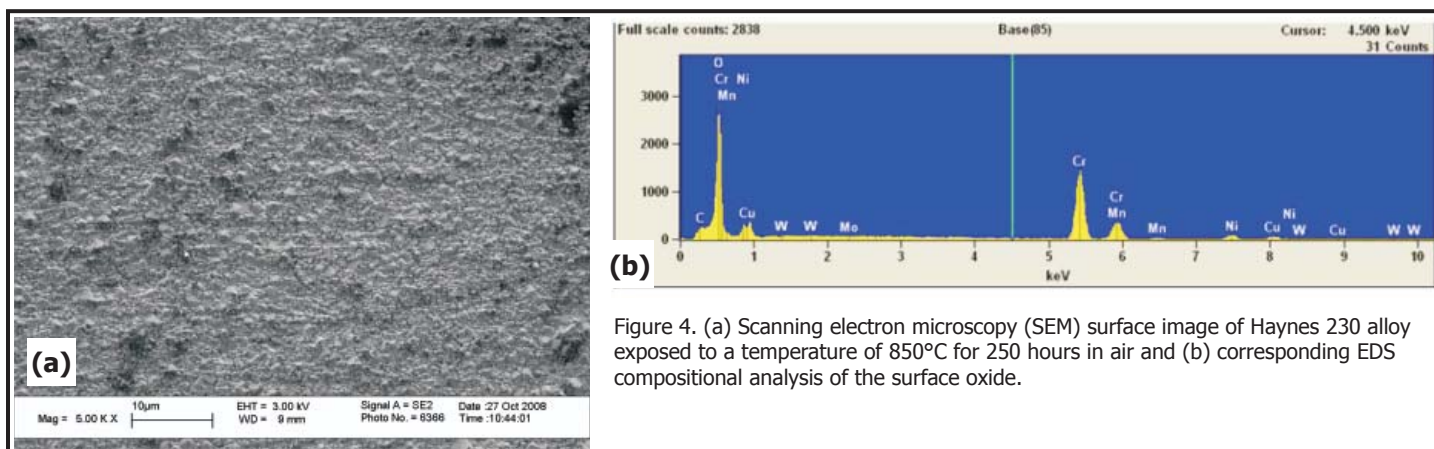
Figure 5. Optical profilometry of the DLC coating deposited for measurements of spectral emissivity.

Planned Activities

The research team will perform emissivity evaluations on three ferritic steels (T91, SA508, and T22) and four austenitic steels (Incoloy 800H, Haynes 230, Inconel 617, and 304 stainless steel). These materials have been selected based on their direct relevance to RPV and other components of the VHTR. The team will measure emissivity at 300°C, 500°C, 700°C, and 900°C after exposure durations of 10 hours, 100 hours, and 200 hours in air (with known humidity) and VHTR-purity helium. The team

has procured VHTR-grade helium (ppm compositions, H_2: 3 ppm, CO: 3, H_2O: 0.2, CO_2: 0.6, CH_4: 0.5, N_2: 0.2, O_2: 0.04) with pre-mixed compositions. Surface treatments to be investigated include shot peening and xenon-ion bombardment for physical topographical surface modification, as well as diamond-like carbon, hafnium-oxide, chromium-oxide, and silicon carbide coatings. Using SEM, Auger electron spectroscopy, and x-ray diffraction, the team will perform detailed characterization of surface oxides and corrosion products in order to correlate surface chemistry changes to changes in emissivity.

NUCLEAR ENERGY RESEARCH INITIATIVE

Materials and Design Methodology for Very High-Temperature Nuclear Systems

PI: James Stubbins, University of Illinois

Collaborators: Stress Engineering Services, Idaho National Laboratory, Massachusetts Institute of Technology, Boise State University, University of Nevada-Las Vegas

Project Number: 07-024

Program Area: Generation IV

Project Start Date: May 2007

Project End Date: April 2010

Research Objectives

The objective of this research project is to address major materials performance and methodology issues for design and construction of high-temperature and very high-temperature nuclear systems. This work will provide a synergy between materials testing and development of simplified-yet-robust design rules for high-temperature systems. The work will also contribute to the systems' performance and improvement. Such systems will have to deal with time-dependent materials properties (creep, creep-fatigue, high-temperature corrosion) in components with complex stress states, long intended service lives, and aggressive operating environments. Routine mechanical properties data and current high-temperature design methodology do not provide adequate information for long-term robust system design; this project will address these deficiencies. In addition, the project team will perform high-temperature materials testing in relevant corrosive environments (such as low-oxygen partial-pressure with substantial carbon activities) to support further code qualification of existing alloys and development of emerging alloys.

Research Progress

The preliminary design of the high-temperature gas corrosion facility is complete (see Figure 1). There are six gas cylinders, one of which contains helium as the main carrier gas, while the other five contain helium with one impurity gas. The mass flow controller (MFC) adjusts the gas flow rate of each gas cylinder, achieving the proposed gas mixture level (H_2 – 400 ppm, CO – 40 ppm, CO_2 – 0.2 ppm, CH_4 – 20 ppm, and N_2 below 20 ppm). After adding a 2 ppm level of H_2O into the gas mixture, part of the gas will pass through the thermally regulated water bath before entering the furnaces. Within the furnaces, researchers will measure thermal creep on a pressurized creep tube with a controllable gas environment. They will apply gas chromatography (GC) supplied by PerkinElmer to monitor both the inlet and outlet gas impurity levels, providing feedbacks to a LabView program used for controlling the MFC of each gas cylinder. Coupled with the automatic selecting value, the GC can monitor all three furnaces in real time. At the end of the flow chart, all of the gases will bubble through an oil bubbler to prevent any air gas entering the system.
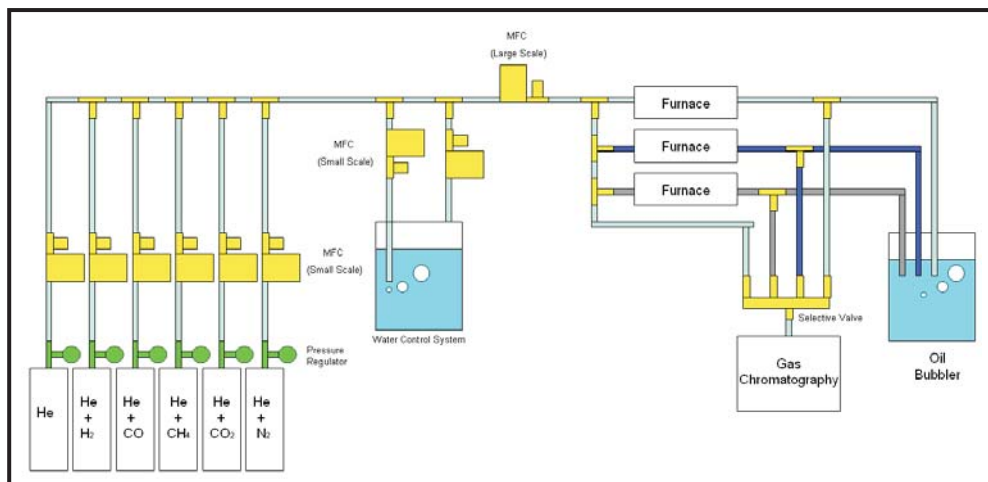

Figure 1. High-temperature gas corrosion facility.

High-temperature alloys of prime interest include Alloy 617, which has received considerable attention for elevated temperature applications, and Alloy 230, which has significant promise for long-term elevated temperature applications. Researchers will test the alloys' systems under a variety of conditions to assess their elevated temperature tensile, creep, and fatigue response. To maximize the creep information generated in this program, the testing will employ miniature pressurized tube specimens. This method covers a wide range of stresses at a variety of high temperatures with a minimum amount of space. Century Tube Inc. is responsible for manufacturing the tubes. The end plugs will be fabricated in the Department of Mechanical Science and Engineering Machine Shop at University of Illinois, Urbana-Champaign. Materials Joining Group at Oak Ridge National Laboratory will execute the electron and laser welding.
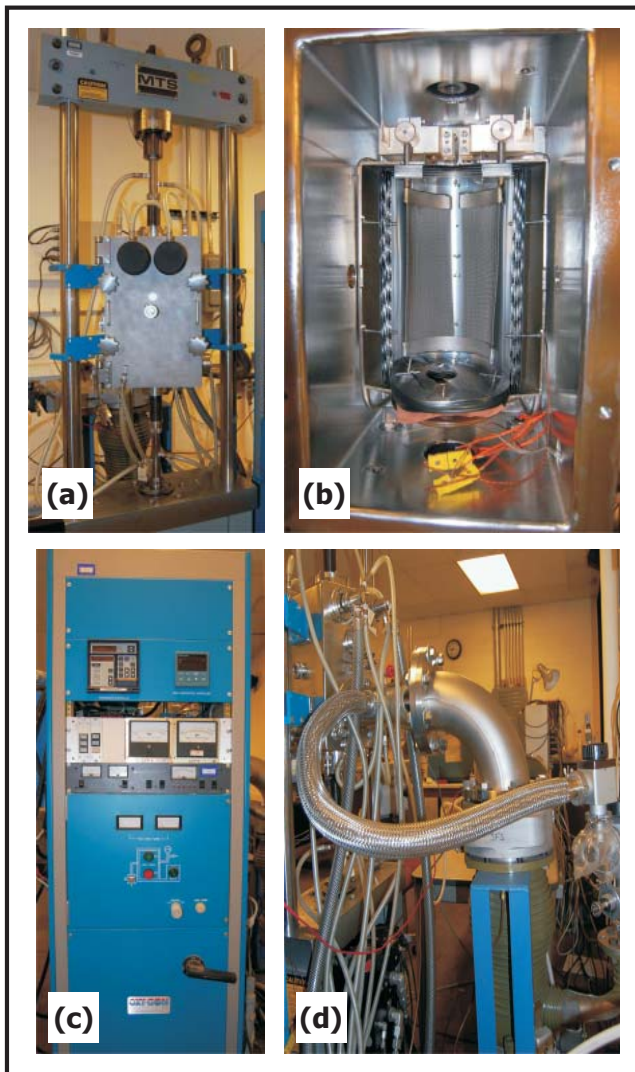

Figure 2. Layout of the high-temperature high-vacuum test facility: (a) test chamber, (b) inside of the test chamber, (c) front control panel, and (d) pumping system.

A dedicated high-temperature high-vacuum test facility is currently under construction in the Advanced Materials Testing and Evaluation Laboratory. This facility is based on an Oxy-Gon FR series universal application furnace supplied by Oxy-Gon Industries, Inc. Coupled with an MTS load frame (Instron controllers), this facility has the capability to do complex high-temperature mechanical loadings on samples in well-controlled test atmospheres, such as a high-vacuum or inert gas environment.

Figures 2(a), 2(b), 2(c), and 2(d) show the test facility's layout. In Figure 2(a), a test chamber made of double-walled 304 L stainless steel is attached to the MTS load frame. All water hoses in this figure are used to cool various parts of the test chamber, which will be subject to high-temperature exposure. Figure 2(b) illustrates the test chamber's inside structures. The heating element, which resembles a metal screen, is in the center of the chamber. Around it are shield assemblies made of molybdenum. The water-cooled heating jacket contains the heating elements and shield packs, further enclosing them. The chamber ports provide channels for various signal measurements, such as temperature and pressure. In addition, the chamber's bottom and top house an inert gas inlet and outlet used to maintain an inert gas environment. Figure 2(c) shows the facility's front control panel, which is used both to control and to monitor pressure and temperature inside the chamber. In addition, safety interlocks are integrated into the control console. When turned on, they can shut down the system if it overheats, loses water cooling, or suffers vacuum failure. Figure 2(d) shows the pumping system. It consists of a roughing pump and a diffusion pump. The pumping port is located at the back side of the test chamber.

Planned Activities

During the next program year, the project team will establish both corrosion testing facilities. The team will complete fabrication of pressurized tubes, in addition to starting creep tests in a controlled atmosphere and corrosion tests in both air and a controlled atmosphere. Team members will finish aging tests up to 3,000 hours for commercial alloys 617 and 230, obtaining aging effects on mechanical behavior.

The project will use all test results, with existing published data, as basic references for development of design guidelines for very high-temperature nuclear systems. The design guidelines would account for properties-based materials performance characteristics and assessment of joint activities on high-temperature crack initiation and growth behavior.

NUCLEAR ENERGY RESEARCH INITIATIVE

Experimental and Computational Fluid Dynamics Analysis of
Advanced Convective Cooling Systems

PI: Victor M. Ugaz and Yassin A. Hassan, Texas Engineering Experiment Station

Collaborators: None

Project Number: 07-058

Program Area: Generation IV

Project Start Date: June 2007

Project End Date: May 2010

Research Objectives

The objective of this project is to study the fundamental physical phenomena in the reactor cavity cooling system (RCCS) of very high-temperature reactors (VHTRs). One of the primary design objectives is to assure that the RCCS acts as an ultimate heat sink, capable of maintaining thermal integrity of the fuel, vessel, and equipment within the reactor cavity for the entire spectrum of postulated accident scenarios. Since construction of full-scale experimental test facilities to study these phenomena is impractical, computational fluid dynamics (CFD) simulations will probably play a key role in the RCCS design process. An important question then arises: To what extent are conventional CFD codes able to capture accurately the most important flow phenomena, and how can they be modified to improve their quantitative predictions?

Researchers are working to tackle this problem in two ways. First, in the experimental phase, the research team plans to design and construct an innovative platform that will provide a standard test setting for validating CFD codes proposed for the RCCS design. This capability will significantly advance the state of knowledge in both liquid-cooled and gas-cooled (e.g., sodium fast reactor) reactor technology. This work will also extend flow measurements to microscale levels not obtainable in large-scale test facilities, thereby revealing previously undetectable phenomena that will complement the existing infrastructure. Second, in the computational phase of this work, numerical simulation of the flow and temperature profiles will be performed using advanced turbulence models to simulate the complex conditions of flows in critical zones of the cavity. These models will be validated and verified so that they can be implemented into commercially available CFD codes. Ultimately, the results of these validation studies can then be used to enable a more accurate design and safety evaluation of systems in actual nuclear power applications (both during normal operation and accident scenarios).

Research Progress

Research activities during the past year have focused on modeling the proposed RCCS design using commercial CFD software. Researchers have selected STAR-CD for use in these initial studies. The basic design to be tested consists of a vertically oriented, heated, cylindrical reactor vessel half-section incorporating a horizontal flange. This assembly is then surrounded by a panel of vertical cylindrical heat exchange tubes. This setup will serve as a basis for experimental and computational cross-validation studies as shown in Figure 1. This geometry has been selected as a benchmark because it combines regions where system codes are in reasonable agreement with experiments (i.e., the central section) and regions where significant discrepancies have been reported (i.e., flange region, top and bottom heads of the vessel). These discrepancies are magnified when the transient cavity response is considered.
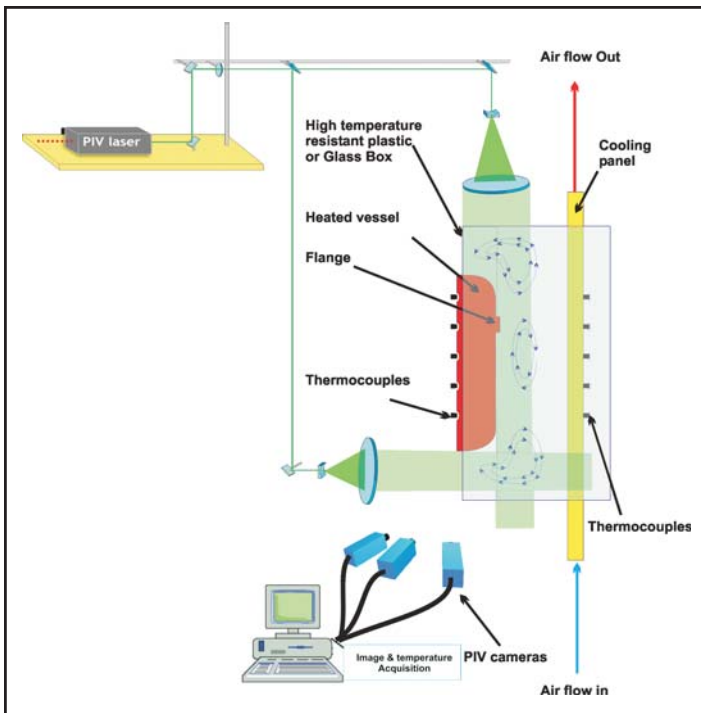
Figure 1. Illustration of setup for simultaneous experimental and computational mapping of the flow velocity and temperature field profiles.

Researchers generated a series of 3-D computational models using STAR-CD software; the models are designed to capture key features of this RCCS configuration. Five specific cases for further analysis and validation were then selected.

- Coarse mesh (900,000 cells) simulation of air at the tube inlets with stagnation boundary conditions and 520 W power generated in the vessel

- Fine mesh (5,500,000 cells) simulation of air at the tube inlets with stagnation boundary conditions and 520 W power generated in the vessel

- Fine mesh (5,500,000 cells) simulation of air at the tube inlets with stagnation boundary conditions and 260 W power generated in the vessel

- Fine mesh (5,500,000 cells) simulation with water flowing through the tubes from bottom to top, and 260 W power generated in the vessel

- Fine mesh (5,500,000 cells) simulation with water flowing through the tubes from top to bottom, and 260 W power generated in the vessel

Computational studies using this geometry and set of flow conditions will allow researchers to optimize parameters associated with the computational simulation method (e.g., convergence of residuals, influence of mesh size, influence of component materials, selection of boundary conditions, etc.) so that the team can be ready to begin validation studies when the test facility is completed (see Figure 2).
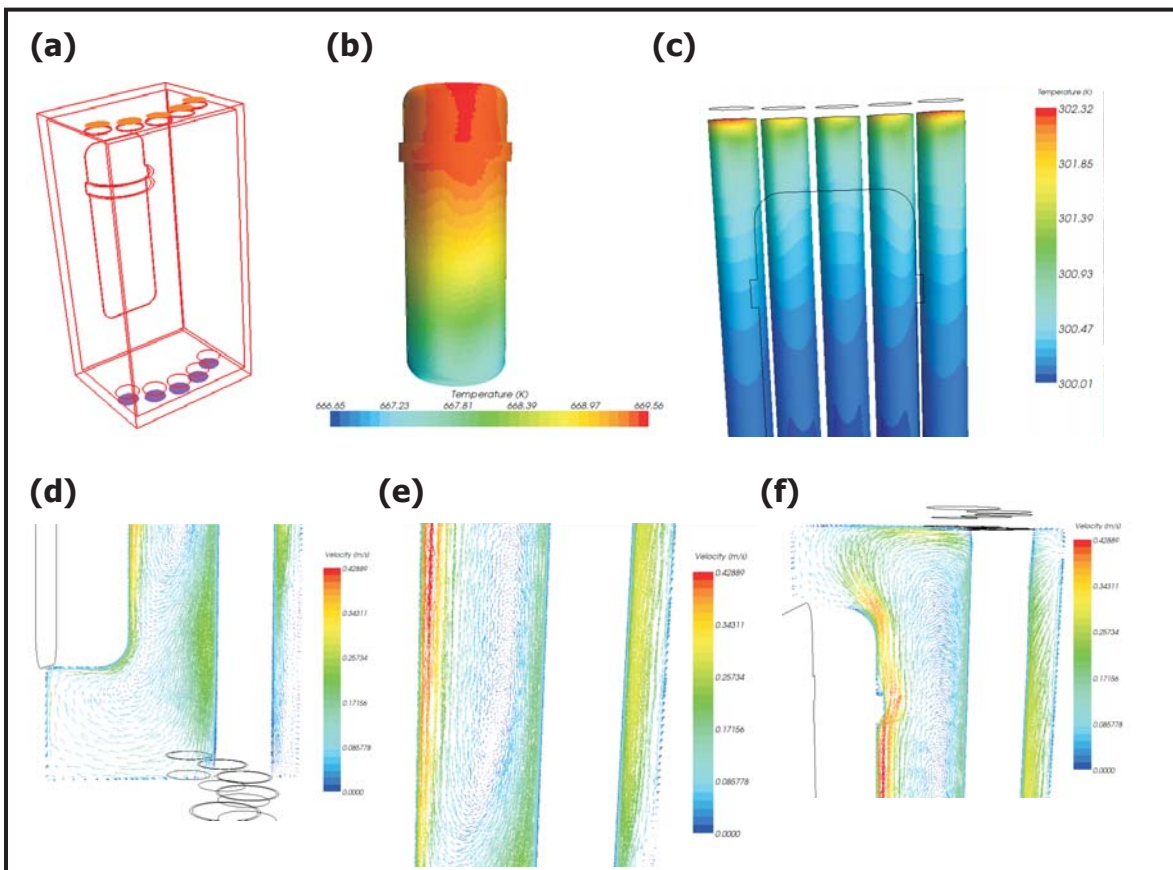
Figure 2. Overview of 3-D computational model setup and preliminary results (plotted data correspond to the first case—coarse mesh—above). (a) overview of RCCS model geometry; (b) reactor vessel surface temperature profile; (c) heat exchanger tube surface temperature profile (Al tubes shown); and (d-f) computed velocity profiles along a central vertical plane corresponding to lower, middle, and upper zones, respectively.
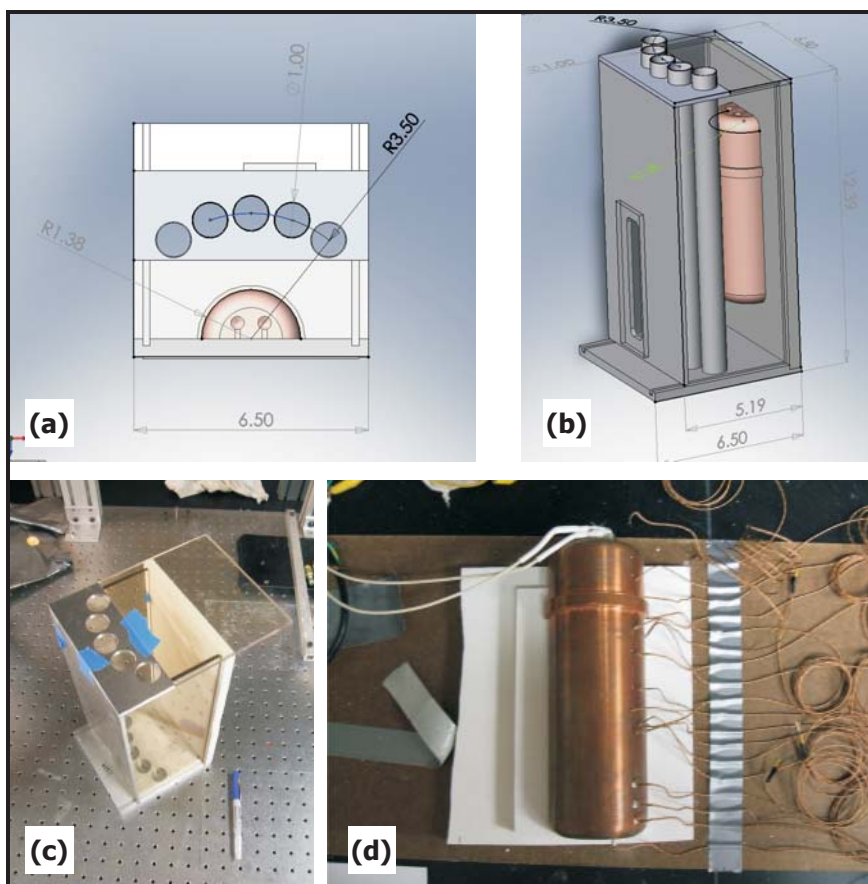
Figure 3. Progress toward the construction of RCCS test geometry: (a,b) overview of RCCS test geometry design, (c) test-section assembly with optical viewing windows, and (d) thermocouple mounting assembly with cartridge heaters.

In parallel with this computational effort, the research team has constructed a flow chamber designed to closely match the RCCS prototype test geometry, as shown in Figure 3. This setup will permit direct quantitative measurement of the 3-D velocity and temperature profiles inside the test chamber so that predictions of the computational simulations can be directly validated and verified. Constructing a test facility compatible with the particle image velocimetry measurement techniques entails a number of design challenges. For example, the use of optically based interrogation methods requires the incorporation of transparent viewing windows at specific locations in the test section. These windows are necessary to allow laser illumination to reach the fluid and to permit imaging using synchronized high-speed cameras. Researchers also found that electrical isolation of the thermocouple temperature probes was necessary because

the temperature readings were affected by cross-talk from the electric field generated by cartridge heaters used for thermal control. The team is also evaluating new fluorescent seeding materials that can be used both as tracers that will enable the flow field within the flow system to be directly visualized and as indicators of local temperature within the flow.

Planned Activities

The primary tasks associated with experimental and computational project phases are listed below. These tasks are in line with the proposed schedule status and milestones.

Experimental Phase:

- Complete construction of test section and develop experimental test plan

- Perform calibration of particle image velocimetry setup and obtain initial measurements to identify key phenomena

- Perform temperature measurements under various flow conditions

- Optimize data-analysis methods

Computational Phase:

- Continue investigation of techniques to accurately model temporal and spatial flow structure. Large eddy simulation will provide the temporal and spatial flow regimes under turbulent, transitional, and laminar conditions. Turbulence phenomena of the turbulent coherent structure will be identified. These flow patterns will help in developing/refining turbulence models and global correlation for RELAP system code.

- Compare computational results with preliminary experimental data

- Investigate modifications/refinements to the computational models in order to capture physical phenomena in the RCCS geometry

NUCLEAR ENERGY RESEARCH INITIATIVE

Establishing a Scientific Basis for Optimizing Compositions, Processing Paths, and Fabrication Methods for Nanostructured Ferritic Alloys for Use in Advanced Fission Energy Systems

PI: G. R. Odette and Takuya Yamamoto, University of California-Santa Barbara (UCSB)

Collaborators: Los Alamos National Laboratory (LANL), Oak Ridge National Laboratory (ORNL), University of California-Berkeley (UCB), South Dakota School of Mines (SDSM)

Project Number: 07-069

Program Area: Generation IV

Project Start Date: August 2007

Project End Date: July 2010

Research Objectives

The objective of this research is to develop high-performance fuel cladding, duct, and internal structural material systems for a variety of future fission reactors—including advanced fast burner reactors envisioned in the Global Nuclear Energy Partnership, Generation IV, and Advanced Fuel Cycle Initiative programs. The goals for alloy performance center on attaining a combination of 1) high-temperature creep strength; 2) thermal and radiation stability, as well as resistance to other sources of in-service degradation, permitting long lifetime (high burn-up) operation to doses of 200 or more displacements per atom (dpa); 3) corrosion resistance and compatibility in advanced reactor coolant environments; 4) a good balance of mechanical properties; and 5) favorable neutronic characteristics and life-cycle costs.

Achieving these ambitious objectives in a practical structural material requires a combination of alloy design and optimization, including development of compatible processing, fabrication, and joining paths. Research will focus on a newly developing alloy class that has shown great promise in achieving all these objectives: nano-structured dispersion-strengthened ferritic alloys (NFAs). NFAs are dispersion-strengthened by a high density of nm-scale Y-Ti-O nano-features (NFs), resulting in remarkable high-temperature creep strength and radiation damage resistance for applications in advanced fission and fusion reactors. NFAs are processed by mechanically alloying (MA) Fe-Ti-Cr powders by ball milling with Y_2O_3, followed by hot-powder consolidation by hot isostatic pressing (HIP) or extrusion. MA dissolves the Y_2O_3 constituents, which precipitate, along with Ti, during high-temperature processing.

The research program consists of the following five tasks:

- **Developing a Deformation Processing Database:** The research team will use a science-based approach to deal with a major current limitation in directionally worked NFA product forms that have anistropic microstructural and strength properties. Researchers have taken a two-step approach: 1) construct a deformation database that will map out deformation-temperature recrystallization regimes that lead to more isotropic behavior; and 2) explore strain, strain rate, and temperature regimes that may allow for dynamic recrystallization or even superplatic deformation. This approach should result in fine, stable grain structures that can be both optimized for creep strength and a good balance of properties in fabricated components such as cladding tubes. The team will also explore new approaches to utilizing γ-α phase transformations to achieve equiaxed microstructures and alternative processing routes to MA.

- **Solid-State Joining:** Researchers will map regimes of efficient diffusion bonding and friction-stir welding, guided by a previously developed understanding for the thermal-deformation stability of NFA microstructures, with the objective of preserving the NFs and maintaining outstanding joint properties.

- **Alternative Alloys and Alloy Optimization:** A semi-combinatorial approach to optimizing NFA compositions will enhance and optimize a variety

of NFA performance indices, including producing alloys with uniform micro-nanostructures, high thermal stability, and high creep strength, as well as resistance to radiation damage and corrosion.

- **Identification and Optimization of Nano-Features:** Researchers will fill in a key missing element in alloy design: the basic character of various NFs. The team will also discover means to manipulate NF character, thus providing a basis of understanding for NFA property optimization.

- **Target of Opportunity Irradiations and Post-Irradiation Examination:** The research team will design and carry out neutron irradiation studies of NFA and other relevant structural alloys on a best-effort basis, as well as coordinating post-irradiation testing to provide information on the use of NFAs in severe nuclear environments.

Research Progress

Task 1: Deformation Processing Database. Researchers are developing a systematic deformation-annealing thermal mechanical processing database. With this database as a foundation, researchers can optimize fabricating components that produce recrystallized microstructures with isotropic properties and controlled grain sizes. The team has performed a preliminary study on a MA957 bend bar. Results showed expected hardness profiles in both the compressive and tensile strained regions. The team has initiated hardness and electron backscattering diffraction (EBSD) studies, as well as strain mapping on deformed specimens and transmission electron microscopy (TEM) examinations of post-strained and annealed microstructure; these studies will continue during the coming year.

Task 2: Solid-State Joining. Standard melt processed welds destroy the beneficial NFs and degrade NFA joint properties. Thus, researchers are pursuing solid-state approaches to joining NFA. The team has recently become part of a research collaboration between LANL, ORNL, UCB Crucible Research, and SDSM to 1) develop larger NFA heats, 2) improve NFA processing paths, and 3) explore friction stir welding (FSW) for solid-state NFA joining. SDSM will carry out the FSW. UCSB will lead an extensive effort to characterize FSW properties and microstructures. The initial bead-on-plate studies will be done on MA956 and PM2000 (supplied by LANL), MA957 (supplied by UCSB), and a 14YWT model alloy (supplied by ORNL). The first stage of this work will be completed by early 2009. Researchers will also initiate diffusion bonding studies in 2009.

Task 3: Alternative Alloys and Alloy Optimization. Achieving a uniform NF distribution by MA is difficult. Regions of lower NF concentrations are softer and experience dislocation recovery and grain growth during hot consolidation, leading to a bimodal grain size distribution and a reduction in the alloy's fracture toughness and strength. Thus, researchers systematically explored a large matrix of milling variables to find combinations that lead to more uniform NF distributions. MA powders were annealed at 1,150°C. The team mounted, polished, and etched the annealed powders, then used scanning electron microscopy (SEM) to examine the powders and characterize the grain size distribution. Three prototypic grain morphologies were observed: large, small (less than 1 µm grains with easily distinguishable boundaries), and heavily etched regions without easily distinguishable grain boundaries that researchers assume are most likely composed of less than 1 µm grains.

The team produced 30 annealed powders with systematic variations in the ball milling parameters. Fine grains were promoted by smaller ball sizes, finer powders, lower ball-to-powder mass ratios, incremental additions of Y_2O_3, and increased milling times. The team further explored various combinations of milling parameters that were found to be attractive in the single-variable experiments. This led to a nominally best-practice milling procedure, resulting in grain structures with a nominal small-grain area fraction of 0.89 (see Figure 1a). This value compares very favorably to the nominal small-grain area fraction of 0.55 for the initial baseline milling parameters shown in Figure 1(b). The best-practice milling variables were:

- High-energy SPEX milling of Fe14%Cr powders MA with the smallest available W (3 percent), Ti (0.4 percent), and Y_2O_3 (0.3 percent) powders

- A 5:1 ball mass-to-charge ratio

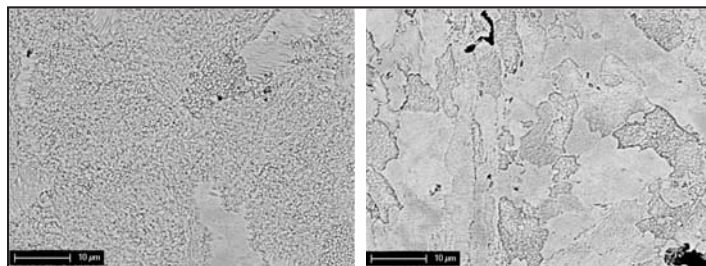- A combination of 6-mm (50 g) and 8-mm (50 g) diameter balls

Figure 1. (a) The etched powder particle surface of the sample using best-practice milling parameters; (b) the etched particle surface for the baseline milling parameters.

- An 8-hour total mill time

- Incremental Y_2O_3 powder additions at 0 hours, 0.5 hours, and 1 hour

More recently, researchers performed EBSD measurements on the best-practice milling powder that was hot-press consolidated at 1,150°C for six hours. EBSD showed a majority of sub-micron-sized grains mixed with some larger grains. Figure 2 shows band-contrast and EBSD grain-orientation images. The area fraction of grains less than 3 µm was 0.63 in the region sampled, with an average size of 284 nm for grains between 50 nm and 3,000 nm in diameter. The corresponding average size of grains larger than 3 µm was 5.05 µm. Figure 3 shows results of a similar EBSD characterization of another NFA alloy, which was processed by attritor milling Fe14Cr3W0.4Ti and $0.3Y_2O_3$ powders, followed by HIP consolidation at 1,150°C for two hours. This alloy contained a bimodal distribution of large grains and clusters of sub-micron grains. The fraction of grains smaller than 3 µm was 0.28, with a corresponding average size of 200 nm for grains between 50 nm and 3,000 nm in diameter. The mean grain size for grains larger than 3 µm was 5.95 µm. Neither of the NFAs shown below exhibited a preferential grain texture.
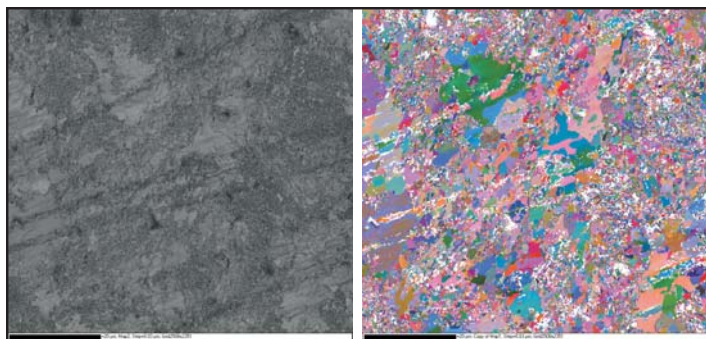
Figure 2. (a) Band-contrast image of the best-practice sample; (b) EBSD grain-orientation map.
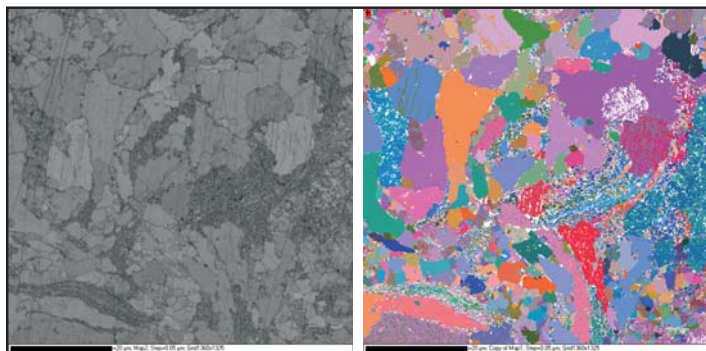
Figure 3. (a) Band-contrast image of 1,150°C HIP consolidated NFA; (b) EBSD grain-orientation map.

Researchers also carried out EBSD on hot-extruded MA957. As shown by the pole-figure map in Figure 4(a),

MA957 has a strong <110> γ-fiber texture in the extrusion direction. Figures 4(b) and 4(c) display EBSD band-contrast and grain-orientation map images in the radial-transverse direction; these images show a distribution of µm-sized grains with a large grain-aspect ratio (GAR) of 5 to 10.
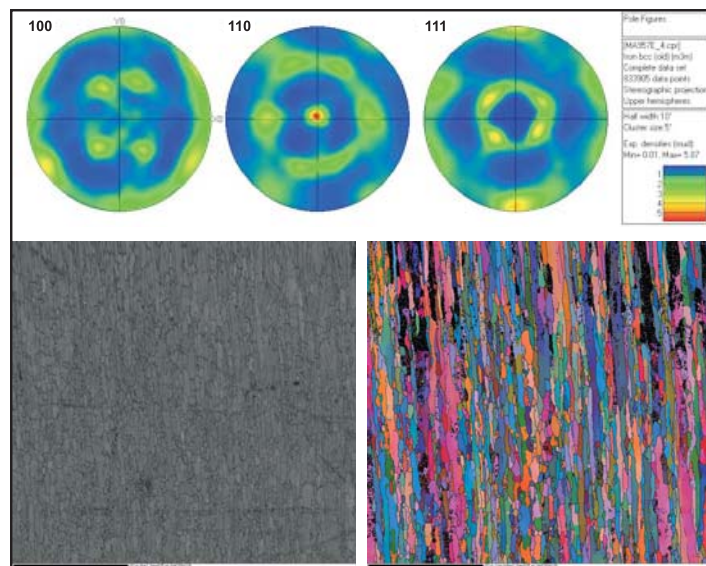
Figure 4. (a) MA957 pole figure in extrusion direction; (b) MA957 band-contrast image in the radial-transverse direction; (c) MA957 grain-orientation map.

Task 4: Identification and Optimization of the NFs. The National Institute of Standards and Technology, Center for Neutron Research in Gaithersburg, MD, used small-angle neutron scattering (SANS) to characterize a subset of the powders produced in this study. The best-practices powder, consolidated by hot pressing at 1,150°C, contained 6.3×10^{17} NFs/cm^3, with an average radius of 1.31 nm and a volume fraction of 1.09 percent. The other NFs in the NFA alloys were similar and compared favorably to those found in MA957: 8.7×10^{17}/cm^3, 1.21 nm, and 0.89 percent, respectively. As part of a collaborative effort with LANL, the project team also processed an MA HIPed heat of NFA containing aluminum (Al) additions to improve corrosion resistance. The team sent the consolidated alloy to LANL in early 2008.

In May of 2007, ORNL researchers characterized several NFAs using the local electrode atom probe (LEAP) as part of the SHaRE program. The qualitative observations from the LEAP analysis have since been reported; however, offsite researchers could not perform a more detailed data analysis, as PoSAP software is available only at ORNL. Thus, project team members spent a week at ORNL in early August 2008 to learn how to use the specialized and proprietary PoSAP and other software needed to analyze LEAP data. The ORNL LEAP characterized MA957, the

ORNL-milled alloy HIPed by UCSB at 1,150°C (described above), and the alloy produced from the same powders HIPed at 1,000°C. Figure 5 shows an example 3-D atom-probe map for MA957 containing the Ti-Y-O NFs. The analysis showed the presence of approximately 3.9×10^{17} NF/cm^3 with an average Guinier radius of 0.72 nm.
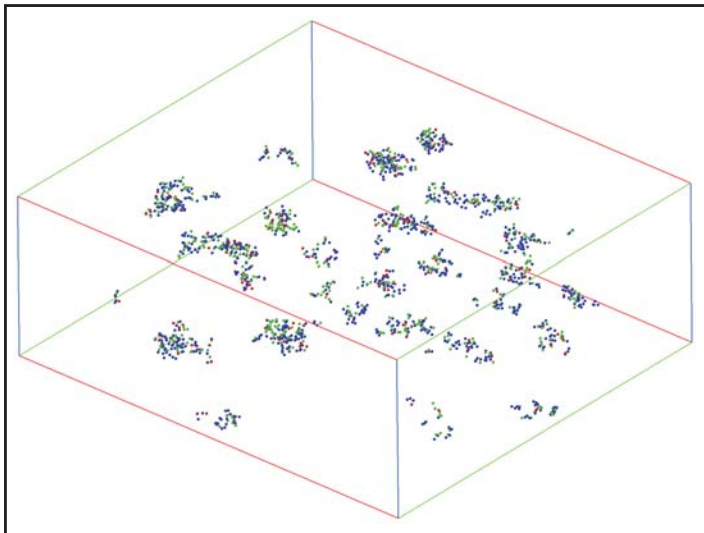

Figure 5. An isometric atom map view of Ti-Y-O nanoclusters in MA957.

Table 1 shows the nominal and LEAP measurements of the composition MA957, along with matrix and NF compositions. Analysis of the other NFA samples is ongoing.

	Fe	Cr	C	Mo	Y	Ti	O	Al	B	Si
Nominal	83.59	14.87	-	0.17	0.12	1.04	0.18	-	-	-
Sample	83.09	15.49	0.01	0.15	0.08	0.84	0.21	0.06	0.01	0.07
Matrix	83.17	15.50	0.01	0.15	0.07	0.78	0.18	0.06	0.01	0.07
NF	72.7	15.51	0.01	-	4.77	5.99	4.58	0.13	0.05	0.07

Table 1. The nominal and LEAP measured sample, matrix, and NFs composition (wt%) of MA957.

In addition to the ORNL LEAP studies, researchers have established collaborations on atom-probe tomography (APT) and advanced TEM characterization of NFAs with Oxford University (UK). A similar collaboration has been established with LANL and Leoben University (Austria). Finally, UCSB will be acquiring its own state-of-the-art atom probe in 2009.

In collaboration with the Illinois Institute of Technology, the research team carried out measurements of extended x-ray absorption fine structure (EXAFS) and x-ray absorption near-edge structure (XANES) at the Argonne National Laboratory Advanced Photon Source; these measurements help clarify the nature of the NFs and the local structure of the Ti and Y atoms in both NFA powders and consolidated alloys. The team characterized the powders in the as-received condition, the as-milled condition, and after annealing the milled powders at 850°C, 1,000°C, and 1,150°C. The consolidated alloys included powders HIPed at 1,150°C and extruded commercial vendor alloys, MA957, and J12YWT. The NFA EXAFS and XANES data compared various Ti- and Y-oxide standards. The annealed and HIPed powders have similar spectra, which show high-temperature heat treatments shift the Y and Ti to more oxidized states that are consistent with combinations of Y_2TiO_5, $Y_2Ti_2O_7$, and, especially, TiO phases. However, the MA957 and J12YWT and annealed-consolidated powder data differ. The commercial vendor alloys produce results that more closely resemble the as-milled powder data, and all show that a significant fraction of substitutional Ti remains dissolved in the (BCC) ferrite matrix. In the case of MA957, the remaining Ti is due to the higher concentration of Ti in this alloy.

Task 5: Target of Opportunity Irradiations and Post-Irradiation Examinations (PIE). As part of the advanced test reactor (ATR) National Scientific Users Facility, UCSB was awarded an irradiation capsule position in the ATR at Idaho National Laboratory. The capsule's basic design has been completed and satisfies the thermal design requirements. Researchers have developed a detailed design of the capsule core for precise temperature control. The design is based on pinned stack-up of specimens with a high precision gas gap, which is provided by press fit spacers on the top and bottom. Researchers have identified specimen matrices for four high and four low irradiation temperatures, with nominal values from 275°C to 750°C. Larger capsule sections at 275°C, 550°C, 650°C, and 750°C will contain various mechanical specimens, such as miniature tensile, disc compact tension fracture, and small deformation and fracture mini-beam specimens, along with disc multi-purpose coupons (DMCs) primarily for micro-hardness and microstructure examination. DMCs will be included in smaller capsules at 350°C, 400°C, 450°C, and 500°C. The current specimen matrices include about 60 materials, such as 7 TMSs, 13 NFAs, 3 stainless steels, 30 model alloys, 4 diffusion multiples, and 5 joints/coatings. The project team will complete the design phase in early 2009 and begin irradiations in June 2009. The team continues STIP-V

spallation proton irradiation of two UCSB capsules at the Pual Sherrer Institute; the process will be completed in the first half of 2009.

Planned Activities

Research on all five tasks will continue in 2009. Anticipated milestones include the following:

Task 1 Deformation Processing Database – Complete characterization of the viscoplastic creep properties and the cold-to-warm deformation high-temperature annealing map for MA957 with extensive application of EBSD and other advanced characterization techniques

Task 2 Solid-State Joining – Complete an initial study of FSW and initiate diffusion bonding studies, including mechanical property and microstructural characterization of the joints

Task 3 Alternative Alloys and Alloy Optimization – Explore a matrix of approximately 60 NFA compositions (Y, Ti, and O variations) processing variable conditions (annealing/consolidation time and temperature) characterized by micro-hardness, SEM, and SANS

Task 4 Identification and Optimization of the NFs – Comprehensively characterize a smaller subset of the alloys cited in Task 4 using TEM, APT, EXAFS/XANES, positron annihilation, and small-angle x-ray scattering measurements to clarify NF composition and structure

Task 5 Target of Opportunity Irradiations and Post-Irradiation Examinations – Initiate the ATR irradiation; complete the STIP-V irradiation and a detailed PIE plan

NUCLEAR ENERGY RESEARCH INITIATIVE

A Research Program on Very High-Temperature Reactors

PI: Sudarshan Loyalka, University of Missouri-Columbia

Collaborators: North Carolina State University, Washington University-St. Louis

Project Number: 08-043

Program Area: Generation IV

Project Start Date: September 2007

Project End Date: September 2010

Research Objectives

Prismatic and pebble-bed very high-temperature reactors (VHTRs) are very attractive both from a thermodynamic efficiency viewpoint and for their hydrogen-production capability. This project addresses numerous challenges associated with the fuel cycle, materials, complex fluid dynamics, and heat transfer.

Consortium members will perform the following tasks:

- Conduct physical experiments for fission product transport phenomena in the overcoating and compact structural graphite, as well as transport through tri-isotopic coating layers

- Develop improved sorption measurement techniques to measure accumulation of condensable radionuclides ("plateout") in the VHTR primary coolant circuit and obtain representative data

- Develop advanced computations of charged radioactive dust (aerosol) transport in the VHTR coolant circuit and confinement by exploring direct simulation Monte Carlo (DSMC) techniques for deposition and resuspension; conduct experiments to verify computational predictions

- Develop a program to measure emissivity for various VHTR component materials, both bare and oxidized, and obtain extensive data

- Develop an experimental program to characterize gas, fission product, and particle flows in the complex geometries of pebble-bed modular reactors (PBMRs); help improve computational approaches and computer programs through experimental understandings

Research Progress

The project requires characterizing and verifying measurement techniques for silver diffused into a graphite matrix or silicon carbide (both spatial and quantitative). To that end, researchers have focused on developing a simple test sample for diffusion of silver into graphite. The research team has tested a 1" cylindrical cell with a threaded plug on one end, as depicted in Figure 1. Inside the cylinder is a small cavity into which silver is placed. The only escape route for the silver is through the threading and a small sealing joint. In order to prevent that release, researchers have explored hermetically sealed designs, resulting in successful development of a graphite cell with a silver kernel that has exhibited measurable diffusion. The test cell depicted in Figure 1 was baked at 1,200°C to 1,300°C for 13 days under an inert atmosphere of argon. The sample was analyzed using computed tomography (CT) scans obtained from the Harry S. Truman Memorial VA Hospital Research Center's Biomolecular Imaging Group. Figure 1 includes a cross-sectional image.
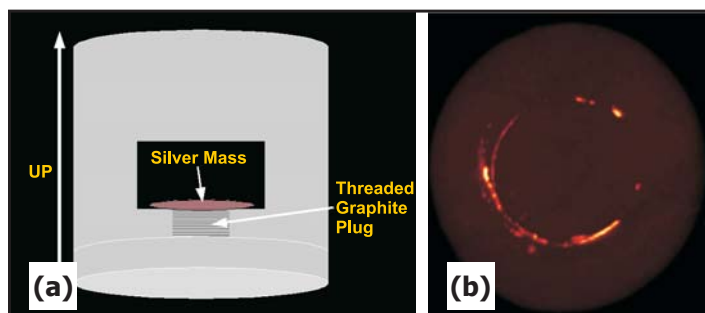

Figure 1. (a) An illustration showing the inside of the sample in roughly the same orientation as placed during the experiment, in which the silver mass rests on threaded plug; (b) a CT image from the top of the cell. This image shows that the diffusion has occurred primarily at the corners.

With respect to adsorption/absorption studies, researchers have focused on literature review, apparatus design, equipment acquisition, and obtaining some initial data. The team extensively reviewed both nuclear and non-nuclear literature. Since availability of accurate vapor pressure data will be crucial to the project research, the team has reviewed literature related to vapor pressures of the elements of interest to the project. The open literature describes the results of this review, and further work in this area continues.

Researchers have begun to measure absorption/adsorption of cesium iodide (CsI) vapor on stainless steel. The team wants to determine under what conditions a detectable level of cesium or iodine is adsorbed onto the stainless steel sample. They have assembled a system with a tube furnace, which is used to heat the fission product sample (initially nonradioactive CsI) to a sufficient temperature to produce vapor. The system now has a ceramic tube mounted vertically with a material sample (initially stainless steel) hanging from a hook inside the tube (as depicted in Figure 2). The CsI vapor is introduced into the top of the ceramic tube, flows over the sample, and exits the bottom of the tube. The vapor then flows into a series of bubblers containing nitric acid in order to scrub the flow stream free of CsI.
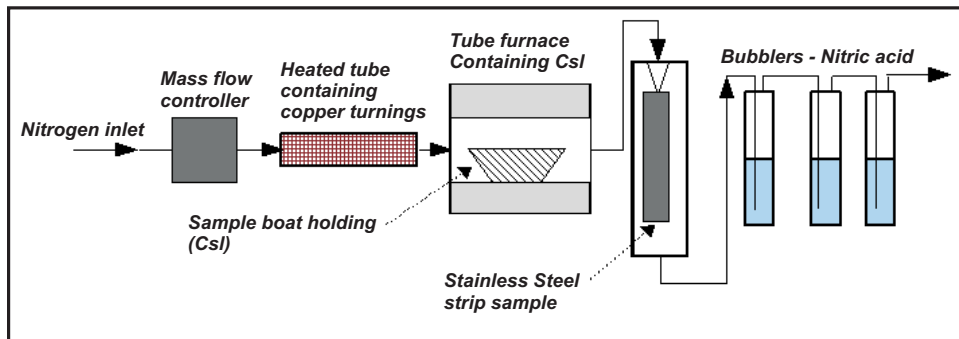
Figure 2. Schematic of the current experimental setup to measure adsorption of CsI on stainless steel.

CsI is being used for all initial tests. Obtaining cesium metal for vaporization has been problematic, and to date, the quantity ordered has not arrived. In its absence, researchers have decided to proceed using several cesium salts that would also be present in a VHTR core. The literature indicates that CsI does exist in VHTR cores and that data on its adsorption properties is necessary since cesium and iodine atoms will compete for adsorption on the stainless steel.

Using the setup described above, researchers heated the furnace tube to 800°C—high enough to produce a significant CsI vapor pressure—and flowing nitrogen at 200 cc/m moved the vapor through the system. This setup ran for an hour, after which the sample strip was analyzed using energy dispersive x-ray spectroscopy (EDS). The steel strip's surface had a significant coating of material. The spectra of these spheres indicated they were CsI. This initial test shows EDS will be a useful method for determining the presence of CsI on the surface of the samples.

Regarding development of advanced computations of dust (aerosol) transport in VHTR primary and secondary, researchers have made considerable progress in both the deterministic and DSMC approaches to the problem. (Deterministic approaches provide benchmarks for the DSMC simulations.) For the deterministic part, and to describe the concentration of suspended particles in a recirculating gas, researchers have been able to solve the Reeks Hall resuspension equation numerically (it is an integro-differential Volterra's equation with a delay kernel). They have found that their numerical results agree precisely with those obtained through analytical solutions of this equation. This work will allow generalizations of the Reeks Hall equation to a number of cases where realistic time-dependent rate processes with respect to coagulation, deposition, and aerosol sources play important roles, and where the equations can now be solved numerically. The research team is presently exploring several similar cases.

Researchers have constructed an initial DSMC program. First they sample the fluid (lift) force on deposited particles from a prescribed fluid force distribution (related to a turbulent flow field). The researchers then allow a fraction of the deposited particles to be resuspended by comparing the fluid force with an adhesive force.

The research team has made considerable progress in four related areas:

- Researchers are close to computing aerosol charging. They have successfully solved the potential theory surface integral equations numerically to calculate the electric field produced by multiple charged bodies of arbitrary shapes (aerosols) arbitrarily situated in a medium. Researchers have parallelized the computations

and tested these computations on an 8-processor cluster. The team has also acquired a 128-processor cluster and made sufficient progress on its installation and testing. This cluster will help researchers substantially in expediting these and other computations to be discussed later. The team will later compute charging of aerosols (due to ionizing radiation emitted by sources both internal and external to the aerosols) and the effect of charging on aerosol processes.

- The team has built an apparatus for generating dust from graphite spheres under controlled pressure, and researchers will acquire initial data on size and mass distributions of the dust in the near future.

- The team has built an apparatus for measuring thermophoretic deposition of aerosol particles and run initial tests. Concurrent to the thermophoresis experimental work, researchers have also developed computational models to estimate the thermophoretic particle deposition efficiencies in cylindrical tube geometries. The team has used the CFD code FLUENT to model the thermophoretic particle deposition and compared the results from the present model with published experimental data. A manuscript relating to this work has been accepted for publication in *Nuclear Technology*.

- Researchers are making considerable progress on modifying an electrodynamics balance to measure the thermophoretic force on single graphite particles.

For measuring emissivity, researchers have set up the apparatus, including a bell jar, data acquisition units, turbopump, water cooling unit, roughing pump, power switch, pressure indicators, turbopump controller, and power supply.

The research team examined the relevant literature to acquire initial emissivity measurements for stainless steel 304 in the 300°C to 800°C range. The team also recently completed additional measurements for pure Ni for a temperature range of 350°C to 900°C. The emissivity measurements match well with the reference data for oxidized Ni within the temperature range studied. The team used EDS to analyze the Ni strip after confirming its post-experimental oxidation. In addition, the EDS analysis detected some carbon on the strip's surface (possibly introduced during the rolling process of fabrication).

The project team has also addressed development of an experimental program to characterize gas, FP, and particle flows, as well as pebble motion in the complex geometries of PBMRs. Researchers have made considerable progress with respect to both single-particle tracking and three-detector approaches for flow characterization. They

Figure 3. The mock-up pebble bed experimental setup.

have completed construction and testing of a mock-up pebble bed (30 cm in diameter), shown in Figure 3. This effort also addresses the project objective of improving computational approaches and computer programs through experimental understandings.

The team has started additional experiments using the current experimental setup to measure residence time distribution of solids by tracking colored particles. Researchers have continued to develop and improve their method for measuring voidage and solids cross-sectional distribution using gamma-ray CT. In such measurements, the pebble bed is mimicked as a fixed bed since the solids' movement in such beds is typically slow. To characterize the cross-sectional solids and voidage distribution of a bed packed with these colored particles, the team packed a cylindrical 18" column with spherical glass balls (marbles). The balls were of 12-mm diameter and 2.55 kg/m^3 density. The team then used gamma-ray CT to measure the bed cross-sectional distribution of solids and voidage, obtaining a range of results. Researchers have further constructed and are testing a 3-D particle-tracking system with three sets of collimated 2" x 2" NaI detectors.

The research team has adapted LABVIEW to carry out motion control of the stepper motors, as well as data acquisition of signals received by the detectors where the counting rate maxima algorithms are used to track the pebbles. The team used the data acquisition system to test a Cs137 point source, and the system has worked well.

The research team is testing this system on a model PBR. They have used a cylindrical container, 30 cm x 30 cm right circular, with a 25° (horizontal angle) bottom bed

for the PBR's vessel. The marbles are spheres of 1.0 cm to 1.2 cm in diameter (these dimensions correspond to the experiment by Gatt, 1970). Initial tests have shown promise, and researchers will continue to test in the next quarter.

Planned Activities

Researchers will continue to acquire additional data, improve experimental designs, and explore computational approaches in the areas discussed above. They have realized initial successes in all project areas and have also identified the challenges toward meeting project objectives.

NUCLEAR ENERGY RESEARCH INITIATIVE

Cladding and Structural Materials for Advanced Nuclear Energy Systems

PI: Gary S. Was, University of Michigan

Collaborators: Alabama A&M University, Pennsylvania State University, University of California-Berkeley, University of California-Santa Barbara, University of Wisconsin-Madison

Project Number: 08-055

Program Area: Generation IV

Project Start Date: September 2007

Project End Date: September 2010

Research Objectives

The goal of this consortium is to address key materials issues in the most promising advanced reactor concepts that have yet to be resolved or that are beyond the existing experience base of dose or burnup. The research program consists of three major thrusts: 1) high-dose radiation stability of advanced fast-reactor fuel-cladding alloys, 2) irradiation creep at high temperatures, and 3) innovative cladding concepts embodying functionally graded barrier materials.

Following are the objectives of this research:

- Develop an understanding of the high-dose radiation stability of candidate sodium-cooled fast reactor cladding and duct alloys under the expected range of temperatures and dose, using a closely integrated program that combines targeted charged particle and neutron irradiation, *in situ* irradiation, and computer simulation of defect microstructure

- Determine the stability of oxide dispersion-strengthened (ODS) steel and ultrafine, precipitation-strengthened (HT-UPS) austenitic steel

- Characterize and understand mechanisms for irradiation creep in silicon carbide (SiC) in TRISO fuel, ferritic-martensitic (F-M) alloys, and ODS and HT-UPS steels

- Develop barrier layers to protect F-M alloys from fuel-clad chemical interaction and to protect Alloy 617 from attack by coolant impurities in the intermediate heat exchanger of the very high-temperature reactor

- Develop modeling tools to explain the behavior of F-M steels under irradiation; develop predictive tools to extend the reach of understanding beyond the experimental database

Beyond scientific achievements, this consortium is expected to provide substantial long-term benefits that will be crucial for the advanced reactor program's success, including establishing pathways to incorporate data into the Amercian Society of Mechanical Engineers Codes and Standards.

Research Progress

Irradiated Microstructures: Experiment and Modeling. The project team intends to extend the range of operation of nuclear fuel-cladding and structural materials in advanced nuclear energy and transmutation systems. To achieve this end, the team must understand the irradiation-induced evolution of the microstructure and the associated changes in bulk properties at relevant temperatures and doses. Researchers are taking a comprehensive approach to developing this understanding; they are performing bulk irradiation, *in situ* irradiation, irradiated microstructure characterization, and computer simulations.

The microstructure of alloys considered for fast-reactor cladding and other structural applications has been analyzed following proton irradiation. The alloys—HT9, T91, HCM12A, NF616, and a 9 Cr ODS steel—were irradiated with protons at 400°C to doses ranging from 1 dpa to 10 dpa. The research team then examined the irradiation-induced microstructures and grain-boundary (GB) compositions using transmission electron microscopy (TEM)

techniques. Varying lots of HT9 do not show significant differences in radiation response when irradiated to 1 dpa at 400°C. HCM12A irradiated to 7 dpa at 400°C shows significant radiation-induced segregation (see Figure 1), which may be related to the formation of copper-rich precipitates. To couple experimental work with modeling efforts, the research team produced two model alloys, Fe-9 Cr-0.1C and Fe-12 Cr-0.1C. The team has performed initial *in situ* irradiations with 1 MeV Kr ions at 400°C, and team members are examining results.
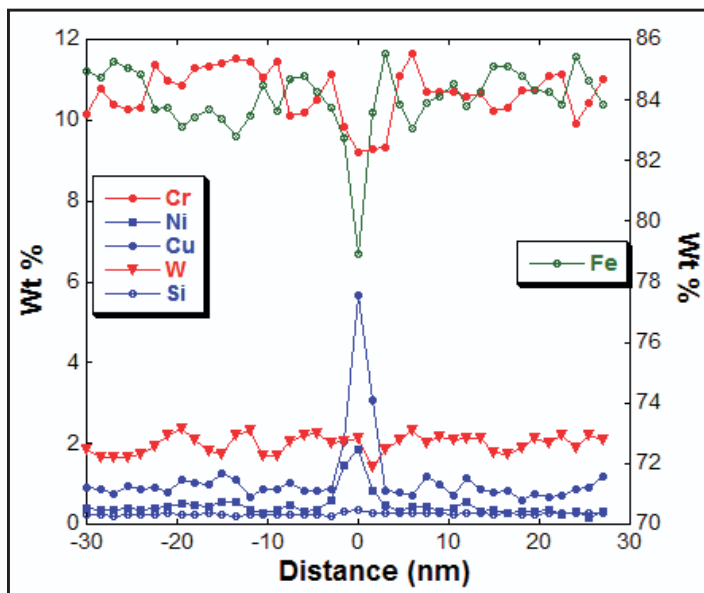
Figure 1. Typical composition profile crossing a GB in HCM12A irradiated to 7 dpa at 400°C.

Computational materials modeling is ongoing to investigate the mechanisms controlling microstructural and microchemical evolutions in ferritic/martensitic alloys following high-dose, high-temperature radiation exposure. One modeling activity is investigating the basic point defect thermokinetics that are at the foundation of radiation-induced segregation and precipitation. Researchers have obtained initial *ab initio* results on vacancy-mediated self-diffusion of Fe, as well as dilute Cr and Ni in Fe. Another modeling task is focused on modeling spatial development of irradiation-induced microstructures using cluster dynamics models.

In September 2008, the team placed tensile and TEM samples of several materials of interest into the advanced test reactor, and these materials will be irradiated to total doses of 3 dpa and 6 dpa at temperatures ranging from 300°C to 700°C.

In Situ TEM Characterization of FM Alloy Creep. The research team used *in situ* straining TEM to study creep mechanisms through observation of dynamic evolution/interaction among various defects (dislocations, stacking faults, and precipitates) under stress at elevated temperatures. For the *in situ* TEM analysis, the team used grinding, jet-polishing, and FIB thinning to prepare uniquely shaped TEM samples that fit into the recently acquired straining-heating holder. This holder can operate at high temperatures (up to 700°C) with large displacements (800 μm). The team conducted preliminary examinations at room temperature on an HT9 specimen. Figure 2 shows four successive images and their corresponding SAED patterns taken from an $M_{23}C_6$ precipitate in the alloy (indicated by a black arrow). Rotation of precipitates relative to the matrix has been observed during straining. A similar phenomenon was reported in polycrystalline Ni foils. Grain rotation during plastic deformation decreases the total GB energy in the system and relaxes stress concentration along the GB efficiently.
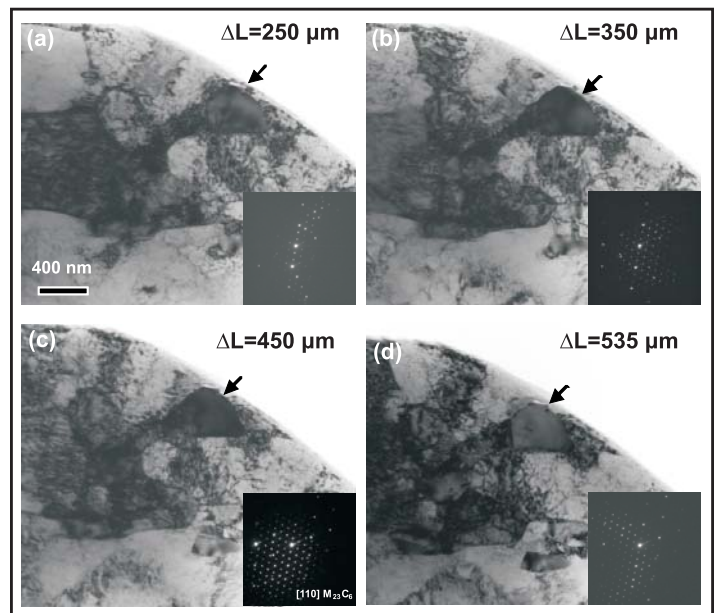
Figure 2. Low-magnification TEM images and SAED patterns of a T91 sample showing the rotation of an $M_{23}C_6$ precipitate under different displacements.

Barrier Layer Development. The project's primary challenge is to develop a science-based approach to modify a structural alloy's surface so it can produce and maintain a layer of dense alpha alumina. This layer acts as a barrier to the ingress of gas-phase contaminants and/or corrosive attack by fuel byproducts. At the temperature of interest (≤1,000°C), most alumina-forming alloys tend to form

transient phases that grow faster than alpha and have undesirable morphologies. The working hypothesis in this research, already demonstrated in the first year, is that alpha alumina may be produced at lower temperatures by reducing the oxidation rate through control of the oxygen partial pressure and suitably modifying the outer layer's chemical composition. Initial emphasis has been on IN617.

Researchers are exploring and comparing two approaches to surface modification: cladding with FeCrAl-Y/RE, a ferritic alloy (known for its ability to readily form alpha alumina), and aluminization by a vapor-phase process. Both approaches have been implemented. The team has successfully performed the first approach, cladding with commercial FeCrAlY foil (100 μm thick) by diffusion bonding. A suitable pre-oxidation approach is under development. Alpha alumina can be produced at pO_2 ≤0.1 ppb and 1,000°C, albeit accompanied by significant Cr interdiffusion with the substrate (even though the Cr content of both alloys is quite similar). Work is under way to create a Cr diffusion barrier layer, whereupon specimens will be supplied to the Michigan group for testing in He with various impurities.

Regarding the second approach, the team has developed a suitable aluminization procedure. Related interdiffusion and oxidation studies are in progress. Researchers have discovered that aluminization may be effected at relatively low temperatures (approximately 650°C), enabling the layer depth to be readily controlled. The team is using heat treatments to develop a surface-level phase constitution that enables alpha alumina to form at low temperatures.

Planned Activities

Continued studies on irradiation's effect on microstructures will focus on proton and heavy-ion irradiation of the multiple alloys of interest, which include a 9 Cr model alloy, 12 Cr model alloy, 9 Cr ODS, 14 Cr ODS, 18 Cr ODS, HT-UPS, HCM12A, NF616, HT9, T91, and D9. Alloys will be irradiated from 300°C to 700°C to doses of 10 dpa (protons) and 100 dpa (ions). After irradiating the alloys, researchers will characterize the materials to understand changes in microstructure and microchemistry. Irradiations will be performed on both bulk samples and TEM disks. Modeling efforts will continue, focusing on spatially dependent microstructural development and the effect of compositions on diffusion under radiation. Specifically, the atomic scale thermokinetic modeling will be extended to include interstitial energetics, and these will be combined with the vacancy energetics to yield a dilute model for defect diffusion and radiation-induced segregation. The program will link computational studies to microstructural features that develop in model alloys and link radiation-induced changes in model alloys to commercial alloys. Finally, researchers will use samples placed in the advanced test reactor to compare microstructural changes in the ion-irradiated materials to microstructural changes of neutron-irradiated materials.

To study creep mechanisms, researchers will conduct *in situ* TEM of rotation and morphological change of precipitates, dislocation, and GB movement under tensile stress in HT9 and T91 during straining at elevated temperatures (up to 700°C). The research team will also begin irradiation creep testing of SiC and T91 alloys at temperatures relevant to expected core conditions.

The team will emphasize identifying the right conditions for generating the alpha-alumina barrier in IN617 and supplying specimens to the University of Michigan for testing. The approach will be extended to the ferritic steels, including assessment of diffusional compatibility with FeCrAlY layers and behavior of aluminized layers.

NUCLEAR ENERGY RESEARCH INITIATIVE

5.2 Advanced Fuel Cycle Initiative

There are 33 NERI research projects currently being performed that closely relate to the research goals of the Advanced Fuel Cycle Initiative. Thirteen were awarded in FY 2006 and 20 were awarded in FY 2007 (12 NERI and 8 NERI-C).

The mission of AFCI is to enable the safe, secure, economic, and sustainable expansion of nuclear energy by conducting R&D focused on nuclear fuel recycling and waste management to meet U.S. needs. In this way, nuclear energy can satisfy the growing energy needs of the United States while improving management of waste requiring geologic disposal.

To meet the program's objectives, several technologies need to be developed to allow closing of the fuel cycle: first, technologies to separate the used nuclear fuel into products that can be reused and wastes that must be disposed of safely; second, technologies to transform the products into fuels that can be reused in reactors; and third, reactors that use the recycled fuel to produce energy. For long-term sustainability, a new type of reactor is needed, using fast neutrons—initially for improved waste management as we transition to a closed fuel cycle and address the stocks of used fuel that have accumulated, and later for resource extension as uranium resources become more scarce and expensive.

Advanced safeguards technologies and techniques will be developed to ensure reduced proliferation risk. Resulting technologies from this work will satisfy requirements for a controlled, proliferation-resistant nuclear materials management system. This is accomplished by division of the program activities into a few key R&D campaigns:

- Separations and Waste Forms
- Transmutation Fuels
- Advanced Safeguards
- Transmutation Science and Engineering
- Sodium Fast Reactor
- Systems Analysis
- Advanced Modeling and Simulation

The chief goals of AFCI are to 1) reduce the environmental and financial burden and uncertainty associated with long-term nuclear waste management; 2) optimize nuclear waste management by minimizing the risk of waste that needs to be handled or stored, producing only solid wastes in robust waste forms, and recycling and reusing materials to the extent practical; 3) recover the unused energy value of materials separated from used nuclear fuel for future use; 4) ensure the ability to safeguard the advanced fuel cycle facilities by developing technologies to more accurately account for, track, and manage nuclear materials; 5) develop options that would make the closed fuel cycle as safe and cost-effective as possible; and 6) support the establishment of a regulatory framework for licensing and permitting of fuel cycle facilities.

During FY 2008, a number of research projects targeted the separation of actinides and lanthanides by several techniques (aqueous process with redox, aqueous process with soft donor atoms, and UREX+). Much work is taking place in the advanced fuel development area. Projects involve analytical studies and modeling techniques, developing and optimizing materials, developing fuel processing and fabrication techniques, and improving fuel coatings. Transmutation projects are targeting alloys for the advanced burner reactor, transuranic transmuters, and minor actinide recycling with boiling water reactors. Systems analysis projects are developing and optimizing computer models for fuel cycle analysis, using those codes to evaluate different scenarios, and conducting fuel cycle economic evaluations. Two new projects are improving SFR simulation methodology and measurement techniques.

Research efforts under the FY 2007 NERI-C projects related to the AFCI program focus on separations systems and analysis; fuel performance, measurements, and radiation effects; risk-informed analysis and computational tools; and small export reactors.

For more information about AFCI, refer to this website: http://www.nuclear.energy.gov/AFCI/neAFCI.html.

An index of the research being performed under this program follows, along with a summary of each project.

NUCLEAR ENERGY RESEARCH INITIATIVE

Directory of Advanced Fuel Cycle Initiative
Project Summaries and Abstracts

NUCLEAR ENERGY RESEARCH INITIATIVE

NUCLEAR ENERGY RESEARCH INITIATIVE

Radiation Stability of Candidate Materials for Advanced Fuel Cycles

PI: Todd Allen and James Blanchard, University of Wisconsin-Madison

Collaborators: None

Project Number: 06-007

Program Area: AFCI

Project Start Date: March 2006

Project End Date: March 2009

Research Objectives

This project will use proton irradiation to further understand the microstructural stability of ceramics being considered as matrix material for advanced fuels. Following are the specific goals of this work:

- To determine the radiation stability of candidate materials in response to proton irradiation at temperatures between 600°C and 900°C. Following irradiation, researchers will examine samples using transmission electron microscopy (TEM) to understand the effect of radiation on lattice stability, phase change, void growth, and other microstructural features.

- To determine the effect of radiation on hardness and fracture toughness in response to proton irradiation at temperatures between 600°C and 900°C. Estimates of the relative changes in fracture toughness as a function of radiation will be made using crack length propagation following Vickers indentation.

- To perform structural analysis using finite element analysis, determine the limiting performance of these ceramic fuel matrices, identify promising candidate materials for advanced reactors, and identify pressing data needs.

Researchers will test the following materials: titanium carbide (TiC), zirconium carbide (ZrC), titanium nitride (TiN), zirconium nitride (ZrN), magnesium oxide (MgO), magnesium oxide-zirconium dioxide (MgO-ZrO$_2$), and magnesium oxide-zirconium dioxide-dierbium trioxide (MgO-ZrO$_2$-Er$_2$O$_3$).

Research Progress

During the past year, researchers performed additional proton irradiation experiments at 900°C to various doses, as listed in Table 1, and initiated characterization of these samples. Additionally, they continued to characterize the samples irradiated to 800°C using TEM, x-ray diffraction (XRD), micro-hardness, and nanoindentation tests.

Material		CERCOM	CEA
Accumulated Damage	ZrC	1.5 dpa, 0.7 dpa	
	ZrN	1.5 dpa, 0.7 dpa	
	TiN		1.0 dpa, 0.5 dpa
	TiC	1.0 dpa, 0.5 dpa	

Table 1. Conditions for proton irradiation testing of candidate ceramic materials at 898±27°C. CERCOM and CEA indicate two different producers of material.

The microstructure of the 800°C irradiated ZrN sample is very different from that of irradiated ZrC. Defect structures are tightly associated with Moiré fringes and the damage structures mainly display as many elongated black spots with some preferential orientations, as shown in Figure 1(a). For 800°C irradiated TiN, the irradiated microstructure was dominated with pre-existing dislocations, as shown in Figure 1(b). In addition, high-resolution micrographs taken of TiN show no loop formation in the material irradiated to 0.5 dpa; the 1 dpa sample remains under investigation.
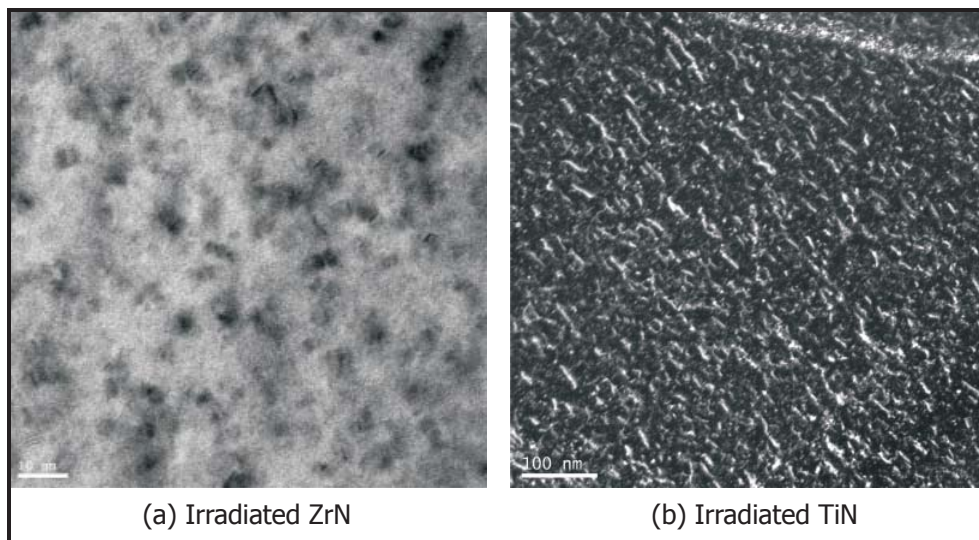
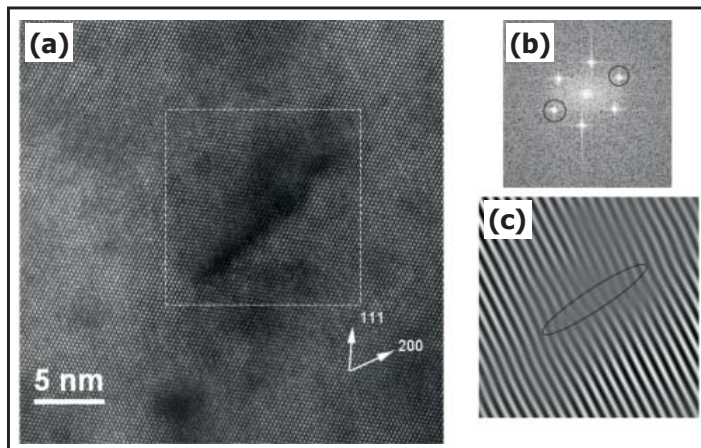Figure 1. TEM images of ZrN and TiN irradiated at 800°C.

Figure 2. (a) [110] lattice image of planer-like defect, (b) Fourier transformation of selected area, (c) Fourier-filtered [200] diffraction lattice images revealing the pyramidal dislocation loops.

Figure 2(a) shows an image of a typical planar-like defect projected as streaks along the = [011] direction. After masking the 200 diffraction spots and applying an inverse Fourier transformation (Figure 2(b)), a pyramidal dislocation loop is clearly displayed. As shown in Figure 2(c), the defects appear as two opposite-signed dislocations (dipole) between which there exists a region of lattice distortion.

The irradiated microstructures for the 900°C irradiation are very different from those of the 800°C irradiation (Figure 3(a)). No high density of faulted loops was observed in ZrC up to a dose of 1.5 dpa. The microstructures are featured with a high density of black spots associated with an orientated streak core. Another clear feature, as shown in Figure 3(b), is the clusters of the nano-size bubbles along the grain boundary, while no bubbles or cavities are found inside the grains. For the TiC irradiated at 900°C (Figure 3(c)), some defect clustering was observed while no distinct line contrasts were found, which are indicative of dislocation loops identified in 800°C irradiations.
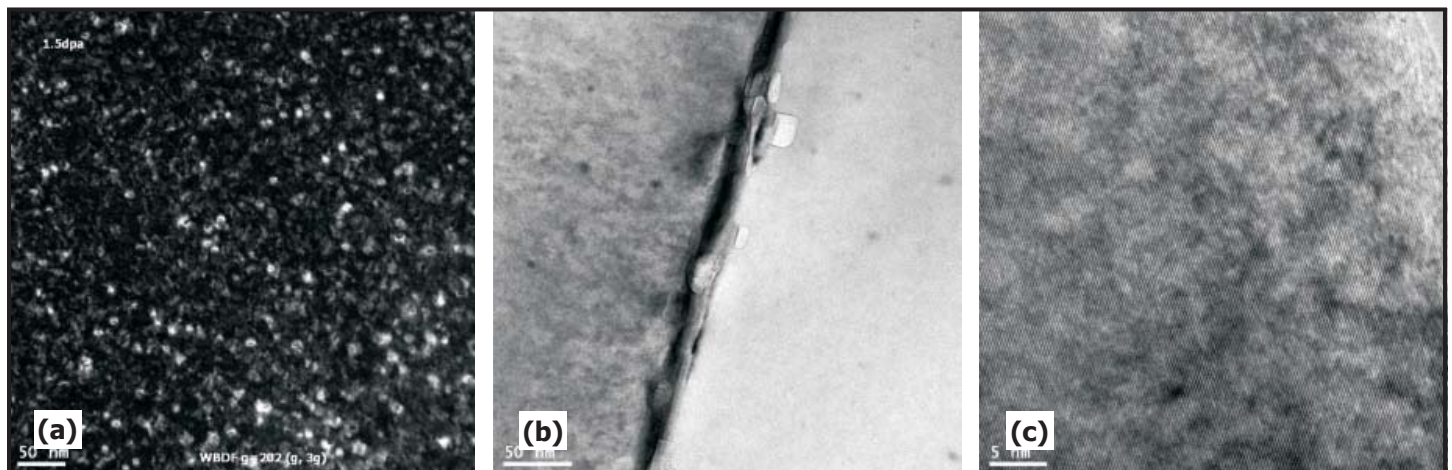

Figure 3. (a) TEM images of 900°C irradiated ZrC and TiC; (b) ZrC irradiated to 1.5 dpa; and (c) TiC irradiated to 1 dpa.

The micro-hardness changes of the four ceramic materials over a range of doses and temperatures are summarized in Figure 4, showing that the hardening effects of 900°C irradiation are much less pronounced than at 800°C.
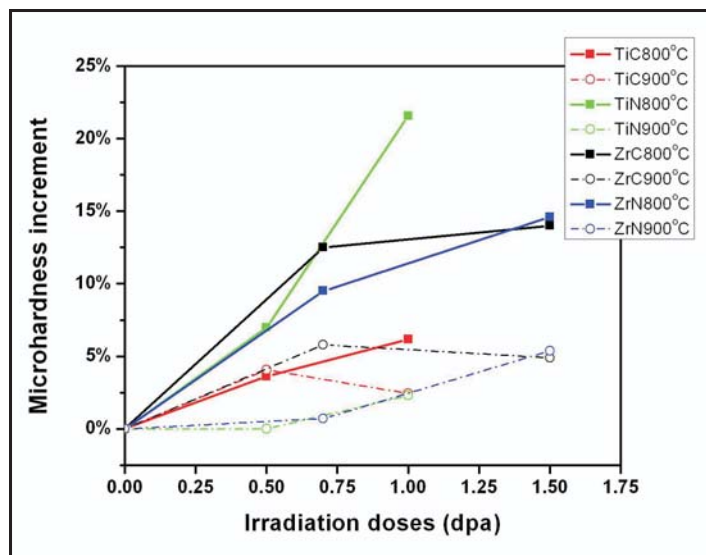

Figure 4. Irradiation hardening of ceramics at various temperatures and doses.

Regarding the inert matrix fuel (IMF), researchers have solidified a procedure for synthesizing $MgO-ZrO_2$ dual-phase ceramics and successfully produced several batches of MgO and $MgO-ZrO_2$. They also evaluated magnesia and dual-phase magnesia-zirconia ceramics as potential inert matrix materials for radiation resiliency under heavy ion irradiation using XRD, micro-hardness, and nanoindentation techniques.

Planned Activities

For the upcoming research year, the characterization of 900°C irradiated samples will continue, along with irradiation at 600°C and higher dose irradiation at two other temperatures. With these three proposed temperatures (600°C, 800°C, and 900°C) and three dose levels (0.5 dpa, 1 dpa, and >2 dpa), the microstructure evolution versus irradiation conditions can be more effectively understood. Additionally, a systematic evaluation of the radiation effects on mechanical properties using micro-hardness testing and nanoindentation will also be continued.

Researchers will perform a comprehensive study on the heat treatment and phase transformation of IMF material during sintering and examine the radiation response of fabricated materials using proton irradiation. Ultimately, this research will provide some understanding on the radiation stability of ceramics being considered as matrix material for the advanced fuels.

NUCLEAR ENERGY RESEARCH INITIATIVE

Solution-Based Synthesis of Nitride Fuels

PI: Ken Czerwinski and Dan Rego, University of Nevada–Las Vegas

Collaborators: Los Alamos National Laboratory, Argonne National Laboratory

Project Number: 06-012

Program Area: AFCI

Project Start Date: September 2006

Project End Date: August 2009

Research Objectives

The objective of this project is to develop a solution-phase process for synthesizing actinide nitrides for use in nuclear fuels. The current process entails carbothermic reduction from the oxide to the nitride, based on a stepwise process of solid-phase reactions from the metal oxide to the carbide, and finally to the nitride. This high-temperature, solid-phase synthesis process is plagued by impurities in the final nitride product and difficulties in production, creating major drawbacks in using nitride fuels for advanced reactor designs. Direct synthesis of the nitride by a solution route could eliminate or minimize the impurities and other synthesis problems. The proposed solution route to nitride has the added benefit of providing several adjustable parameters that would allow control over properties of the final solid product.

This project builds upon recent investigations by collaborators into amido reactions in non-aqueous solvents:

$$AnI_3(solv)_4 + 3\ NaNR_2 \rightarrow An(NR_2)_3 + 3\ NaI + solv$$
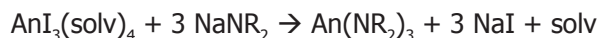
From this result, the following is a plausible route for the synthesis of nitride fuels:

$$AnI_3 \xrightarrow[NH_3(l)]{} AnI_3(NH_3)_4 \xrightarrow[3NaNH_2]{} An(NH_2)_3 \xrightarrow{\Delta, -2NH_3} AnN$$
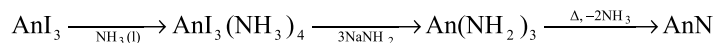
where An is an actinide fuel (uranium, neptunium, plutonium, or americium). The non-aqueous synthetic route based on amido chemistry potentially provides property control over the nitride product similar to the sol-gel methods for actinide oxides. The resulting nitride product should be free of the impurities inherent in the carbothermic reduction technique.

The project is divided into three primary tasks: 1) characterization and optimization of uranium amide/imide formation from both trivalent and tetravalent starting materials and their further conversion to nitrides, 2) examination and optimization of nitride metathesis reactions, and 3) investigation of the above routes via inorganic and organoactinide modeling complexes.

Research Progress

Researchers obtained and set up equipment necessary for low-valent (i.e., U^{3+} and U^{4+}) chemistry, including the Schlenk line, an inert atmosphere glove box customized for solvent handling and work-up, and basic vacuum-line work. They also obtained starting materials for uranium (U), including $UI_3(THF)_4$, UI_3, and UCl_4, as well as various organouranium halide modeling compounds and other materials.

The research team has undertaken both $UI_3(THF)_4$ and UCl_4 reactivity with $NaNH_2$ in liquid NH_3. Infrared (IR) identification of amide/imide overtone absorbances indicates formation of amide/imide complexes from this low-temperature reaction. Elemental analyses are under way, as are further attempts at conversion via application of mild heat and vacuum.

Researchers are investigating the chemistry and product formation of these systems via modeling compounds. The $UI_3/NaNH_2$ reaction was investigated using $(C_5Me_5)_2UI(THF)$ as a UI_3 analog, as shown in Equation 1.
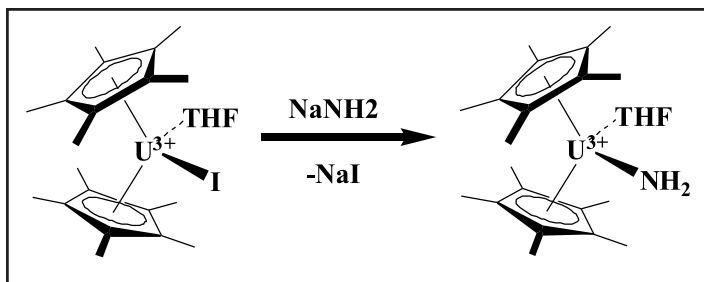
Equation 1.

The uranium oxidation state can be monitored by the near IR. In this region, U(III) shows Laport forbidden $f \rightarrow f$ transitions. The near IR of the above reaction shows the reaction product to have lost much of the absorbances attributed to the starting material's trivalent state (see Figure 1). This may suggest a subdued absorbance in the region of the near IR while retaining trivalent oxidation; however, additional examination of both U(III) and bonafide U(IV) compounds indicates oxidation of the uranium to U(IV), perhaps via conversion of the amide to an imide. Researchers are employing various ligands such as (C_5Ph_5)-, (C_5Me_5)-, $[N(SiMe_2Ph)_2]$-, and scorpionates (e.g., $[HB(3PhPyrazole)_3]$-) to model these reactions and help investigate other non-aqueous nitride syntheses, as shown in Figure 2.

Use of these ligands also allows for a non-aqueous-based solvent synthesis of nitrides via metathesis with other nitride salts, such as Li_3N. Researchers have already seen positive reactivity with the use of uranium scorpionate ligands and have begun analyzing these reactions.

Metathesis with Li_3N also indicates potential for uranium nitrides via solid state routes. As is shown in Figure 3, researchers have already achieved the formation of UN via UI_3 and Li_3N, albeit in low initial yield. Optimization of this process is currently under way.
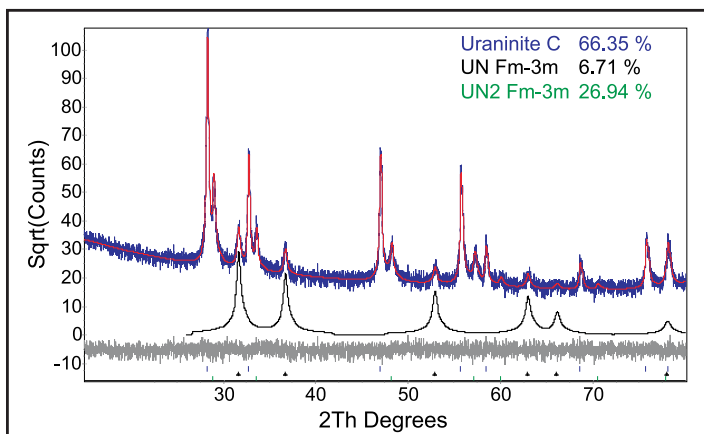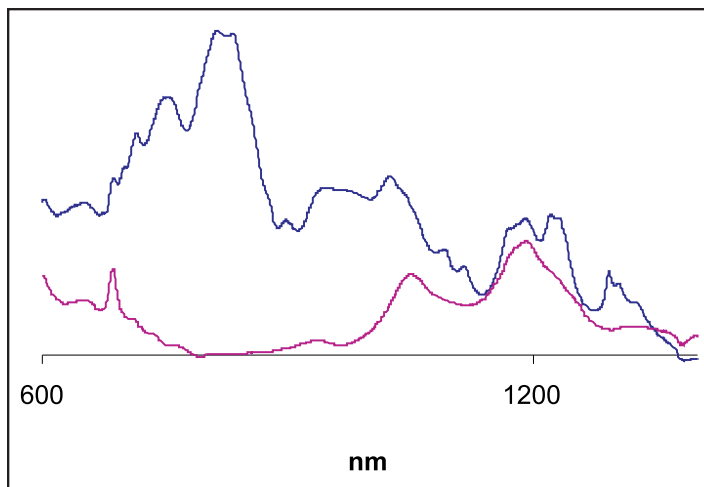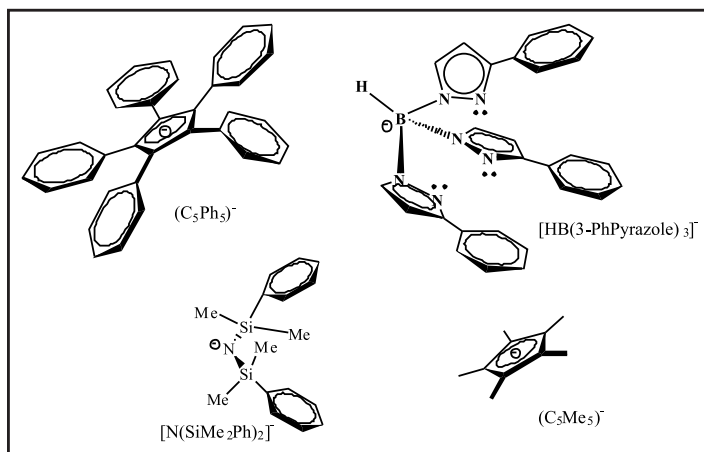

Figure 1. Comparison of $(C_5Me_5)_2UI(THF)$ near IR (top) and its reaction product with $NaNH_2$ (bottom).

Figure 2. Various ligands used with uranium.

Planned Activities

The following planned activities are associated with each of the three primary tasks:

1) Further characterization and optimization of uranium amide/imide formation from both trivalent and tetravalent starting materials and their further conversion to nitrides

   ➤ Full identification of initial mixture formed from liquid NH_3 reaction

   ➤ Examination of conversion to nitride via monitoring of heat/vacuum variations

   ➤ Extension to other actinides—both trivalent and tetravalent starting materials

Figure 3. Powder x-ray diffraction pattern of washed and sintered reaction products from UI_3/Li_3N reaction, with UN spectrum highlighted.

2) Examination and optimization of nitride metathesis reactions

- ➤ Optimization with U^{3+} starting material

- ➤ Extension to U^{4+} starting materials

- ➤ Extension to other actinides (both An^{3+} and An^{4+})

- ➤ Formation of An^{3+} nitrides via subsequent use of alkali metal-reducing agents

- ➤ Formation of An^{3+} from An^{4+} starting materials via trimetallic reduction/metathesis concomitant co-reaction

3) Investigation of the above routes via inorganic and organoactinide modeling complexes, including investigation of reactivity beyond liquid NH_3 in less reactive non-aqueous solvents

NUCLEAR ENERGY RESEARCH INITIATIVE

The Development and Production of Functionally Graded Composite
for Lead-Bismuth Service

PI: Ronald G. Ballinger, Massachusetts Institute of Technology (MIT)

Collaborators: Los Alamos National Laboratory (LANL)

Project Number: 06-038

Program: AFCI

Project Start Date: April 2006

Project End Date: April 2009

Research Objectives

The objective of this project is to produce materials that meet both the corrosion and structural requirements of liquid lead and supercritical water systems at temperatures up to 700°C in a neutron flux environment. Lead and lead-bismuth (Pb/Pb-Bi) eutectic corrode fuel cladding and structural materials, which limits the compounds' use as coolants in advanced liquid-metal-cooled fast reactor and transmutation systems. In addition, the existing upper temperature limit—approximately 550°C for operation of these systems, dictated by corrosion concerns—is insufficient.

A new series of iron-chromium-silicon (Fe-Cr-Si) alloys provides several advantages: 1) formation of a protective film over a wide range of oxygen potentials; 2) minimal solubility in liquid metals, which may occur in crevices or other oxygen-depleted areas; and 3) resistance to corrosion in Pb/Pb-Bi eutectic at temperatures up to 700°C. Initial testing indicates that these materials are resistant to stress corrosion cracking degradation in supercritical water systems and that the formation of a Cr-Si-based dual oxide layer provides a high degree of protection.

In this work, researchers will produce functionally graded composites, consisting of a corrosion-resistant layer on a structural alloy, in two forms of tubing suitable for either pipe or fuel-cladding applications. Two structural alloy systems will be used for each product form: quenched and tempered (Q&T) and—resources permitting—oxide dispersion strengthened, which will be fabricated using standard commercial practice. The researchers will test the materials produced for corrosion resistance and structural properties. The clad alloy can also be fabricated in the form of welding wire for use as an overlay for more complex shapes.

Research Progress

The project is being conducted in four major tasks: 1) cladding/piping procurement, 2) corrosion testing, 3) diffusion testing, and 4) mechanical properties determination.

Cladding/Piping Product Procurement. Researchers are attempting to produce a functionally graded composite material consisting of a dominant structural layer based on the Fe-Cr-C alloy system, with a surface overlay layer of a high Si ($\geq$ 2.55 wt%) Fe-12%Cr-Si alloy. The structural layer materials will be a 9Cr-1Mo-based commercial Q&T alloy—currently identified as T/P91. The cladding production process makes use of standard commercial practice: 1) produce an extrusion billet by direct melting, 2) process the starting ingot to extrusion billet size by forging, 3) weld overlay the extrusion billets, 4) pre-machine the extrusion billets, and 5) reduce the extrusion billets by a combination of hot extrusion/roto-rolling (Pilgering) to final pipe-product dimensions for that form and to pre-drawing dimensions for the fuel-cladding final product form. The cladding product form will then be further reduced by redrawing to the final product dimensions.

Weld wire is being produced for use in the cladding process. The weld overlay wire composition chemistry has been fixed at Fe-12%Cr-2.5%Si, and the final diameter is 0.035". Special Metals processed the material and shipped it to researchers at MIT. The process yielded 120 pounds of 0.218" wire rod and about 440 pounds of 0.525" rod in

various lengths from 8' to 20'. MIT retained some samples for mechanical properties' testing; the remainder was sent to Electrode Engineering for fabrication of the final product.

The project has identified Artisan Welding to provide weld overlay services. The team located an automatic welding robot at Bor-Tech.

To produce the Q&T steel-based product, the project has settled on T91 tubing as the basis for the material. The H.C. Starck Company is processing extrusions to a diameter of 3". The Timken Company is then drawing the Starck product to approximately 2"; Timken is producing both the pipe product form and the initial tube-reduced extrusion (TREX)/draw of the fuel-cladding product form. The TREX/draw product is then redrawn by Superior Tubing Company to produce the final fuel-cladding product form.

Corrosion Testing. The product forms will be tested for corrosion resistance in three MIT facilities: 1) a supercritical water testing facility, 2) a thermal convection loop that will be constructed using the piping product form produced during the first task of the project, and 3) the rotating electrode high-temperature facility. All product forms will be tested.

The team has cleaned the liquid Pb-Bi furnace, calibrated its sensors, and set up a new data acquisition system to replace an older, more limited system. The system now has the capability to deliver 5%H_2 in argon reliably, remove all moisture and oxygen from the stream, and analyze multiple inlet and outlet gas streams at once. The system also now has computer control over the gas streams, allowing a multiplexed gas analysis system to analyze many streams in one pair of sensors, saving money and providing sensor redundancy in the system. Sensor redundancy ensures that if a sensor fails, the computer will recognize it and switch to a new sensor, continuing the test.

The loop has been modified to accommodate both oxidizing and reducing conditions at the same time in parallel furnaces, allowing experiments to proceed at double the speed.

The first samples of T91 and 12Cr2Si finished their 168-hour run in the furnace. The project team sectioned and polished the samples to prepare them for analysis.

The team also performed 700°C lead-bismuth eutectic (LBE) testing for the two materials. Team members set up a reducing furnace with an H_2/H_2O ratio of over 1,000, making the furnace condition reducing to all oxides except for Cr_2O_3 and SiO_2. The oxidizing furnace has a carefully controlled H_2/H_2O ratio between 8 and 18, depending on the temperature of the test, in order to keep the oxygen potential between that of $FeSi_2O_4$ and Fe_3O_4.

Researchers are conducting a detailed microstructural analysis of each sample. Analysis techniques include standard metallographic, scanning electron microscopy, and x-ray techniques. Both alloys appear to resist LBE corrosion quite well. The presence of oxides has been suggested by the formation of a thin film at the LBE liquid line, but sample integrity appears to have been completely preserved. The team used ICP-mass spectroscopy to analyze small samples of T91, 12Cr2Si, the as-received lead, bismuth, and post-corrosion LBE. Researchers looked for impurities and solutes to determine both impurity levels in the setup and dissolution rates into the LBE. The team concluded that contamination from the furnace sealant may have affected the test results, so these experiments will be repeated. Figure 1 shows samples as they exited from the highly reducing LBE furnace after 168 hours.
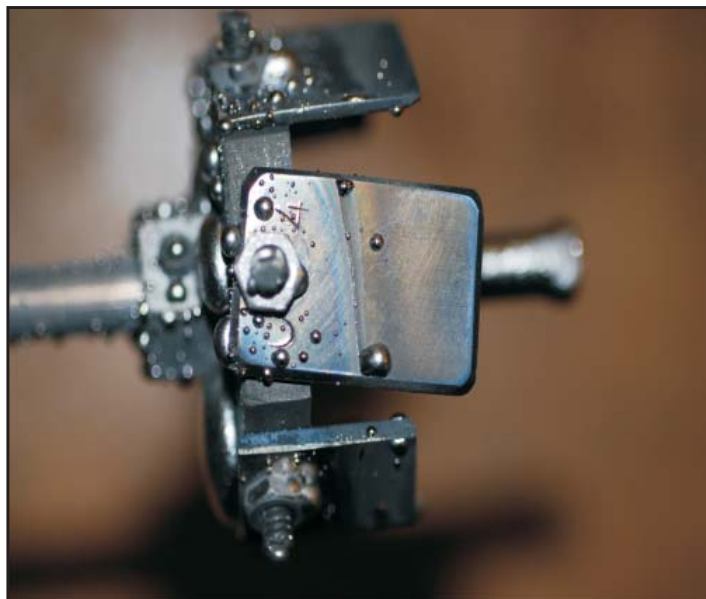

Figure 1. An example of 12Cr2Si sample after 168 hours of exposure to LBE at 700°C.

The results of the corrosion testing, both at MIT and in the DELTA loop at LANL, are being incorporated into an overall model for the corrosion process. The model will be used to allow extrapolation of test data to engineering system-relevant times.

Researchers have performed simple models of the diffusion of Si through T91 to get a rough estimate of the expected diffusion constant. The simple model predicted that in a sharp interface between the alloys, it will take months to notice a one percent change in Cr or

Si concentration at a distance of one micron, indicating initially that diffusion may not be much of a problem in terms of the materials staying resistant to LBE over their lifetimes. More importantly, longer-term modeling has shown that the Si level is expected to drop to 1.25 percent (the project's lower limit) at a distance of 3.9 mils into the material over 50 years, which would mean that diffusion would not compromise the fuel cladding before the end of its life.

Researchers determined that they will need a full diffusion model that allows for concentration-dependent diffusion coefficients. The team has defined and is now developing a more detailed model.

Diffusion Testing. The composite system will achieve its corrosion resistance via the presence of a high Si layer on the surface exposed to the environment. The project has initiated a task to evaluate the diffusion of Si between the protective layer and the T/P91 material that will be used for the structural substrate material.

Six diffusion couple "blanks" have been produced by hot isostatic pressing at Ultraclad, Inc. Having aged the blanks, the team is now evaluating the degree of Si mixing. After optically analyzing the 800°C diffusion couples, researchers believe that the A1 phase transformation for Fe-12Cr-2Si with carbon may be lower than 800°C, due to the lack of pearlite in the carbon-rich area of the 12Cr2Si-side interface. Therefore, the team will carry out tests at 700°C to determine the validity of the 800°C tests. Diffusion couples for these tests have been HIPed and are currently being ampouled.

The team has performed electron microprobe analysis on the 300-hour, 600-hour, and 1,200-hour samples, and all show a characteristic "error function" diffusion profile. Calculated diffusion constants have been used in the diffusion model to predict end-of-life corrosion resistance. Figure 2 shows a graph of the predicted diffusion profile results for this composite, and Figure 3 shows the Si diffusion profiles for all samples tested so far.

Mechanical Properties Testing. In order for the program to be successful, the materials must meet both the corrosion and the structural alloy requirements. Mechanical properties of the fabricated components must be explored both at room temperature and in the 600°C to 700°C temperature range. The mechanical testing takes the form of tensile and 1,000-hour stress rupture tests.
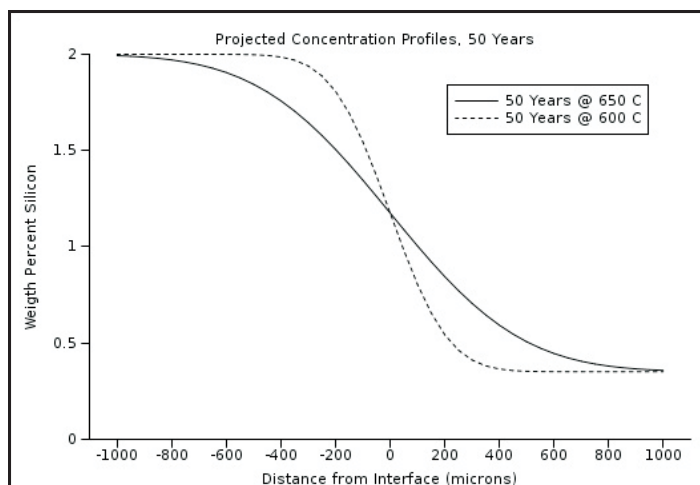

Figure 2. Projections of the expected Si profile at end-of-life for a typical high-temperature LBE fast reactor.
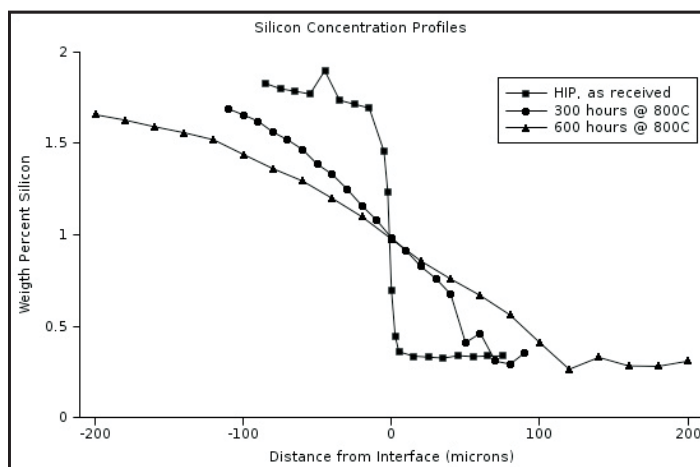

Figure 3. Actual data from the 800°C diffusion couple tests.

Researchers used a LECO microhardness testing machine to test all the 800°C diffusion couples and as-received specimens of T91 and 12Cr2Si. Knoop hardness tests show that T91 is much harder than 12Cr2Si, as expected. The team acquired hardness profiles for each diffusion couple in order to indirectly measure carbon content and diffusion. Carbon diffusion has been shown to be very fast, even when compared to Si diffusion. The speed suggests that there will be a gradual hardness profile, rather than a step change, that will further enhance the mechanical properties of the cladding and interfacial layer of the composite.

Planned Activities

The project is now focusing on the following areas:

- Producing the weld wire
- Producing the composite, including overlaying the weld wire and extruding the composite
- Continuing corrosion testing of both archived and new material from the composite program
- Continuing the diffusion studies, including tests at 700°C
- Commissioning the supercritical water experimental facility

NUCLEAR ENERGY RESEARCH INITIATIVE

Flexible Conversion Ratio Fast Reactor Systems Evaluation

PI: Neil E. Todreas and Pavel Hejzlar, Massachusetts Institute of Technology (MIT)

Collaborators: None

Project Number: 06-040

Program Area: AFCI

Project Start Date: March 2006

Project End Date: May 2008

Research Objectives

The objective of this project is to design a flexible conversion ratio (CR) fast reactor system that enables time-dependent management of fissile inventories and higher actinides. The goal is to produce a single reactor design capable of being configured to achieve 1) CRs near zero in order to transmute legacy waste and 2) CRs near unity for operation in a sustainable closed cycle.

Both designs utilize a consistent plant rating of 2,400 MWt, and forced circulation will cool the reactor cores during normal operation to achieve high power density of at least 100 kilowatts/liter. To be more economically competitive, power conversion systems will eliminate the intermediate heat transfer loop. Safety and core integrity will be achieved through a self-controllable reactor design that ensures safe shutdown for all key transients. Eliminating blankets will enhance proliferation resistance, as will using transuranics (TRUs) as fuel without separating plutonium.

The research team will develop two candidate liquid coolant core designs—lead and liquid salt—which the team will then cross-compare against each other and two other reactor designs: 1) a supercritical carbon dioxide-cooled reactor (being developed for another MIT project) and 2) the sodium-cooled reactor (being developed by Argonne National Laboratory [ANL]). This comparison will help decision-makers select the most attractive large high-power-density fast system for closed fuel cycles in countries with fuel service centers.

Research Progress

Researchers have developed four candidate flexible CR fast reactor coolant designs. The designs utilize a 2,400-MWt rating and a four-train supercritical CO_2 power

conversion cycle, and their performances were compared on a consistent basis. Figure 1 depicts one 300-MWe train. The lead-cooled fast reactor (LFR) and liquid salt-cooled fast reactor (LSFR) fully designed in this project have cores placed in a large pool-type vessel with a dual-free level, which also contains four intermediate heat exchangers (IHXs) coupling a primary coolant to a compact and efficient supercritical CO_2 Brayton cycle power conversion system. An enhanced reactor vessel auxiliary cooling system (RVACS) and a supplementary passive secondary auxiliary cooling system (PSACS) passively remove decay heat. The team adopted several of the most promising RVACS enhancements: a combination of a liquid metal bond in the gap between the reactor vessel and guard vessel, a perforated plate in the air gap, and a dimpled guard vessel wall. The PSACS consists of 4x50 percent safety-grade cooling loops connected to CO_2 IHX inlets, which remove decay heat through natural circulation of CO_2 into a passive auxiliary heat exchanger, which is submerged in an in-containment water storage tank.
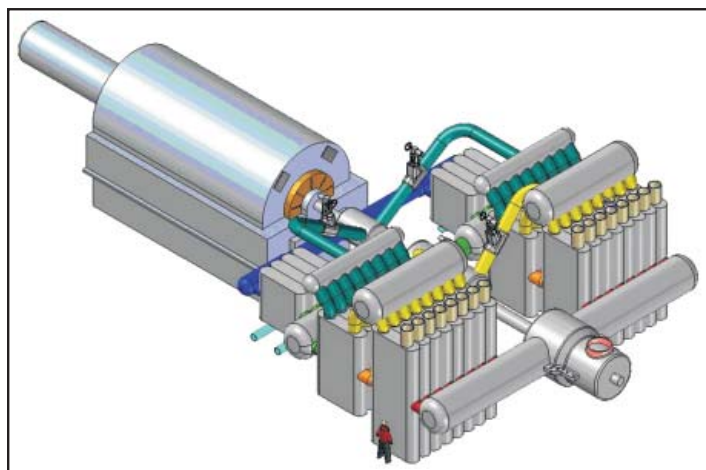

Figure 1. One of four 265-MWe trains of an SCO_2 power conversion system.

The lead-cooled core contains 349 canned fuel assemblies, each having 21x21 pin positions in a square lattice. In the CR=0 core, each fuel assembly has control rods with 25 rodlets inserted into guide tubes in the central 5x5 positions of the assembly. All control rods are double-entry design to minimize reactivity changes during seismic events and to flatten the axial power profile. The CR=1 core requires significantly fewer control rods due to its smaller reactivity swing; hence, only one-third of the assemblies are equipped with control rods. During the transition from the CR=0 to the CR=1 core, excess control rods can be removed and head penetrations plugged.

The CR=1 core is a one-batch, three-region core using metallic uranium-transuranic-zirconium (U-TRU-Zr) fuel, where the composition of TRUs corresponds to that of discharged light water reactor fuel with 50 MWd/kg burnup. To maintain low power peaking during core life, the project uses Zr content adjustment, rather than TRU enrichment grading, to vary heavy metal loading between different core regions. Therefore, the core contains three regions, each with a different Zr weight fraction (10 wt%, 15 wt%, and 19 wt%) and thus different U (75 wt%, 70.8 wt%, and 67.5 wt%) and TRU (15 wt%, 14.2 wt%, and 13.5 wt%) weight fractions, while the TRU-to-heavy metal ratio remains fixed. The maximum radial power peaking is maintained low, that is, 1.21 at middle of life. The cycle length for a single-batch core reload is 1,800 effective full power days (EFPD) (about 5.5 years at 90 percent capacity factor) and is limited by cladding peak fluence.

The CR=0 lead-cooled core is a three-batch core with TRU-Zr fuel to accommodate a large reactivity swing. The initial fuel composition of 34 weight-percent TRU and 66 percent Zr matrix resulted in a fuel cycle length of about 550 EFPD, corresponding to 1.7 years of operation at a 90 percent capacity factor. Fuel was driven to a discharge burnup of 400 MWd/kgHM. This high burnup was achieved because of a small heavy metal weight fraction in the pins. This is not expected to pose a problem for two reasons: 1) the fission gas release that drives fuel swelling is comparable to that of a CR=1 core because the total number of fissions for the two cores is comparable, and 2) more Zr diluent in the pins provides more volume, which can accommodate heavy metal swelling. The CR=0 core has higher power peaking than CR=1, but the proposed fuel-management strategy makes it possible to maintain radial power peaking below 1.35. The TRU consumption rate is 1,282 kg/yr, or 0.32 kgTRU/yr/MWth. This exceeds the TRU destruction rate of accelerator-driven systems, such as accelerator transmutation of waste (ATW), which reported the value of 0.262 kgTRU/yr/MWth and is due to the higher capacity factor of a critical reactor. Reactivity coefficient ratios for both CR=1 and CR=0 cores fell within the range, also satisfying the ANL self-controllability criteria.

For the salt-cooled reactor, the project team developed the CR=1 core design with lithium expansion modules (LEMs) that satisfies the core self-controllability criteria. The design employs a hexagonal lattice with a P/D of about 1.19 and a larger heavy metal loading than the lead-cooled core. The core features a reasonable radial power distribution and low peaking factor—below 1.3—throughout the fuel cycle. The achievable power density is 130 kW/l. Similar to the lead-cooled core, the CR=1 liquid NaCl-KCl-MgCl$_2$ salt-cooled core has three radial zones with different Zr-to-HM ratios in order to tailor the power peaking and maintain a nearly steady power profile during irradiation. The cycle length is about 1,900 EFPD to satisfy the 4×10^{23} n/cm^2 fast fluence limit. Figure 2 shows the final core layout indicating three zones and positions of double-entry control rods.
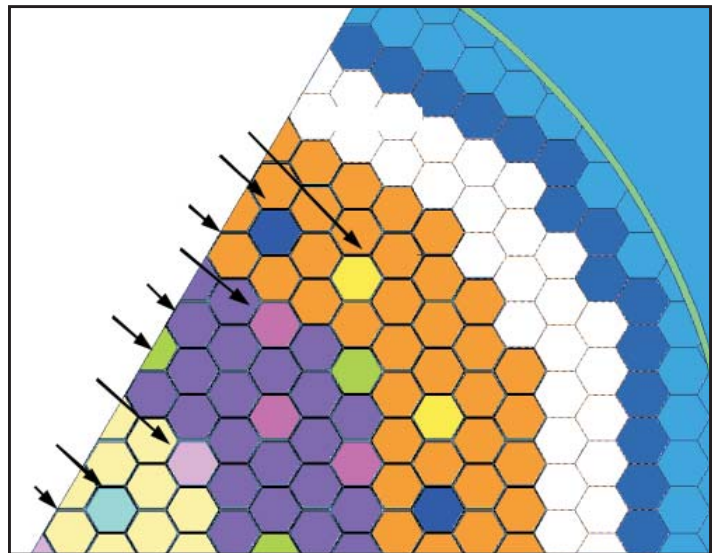

Figure 2. Liquid salt-cooled core layout.

The project team based the design of the CR=0 salt-cooled core on the tight lattice core (P/D=1.19) with 130 W/cc power density. As in the lead-cooled case, the team adopted three-batch fuel management for the salt-cooled core, which achieves fuel cycle length of about 540 EFPD. They developed the fuel-loading pattern to provide reasonable radial power peaking factors. In the current design, the maximum radial power peaking factors are below 1.35, which is comparable to the lead-cooled core. The achievable discharge fuel burnup is 340 MWd/kg, which corresponds to about a 36 percent TRU burnup fraction. Because of the less positive coolant temperature reactivity coefficient and less negative Doppler feedback of the CR=0

core, the CR=0 core needs half the LEMs required by the CR=1 core (12 versus 24).

To confirm that the proposed lead- and salt-cooled core designs can satisfy cladding and fuel-temperature limits, the project team performed three transient analyses using RELAP5-3D models: unprotected station blackout (SBO) using RVACS/PSACS, unprotected loss of flow using the power conversion system for decay heat removal (DHR), and unprotected overpower. In addition, the team also simulated protected SBO to assure that the system could maintain sufficient margin to freezing of coolant. The results confirmed that both the lead-cooled and liquid salt-cooled reactors can accommodate these accidents without exceeding temperature limits.

Overall, the most important findings for the lead- and salt-cooled reactor designs are that 1) it is feasible to design these reactors with the flexible CR in the range of CR=0 and CR=1 in a manner that achieves inherent reactor shutdown in unprotected accidents; 2) the salt-cooled reactor requires LEMs to overcome the inherent salt coolant's large positive coolant temperature reactivity coefficient; and 3) the preferable salt for fast-spectrum, high-power-density cores is $NaCl-KCl-MgCl_2$, as opposed to fluoride salts, due to its better thermal-hydraulic and neutronic characteristics.

The gas-cooled fast reactor (GFR) previously developed at MIT is a CR=1-only design. It uses oxide fuel (with BeO diluent) for chemical stability with the selected CO_2 coolant maintained at 20 MPa and directly coupled to an S-CO_2 power conversion cycle. The sodium-cooled fast reactor (SFR) design is the ANL modular 1,000-MWt advanced burner reactor (ABR) concept, which is based on the GE S-PRISM design. For comparison, the team took the 1,000-MWt core as a starting point and increased the number of core assemblies to achieve the 2,400-MWt power rating. They changed the number of batches from three to one and used Zr weight fraction grading rather than enrichment grading, as for the LFR and LSFR cores. The team performed full neutronic analysis of the 2,400-MWt SFR core to obtain reactivity coefficients, power distribution, and heavy metal mass balances. Core thermal hydraulics will be similar to the original ABR core because core temperature rise is preserved, core peaking is smaller than in the original design, and flow rate per fuel assembly is also preserved. Transient analysis including plant and DHR system design were beyond the scope of this project, but adequate DHR systems, using either enhanced RVACS and PSACS or a direct reactor auxiliary cooling system, may be developed for the SFR.

The comparison of the four concepts focused on relative economic and safety performance. Regarding economics, economy-of-scale and power conversion system compactness are the same due to the consistent 2,400-MWt rating and use of the S-CO_2 power conversion system; therefore, the team compared the achievable plant thermal efficiency, core power density, and core-specific powers. Operating coolant temperatures and fuel linear power and compactness become the dominant factors. The potential to achieve the highest efficiency among the four reactor concepts can be ranked from highest to lowest as follows: 1) GFR, 2) LFR and LSFR, and 3) SFR. Both the lead and salt designs achieve about 30 percent higher power density than the gas-cooled reactor, but attain power density three times smaller than that of the sodium-cooled reactor. However, for the sodium concept to benefit from capital cost savings from this smaller potential core size, the DHR approach needs to keep the reactor vessel size suitably bounded. The SFR provides the best fuel-cycle costs because of its high specific power of 65 kW/kgHM compared to the lead, salt, and gas reactor values of 45 kW/kgHM, 35 kW/kgHM, and 21 kW/kgHM, respectively.

Regarding safety, all concepts can be designed to accommodate unprotected limiting accidents. However, this option is not preferable in the GFR, where the active or semi-passive approach would likely result in a more economic and reliable plant. The benefit of using the S-CO_2 power conversion system is that it provides an additional heat removal option since the decay heat can drive the turbine, which in turn drives the compressors to circulate CO_2 through the IHXs in a self-sustaining operational mode. This approach is feasible and effective for the LFR and LSFR and could also be used in the SFR and GFR. Protected accidents need to be given special attention in the LSFR and LFR due to their small margin to freezing, and to a lesser extent in the SFR. The GFR does not pose this challenge. Finally, the well-known vulnerability of sodium to its chemical reaction with water is to be noted should the Rankine power conversion cycle be utilized. The opacity of both sodium and lead should also be noted, which would affect under-surface in-vessel fuel-handling operations.

Planned Activities

This project concluded in May 2008. All activities have been completed.

NUCLEAR ENERGY RESEARCH INITIATIVE

Development and Utilization of Mathematical Optimization in Advanced Fuel Cycle Systems Analysis

PI: Paul J. Turinsky, North Carolina State University (NC State)

Collaborators: Argonne National Laboratory, Idaho National Laboratory (INL)

Project Number: 06-047

Program Area: AFCI

Project Start Date: March 2006

Project End Date: March 2009

Research Objectives

The objective of this project is to develop mathematical techniques to optimize deployment strategies for advanced nuclear fuel cycle/reactor/fuel facilities. Researchers will employ a stochastic optimization approach, which will determine the tradeoff surface of this multi-objective optimization problem. The optimization will consider economic, energy, environmental, and nonproliferation resistance metrics of the fuel cycle, which will be modeled using the verifiable fuel cycle simulation (VISION) code.

This project will accomplish several goals:

- The capabilities developed will assure that optimum deployment strategies are determined with reduced scientist/engineering effort, providing higher confidence in utilizing the results in policy decision-making.

- The automated capability should make it possible for less technically sophisticated individuals to utilize fuel-cycle simulation capability.

- The multi-objective mathematical optimization will determine the tradeoff surface, resulting in different optimization deployment strategies as one moves across the surface, which will provide quantitative data on such items as the relationship of repository capacity to energy costs.

Decision-makers could use resulting data to establish policies concerning incentives and requirements to encourage the preferred evolution of the commercial nuclear power enterprise.

Research Progress

An improved forecasting method for building reactors and nuclear fuel cycle facilities was added to the VISION code. The goal of this research was to develop a forecasting method for building light water reactors (LWRs), fast recycle reactors (FRRs), and their required support facilities in an advanced fuel-cycle model. A forecasting method is necessary for evaluating realistic fuel-cycle planning strategies. As FRRs utilize LWR used fuel as their makeup fuel source, this method must minimize excess LWR used fuel in the fuel cycle while ensuring that there are no shortages of used fuel at any point over the simulation time span. None of the existing or developing advanced fuel-cycle models have a forecasting method that can solve the problem of building an appropriate number of FRRs; therefore, it was decided to build this logic into the VISION code, currently being developed at INL.

VISION utilizes a system dynamics model of advanced nuclear fuel cycles related to the Advanced Fuel Cycle Initiative at the U.S. Department of Energy. VISION will indicate the need to build reactors and their support facilities based on projected U.S. energy growth rates and the nuclear market share. The VISION code has the capability of modeling several different reactor types and separation processes such as uranium recovery by extraction, co-extraction, and electrochemical. VISION can run several different combinations of reactor and reprocessing options. The two main options VISION analyzes are the one-tier and two-tier cases. In the one-tier case, all LWR used fuel is sent directly to FRRs; in the two-tier case, the used fuel will be recycled before it is sent to the FRRs. The results presented here apply only to the one-tier case.

The forecasting methodology requires the program to look ahead for a specified number of years in order to determine the energy requirement and the amount of LWR used fuel that can be used in an FRR. The number of years that the system looks ahead, Δt_{look}, should be equal to or greater than the maximum construction time for a reactor support facility (fuel fabrication facilities, separation facilities, etc.). The energy requirement is the exponential growth rate that the user specifies. The amount of LWR used fuel that can be used in an FRR is denoted by the symbol $\overline{uSF_t}$ and is also referred to as the unmortgaged spent fuel stock.

As the simulation and the prediction program progress, $t + \Delta t_{look}$, the forecasting logic will calculate the lifetime supply of spent fuel from LWRs coming online at the following time:

$$t + \Delta t_{look} - \Delta T_{look} \qquad (1)$$

and will send that amount of spent fuel to the $\overline{uSF_t}$. In Equation 1, ΔT_{look} is equal to the amount of time it takes LWR used fuel to go through wet storage, plus separations, plus fuel fabrication, plus the amount of time it takes to produce one full core for an FRR given the yearly production rate of LWR used fuel. The maximum number of FRRs that can be ordered by the prediction at t and come online at $t + \Delta t_{look}$ in the simulation is then calculated using the equation below:

$$\#\mathrm{FBR}_{SF,t+t\Delta_{look}} = \frac{\overline{uSFt}[PuControl]}{F_{Total}^{LWRsf}[PuControl]} \qquad (2)$$

where the $F_{Total}^{LWR_{sf}}$ is the lifetime requirement of LWR used fuel for one FRR and the *PuControl* is an isotopic control switch that the user defines. Once the system orders an FRR, the $F_{Total}^{LWR_{sf}}$ amount of fuel is taken out of the $\overline{uSF_t}$ and sent to a mortgaged spent fuel stock. The use of these equations ensures that the system will not overbuild FRRs and that there will always be a supply of fuel for FRRs.

Now that the prediction has the energy demand and the maximum number of FRRs that the system can support ($\#\mathrm{FBR}_{SF,t+\Delta t_{look}}$) at $t + \Delta t_{look}$, the program can determine the number and mix of reactors at this given time. If there are not enough FRRs to meet the energy demand, then the system will build LWRs. With the number and mix of reactors known, the program can perform a supply and demand calculation on the fuel fabrication and separation facilities in order to determine if new facilities are needed. Inventories of separated material and fabricated fuel are also used, and if the predicted supply plus the predicted inventory is greater than the predicted demand, then no new facilities are built. If the predicted supply plus

inventory is less than the predicted demand, then new facilities are ordered and will come online in time for their services to be used by the reactors.
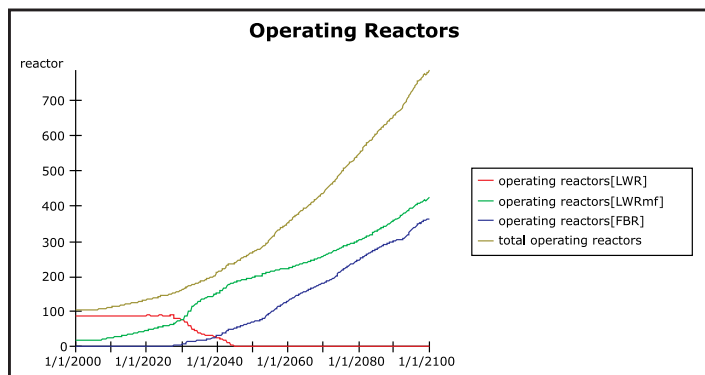

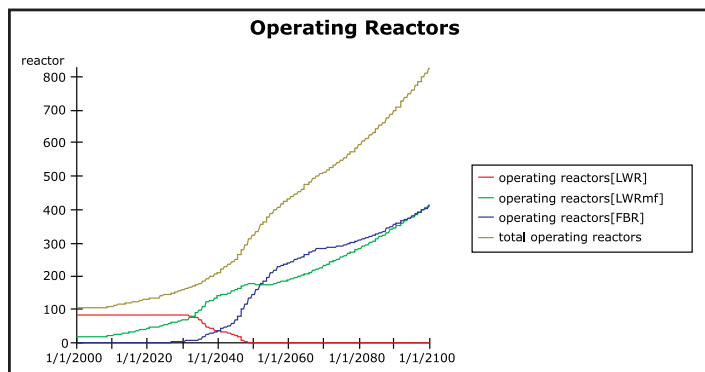Figure 1. Operating reactors with old methodology.

Figure 2. Operating reactors with new forecasting logic.

The graphs in Figure 1 and Figure 2 show reactors coming online as the simulation progresses from the year 2000 to the year 2100. The blue line is the number of FRRs operating and the green line is the number of LWRs operating. The results of this methodology show a smoother reactor build rate for FRRs. Incorporating the forecasting method also allows the system to reach an equilibrium growth rate of LWRs to FRRs, starting around the year 2070. In the old methodology, the system never reaches equilibrium. This equilibrium growth rate is important because it provides scientists and industry leaders with a support ratio that will allow for proper planning of fuel-cycle strategies. This addition has been a major improvement in advanced fuel-cycle modeling because it allows the system to build the maximum number of FRRs without running out of fuel and the system to reach an equilibrium growth rate.

The unavailability of fuel-cycle facilities can disrupt FRR energy-generation capability, which is limited by the availability of fresh FRR fuel. To help researchers analyze the impact of disruptions of fuel-cycle facilities, the research team added additional capability to VISION. They

completed this study to obtain a better understanding of uncertainties in construction schedule and operations of fuel-cycle facilities for an advanced nuclear fuel cycle. This analysis was performed on separation facilities (also called reprocessing facilities), but has similar implications on fuel-fabrication facilities and other facilities in an advanced nuclear fuel cycle. In particular, this analysis showed the importance of a separation facility having a separated material inventory—and how lead-time for a separation facility's construction, as well as the facility's size, impacts that inventory. Specifically, this analysis considered effects of a delay in a separation facility's construction, as well as effects of temporarily shutting down a separation facility. Using the VISION code, the analysis was performed again after modifications.

One of the relationships that this research examined is the relationship between separation facility size, construction lead time, and separated material inventory. When an FRR first comes online, LWR used fuel supplies the initial core load and first few reloads from thermal separations. Then, when fast recycling is initiated, the amount of LWR used fuel required for each reload is roughly 1/5 of the total reload for a 0.5 conversion ratio. If thermal separation facilities are built based on the long-term demand for LWR used fuel (1/5 of each FRR reload), then that facility would have to come online approximately 35 years before the reactor starts in order to meet demand for the first core and subsequent four reload cores. On the other hand, if thermal separation facilities are built based on initial demand of an FRR, then the system would drastically overbuild separation capacity. In order to get around this problem, a separation facility must begin construction based on total demand of an FRR; however, that separation facility should start up a couple of years before the FRR. This will allow the separation facility to accumulate an inventory to supply the FRR with fuel for the first core and subsequent reload cores.

The research team completed a study to determine optimal lead time and separation facility size for a specified FRR growth rate. This optimum combination is important because if the lead time is too long or if the separation facility is too large, the separated material inventory will become large. The team ran the simulation many times to determine the desired results.

The team completed an additional study to determine the effect of upset scenarios on the fuel cycle. The first upset event analyzed was a nine-year delay in construction of the first few separation facilities. The last upset event analyzed involved taking one separation facility offline for

five years after five years of operation. The results will show the best mitigation strategy for each upset event.

Table 1 shows results for the lead-time-versus-separation-facility-size study. The results were as expected: In order to build inventory, the preferred separation facility size decreases as the lead time increases.

Facility Size	Lead Time		
	10 Percent FRR Growth	20 Percent FRR Growth	FRR Ramp up to 100 Percent
1 kt/yr	Not Feasible	1 yr	Not Feasible
0.5 kt/yr	1 yr	4 yr	7 yr
0.25 kt/yr	3 yr	5 yr	7 yr

Table 1. Optimum lead time versus separation facility size.

The graph in Figure 3 shows the predicted inventory (red line), actual inventory (blue line), and minimum bank limit (green line). This is a plot of the inventory graph for the 20 percent FRR growth case with a separation facility size of 0.5 kt/yr and a lead time of four years. This graph shows how the inventory stays fairly close to the specified bank limit, thus indicating an optimum lead time and separation facility size.
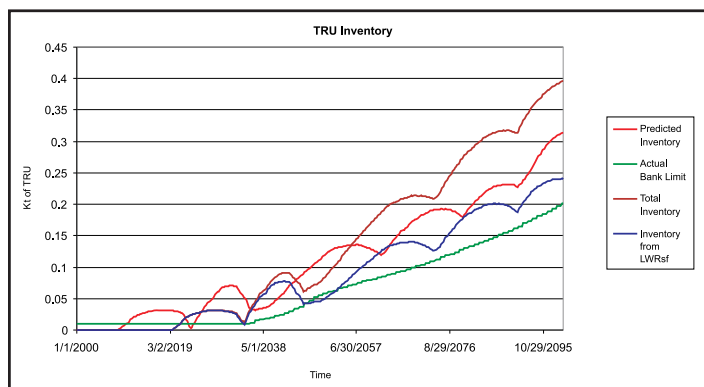

Figure 3. Plot of inventories.

The next analysis shows the negative impact on the fuel cycle and the best mitigation strategy caused by construction delay of a separation facility.

Table 2 shows results of a nine-year delay in construction of the first separation facilities ordered. The lost FRR GWe years are the total amount of GWe production that would be lost due to not having a separation facility up and running on time, hence requiring FRRs to down-power due to lack of fuel. As comparing Scenarios One and Three shows, constant facility size paired with increased lead time decreases lost energy

generation by 12.24 GWe-yr. Also, as comparing Scenarios Two and Three shows, simply increasing separation facility size while keeping lead time constant decreases the negative impact by only 2.52 GWe-yr. Based on this analysis, the best mitigation strategy is to have a longer lead time for a separation facility.

| Scenario Number | 10 Percent FRR Growth | | Lost FRR GWe Years |
	Facility Size	Lead Time	
1	0.5 kt/yr	1 yr	35.28 GWe-yr
2	0.25 kt/yr	3 yr	25.56 GWe-yr
3	0.5 kt/yr	3 yr	23.04 GWe-yr

Table 2. Results of construction delay.

As mentioned above, the research team investigated another upset scenario: Separation facilities were taken offline for five years after five years of operation. The best mitigation strategy for this upset event was to build smaller separation facilities. Smaller facilities are preferred because this implies that multiple facilities will be built at the same time; therefore, when one facility is taken offline, other facilities will remain in operation. In addition, lost capacity is lower when shutting down a smaller facility. In summary, these results give a better understanding for the best process for building facilities in an advanced nuclear fuel cycle in order to minimize the economic impact of upset events.

Finally, additional work was completed to get VISION to a state where it can be used with an optimization engine, implying access to decision variables, objectives, and constraints.

Planned Activities

The team will complete work on integrating the simulated annealing optimization engine with the VISION code. Once completed, they will undertake the same task using a genetic algorithm as the optimization method, first for a single objective function and then for a multiple objective function. As the optimization capability is made available, the team will exercise it to both verify and validate this aspect of the software and to complete advanced fuel-cycle studies that would be of current interest.

NUCLEAR ENERGY RESEARCH INITIATIVE

Engineered Materials for Cesium and Strontium Storage

PI: Sean McDeavitt, Purdue University

Collaborators: Texas A&M University (TAMU), Argonne National Laboratory (ANL)

Project Number: 06-058

Program Area: AFCI

Project Start Date: April 2006

Project End Date: March 2009

Research Objectives

Next-generation spent fuel reprocessing methods being developed under the Advanced Fuel Cycle Initiative include solvent extraction schemes to isolate cesium (Cs) and strontium (Sr) from spent nuclear fuel. Isolating these isotopes for short-term decay storage eases design requirements for long-term repository disposal; a significant amount of radiation and decay heat in fission product waste comes from Cs-137 and Sr-90. For the purposes of this project, the fission product extraction (FPEX) process is considered the baseline extraction method.

Final year objectives are to synthesize and characterize a series of bentonite ceramics (an aluminosilicate structure) with up to 40 weight percent (wt%) simulated fission products. This project began as a complementary effort to engineering development of a fluidized bed steam reformer at Idaho National Laboratory (INL). However, both INL and TAMU results indicated that steam reforming is too vigorous for efficient immobilization. Therefore, this project expanded its focus to examine alternate fabrication options and to develop and characterize novel ceramic forms for the Cs and Sr isotopes.

Research Progress

The project progressed in two phases in FY 2008. First, the project team completed final experiments to synthesize Cs/Sr-bearing ceramic materials using the TAMU steam reformer. This led to the termination of that research direction in favor of a gentler ceramic synthesis process using Cs- and Sr-loaded kaolinite and bentonite clays, as described below. This second research phase began in collaboration with ANL.

Steam-Reforming Experiments. The team combined aqueous precursor solutions containing Cs and Sr nitrates ($CsNO_3$ and $Sr[NO_3]_2$) with solid powder reactants (e.g., kaolin $[Al_2Si_2O_5(OH)_4]$, carbon, and titanium oxide). In the project's first year, steam reforming produced cesium aluminosilicate ($CsAlSi_2O_4$) and strontium carbonate ($SrCO_3$) as stable reaction products, but only a fraction of the Cs and Sr reagents were actually immobilized in the final ceramic product. This was due, in part, to the steam's high flow rate and the reagents' short residence time through the process vessel.

This past year, experimenters used a modified scheme that still relied on reactions between H_2O and various solid reagents; however, internal energy of the system was reduced by switching to a low flow-rate argon cover gas along with a low-flow systaltic pump to inject Cs- and Sr-bearing solutions. Vaporized water from the feed solution provided the requisite oxygen and hydrogen to the synthesis reactions. The system was used to synthesize cesium aluminosilicate ($CsAlSi_2O_4$) and strontium carbonate ($SrCO_3$), but effectiveness was poor. Some experiments produced negligible reaction products, and these products frequently contained unreacted strontium nitrate. Furthermore, in final tests with titanium oxide, the system was clearly unable to synthesize titanate and zirconate ceramics without going to much higher temperatures. In the end, the steam-reforming option was set aside due to the high-energy system's poor efficiency and the low-energy system's ineffective conversion.

Clay-Loading/Sintering Experiments. In conjunction with ANL, the project team developed a new strategy for waste form synthesis during a summer internship. In this method, nitrate solutions containing

Cs, Sr, barium (Ba), and rubidium (Rb), based on the expected FPEX effluent concentrations, are loaded into aluminosilicate clays and converted into ceramic pellets via high-temperature sintering. The simulated waste solution is prepared with concentrations of Cs, Sr, Ba, and Rb increased to their solubility limit to minimize volume. The simulated waste solution is mixed with the clay to produce a slurry, which is heated at low temperatures and dried into a waste-loaded powder. This powder is pressed into a pellet and sintered to produce a solid pellet.

Variables being explored include the type of clay, waste loading of the solution (and thus the final waste form), and sintering time and temperature. Experimenters used 1) bentonite clay loaded with a simulated waste solution and 2) kaolin clay loaded with dry nitrate salts. The team varied sintering temperatures from 1,100°C to 1,400°C and the waste concentrations from 18 mass percent to 30 mass percent Cs, Sr, Ba, and Rb. In the initial experiments, kaolin samples expanded and cracked extensively upon sintering when loaded with dry nitrates. Furthermore, the bentonite samples densified into a strong monolith upon sintering between 1,100°C and 1,300°C; sintering at 1,400°C caused local melting and vitrification. These initial tests with bentonite not only revealed that higher temperatures (i.e., 1,300°C) produced higher densities but also showed a significant loss in mass during sintering above 1,200°C. Therefore, the current focus of this research is to optimize waste loading and sintering conditions to minimize mass loss while achieving high density.

The team is currently performing differential scanning calorimetry (DSC) analyses with *in situ* mass-loss measurements using loaded but unsintered bentonite clay powders. The sintered samples noted above displayed some mass loss during densification, which was consistent with the loss of water and nitrates from the loaded clay structure. The DSC measurements confirm this phenomenon. The object is to determine a threshold temperature below which waste elements will not be appreciably expelled from the clay as it sinters. As part of this effort, the team will use neutron activation analysis to quantify concentrations of waste elements in the final monoliths, and transmission electron microscopy to assess structure and overall uniformity of the proposed waste material.

Planned Activities

This project made a significant advance in synthesis and fabrication of Cs- and Sr-bearing waste forms from the FPEX effluent despite the determination that steam reforming is not a viable process for this purpose. The project was originally projected for March 2009 completion, but is pursuing a no-cost extension to enable further development of the new clay-loading process and continued collaboration with ANL. A test matrix is under way to systematically evaluate the bentonite clay-processing route. The matrix will include three different waste loadings and three different sintering temperatures. Each sample will be analyzed using electron microscopy, x-ray diffraction, neutron activation analysis, leach testing, and other methods as deemed appropriate within project means.

NUCLEAR ENERGY RESEARCH INITIATIVE

Feasibility of Recycling Plutonium and Minor Actinides in Light-Water Reactors Using Hydride Fuel

PI: Ehud Greenspan, University of California-Berkeley

Collaborators: Massachusetts Institute of Technology, Argonne National Laboratory

Project Number: 06-065

Program Area: AFCI

Project Start Date: March 2006

Project End Date: February 2008

Research Objectives

The objective of this project is to assess the feasibility of improving the plutonium (Pu) and minor actinide (MA) recycling capabilities of pressurized water reactors (PWRs) by using hydride instead of oxide fuels. There are four general parts to this assessment:

1) Identifying promising hydride fuel assembly designs for recycling Pu and MAs in PWRs

2) Performing a comprehensive systems analysis that compares the fuel cycle characteristics of Pu and MA recycling in PWRs using the promising hydride fuel assembly designs identified in Part 1 versus using oxide fuel assembly designs

3) Conducting a safety analysis to assess the likelihood of licensing hydride fuel assembly designs

4) Assessing the compatibility of hydride fuel with cladding materials and water under typical PWR operating conditions

Research Progress

The safety analysis of PuH_2-U-$ZrH_{1.6}$ (PUZH)-loaded cores was completed through the assessment of the reactor performance upon a complete loss of flow accident (CLOFA)—a Condition III incident consisting of the complete loss of forced reactor coolant flow which may result, among other causes, from a simultaneous loss of electrical supply to all reactor coolant pumps (RCPs). Following this loss, RCPs start coastdown, causing the coolant flow rate through the core to decrease and the whole primary system to heat up. Even though the negative feedback through the moderator temperature coefficient (MTC) of reactivity causes core power to slowly decrease, the lack of cooling can yield fuel pin failure

and thus core damage. The reactor is protected from this occurrence by automatic scram, which occurs a few seconds after accident initiation. The severity of a CLOFA is measured by monitoring the evolution of the minimum critical heat flux ratio (MCHFR) in the short time period between accident initiation and reactor scram.

Consistent with the analysis methodology used for other accident scenarios analyzed throughout the project, a CLOFA was assumed to occur in four different PWRs. These plants are identical in all of their components except for the types of fuel assemblies loaded in the core: 1) all-UO_2 assemblies, 2) combined non-fertile and uranium (CONFU) assemblies, 3) CORAIL assemblies, and 4) PUZH assemblies. These assemblies have the same geometry and differ only in the type of fuel and/or the fuel rods arrangement in the assembly lattice. The plant modeling technique was validated by comparing the results obtained for the all-UO_2 core with those reported for the Seabrook plant, which is the reference plant for this project; the agreement is satisfactory.

It was found that the MCHFR of a PUZH-loaded core undergoing a CLOFA is larger than that of the competitor cores, i.e., CONFU- and CORAIL-core, which are also aimed at Pu/MA recycling but use oxide fuel. The reason for this is twofold. First, PUZH assemblies have a uniform lattice, as opposed to CONFU and CORAIL assemblies, which are heterogeneous. This allows a PUZH assembly to operate with a smaller pin peaking factor, which translates into a higher steady-state MCHFR, as shown in Figure 1. Second, the PUZH core has the most negative MTC/β ratio among the cores analyzed, which yields a more rapid core power reduction between accident initiation and reactor scram and, therefore, a smaller MCHFR reduction after accident initiation. This is quantified in Table 1.
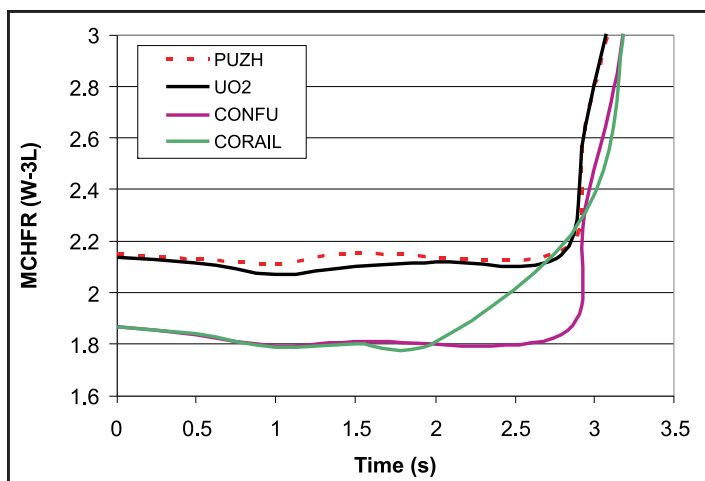
Figure 1. Evolution of MCHFR during CLOFA.

MCHFR During CLOFA Scenario			
	MCHFR (W-3l correlation)		MCHFR Variation % Relative to Steady State Value
Core Type	At Steady-State	Minimum During CLOFA	
All-UO$_2$	2.138	2.073	-3.0
CONFU	1.866	1.791	-4.0
CORAIL	1.870	1.788	-4.4
PUZH	2.146	2.110	-1.7

Table 1. MCHFR during CLOFA scenario.

Consistent with results obtained for other accident scenarios, i.e., large break loss-of-coolant accident and main steam line break, the analysis of CLOFA showed that a PWR core loaded with PUZH assemblies would operate with larger safety margins than the oxide-fueled cores aimed at Pu/MA recycling, and its performance would resemble that of a typical all-UO$_2$ core. The transmutation capability of the hydride-fueled PWR was found significantly superior to those of the oxide-fueled PWR.

The transuranic (TRU) transmutation capability of hydride-fueled PWR was compared against that of the "deep-burn" graphite-moderated reactors (high-temperature reactors [HTRs]). It is found that the achievable burnup is approaching 700 GWd/MT in deep-burn HTRs versus approximately 540 GWd/MT in hydride-fueled PWRs.

A PWR core fueled with PuH_2-$ZrH_{1.6}$ was found to have a positive fuel temperature coefficient of reactivity (FTC) in the third batch of the first recycle. One of the options to avoid the positive FTC identified is to substitute the hydride fuel deuterium (D) for hydrogen (H). After the first recycle, there is no need for D. Another approach identified for maintaining the FTC negative is to add some U to the hydride fuel. This approach penalizes the attainable fractional Pu transmutation, whereas the substitution of D for H does not.

The effect of coolant voiding on the neutron leakage probability from a PWR core was investigated. Knowing this leakage probability is important for determining the maximum number of times it is possible to recycle TRU in PWRs. The leakage probability was found to strongly depend on the shuffling scheme adopted—for a standard PWR it can be as high as 12.5 percent for a high-leakage fuel management scheme and as low as 0.34 percent for a low-leakage fuel management scheme. The leakage probability assumed throughout this project is 5 percent, which is quite conservative with respect to the achievable burnup. For example, the attainable burnup in the first recycle of HTR TRU in PWRs varies from 510 MWd/tHM at 5 percent leakage probability to 540 MWd/tHM at 3 percent leakage probability. With 5 percent leakage probability, it is possible to recycle Pu+Np in a PWR at least 6 times when using hydride fuel before getting a positive void reactivity feedback.

Planned Activities

Researchers will compare the impact of recycling Pu and MA using hydride fuel versus using oxide fuel on the following Yucca Mountain Repository (YMR) performance characteristics:

- TRU and fission product quantity and composition that will need to be disposed

- Radiotoxicity and decay-heat of the high-level waste (HLW)

- Inventory of [237]Np and its precursors—a major contributor to the long-term radiation level in the vicinity of the repository due to HLW leakage into the environment

- HLW storage capacity—to be measured by the cumulative amount of energy that could be generated in PWRs as well as the HLW that could be stored at the YMR

Researchers will also complete the study of the feasibility of an inverted hydride fuel design for the PWR.

NUCLEAR ENERGY RESEARCH INITIATIVE

Accelerator-Based Study of Irradiation Creep of Pyrolytic Carbon Used in TRISO Fuel Particles for the Very High-Temperature Reactor

PI: Lumin Wang and Gary S. Was, University of Michigan

Collaborators: Oak Ridge National Laboratory, Idaho National Laboratory

Project Number: 06-113

Program Area: AFCI

Project Start Date: March 2006

Project End Date: March 2010

Research Objectives

Pyrolytic carbon (PyC) is one of the important structural materials in the TRISO fuel particles that will be used in the next generation of gas-cooled very high-temperature reactors. When the TRISO particles are under irradiation at high temperatures, creep of the PyC layers may cause radial cracking, leading to catastrophic particle failure. Therefore, predicting overall fuel performance requires a fundamental understanding of PyC creep behavior during irradiation.

This project's primary objective is to characterize PyC creep behavior through a systematic program of accelerator-based proton irradiation and *in situ* measurements under stress at various temperatures between 400°C and 1,200°C. The project team will analyze test data to determine creep coefficients, which will then be correlated to existing coefficients measured under neutron irradiation. In addition, the team will conduct initial experiments on transport of select fission products (e.g., Ag and Sr) in PyC under irradiation and stress; these experiments will entail implanting ions into the material.

Research Progress

In FY 2008, the research team designed and constructed a unique ion accelerator target chamber for *in situ* creep tests during proton ion beam irradiation. Also, University of Michigan researchers successfully produced and characterized PyC samples of suitable dimensions. During this reporting period, researchers have encountered several challenging problems for conducting the *in situ* PyC creep test during proton beam irradiation at elevated temperatures; the difficulties include determining PyC's thermal emissivity and thermal expansion, as well as breakage of the thin PyC samples during stress due to the material's brittleness. Researchers expect future irradiation creep experiments to run smoothly, as the team has resolved most of the problems by conducting a series of experiments and by improving the sample holder's design.

Determination of PyC Emissivity. Temperature control is a key factor in irradiation creep experiments. Sample temperatures are monitored using the infrared pyrometer, which requires knowledge of sample emissivity. Thus, knowing the PyC samples' emissivity is crucial in performing the irradiation creep testing properly. Typically, sample emissivity is determined by spot-welding thermocouples to a sample and adjusting sample emissivity until the pyrometer output matches the temperature measured by the thermocouples. Because metal thermocouples cannot be spot-welded to a nonmetallic PyC foil, researchers performed multiple experiments to determine emissivity of the PyC samples. The final experiment consisted of sandwiching the thermocouple between two pieces of PyC. The successful technique allowed for higher temperatures without the constraints of the other options. The experiments were performed at temperatures up to 700°C, and the emissivity of the samples was determined to be 0.350. Previous research has found that, from 250°C to 1,500°C, the emissivity of highly polished carbon and graphite samples is independent of temperature. Because the PyC samples have a highly polished surface, these reported trends of emissivity are applicable. Therefore, an emissivity of 0.350 will be used for the full range of experiments between 600°C and 1,200°C.

Thermal Expansion of PyC.

While testing the deposited heater, the team performed a set of experiments to observe PyC's thermal expansion. The team found a lower value for thermal expansion than that in the literature data. However, the trends with increasing temperature were very similar. The literature data resulted from measuring a completely isotropic PyC sample, but this project has been using PyC with a slight level of anisotropy. The literature presents thermal expansion of anisotropic PyC in the a-direction and with a lower value than isotropic PyC's thermal expansion. Thus, the observed anisotropy in the current samples could explain, at least in part, why the PyC sample data did not exactly match the literature values. Researchers now have accurate thermal expansion data for the PyC used in this project, which will enable them to obtain accurate creep data in future experiments.

Irradiation Effects on PyC Anisotropy.

PyC produced by chemical vapor deposition has different degrees of anisotropy. The samples' microstructure consists of nano-sized crystals. In the basal plane, the nanocrystals appear to have a random orientation. However, when the sample is viewed parallel to the basal plane, the anisotropy is more visible. This occurs because even though the small crystallites on the basal plane have a random orientation, the c-axes of the crystallites are more likely to have a similar orientation that is perpendicular to the film surface. This preferred orientation can be seen in diffraction patterns taken from the cross-sectional sample. Unlike the plan view diffraction pattern, which has continuous and uniform rings, the cross-sectional diffraction pattern has regions that are more intense. The arc length of these intense regions is inversely proportional to the level of preferred orientation (texture). Intense regions that have shorter arc lengths correspond to samples that have higher levels of anisotropy.

Proton irradiation changes the sample anisotropy. To observe this change, researchers tested the samples that were used for temperature and beam-current correlation experiments. The research team irradiated the samples with 2 MeV protons. Initial sample temperatures were room temperature, 200°C, and 400°C; dose rates ranged from 2×10^{-7} dpa/s to 4.2×10^{-6} dpa/s; samples received a total dose of less than 1 dpa. The team analyzed
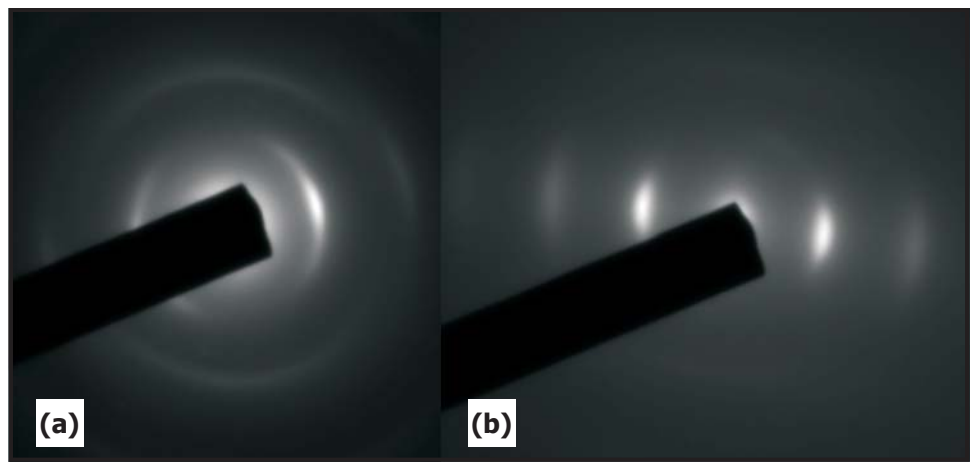

Figure 1. Cross-sectional electron diffraction patterns for irradiated PyC samples: (a) near the front surface of the sample that received little proton dose and (b) near the back surface that received higher displacement dose.

electron diffraction patterns taken before and after proton beam irradiation. The analyses indicated that irradiation enhanced the PyC film's undesirable anisotropy, with the c-axes of the graphite nanocrystals more favorably aligned in the direction normal to the film surface (see Figure 1). However, the irradiated microstructure remains isotropic in directions parallel to the film plane.

Modifications on the Sample Stage and Stress-Loading Process.

The research team encountered several difficulties in the initial irradiation creep experiments. The majority of these setbacks were due to the samples' brittleness and small thickness (30 microns to 40 microns), requiring adjustments to the stage and to the sample-loading process. Researchers have developed a precise sample-alignment method and a stress-application process that greatly reduced the probability of sample breakage during the loading process.

During prior attempts at creep experiments, researchers usually went through multiple samples before they could load a set into the irradiation chamber and seal the samples. Attaching the stress to the sample was a very delicate process, and unless it was done perfectly, the slightest shake of the hand was highly likely to break the sample. The research team has recently worked out a process that uses a 1-mm-wide rod with a hook at each end. A researcher first hooks one end into the sample clamp, as shown in Figure 2(a); then, using a hand-crank jack that can slowly raise and lower the weight, the researcher hooks the bottom end to the weight, as shown in Figure 2(b). Since using this process, combined with the sample alignment procedure, researchers have had a 100 percent success rate for attaching the stress to the samples once they have been loaded into the irradiation chamber.
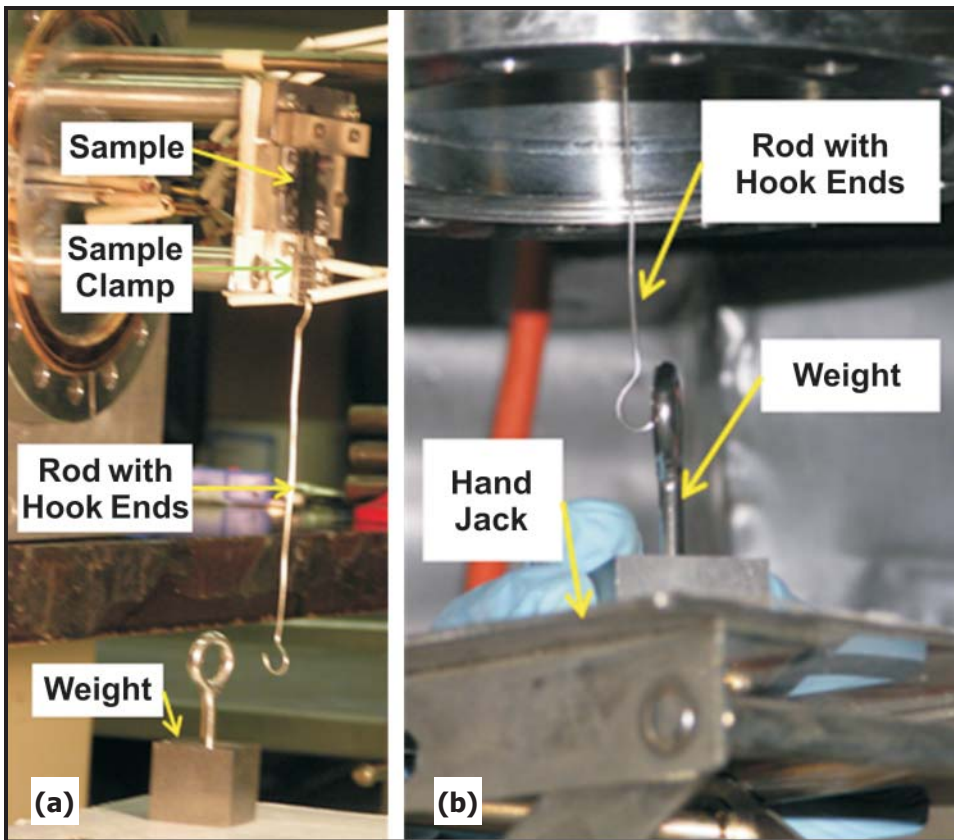
Figure 2. Photographs taken during a new sample-loading procedure showing (a) attaching the hooked-rod to the sample clamp and (b) using the hand jack to apply the weight to the rod.

An initial irradiation test on PyC has been successfully conducted with stress at 1,000°C and the proton beam penetrating the entire sample thickness. The researchers have measured small-sample elongation due to the initial stage of creep, and they have begun detailed data analysis.

Planned Activities

The following activities are planned for the upcoming year of this project:

- Conduct high-temperature irradiation (800°C, 1,000°C, and 1,200°C), and perform data analyses

- Implant selected fission-product elements (e.g., Ag and Sr), and perform irradiation of samples with pre-implanted fission product and cross-sectional transmission electron microscopy analyses

- Conduct final data analyses and empirical modeling

NUCLEAR ENERGY RESEARCH INITIATIVE

Development of Acetic Acid Removal Technology for the UREX+ Process

PI: R. M. Counce and J. S. Watson, University of Tennessee

Collaborators: Oak Ridge National Laboratory (ORNL)

Research Objectives

The overall goal of this project is the selection and experimental verification of the most appropriate technology to separate or destroy acetic acid produced from the decomposition of acetohydroxamic acid in the UREX+ process. Acetic acid accumulation would hamper the reuse of nitric acid and increase waste volume. The goals for this period were to 1) conduct an in-depth analysis of the leading technologies selected from the literature review performed earlier and 2) select the best method with which to proceed into the final project year. Studies performed this year include an evaluation of the chemistry of selected systems, flow-sheet studies of the most promising approach, and selective engineering tests. The project objective, then, is to provide reference studies sufficient for incorporating an acetate-removal step into the UREX+ process conceptual flow sheet when needed.

Research Progress

The research team conducted a review of appropriate technologies and an evaluation of available thermodynamic information for simulated UREX+ aqueous solutions containing nitric and acetic acids. The team determined that the most feasible separation/destruction method for general flowsheet application is solvent extraction; therefore, subsequent analysis has focused on solvent extraction options. Distillation is an important competitive technology if the only reason to remove acetic acid is to purify recycled nitric acid, which will likely involve distillation.

In proceeding with contactor studies, the team chose 1.5 M tributyl phosphate (TBP)-dodecane as the solvent system. They conducted tests for a 1 M nitric acid and 0.1 M acetic acid aqueous system as well as a 0.5 M nitric acid and 0.05 M acetic acid system (M = kmol/m^3). Table 1 shows the results. The team found that the 1.5 M TBP-dodecane system showed the highest separation factor with a sufficiently high distribution coefficient for acetic acid at 0.05 M. The highest separation factor for the 1 M nitric acid/0.1 M acetic acid system is at 1 M TBP-dodecane; however, the distribution coefficient (K_D), at 0.342, is not sufficient.

AQUEOUS SYSTEM	ORGANIC SYSTEM	K_D Nitric Acid	K_D Acetic Acid	Separation Factor
0.5 M Nitric Acid 0.05 M Acetic Acid Water	dodecane	0.022	-0.021	N/A
	1 M TBP-dodecane	0.049	0.183	3.735
	1.5 M TBP-dodecane	0.166	0.998	6.012
	2.5 M TBP-dodecane	0.308	1.481	4.808
	TBP	0.620	2.573	4.150
1 M Nitric Acid 0.1 M Acetic Acid Water	dodecane	-0.003	-0.043	N/A
	1 M TBP-dodecane	0.078	0.342	4.385
	1.5 M TBP-dodecane	0.150	0.525	3.500
	2.5 M TBP-dodecane	0.299	1.038	3.472
	TBP	0.660	1.751	2.653

Table 1. Distribution coefficients and separation factors for the TBP-dodecane solvent system.

Figure 1 shows a proposed removal step for acetic acid. The team then sought to determine where to optimally place this removal step in the UREX+ process. They employed literature information to estimate interference from acetic acid with each step of the specific task (separation). Researchers may also use the results of this analysis as a basis to create flow sheets of the UREX+ process with the removal step of acetic acid inserted.
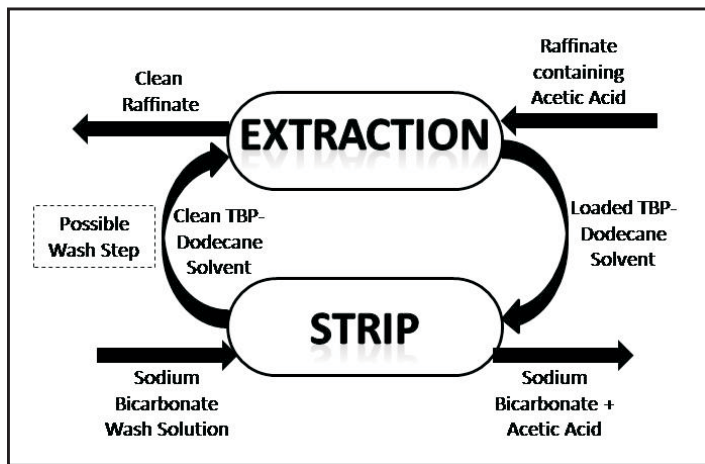

Figure 1. Acetic acid removal step.

If researchers estimated an adverse effect, this was taken as reason for placing the acetic acid removal prior to this step. Using an organic-to-aqueous (O/A) ratio from the literature or assuming an extraction factor of 1 when an O/A ratio was not given, researchers calculated and compared extraction factors for both acetic acid and extracted metals in each step.

$$E = K_D \bullet \frac{ORG}{AQ} \tag{1}$$

The presence of acetic acid is not expected to interfere with uranium extraction. No interference is expected in the cesium and strontium removal step—either CCD-PEG or FPEX. NPEX uses the same TBP-dodecane solvent used for the UREX step, and this solvent removes acetic acid; however, based on both the plutonium and neptunium extraction factors found in the literature, it should not cause interference. For the next step, TRUEX uses CMPO-TBP-dodecane solvent for the removal of americium and curium. Table 2 shows results from experiments for acetic acid using 0.2 M CMPO-1.2 TBP-dodecane solvent. After calculating extraction factors, researchers determined that acetic acid was not a likely problem for extracting these metals. The final step was TALSPEAK. It uses HDEHP-DIPB solvent to remove both actinides and lanthanides. Acetic acid was tested in a nitric acid phase contacting the HDEHP-DIPB solvent. This resulted in no extraction of

either acetic acid or nitric acid. In addition, very little acetic acid is likely to reach the TALSPEAK step; therefore, acetic acid is unlikely to interfere in this step either.

Acid	K_D
Acetic Acid 0.05 M	0.952
Nitric Acid 0.5 M	0.328

Table 2. Acid distribution in TRUEX solvent.

Another factor examined was simultaneous metal extraction in the acetic acid removal step. Seeing no compelling reason to add complexity to the process, the project team decided to recommend putting the acetic acid removal step at the end of the UREX+ process after TRUEX, as Figure 2 indicates. The arrows pointing down are the aqueous streams, while the arrows pointing right are the organic streams.
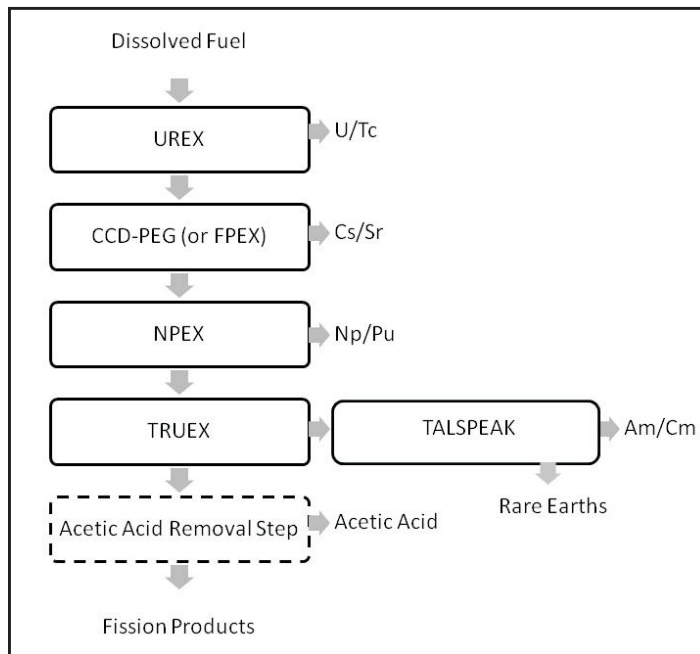

Figure 2. Flowsheet proposal.

During this reporting period, the team also investigated the behavior of water during acetic acid extraction. The aqueous phase comprises a 1:1 volume ratio of the two acid concentrations mixed with the organic phase of various TBP concentrations in selected diluents. Table 3 shows solubility tests for an aqueous phase of pure deionized water. The results on solubilities with the addition of acids are in Table 4. For the pure water system, molarities are given in terms of $kmol/m^3$ of "wet organic" organic solution after equilibrium water absorption. This is done in order to better understand the molar ratio of TBP to water in the organic after contact.

M of TBP in Wet Organic Phase	AVERAGE M of Water in Organic
Dodecane	
0	0.003
0.937	0.365
1.48	0.741
2.42	1.80
3.45	3.60
1,2 Dichloroethane	
0	0.131
0.935	0.461
1.48	0.754
2.41	1.93
3.45	3.60
FS-13 (phenyltrifluoromethyl sulfone)	
0	0.149
0.935	0.486
1.48	0.783
2.41	1.77
3.45	3.60

Table 3. Water solubility results from contact between deionized water and TBP-organic diluent mixtures.

M of TBP in Dry Organic Phase*	AVERAGE M of Water in Organic
Dodecane	
0	0.0117
1	0.4052
1.5	0.7494
2.5	1.763
3.67	3.857
1,2 Dichloroethane	
0	0.1574
1	0.5346
1.5	0.7904
2.5	1.577
3.67	3.857

*M of TBP is given in moles/liter of TBP in the organic solution prior to contact with the aqueous solution. Given the relatively small amount of acid and water extracted, the molarity of TBP in the dry solution is approximately the same as the molarity of TBP in the organic after contact.

Table 4. Water solubility results after contact of deionized water containing 0.5 M nitric acid and 0.05 M acetic acid with various concentrations of TBM in organic diluents.
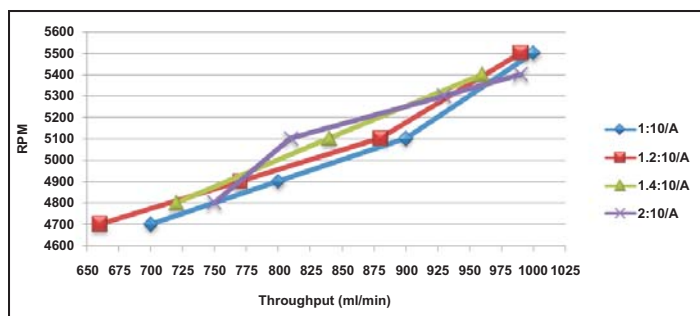
Figure 3. RPM versus throughput.

The centrifugal contactor is operational, and hydraulic tests have been completed for the extraction step. The team tested O/A volume ratios of 1:1, 1.2:1, 1.4:1, and 2:1. Figure 3 shows the points where the contactor transitions between acceptable phase separation (99 percent separation) to unacceptable. The organic phase used was 1.5 M (41 volume percent) TBP in dodecane, and the aqueous phase consisted of 0.5 M nitric acid. For simplification purposes, the team did not introduce acetic acid into the hydraulic tests.

Mass transfer efficiency data for the extraction step is currently under way. Once completed, the team will begin stripping the organic with hydrolic tests under strip conditions and progress to mass transfer efficiency testing.

Planned Activities

Work with the centrifugal contactor will continue. Mass transfer efficiency testing is under way, with an organic phase consisting of 1.5 M TBP in n-Dodecane and an aqueous phase containing an equal-volume mixture of nitric acid and acetic acid.

The organic phase is recycled between runs after being washed with 0.001 M nitric acid, stripped with 0.01 M sodium hydroxide, and rinsed with deionized water. The research team performs all three steps in triplicate to ensure full contact with the entirety of the organic solution, and replaces any loss in organic solvent with newly mixed solvent.

The procedure for the test begins by acquiring the equilibrium extraction values. These are calculated separately for each test to ensure accurate efficiency data. With the addition of a new organic solvent to the recycled organic from previous tests, these numbers vary with each test. The team then sets a total flowrate and O/A ratio and runs the test with aqueous phase samples taken at each minute until all the organic phase has run through the contactor. The team then titrates both the equilibrium sample and multiple aqueous phase samples to determine extraction efficiency.

Researchers have collected initial data for runs at both 1:1 and 2:1 O/A ratios; analysis of the data is currently under way.

Once flow-sheet development and key engineering tests have been completed, the team will prepare an approximate cost analysis for adding an acetate removal step to the UREX+ process. Both the engineering tests and the economic analyses will involve close association with the ORNL partners.

NUCLEAR ENERGY RESEARCH INITIATIVE

Separation of Nuclear Fuel Surrogates from Silicon Carbide Inert Matrix

PI: Ronald Baney and James Tulenko, University of Florida

Collaborators: None

Project Number: 06-126

Program Area: AFCI

Project Start Date: March 2006

Project End Date: September 2008

Research Objectives

The objective of this project has been to identify a process for separating transuranic species from silicon carbide (SiC), a prime candidate for inert matrix fuel materials. Viable processes for separating the unspent fuel from the SiC matrix have not been previously reported. This project has addressed this void. Specifically, this project aims to demonstrate a process for dissolution and separation of ceria from the SiC matrix, a surrogate for PuO_2. Only technologies compatible with traditional fuel-handling processes have been examined. Processes to dissolve either the fissile material or the SiC matrix were considered. Researchers performed a literature survey to identify and evaluate available methods that could be used for dissolving SiC and recovering the fissile material. After evaluating various candidate methods for ease of separation, degree of safety, and cost, researchers selected a hot corrosion (potassium carbonate molten salt) method as the most promising. A related process involving oxidation of SiC with chlorine gas in molten chloride salts was reported to be slow and inefficient, leaving non-oxidized carbon residues.

SiC is thermodynamically an unstable ceramic for reaction with oxygen; however, a passivating silica layer is formed that inhibits oxidation by preventing oxygen from reaching the underlying SiC. In a molten sodium carbonate environment, sodium ions can flux the silica layer by forming sodium silicate, thus destroying the silica's passivation effect. The process continues until the SiC is consumed, as occurs in immersion in a melt bath. Researchers have known about the dissolution of SiC by alkali and alkali earth compounds since the 1970s, and research has continued well into the early 2000s. Previous reported studies have shown that the rate and degree of corrosion varied based on oxygen partial pressure and the type of carbonate salt used for the melt bath. The University of Florida has examined the roles of the cation Na^+ or K^+ and the SiC particle or pellet effects upon rates.

Research Progress

Previous reports described experiments in which SiC pellets and powders reacted with sodium carbonate at 1,050°C in an open-ended tube furnace. The powders reacted completely after two hours. Ceria pellets were unchanged under the same reaction conditions. These preliminary studies demonstrated the process' viability. Subsequently, the research team examined parameters affecting the rates of SiC dissolution. The rate of SiC powder dissolution leveled off; the team traced that effect to inadequate premixing of the sodium carbonate and SiC powders. This observation suggested that islands of SiC would become surrounded with sodium silicate salts, which would retard the fluxing sodium ions' ingress to the passivating silica layer surrounding the SiC particles.

The team recognized that a practical process must not involve an attrition step but rather direct dissolution of pellets because of the significantly high added cost of highly radioactive contaminated grinding equipment. The need for direct dissolution of pellets, the observed leveling-off effect, and first-year reports that corrosion rates were rather slow for pellets: these combined facts prompted a search for a more reactive system, which was the subject of this last period of research.

In the past year, research has focused on the following areas.

SiC Pellet Dissolution – The Effect of the Cation.
Researchers cut into pellets a 5 mm diameter reaction-bonded silicon carbide rod (RB-SiC from Goodfellow Corporation); then they ground the pellets with fine-grit grinding paper to remove the tool marks. For two experiments, the researchers used a crucible containing an RB-SiC pellet and K_2CO_3 or Na_2CO_3, at approximately a 1-to-1½ molar ratio of SiC to carbonate salt; they placed this crucible midway in the tube furnace and heated it at 1,050°C for 15 hours.

Table 1 summarizes the results: potassium salt is clearly much more effective than sodium salt.

Figure 1. SiC pellet cumulative weight loss percent versus reaction time.

Experiment	SiC Pellet Composition	Pellet Dimension (mm)	Molten Salt	% Dissolved after 15 hours/1,050°C
I	SiC	D=4.98 h=1.74	Na_2CO_3	22
II	SiC	D=5.01 h=1.91	K_2CO_3	60

Table 1. Effect of the cation upon the rate of dissolution.

Potassium silicate has a lower liquid range than sodium silicate, which explains these results; thus formation of a solid phase of the silicate salt formation does not inhibit the cations' fluxing effect on the passivating silica layer.

SiC Pellet Dissolution – Time for Total Dissolution. The research team placed pellets of RB-SiC, along with about a 50-mole excess of K_2CO_3, into an open-ended tube furnace and heated them at 1,050°C. After every 10 hours of heat treatment, the researchers quenched the SiC pellet residue in lab air, and then washed the residue in boiling water. They calculated the SiC pellet weight loss, and then returned the residue to the furnace with fresh K_2CO_3 salt for the next run. The team repeated this process until the SiC pellet was totally dissolved in the molten salt.

The following results were obtained:

- SiC nanoparticles and one micron-size particle are rapidly oxidized in molten sodium carbonate at temperatures as low as 950°C to form water-soluble silicates.

- Ceria pieces do not react under similar conditions.

- SiC pellets are slow to react in molten sodium carbonate, even at temperatures as high as 1,050°C.

- SiC pellets can be completely reacted and dissolved to form water-soluble silicates in molten potassium carbonate at 1,050°C after about forty hours.

- Potassium salt is clearly much more effective than sodium salt.

Planned Activities

The team has completed this project. The one remaining planned effort is a manuscript, which is now in draft form and will be submitted for publication.

NUCLEAR ENERGY RESEARCH INITIATIVE

Enhancements to High-Temperature In-Pile Thermocouple Performance

PI: John Crepeau, University of Idaho (UI)

Collaborators: Idaho National Laboratory (INL)

Project Number: 06-134

Program Area: AFCI

Project Start Date: March 2006

Project End Date: March 2008

Research Objectives

The overall objective of this joint UI and INL project was to develop recommendations for an optimized thermocouple design for high-temperature long-duration in-pile testing by expanding upon results from initial INL efforts to develop doped molybdenum/niobium (Mo/Nb) alloy high-temperature irradiation-resistant thermocouples (HTIR-TCs). The project team completed tasks at INL's High-Temperature Test Laboratory, a state-of-the-art facility with specialized equipment and staff trained in high-temperature instrumentation development and evaluation. This section highlights results from tasks completed to quantify the impact on thermocouple performance of candidate enhancements, such as alternate alloys, alternate geometries, and alternate thermocouple fabrication techniques.

Research Progress

In Task 1, the research team evaluated alternate alloys of Mo and Nb for the INL-developed HTIR-TCs. The team proposed three types of high-temperature testing: 1) ductility evaluations, 2) resolution evaluations, and 3) long-duration testing (if results from the prior two subtasks were to appear promising).

Results from Task 1 evaluations indicated two alloys that yielded a thermocouple that best retained its ductility and exhibited the best resolution over the temperatures of interest: oxide dispersion-strengthened (ODS)-Mo and KW-Mo paired with Nb-1%Zr. Because the ODS-Mo is not commercially available, this material is significantly more expensive to obtain. Hence, pairing KW-Mo with Nb-1%Zr yields the best thermocouple combination. Because other

project tasks were investigating this thermocouple in various long-duration high-temperature tests, the project team did not perform additional long-duration testing as part of Task 1.

In Task 2, the team investigated the performance of thermocouples with alternate geometries. As part of this task, the team developed techniques for fabricating each thermocouple's geometry so that the thermocouple could withstand high temperatures for a long duration and transient testing. Representative samples of each alternate-geometry thermocouple were prepared and subjected to thermal cycling tests (two cycles up to 1,600°C) and a long-duration test (over 2,000 hours) at 1,500°C. Results showed that thermocouples containing larger-diameter wire (0.020"/0.508 mm) remained stable for longer time periods.

In Task 3, which was completed in the project's final year, the team explored several alternate techniques for fabricating doped Mo/Nb-1%Zr thermocouples. In particular, team members explored the impact of heat treatment temperatures and durations on thermocouple performance, and compared a "loose-assembly" thermocouple configuration with the "swaged" type of HTIR-TCs; this comparison was the subject of prior INL evaluations.

HTIR-TC fabrication requires that grain growth in the thermoelement wires be stabilized by heat treating. However, limited data were available to select appropriate temperatures and durations for this heat treatment. Heat treatment evaluations completed in this project focused on thermocouples designed to operate at 1,200°C and 1,500°C. Figure 1 compares results from calibration

runs obtained for thermocouples heat-treated at various temperatures (1,300°C to 1,500°C) for 20 hours. Results indicated that the peak emf is reduced as the heat treatment temperature increases, but that the decrease in emf is reduced at temperatures greater than 1,400°C.
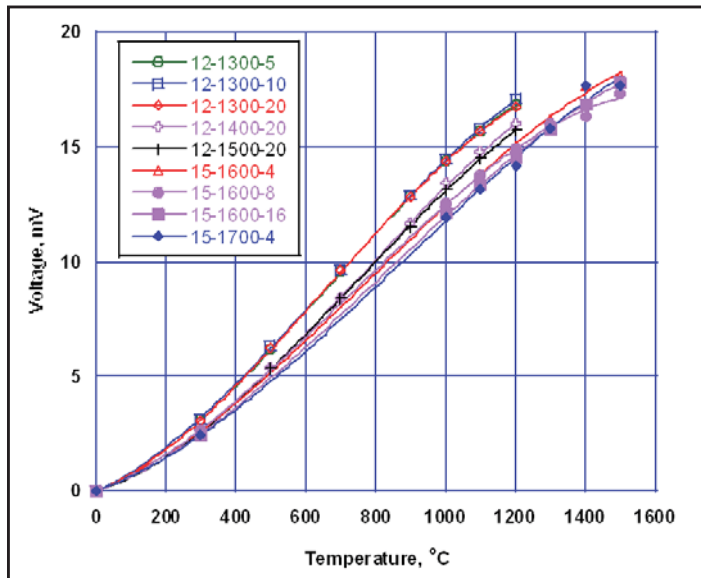

Figure 1. Calibration evaluations on HTIR-TCs heat-treated at different temperatures and durations.

Task 3 also explored viability of a loose assembly HTIR-TC design. Loose assembly fabrication required developing unique HTIR-TC thermocouple components and fixturing designs. For example, Figure 2 shows the specialized splice sleeves and transition insulator components developed as part of this project. Researchers used a trial-and-error approach to fabricate process and parameters. For
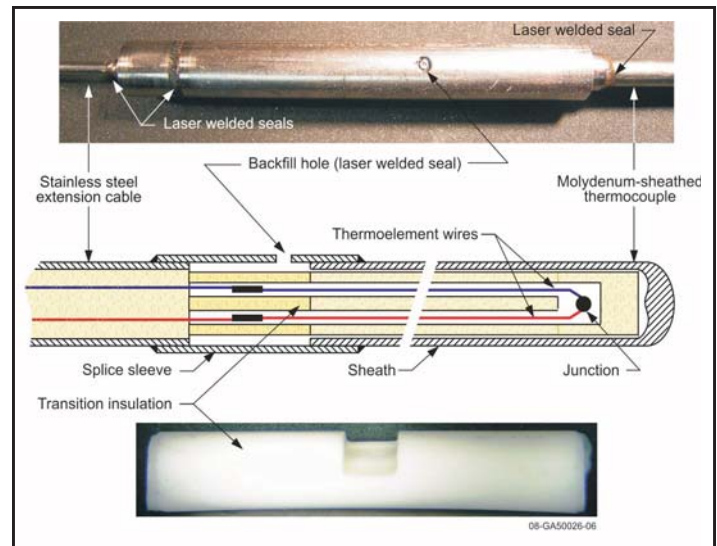
Figure 2. Specialized components for HTIR-TC loose-assembly design.

example, the team included a high-temperature "off-gas" step to prevent degradation of thermocouple wires due to oxygen release from hard-fired insulators. The team evaluated performance of prototype HTIR-TCs in a long-duration test at 1,500°C. Initial results indicated that the loose-assembly and swaged HTIR-TCs have similar stability. The team plans to perform additional investigations into the performance of loose-assembly HTIR-TCs using an alternate source of funding.

Planned Activities

The project team completed all tasks within schedule and budget in March 2008. No additional activities for this project are planned.

NUCLEAR ENERGY RESEARCH INITIATIVE

Design and Development of Selective Extractants for An/Ln Separations

PI: Robert T. Paine, University of New Mexico

Collaborators: Washington State University (WSU), Idaho National Laboratory (INL)

Project Number: 06-137

Program Area: AFCI

Project Start Date: April 2006

Project End Date: March 2009

Research Objectives

This project is designed to remove transuranic elements from spent nuclear fuel for storage or for reuse in transmutation processes. The proposed method will develop an efficient aqueous separation scheme for recovering americium (Am) and curium (Cm) from the acidic liquid remaining after UREX+2-processing to remove uranium, plutonium, neptunium, cesium, and strontium. The method will also separate trivalent actinides from fission product lanthanide ions. The project focuses on continued development and optimization of "NOPOPO ligands," which researchers previously demonstrated are effective extractants under laboratory-scale conditions and show promise as a large-scale process add-on to UREX+2.

The primary objectives of this project include 1) design, synthesis, and extraction performance characterization of 2,6-bis(phosphinomethyl)pyridine N,P,P'-trioxides (NOPOPO) as potential reagents for separating Am, Cm, and fission product lanthanides from other transuranics and fission products; and 2) development of a separations "platform" for mutual separation of Am/Cm from the lanthanides. Preliminary analyses indicate that one member of the ligand family, (EtHx)$_4$NOPOPO, offers improved separation of Am^{3+} ions from acidic aqueous solutions compared to the CMPO ligand used in the transuranic extraction (TRUEX) process. The research is expected to produce a best-case extractant compound, which will undergo a complete round of synthesis optimization and performance characterization with a realistic raffinate stimulant representative of the uranium extraction (UREX+) process.

Specific project tasks include the following:

- Optimize the NOPOPO synthesis
- Conduct further extraction testing of (EtHx)$_4$NOPOPO
- Study extractant phase compatibility, as well as hydrolysis and radiolytic stability
- Design and synthesize new NOPOPO derivatives with improved solubility, phase compatibility, and stability characteristics
- Conduct extractive testing of the new derivatives to determine their relative efficacy
- Conduct focused testing on the best-case extractant compound to optimize synthesis and characterize performance with realistic waste solutions
- Perform a cost analysis for the new process

Research Progress

The research team has previously shown that they can use three different synthesis protocols to prepare modest quantities (2 grams to 10 grams) of the family of NOPOPO ligands, shown in Figure 1, with a wide variety of aryl and alkyl R groups.

Subsequent work that focused on developing a hydrocarbon solvent soluble derivative suitable for actinide ion extractions showed that the derivative 3 with R = R' = 2-ethyl hexyl (EtHx) could be obtained in 10-gram batches with good overall
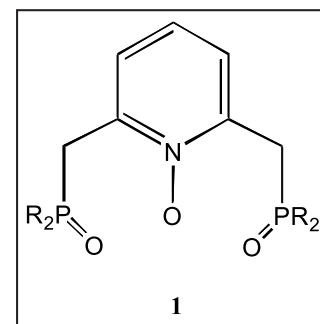

Figure 1. New family of NOPOPO ligands.

yield. However, as initially described, synthesis yields varied from batch to batch, and the crude ligand often required extensive efforts to obtain in suitably pure form. Therefore, the new program's initial objective involved development of a reliable procedure for synthesis and purification of 3 with R = R' = 2-EtHx.

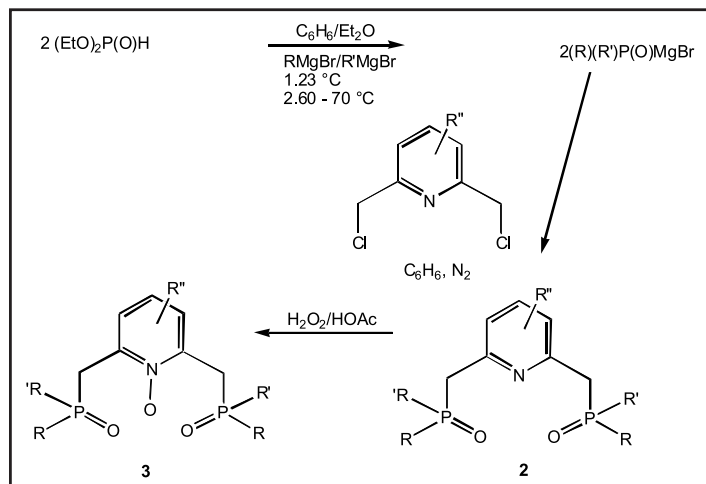During the first 12 months of the project, researchers optimized the procedure summarized in Figure 2.

Figure 2. Scheme for synthesis and purification of 3 with R = R' = 2-EtHx.

The synthesis has now been performed on a 20-gram scale with yields of 80 percent or better. The team also identified the source of the troublesome impurities: they appear to originate from the commercial starting material. Efforts to eliminate the originating species have been partially successful. At present, the purification approach involves a column purification on silica gel, followed by a Na_2CO_3 scrub to remove acidic impurities. This removes the impurity that is responsible for depressed distribution ratios at low [H$^+$]; however, the high acid Ds are still two orders of magnitude smaller than observed earlier. Work continues in an effort to reveal the source of this problem.

The synthesis effort has been expanded to include derivatives that might be soluble in the process solvent FS-13. In this regard, the team has prepared the analogs of 2 and 3, having R = R' = 2-CF$_3$C$_6$H$_4$ and 3,5-(CF$_3$)$_2$C$_6$H$_3$. Researchers have fully characterized these compounds and, during the project's second year, examined the coordination chemistry. The coordination chemistry with Ln(III) ions indicates the CF$_3$ decorated NOPOPO ligands also bind in a tridentate fashion; however, only 1:1 ligand metal complexes have been isolated and structurally characterized. The lack of formation of 2:1 complexes may be due to the added steric bulk of the CF$_3$ substituents.

Studies of aqueous acid stability of 3 (R = R' = 2-EtHx) continued during the second year. The compound is stable when stored at 20°C to 25°C and while exposed to 0.5–4M HNO$_3$ as determined by ^{31}P NMR analysis. During the first year of research, INL undertook an initial radiolysis test. The results suggested that some degradation occurred, as indicated by reduced extraction performance for Am and Cm. INL undertook a second round of studies in the second year of this project. These showed that, with more reasonable radiation dose levels, the NOPOPO is stable and extracts Am with performance close to that shown with undosed extractants.

Planned Activities

The scale-up and purification optimization studies for 3 (R = R' = 2-EtHx) continues with specific attention given to purification of the starting material. In addition, researchers plan to continue the synthesis development and purification of trifluoromethyl derivatives of 3, which may have useful performance in the FS-13 process solvent. The research team will also work toward developing the R=R'=n-octyl derivative.

The radiolysis behavior and subsequent extraction performance testing at INL will continue, as will the extraction testing at WSU.

NUCLEAR ENERGY RESEARCH INITIATIVE

Microwave Processing of Simulated Advanced Nuclear Fuel Pellets

PI: D. Clark and D. Folz, Virginia Polytechnic Institute and State University (VT)

Collaborators: University of Tennessee (UT)

Project Number: 06-141

Program Area: AFCI

Project Start Date: March 2006

Project End Date: March 2009

Research Objectives

The objective of this project is to sinter simulated (non-radioactive) oxide and nitride inert matrix fuel pellets using microwave energy. Researchers will characterize the sintered pellets with respect to density and grain morphology. Researchers on the VT team will use microwave hybrid heating (multi-mode and single mode) to sinter the pellets, while the UT researcher will use direct microwave sintering (no microwave susceptor).

Following are the primary tasks of this work:

- Prepare green pellets
- Demonstrate direct microwave heating to achieve sintering
- Demonstrate microwave hybrid heating to achieve sintering
- Characterize pellets before and after microwave processing
- Evaluate microwave processes

Research Progress

Cubic Zirconium Oxide (8 mol% Yttria). In an effort to increase the sintering density at lower temperatures for a given process (conventional or microwave), researchers must identify methods that can maximize the green density. In all of the previous experiments, the starting green density for approximately 50 μm-sized 8 mol% Yttria-Zirconia (8YZ) particles was 45 percent theoretical density (TD). One method to increase green density is to add a smaller-sized particle, which can maximize the density by filling the pores (~ 55 percent) present in the green sample. Nano-sized 8YZ particles and micron-sized particles were mixed at different ratios on a roller mill for 10 hours. Figure 1 shows the results.
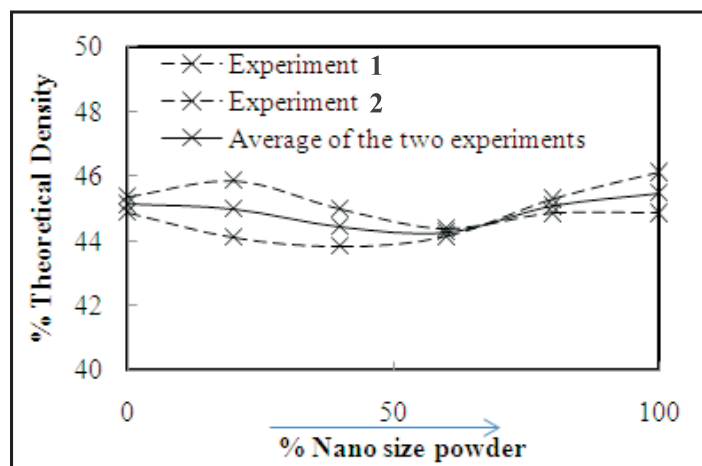
Figure 1. Effect of nano-sized 8YZ particles on green density.

This plot shows green density variation with addition of nano-sized 8YZ particles. The density did not increase appreciably with the addition of a second size particle. Possible random arrangement among the particles during pressing could explain why researchers observed no increase in green density with the addition of the nano-particles. The research team is designing different trial-and-error experiments to increase the initial density for 8YZ green pellets. For example, the team is using sonication on the particle mix in the mold before subjecting the mix to isostatic pressing.

Sintering – 8 mol% Yttria-Zirconia (8YZ). Previous reports presented sintering results obtained in a home model microwave oven. As the researchers wished to determine the results' repeatability, they performed sintering runs for 8YZ in the newly installed multimode

microwave applicator (MMA) furnace. Figure 2 is a plot that shows the densification behavior of 8YZ in different types of heating furnaces. A 20-minute soak time was maintained for all sintering runs. As seen in Figure 2, 8YZ densified to about 97 percent TD at 1,300°C in the new MMA furnace. This result was in agreement with the results obtained in the single-mode microwave furnace.
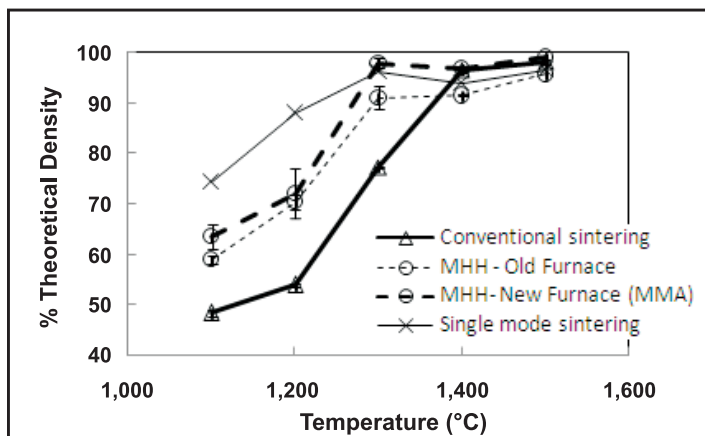

Figure 2. Densification behavior of 8YZ with respect to temperature and processing technique.

Researchers also observed a slight increase in 8YZ densities in the new MMA furnace (compared to those in the old microwave furnace). Researchers also noted a significant difference in densities between a microwave furnace and a conventional furnace at temperatures below 1,300°C.

Previous quarterly reports described 8YZ's sintering behavior in a microwave hybrid system and a conventional system. Using micro-indentation techniques, researchers are now trying to predict fatigue behavior of the 8YZ sintered pellets. The work of Vaughan (et al.) and Govindan inspired these tests. These scientists have predicted the mechanical cyclic fatigue behavior of alumina and uranium oxide fuel pellets using a micro-indentation technique. In this technique, experimenters make a Vickers indentation on the sample, as in Figure 3(a). They repeat indentations at the same spot until the corners chip out (Figure 3(b)).

During this test, experimenters kept the applied load constant and recorded the number of cycles required to chip out the indentation at a particular load. They repeated this technique for different loads in order to obtain a relationship between the load and number of cycles required to chip the indentation. This method of predicting fatigue behavior is relatively simple when compared to conventional fatigue testing because this method requires less material and time.
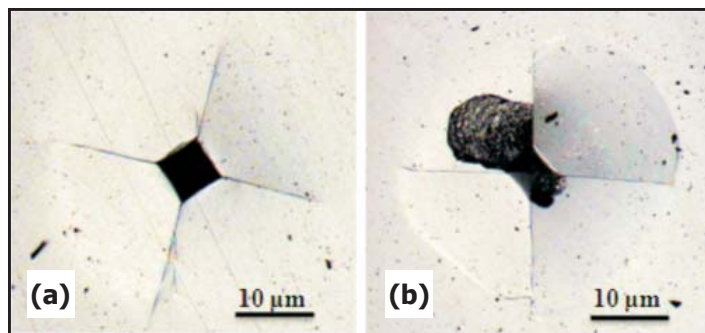
Figure 3. Representative tests performed at VT on 8YZ samples illustrating (a) Vickers indentation and (b) lateral chips coming out of the initial indentation after N number of cycles at constant load.

For the fatigue tests, the team selected 8YZ pellets sintered at 1,500°C for a soak time of 20 minutes. The team performed indentation fatigue testing on two samples, one processed in a microwave hybrid system and the other in a conventional system. Both of these samples were polished down to 0.25 µm diamond paste. Figure 4 shows the results.
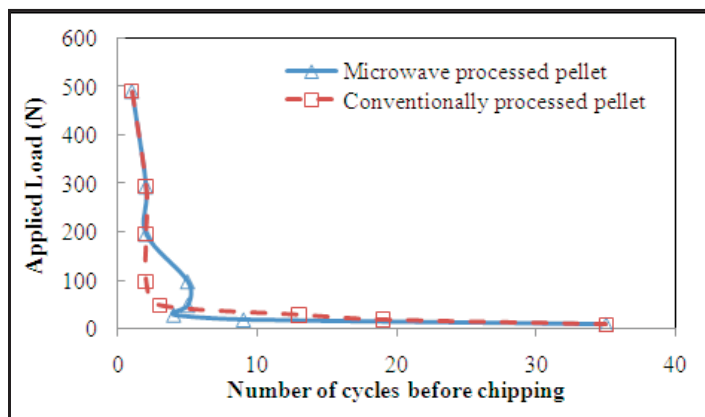

Figure 4. Fatigue curve for 8YZ: load versus number of cycles before lateral chips form.

The number of cycles required to cause chipping of the indentation increased as the indentation load decreased. At a load of 100 N, the microwave-processed sample survived a greater number of cycles than the conventionally processed pellet. The above plot shows no threshold indentation load level (fatigue limit). The research team is conducting further tests to evaluate reliability of these tests.

Cubic Zirconia – Dysprosia Composite Pellets.
During the last quarter, the team performed sintering runs for 20 wt% Dy_2O_3-8YZ (8YZ-20 D) in both conventional and microwave hybrid furnaces. Figure 5 shows evaluation of data corresponding to the sample's loss in weight before and after evaluating sintering. The percent weight loss for all the sintering runs was always less than one percent.
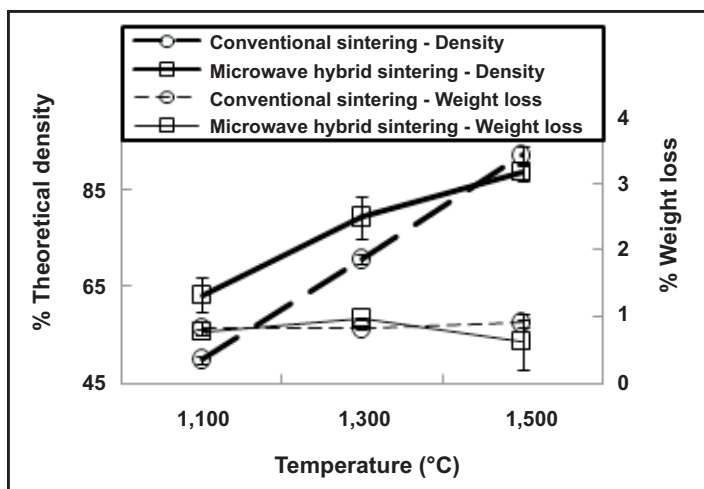
Figure 5. Densification and percent weight loss behavior of 8YZ-20 D in a conventional furnace and a microwave hybrid furnace.

Also during this quarter, the team performed isothermal sintering runs at 1,300°C for the 8YZ-20 D composite. Figure 6 shows the results.
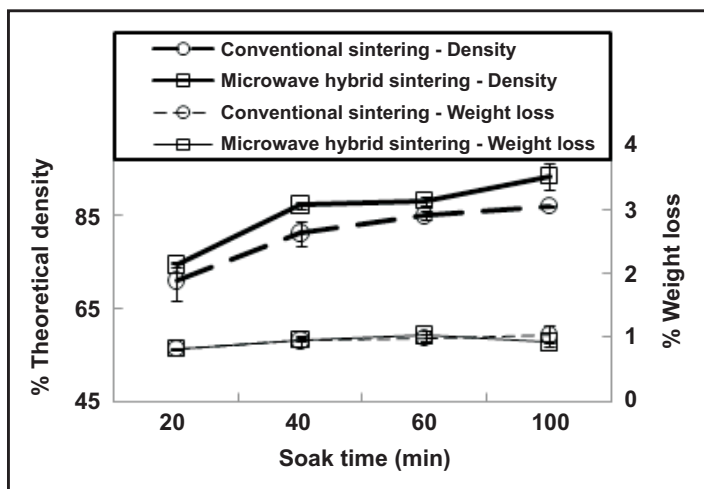

Figure 6. Isothermal densification and percent weight loss behavior of 8YZ-20 D in a conventional furnace and a microwave hybrid furnace.

For all soak times, the microwave hybrid sintered samples exhibited a higher density than conventionally sintered samples. The percent weight loss for all the sintering runs was less than one percent. This behavior indicates that dysprosia, which was selected as a simulant to americium, is not exhibiting a significant weight loss (i.e., > 10 percent).

Since dysprosia is not as volatile in nature as americium, researchers selected an alternative simulant with a melting point of approximately 1,200°C: manganese sequoxide (Mn_2O_3; Tm = 1,080°C). The team performed a thermogravimetric analysis run on Mn_2O_3. Mn_2O_3 showed a maximum weight loss of four percent, whereas Dy_2O_3 showed less than one percent. Figure 7 shows the results.
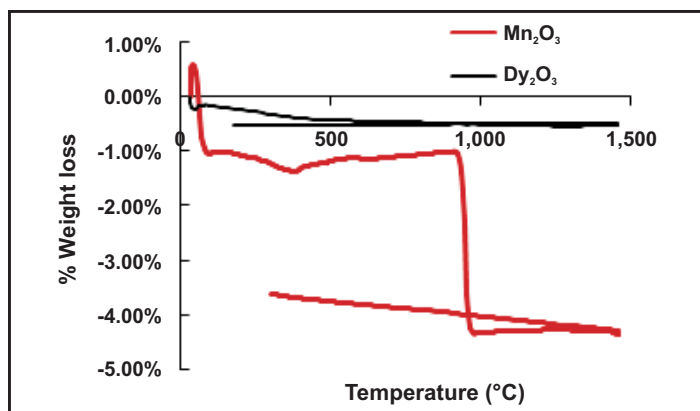
Figure 7. Thermogravimetric analysis of Mn_2O_3 and Dy_2O_3.

Zirconium Nitride. The team began performing sintering on ZrN pellets in an argon atmosphere in MMA; however, they could not complete these sintering runs because the controlled atmosphere chamber developed an argon leak.

Characterization and Testing. Sintering 8YZ at 1,300°C in the MMA furnace achieved a density of about 97 percent theoretical. The conventional furnace achieved a similar density at 1,400°C. To study the differences in processing technique, the research team selected approximately 97 percent TD dense samples for characterization and testing studies.

The team cut longitudinal sections using a diamond blade saw and mounted these samples into epoxy resin, which the researchers then cured for nine hours. Furthermore, they subjected these samples to a series of coarse polishing through a standard progression of SiC papers (180 grits, 320 grits, 400 grits, 600 grits, and 1,000 grits). Fine polishing was done using 15 microns, 6 microns, and 1 micron diamond suspensions in oil.

The team etched these polished samples using 1) chemical (H_3PO_4, HF) and 2) thermal etching. Thermal etching revealed the grain structure, whereas chemical etching did not reveal any grain structure. Figures 8(a) and 8(b) are the scanning electron microscope micrographs of the MMA-sintered sample and conventionally sintered sample. Mean intercept length method was used to calculate average grain sizes on these micrographs.

Conventionally processed samples showed a grain size of 0.66 μm, while an MMA-processed sample showed a grain size of 0.51 μm. The team also did hardness testing, using a Vickers micro-indentor. A difference in the hardness testing reflected the slight difference in grain size mentioned above. Table 1 summarizes the processing conditions and testing results. The team used Archimedes liquid displacement method to determine density and porosity.
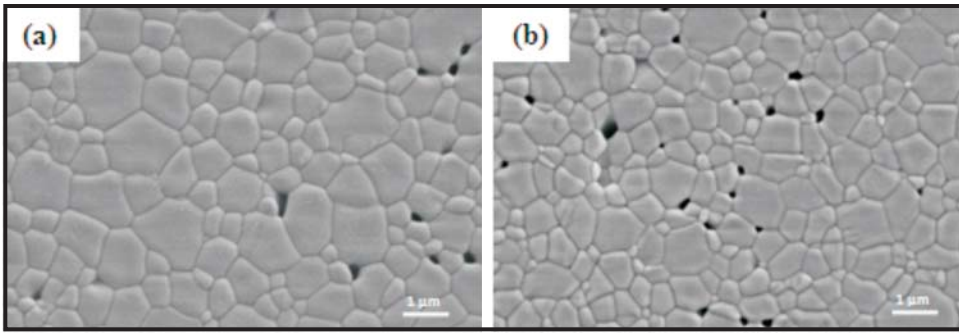
Figure 8. (a) Conventionally sintered sample 1,400°C (20 minutes) and (b) MMA-sintered sample 1,300°C (20 minutes).

	Conventionally sintered 1,400°C (20 min)	Microwave sintered 1,300°C (20 min)
Density (%TD)	97.59±0.53	97.68±0.36
% Pores (Open)	0.84±0.36	0.50±0.09
% Pores (Closed)	1.47±0.37	1.90±0.28
Hardness (MPa)	8.58±2.26	9.37±1.07

Table 1. Comparison of similarly dense 8YZ sintered pellets.

Upon comparing similarly dense samples, open and closed pore distribution differed. The microwave samples appeared to have a higher percentage of closed pores as compared to the conventionally processed sample. These differences in properties are minute. However, they imply that 8YZ processing can be done at lower temperatures in a microwave furnace without any compromise to the properties.

Planned Activities

In the final three months of this funded study, the research team will focus on developing *in situ* measurement techniques to compare linear shrinkage as a function of time and temperature in the conventional and microwave ovens. This process requires that the researchers construct a microwave dilatometer, which is already in progress. From this data, master sintering curves for the stabilized zirconia will be constructed during further work that is being proposed for this project. This data will allow the team to propose a methodology for controlling the sintering process for oxide and inert matrix materials of interest to the U.S. Department of Energy. The microwave dilatometer could provide an excellent *in situ* method for process monitoring during an eventual production phase. Additional attention is being paid to the effects of particle size and particle size distribution on the green and sintered densities of the materials under study.

Further work will also propose more integrated exploration of this method with Los Alamos National Laboratory to develop instruments that could be tested as remote process equipment in a hot cell environment.

NUCLEAR ENERGY RESEARCH INITIATIVE

Radiation-Induced Segregation and Phase Stability in Candidate Alloys for the Advanced Burner Reactor

PI: Gary S. Was, University of Michigan and Brian Wirth, University of California-Berkeley

Collaborators: Los Alamos National Laboratory, Oak Ridge National Laboratory

Project Number: 07-015

Program Area: AFCI

Project Start Date: September 2007

Project End Date: August 2010

Research Objectives

The objective of this project is to determine irradiation's effect on segregation and phase stability in candidate alloys that may be used as structural materials for transmutation in the advanced burner reactor (ABR). This project will focus on ferritic-martensitic (F-M) alloys T91 and HT-9; an experimental oxide dispersion-strengthened alloy; and an advanced austenitic alloy, D9, to investigate the electronic-magnetic-elastic interactions between chromium and radiation-induced defects. The project seeks to provide an understanding of radiation-induced segregation (RIS) and phase stability that can be used to develop predictive irradiation performance models.

Researchers will conduct experiments by proton and heavy-ion irradiation over a dose range of 3 dpa to 100 dpa and a temperature range of 400°C to 600°C. Analysis of RIS, phase microstructure, dislocation microstructure, and hardening will be conducted on all conditions. Investigators will also use *ab initio* electronic structure calculations to investigate the configuration-dependent binding and migration energies of chromium (Cr) with vacancy and interstitial defects. These calculations will enable development of atomistic-based kinetic Monte Carlo models to investigate the Cr diffusivity and segregation behavior by interstitial and vacancy mechanisms.

Research Progress

The primary objective of this program is to understand RIS and phase stability in candidate alloys for application as structural materials in the ABR. The team irradiated alloys T91, HT9, and D9 with 2.0 MeV protons to doses of 3 dpa, 7 dpa, and 10 dpa at both 400°C and 500°C. T91 and HT9 are ferritic-martensitic alloys, both of which are viable candidates for the ABR structural materials. The austenitic alloy D9 is also a leading candidate, yet it can potentially suffer from the RIS of silicon.

Following irradiation at 400°C to 3 dpa, 7 dpa, and 10 dpa, the team performed RIS measurements by scanning transmission electron microscopy with energy dispersive x-ray spectroscopy. Team members observed no pre-existing segregation in any of the grain boundaries in any of the three alloys. Thus far, researchers have analyzed the T91 and HT9 specimens irradiated at 400°C. The RIS analysis considered only prior austenite grain boundaries aligned edge-on to the electron probe. Alloy T91 exhibited Cr enrichment and Fe depletion at all three doses at 400°C, as Figure 1(a) shows. The magnitude of the Cr enrichment is ≤1.5 wt% at all boundaries studied. The point-to-point change in Cr concentration is inversely related in a nearly 1:1 ratio to the point-to-point change in Fe concentration. At all three doses at 400°C, T91 exhibits Si, Ni, and Cu enrichment. Alloy HT9 exhibits Cr enrichment at 3 dpa, but exhibits Cr depletion at 7 dpa and 10 dpa, as Figure 1b shows. However, the magnitudes of all observed Cr concentration changes are <1.0 wt%—less than the inherent uncertainty of the measurements. Ni enrichment of about 1.0 wt% is observed at all three doses in HT9 at 400°C.
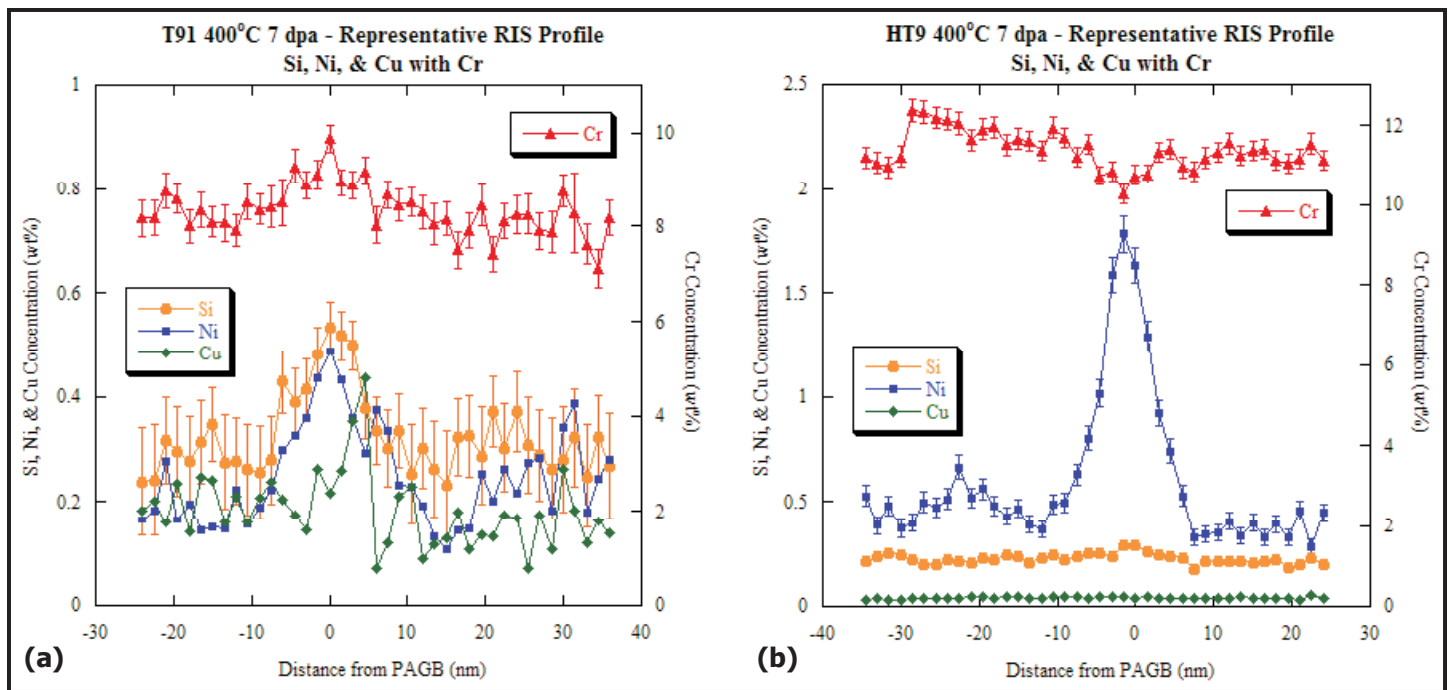
Figure 1. Grain boundary composition profiles following irradiation at 400°C to 7 dpa in (a) T91 and (b) HT9.

Researchers performed hardness measurements on all alloys before and after irradiation. Irradiation-induced hardening is greater at 400°C than at 500°C, as expected. Hardening saturates around 7 dpa, and the values compare well to those found in literature.

The research team has developed a lattice-based kinetic Monte Carlo (KLMC) model to simulate vacancy-mediated Cr transport and segregation to grain boundaries in concentrated Fe-Cr alloys. *Ab initio* electronic structure calculations informed the model, and comparison to Cr diffusivity data validated the model. The initial simulations involve calculating the radiation-induced segregation of Cr in a Fe-10%Cr alloy to a grain boundary sink for electron irradiation at 10^{-6} dpa/sec at 1,000°C. The initial KLMC results indicate Cr enrichment at the grain boundary located at the 0th atomic plane, and that Cr enrichment is increasing with fluence. Future simulations will verify these results and extend the method to simulating ion and neutron irradiation conditions.

Planned Activities

In this project's second year, the project team will conduct irradiations at 600°C to 3 dpa, 7 dpa, and 10 dpa, and also at higher doses approaching 100 dpa using heavy ions. The team will also use local electrode atom probes to analyze the grain boundary segregation of alloys in this study.

The KLMC code for vacancy-mediated Cr transport has recently been extended to incorporate interstitial-based diffusion. During the project's second year, the team will verify and validate both of these codes, then extend them to predict Cr segregation tendencies as a function of irradiation temperature, irradiating particle (ion or neutron), and dose. In addition, the team will begin a second modeling task focusing on the dislocation loop evolution in F-M alloys as a function of irradiation temperature and dose. In particular, the modeling will use atomistic molecular dynamics simulations, atomic-scale kinetic Monte Carlo, and rate theory methods as a means to 1) evaluate the formation mechanism of interstitial loops with Burger's vector of a<100> and 2) predict the size and density of evolution of both a/2<111> and a<100> loop populations. The team will benchmark predictions against the experimental database generated by the proton and heavy-ion irradiations, in addition to available neutron irradiation data.

NUCLEAR ENERGY RESEARCH INITIATIVE

Chemistry of Transuranic Elements in Solvent Extraction Processes:
Factors Controlling Redox Speciation of Plutonium and Neptunium in
Extraction Separation Processes

PI: Alena Paulenova, Oregon State University

Collaborators: Argonne National Laboratory (ANL)

Project Number: 07-023

Program Area: AFCI

Project Start Date: April 2007

Project End Date: March 2010

Research Objectives

The objective of the project is to examine the factors controlling redox speciation of plutonium (Pu) and neptunium (Np) in UREX+ extraction in terms of redox potentials, redox mechanisms, kinetics, and thermodynamics. Researchers will employ radiochemical redox-speciation extraction schemes in parallel to the redox experiment. The resulting distribution of redox species will be studied using spectroscopic, electrochemical, and spectro-electrochemistry methods. Other methods, such as x-ray absorption spectroscopy and laser spectroscopy, are available at ANL. This work will result in creation of a database on redox stability and distribution of redox couples in the nitric acid/nitrate electrolyte, as well as development of redox buffers to stabilize the desired oxidation state of separated radionuclides. Researchers will evaluate effects of temperature and concentrations of acid and salt on actinide nitrate's redox potential, considering a range of chemical matrix conditions. The database generated from the experimental work will be integrated into a selected existing actinide speciation code.

Research Progress

The relationship between redox activity and complexation in Pu and Np chemistry presents a challenge to scientists attempting to model speciation of these metals in multicomponent matrices. Ultimately, a predictive approach can accomplish the modeling. This approach is based on a new level of understanding of redox behavior of Np, Pu, HNO_3, HNO_2, and other redox-active species (organic molecules) present in separation matrices. The redox mechanisms of actinide ions in solutions are complex processes; they are complicated by radiolysis and hydrolysis of solution components. Due to the rich redox chemistry of Pu and Np, some oxidation states can be disproportionate or unstable; and some reactions are reversible, and their reaction direction depends on the reaction conditions. To optimize separation processes, researchers noted pentavalent vanadium (V) for the oxidation of Np(V) to Np(VI) instead of the traditional reduction of Pu(IV) and Np(IV) with Fe(II). Because V is very easily oxidized or reduced, its behavior in reverse redox reactions with Np was of great interest.

Reaction Between Np(V) and V(V). During the reporting time, researchers have conducted a deeper study of the oxidizing action of V(5+) on Np(5+) in solutions of nitric acid. The studied redox reaction follows:

$$NpO_2^+ + VO_2^+ + 2H^+ \leftrightarrow NpO_2^{2+} + VO^{2+} + H_2O \qquad (1)$$

It is a reverse reaction, and Equation 2 describes its kinetics:

$$-\frac{d[Np(V)]}{dt} = k_1'' \cdot [Np(V)] \cdot [V(V)] - k_2'' \cdot [Np(VI)] \cdot [V(IV)] \qquad (2)$$

where k_1'' and k_2'' are the apparent second-order rate constants of the forward and backward reaction, respectively; they are independent on actual concentrations of the metal redox species, but dependent on hydrogen ion concentration, ionic strength, and temperature. The apparent equilibrium constant K' for the studied reverse reaction can be written as follows:

$$K' = \frac{[Np(V)]_{eq.} \cdot [V(V)]_{eq.}}{[Np(VI)]_{eq.} \cdot [V(IV)]_{eq.}} \qquad (3)$$

For a given constant ionic strength and temperature, K' becomes a function only of proton concentration and, when

measured for several acid concentrations, provides the data necessary for quantification of the reverse redox process (K'= k_2''/k_1''). The experiment targeted the apparent rate constants (k_1'' and k_2'') for selected concentrations of hydrogen ions (HNO_3) and constant ionic strength ($LiNO_3$). The reaction was monitored by VIS-NIR spectrophotometry, with the fast-scanning RMS1000™ (OLIS) at 980 nm for Np(V) and at 1,225 nm for Np(VI).

Two methods were employed to determine the kinetic characteristics of studied reactions: the method of initial rates and the Runge-Kutta 4th order (RK4) method. Figure 1 displays the correlation plot of experimental initial oxidation rates (symbols) against the numeric product of initial concentrations of the reactants [Np(V)] x [V(V)] for two different four-molar concentrations of total nitrate; the slope of each linear fit estimates the value of the apparent rate constant k_1'' for the forward reaction. The numeric RK4 model was applied for both apparent constants k_1'' and k_2'' calculations. Including all measured data points in the RK4 model, this method determined the constants with a much higher degree of confidence than the method of initial concentrations, which employs only the first 10 percent of data (Figure 2). The constants k_1'' and k_2'' can be expressed as a power function of the proton concentration and reported as the following:

$$k_1'' = (1.0 \pm 0.1) \times [H^+]^{+1.20} \quad (M^{-1}/s)$$
$$\text{and}$$
$$k_2'' = (34 \pm 4) \times [H^+]^{-0.78} \quad (M^{-1}/s)$$

Reaction Between Pu(IV) and V(V). A long-term experimental run with Pu(IV) and V(V) in 4 M HNO_3 resulted in no detectable oxidation and confirmed that selective oxidation of Np(V) in the presence of Pu(IV) is possible, thus allowing oxidation of unextractable Np(V) into easily extractable Np(VI), followed by a simultaneous extraction and separation of Np and Pu from the aqueous matrix.

Planned Activities

The research team plans to conduct the following tasks in the upcoming year:

- Extend the electrochemical and spectroelectrochemical measurements of the redox kinetics of actinides (cyclic voltammetry, redox potentiometry) under a variety of conditions relevant to extraction separation processes (different concentrations of acids and salts, temperatures)
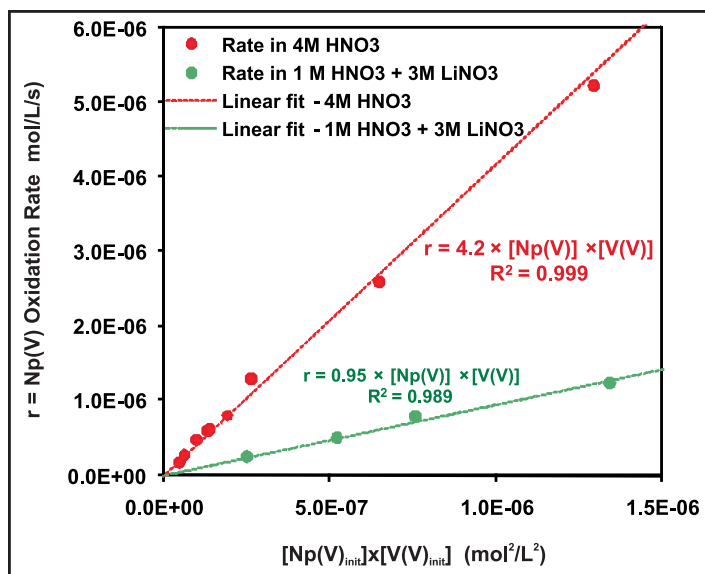

Figure 1. The initial rates for the Np(V) oxidation versus product of initial concentrations in the solutions of 4 M HNO_3 and 1 M HNO_3+3 M $LiNO_3$ at 25°C.
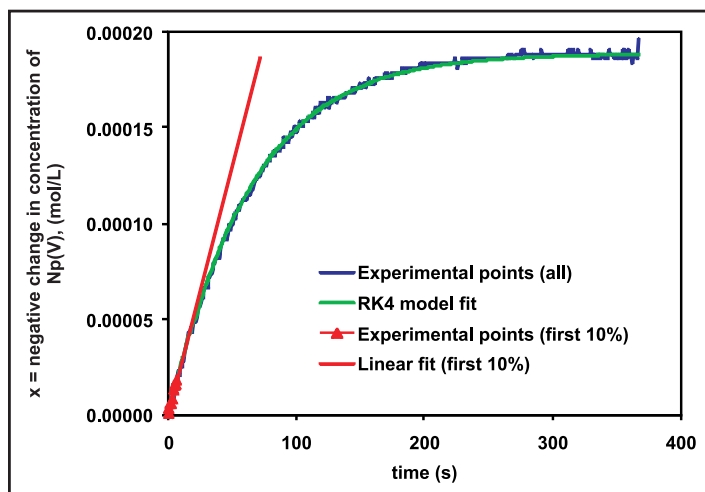

Figure 2. Experimental data for the oxidation reaction of Np(V) in 4 M HNO_3 at 25°C for 0.36 mM Np(V) and 1.8 mM V(V).

- Examine the redox kinetics of actinides (Pu and Np) with various concentrations of nitric and nitrous acid, nitrates, and selected redox agents, utilizing existing modeling programs for both the ionic equilibrium (Fiteql 4.0, SQUAD) and kinetics (GlobalWorks, RK4)

NUCLEAR ENERGY RESEARCH INITIATIVE

New Fission Product Waste Forms: Development and Characterization

PI: Alexandra Navrotsky, University of California-Davis (UC Davis)

Collaborators: Sandia National Laboratories (SNL); Eltron Research, Inc.; Brigham Young University

Project Number: 07-027

Program Area: AFCI

Project Start Date: June 2007

Project End Date: May 2010

Research Objectives

This project will identify advanced methods for chemical partitioning of spent nuclear fuel into cesium (Cs), strontium (Sr), and minor actinide (MA) constituents that can be stored for future disposition. Researchers will study new waste forms and disposal strategies for the steam reforming process to produce a Cs/Sr storage form that incorporates Sr and Cs, their decay products, and rare earth fission products. The project team will conduct a broad characterization study of inorganic ceramic waste form phases and the thermochemistry of these phases; this study will provide a comprehensive data set from which to select the appropriate waste form. Emphasis will be on perovskite phases as a major constituent of the final waste form. Project goals are to reduce costs of the guanidinium carbonate steam reforming waste process; to minimize risk of environmental contamination during waste processing; and to provide the U.S. Department of Energy with technical solutions to various issues related to Cs, Sr, and MA disposal.

Project objectives include the following:

- Establish ceramic waste forms for disposing of Cs, Sr, and MAs, which consist of transition metal oxides loaded *in situ* with minimal additional processing steps, minimizing waste volume, and producing durable waste forms for all cations and their decay products

- Fully characterize phase relationships, structures, and thermodynamic and kinetic stabilities of promising waste forms

- Establish a sound technical basis for understanding key waste-form properties, such as melting temperatures and aqueous durability, based on an in-depth understanding of waste form structures and thermochemistry

- Establish synthesis, testing, scaleup, and commercialization routes for waste-form implementation throughout in-kind collaborations with Eltron Research

The proposed work will provide information on durability and stability of these waste forms, supporting evaluation of their potential for viable storage or disposal scenarios. Since Cs and Sr form new elements by radioactive decay over several hundred years, researchers will study the behavior and thermodynamics of these waste forms using non-radioactive analogues.

Figure 1. A unique high-temperature calorimeter used for heat measurements of ceramics formation.

Research Progress

The project started with a major literature search in Fall 2007, and the team made a list of references available to all participants. Researchers then started work on Cs, barium (Ba), and Sr silicates, as well as on perovskites.

Synthetic efforts based on solid-state and sol-gel reactions have been performed for $Cs_2TiSi_6O_{15}$ and $CsTiSi_2O_{6.5}$ phases, respectively. In addition, molten salt synthesis for the fresnoite ($Ba_2TiSi_2O_8$) phase has been performed.

Calorimetric measurements on glass and crystallite fresnoite samples have been performed. All samples dissolved reproducibly, with a return to calorimeter baseline signal within 28 minutes to 32 minutes, indicative of problem-free calorimetry. Measured-drop solution enthalpies (ΔH_{ds}) of glass (A), crystalline with glass (B), and crystalline (C) fresnoites were 187.6 ± 1.2, 254.2 ± 1.7, and 259.4 ± 1.9 kJ/mol, respectively. The enthalpies of formation from the oxide ($\Delta H^o_{f,ox}$) were calculated via the thermodynamic values of binary oxides—such as BaO, TiO_2, and SiO_2—as well as their thermodynamic cycles. The enthalpies of formation of fresnoite phases (A, B, and C) from the elements ($\Delta H^o_{f,el}$) could be derived to be -4098.6 ± 6.3 (A), -4165.2 ± 6.5 (B), and -4170.4 ± 6.5 (C) kJ/mol, respectively. Furthermore, the enthalpy of vitrification is calculated to be 71.8 ± 2.2 kJ/mol, taking sample A as a representative of "completely glassy" and sample C as "well crystallized." On a two-oxygen basis, this value is 18.0 ± 0.6 kJ/mol, or about twice that of SiO_2/cristobalite (9 kJ/mol). In addition, if one assumes that sample A is completely glassy and sample C completely crystalline, while B contains a mixture of glass and crystals, then sample B would contain about 7 percent glass.

Via solid-state synthesis, researchers synthesized perovskite and pyrochlore phases in the systems $CaTiO_3$-Y_2O_3, $SrTiO_2$-Y_2O_3, and $BeTiO_3$-Y_2O_3. The team performed a second synthesis set using a mix of TiO_2, Y_2O_3, and MCO_3 precursors, with molar composition of M:Y:Ti 0.75:0.25:1. These syntheses differed from the previous experiment in two ways: a wet mixing of the powders using acetone (presumably to increase homogeneity) and rapid cooling after sintering ("quench-like"). For the Ca-Y-Ti-O system, two phases have been formed: a perovskite $CaTiO_3$-like phase with an average Y solubility of 1.28 at% and a pyrochlore $Y_2Ti_2O_7$-like phase with an average Ca solubility of 1.88 at%. For the Sr-Y-Ti-O system, two phases have been formed: a perovskite $SrTiO_3$-like phase and a pyrochlore phase with small particles embedded in the perovskite structure. The small $Y_2Ti_2O_7$-like particles prevented composition analysis due to the detection limit. For the Ba-Y-Ti-O system, three phases have been formed: a perovskite $BaTiO_3$-like phase with an average Y solubility of 0.76 at%; a $Y_2Ti_2O_7$ pyrochlore-like phase with an average Ba solubility of 0.08 at%; and a third Ba-rich phase, about 7 percent to 9 percent volume fraction, with an average Y solubility of 0.09 at%. For the Ca-Y-Ti-O and Ba-Y-Ti-O systems, results are similar to previous observations, with some changes in solubility limits. For the Sr-Y-Ti-O system, previous observations with x-ray dot mapping (Sr and Y cannot be distinguished by BSE) showed two distinct phases rich in Sr and Y. It is therefore assumed that with the Sr-Y-Ti-O system, the $Y_2Ti_2O_7$-like phase forms in small particles and may have a tendency to segregate if not immediately cooled.

Researchers attempted to synthesize $YTiO_3$ in a reducing atmosphere. A mixture of TiO_2/Eu_2O_3 was partly reduced to $EuTiO_3$ using Ar/5%H2 at 1,000°C. The team attempted to synthesize $YTiO_3$ from reducing a) $Y_2Ti_2O_7$ and b) a mixture of oxides using the same conditions; however, the $YTiO_3$ phase did not form. Both mixtures, TiO_2/Eu_2O_3 and TiO_2/Y_2O_3, showed an absence of crystalline Ti-O phase after the reduction treatment. An attempt by arc melting was also unsuccessful.

Researchers also attempted to synthesize a set of $Cs/MTiO_3$ (M=Ca, Sr, Ba) and $Cs/Y_2Ti_2O_7$ samples at 1,200°C; because of Cs volatility, the samples formed were porous. Using synthetic techniques based on an aqueous precipitation reaction, the team prepared the crystalline and glass phases of $CsTiSi_2O_{6.5}$. In addition, A_2TiSiO_5 (A = Cs, Rb, K, and Na) and $A'TiSiO_5$ (A' = Ba, Sr, Ca, and Mg) glass samples have been prepared using solid-state reactions.

The research team prepared samples of perovskites in the $BaTiO_3$-$SrTiO_3$, $BaTiO_3$-$CaTtO_3$, and $SrTiO_3$-$CaTiO_3$ systems. Calorimetry was partially completed. In an attempt to form solid solutions of $YTiO_3$ in $SrTiO_3$, Los Alamos National Laboratory prepared samples of $SrTiO_3$-$YTiO_3$ in varied compositions. Preliminary characterization showed that the samples contained the $Y_2Ti_2O_7$ phase; the process needs further reduction. Longer runs are planned. Ben-Gurion University of the Negev synthesized varied compositions of M:Y:Ti xerogels in order to estimate diffusion limits versus thermodynamic stability of Y-Ti-O incorporating in $MTiO_3$. Preliminary characterization of Ca:Y:Ti samples showed that the atomic ratios of the elements were different from what was expected. Further synthesis is needed.

	ΔH_{ds} (Jg^{-1})	ΔH_{ds} (kJmol^{-1})	$\Delta H^{o}_{f,ox}$ (kJmol^{-1})	$\Delta H^{o}_{f,el}$ (kJmol^{-1})
A (glass)	408.9 ± 2.6	187.6 ± 1.2	-237.0 ± 4.2	-4098.6 ± 6.3
B (crystal)	554.0 ± 3.8	254.2 ± 1.7	-303.6 ± 4.4	-4165.2 ± 6.5
C (crystal)	565.3 ± 4.2	259.4 ± 1.9	-308.8 ± 4.5	-4170.4 ± 6.5

A: amorphous sample (BTS-1/4 "glass")
B: a fully crystallized sample from the "old" glass (BTS-1 "fully crystallized")
C: a fully crystallized sample from the "new" glass (BTS-1/4F "ceramized")

Table 1. Enthalpies of drop solution in lead borate at 701°C (ΔH_{ds}) and enthalpies of formation from the oxides ($\Delta H^{o}_{f,ox}$) and from the elements ($\Delta H^{o}_{f,el}$) at 25°C for fresnoite ($Ba_2TiSi_2O_8$) phases.

UC Davis has made progress with several phases, including $Ba_2TiSi_2O_8$ (fresnoite), $(Cs_{1-x},Ba_{0.5x})TiSi_2O_{6.5}$ (pollucite), $(Cs_{2-x},Ba_{0.5x})TiSiO_5$, $CaTiSiO_5$, $SrTiSiO_5$, and $BaTiSiO_5$; researchers have presented updates at SNL. Pollucite phases were synthesized: $(Cs_{1-x},Ba_{0.5x})TiSi_2O_{6.5}$ (x = 0, 0.2, 0.4, 0.6, 0.8, and 1), and $(1-x)CsTiSi_2O_{6.5}$-$xBaTiSi_2O_7$ (x = 0, 0.2, 0.4, 0.6, 0.8, and 1.0). A product consistency test (PCT) was performed on $Ba_2TiSi_2O_8$ (fresnoite) and $(Cs_{2-x},Ba_{0.5x})TiSiO_5$.

Researchers are preparing the calorimetric and PCT work on fresnoite for publication. They have prepared crystalline and glass phases of $CsTiSi_2O_{6.5}$ using synthetic techniques based on an aqueous precipitation reaction. In addition, they have synthesized several glass samples: $(Cs_{1-x},Ba_{0.5x})TiSi_2O_{6.5}$ (x = 0, 0.1, 0.2, and 0.3), and $(Cs_{2-x},Ba_{0.5x})TiSiO_5$ (x = 0, 0.5, 1, 1.5, and 2). Using solid-state reactions, the research team has prepared

Sr-fresnoite ($Sr_2TiSi_2O_8$) glass and $(Sr_{1-x},Y_{0.67x})TiSiO_5$ (x = 0, 0.25, 0.5, 0.75, and 1) glass. The team will perform calorimetry, including simultaneous thermogravimetry and differential scanning calorimetry, and oxide melt drop solution will be done.

Note: although work at UC Davis is progressing well, the project is still proceeding slowly owing to inadequate and late funding at SNL.

Planned Activities

Following is a list of tasks for the coming year:

- Publish paper on fresnoite

- Complete calorimetry and write paper on Ca, Sr, Ba perovskite thermochemistry

- Continue attempts to synthesize $YTiO_3$

- Synthesize and measure enthalpy of formation of benitoitie and its analogues

- Continue work on Cs phases

- Investigate Zr-containing systems since the final decay product of Sr is Zr, with Y a shorter-lived intermediate

- Continue phase diagram analyses

NUCLEAR ENERGY RESEARCH INITIATIVE

Computations for Advanced Nuclear Reactor Fuels

PI: Sudarshan K. Loyalka, University of Missouri-Columbia

Collaborators: None

Project Number: 07-035

Program Area: AFCI

Project Start Date: July 2007

Project End Date: June 2010

Research Objectives

To successfully implement an efficient and effective nuclear power strategy, it is essential to develop new fuels that can provide optimal performance over long periods of time. This research will explore advanced computational techniques to improve understanding of fission gas distribution and heat transfer in solid fuel under normal and accident conditions.

Research Progress

The project team extensively reviewed literature on molecular, particulate, and phonon transport. Team members constructed and tested a direct-simulation Monte Carlo (DSMC) program for free-molecular fission product transport in arbitrarily shaped nano-pathways in TRISO coatings. The program provided good visualization and animation of the transport. Researchers have also conducted a number of parametric studies relating to pathway shapes, sizes, lengths, and boundary conditions. Additionally, the team constructed and tested two DSMC programs for nano-particle flows in cracks. Also successful were tests of algorithms needed for collisions, as described by simple intermolecular potentials. Figure 1 shows a typical binary molecular flow realization in a straight pathway.

The team also explored various algorithms for improving efficiency of collisional sampling potentials, as well as convective and diffusive flows.
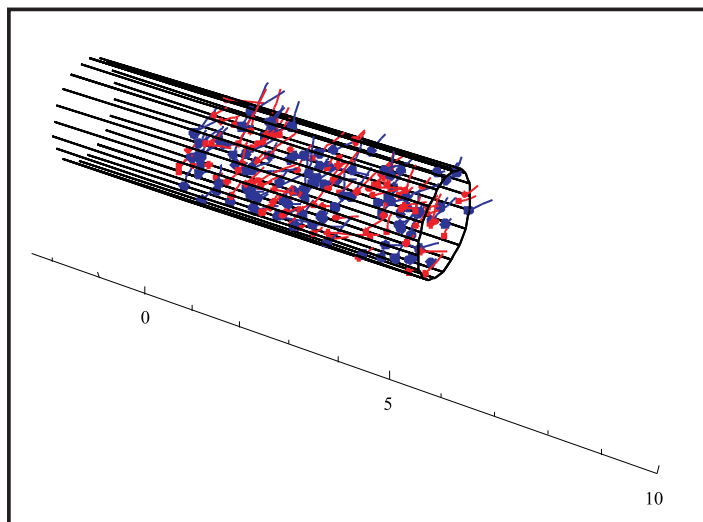
Figure 1. A simulation of fission product transport.

For heat transfer and temperature distribution, researchers have explored both deterministic and DSMC calculations directed at the phonon transport equation. A model phonon equation that applies to all thicknesses produced a range of results. These results are useful in removing divergence from the previous expressions for heat flux at low temperatures. The researchers have also constructed a DSMC program based on the model equation. They have explored construction of the full three-phonon collision operator in a computationally useful form for both deterministic and DSMC calculations, and have identified a technique enabling rapid progress once construction can begin (within the upcoming year).

Regarding journal publications, researchers have made substantial progress with several manuscripts that describe the above research results. Some documents are near completion and will be submitted in the upcoming year.

Planned Activities

The research team will complete and submit several manuscripts for publication in archival journals; topics include fission-gas distribution and phonon heat transfer. In both areas, researchers will explore increasingly more realistic cases with respect to molecular and phonon interactions with surfaces, geometries, and material compositions. The team will parallelize the calculations on a recently acquired 128-node computer, while exploring combinations of different computational languages.

NUCLEAR ENERGY RESEARCH INITIATIVE

Experimental Development and Demonstration of Ultrasonic Measurement Diagnostics for Sodium Fast Reactor Thermohydraulics

PI: Akira Tokuhiro, Kansas State University

Collaborators: Argonne National Laboratory (ANL)

Project Number: 07-037

Program Area: AFCI

Project Start Date: June 2007

Project End Date: May 2010

Research Objectives

This research project will address some of the principal technology issues related to sodium-cooled fast reactors (SFRs), primarily development and demonstration of ultrasonic measurement diagnostics linked to effective thermal convective sensing under normal and off-normal conditions. Sodium is well-suited as a heat-transfer medium for the SFR. However, because it is chemically reactive and optically opaque, sodium presents engineering accessibility constraints relative to operations and maintenance (O&M) and in-service inspection technologies that are currently used for light water reactors. Thus, there are limited sensing options for conducting thermohydraulic measurements under normal conditions and during off-normal events (maintenance, unanticipated events). Acoustic methods, primarily ultrasonics, are a key measurement technology with applications in non-destructive testing, component imaging, thermometry, and velocimetry.

This project will yield a better quantitative and qualitative understanding of sodium's thermohydraulic condition under varied flow conditions. The work scope includes evaluating and demonstrating ultrasonic technologies and defining instrumentation options for the SFR.

The researchers will demonstrate ultrasonic technology through the following activities:

- Design, construct, and operate a small, simple, university-based sodium flow loop with inventory of approximately 5 liters to 6 liters

- Develop and demonstrate ultrasonic velocimetry and thermometry, with a focus toward improved SFR O&M (i.e., using velocimetry and thermometry as diagnostic tools during normal and off-normal operations)

- Test a compact sodium-to-supercritical CO_2 heat exchanger and generate convective heat-transfer data, correlations, and operational experience during normal and off-normal operations

Research Progress

Previous Year's Activity. Kansas State University researchers have established a collaboration with ANL in order to participate in the university's Sodium Plugging Experimental Facility test program (see below). The present project will contribute to the ANL facility for overall coordination research and development in SFR technologies.

With respect to ANL's Sodium Plugging Experimental Facility, the advanced burner reactor (ABR) concept employs a supercritical CO_2 Brayton-cycle power-conversion technology. A key component for efficient power conversion is a compact heat exchanger known as the printed circuit heat exchanger (PCHE). In the ABR (or similar SFR), this would be a sodium-to-CO_2 heat exchanger. Each PCHE is essentially a monolithic block of stainless steel containing embedded narrow flow channels. Plugging of these narrow flow channels due to an impurity (e.g., oxides) present in the sodium is possible if the sodium should become supersaturated with impurities. Researchers need experimental data to assess plugging characteristics; with this data, the team can determine the optimum design of the PCHE sodium-CO_2 heat exchanger.

Following are the two specific objectives of the Sodium Plugging Experimental Facility test program:

1) To demonstrate that, for the PCHE flow-channel sizes being considered for the sodium-to-CO_2 heat exchanger, no plugging occurs if the sodium temperature is well above the impurity saturation temperature

2) To collect experimental data that can be used to model the plugging behavior as a function of the channel size, as well as the amount of impurity super-saturation
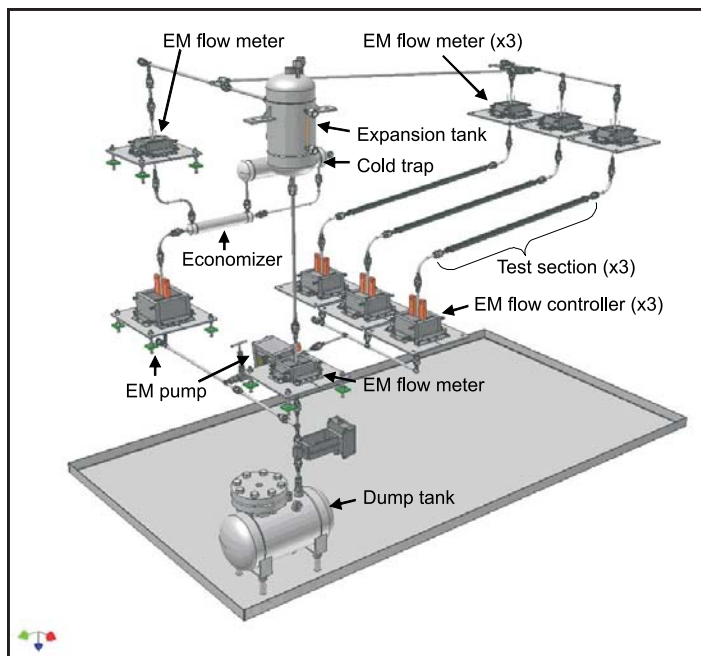

Figure 1. Schematic of a small sodium loop facility at ANL.

As shown in Figure 1 above, the apparatus consists of a main sodium loop with three test sections, a bypass sodium loop including a cold trap/economizer assembly, and an auxiliary system comprising Argon and vacuum lines. The main loop, as well as the bypass loop, is constructed from stainless steel tubing. Other major components include electromagnetic (EM) flow controllers, EM pumps, EM flow meters, and expansion and dump tanks. The sodium-loop system is about 1.8 m tall and is heated by a number of ceramic band heaters. The loop's maximum operating temperature and pressure are 510°C and 207 kPa (= 30 psig), respectively. At about 800 A, the nominal flow rate and pressure head are 4×10^{-5} m^3/s

(= 2.4 liters/min) and 40 kPa, respectively; however, the EM pumps can operate at up to 1,000 A for higher flow-rate and pressure-head operations.

Based on experimental results, under "clean" sodium flow conditions, there is no apparent plugging of the micro-channels tested in the above sodium loop.

Ultrasonic Doppler Velocimetry, Thermometry, and Sensor Design. The principles of ultrasonic Doppler velocimetry (UDV) are noted in a well-documented list of publications at www.met-flow.com.

UDV can be used with gases; however, the acoustic velocity in gas is roughly 300m/s versus >1,500m/s in liquids, so UDV can be used as a quasi-live velocimetric "tool" in liquids. That is, it provides both spatial velocity information (distribution) and temporal velocity information. The former can be derived along the acoustic beamline by measuring and sufficiently sampling the Doppler shift (per channel) at the time of echo detection (thus requiring "seeding" of some sort); the latter can be derived as the ultrasonic burst and echo reception (Doppler shift measurement) is rapidly (electronically) cycled. Thus, spatio-temporal velocimetric information is acquired much like a laser-based velocimetry method (laser Doppler, particle image, etc.). Specifics about the Met-Flow Ultrasonic Velocity Profile (UVP) monitor used here can be found at www.met-flow.com. The UVP was procured using leverage funds.

The project has purchased and begun initial testing of a Met-Flow SA UVP Model DUO. For ultrasonic thermometry, the project has ordered additional digital signal-processing instrumentation, which will be tested upon delivery in late 2008. Further, in order to realize ultrasonic velocimetry and thermometry at SFR-relevant temperatures, the project requires transducers that can operate in excess of 500°C. The Curie temperature limits Piezoelectric (Pz) elements commonly used in ultrasonics; the highest Curie temperature for commercially available piezoelectrics is 650°C for bismuth titanate. Although plans are under way to procure these Pz elements, the project has initiated a design effort to integrate gas cooling of lower-temperature transducers. One current design is shown in Figure 2.
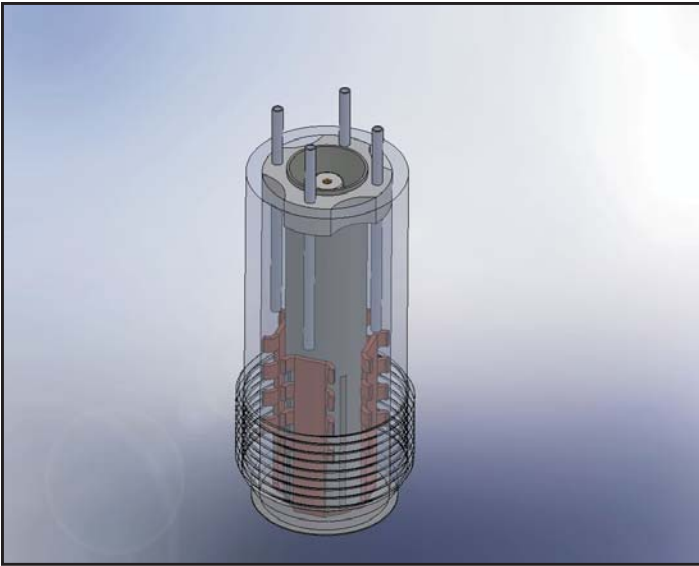
Figure 2. Current design of the cooled ultrasonic transducer.

Planned Activities

Based on the objective to develop and demonstrate ultrasonic technologies for the SFR, a scope of work was defined in terms of project tasks and associated metrics. Researchers plan to undertake the following:

- Continue with design of the pipe flow test section for velocimetry and thermometry

- Continue with design of the active "economizer" (cold trap)

- Continue with considerations and negotiations with Heatric, who has provided a quotation for a potential sodium-to-CO_2 heat exchanger

- Perform shakedown testing of ultrasonic signal-processing instrumentation for thermometry in early 2009 after the instrumentation is delivered (already ordered and expected in late 2008)

- Develop a generalized capability to analyze compact heat-exchanger designs using CFD; develop a methodology to optimize design for a given set of desired design parameters. This methodology will be applied to a sodium-to-CO_2 heat exchanger design.

- Hold a meeting with ANL to prepare for delivery of the test section, active cold trap, and ultrasonic instrumentation. The team and ANL will work collaboratively to develop operations, safety, and experimental plans.

NUCLEAR ENERGY RESEARCH INITIATIVE

Fundamental Processes of Coupled Radiation Damage and Mechanical Behavior in Nuclear Fuel Materials for High-Temperature Reactors

PI: Simon Phillpot, University of Florida

Collaborators: Idaho National Laboratory, Los Alamos National Laboratory

Project Number: 07-046

Program Area: AFCI

Project Start Date: June 2007

Project End Date: May 2010

Research Objectives

A longstanding issue for the nuclear industry is degradation of mechanical properties of nuclear fuels under irradiation, including both fissionable material and cladding. Developing fuel systems with improved resistance to radiation damage will allow longer burnups, improved usage efficiency, increased time between refueling, and decreased waste. The objective of this project is to elucidate the relationship between the microstructure, radiation damage, and mechanical properties of nuclear fuel materials. This research focuses on developing an understanding of 1) fundamental mechanisms of radiation damage in polycrystalline materials, 2) the effect this damage has on plastic deformation, and 3) the effect of mechanical deformation on radiation tolerance.

Researchers use hexagonal close-packed (HCP) titanium (Ti) (representing HCP Ti alloys for fast reactors and zircaloy for cladding in thermal reactors) and uranium dioxide (UO_2). To simulate radiation damage, the research team applies state-of-the-art, large-scale, atomic-level simulation through a judicious combination of conventional molecular dynamics (MD) and accelerated MD methods. The team applies large-scale MD simulations to elucidate mechanical behavior. This systematic program simulates irradiation's effects on structural and mechanical properties of polycrystalline Ti and UO_2; the simulations will help identify radiation damage mechanisms and provide insights into the expected behavior of nanocrystalline microstructures and nanocomposites. This work will ultimately help researchers design microstructures that are less susceptible to radiation damage and thermomechanical degradation.

Research Progress

Defect Clustering in UO_2. Using a method developed under this project, researchers have simulated long-term effects of radiation damage on UO_2's defect properties. The team found that all defects rapidly recombine and annihilate when Frenkel pairs are introduced into only one sublattice—i.e., on either uranium or oxygen, but not both. In contrast, when the defects are present on both sublattices, they form clusters. The uranium defects are immobile, but the oxygen defects diffuse through the system. Four interstitial oxygen ions penetrate a unit cell of UO_2, resulting in twelve oxygen atoms present in a single unit cell. As a result, all twelve oxygen ions are present on the interstitial position after knocking the original eight from their lattice sites; all original oxygen sites become vacant (see Figure 1). This kind of cluster has also been previously observed experimentally, but has not been previously seen in simulation. The simulation approach used here holds significant promise for providing new insights into radiation damage in materials.
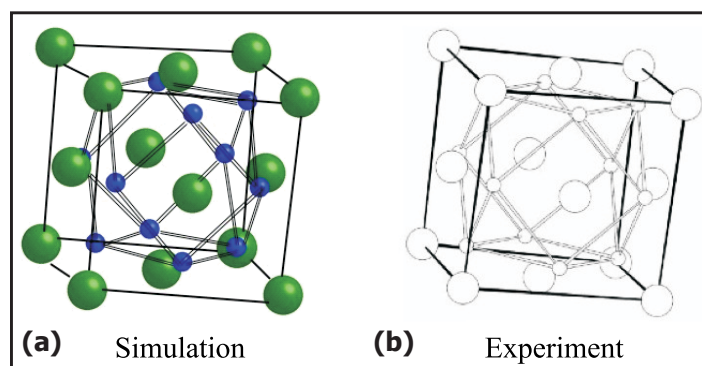

(a) Simulation   (b) Experiment

Figure 1. (a) Cluster of 12 oxygen atoms in UO_2 that represent (b) the same cluster seen in simulation and experiment.
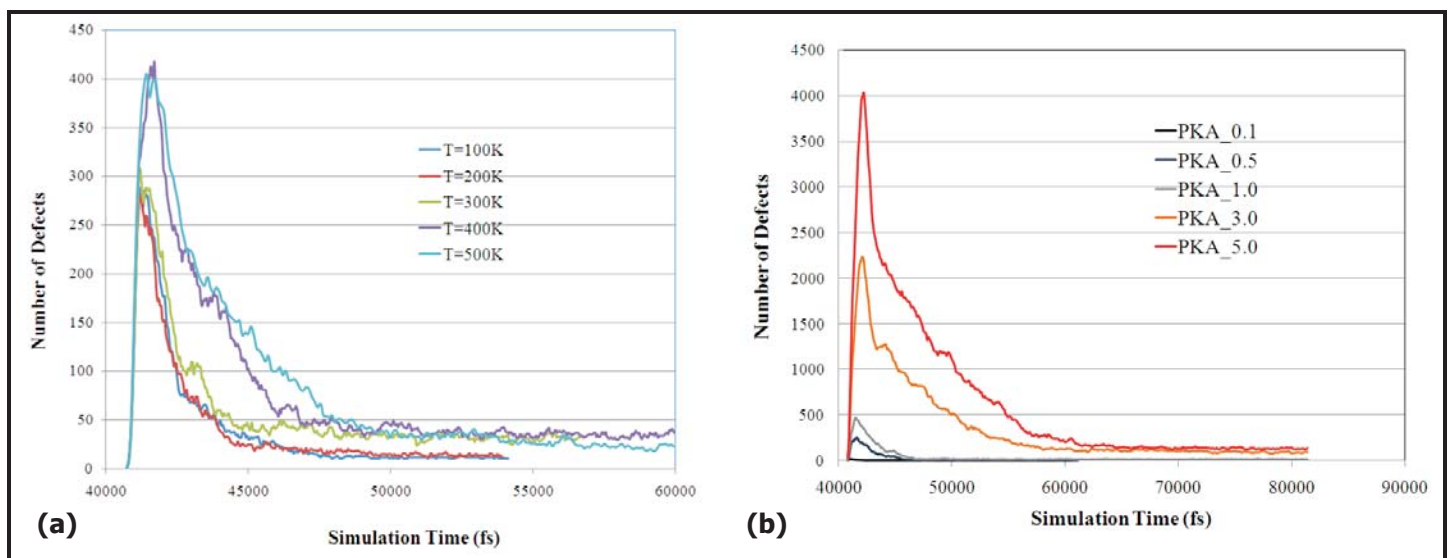
Figure 2. (a) The dependence of the number of defects on simulation time at different temperatures; (b) effects of PKA energy on number of defects.

Radiation Cascades Simulations in Titanium. The team has conducted radiation cascade simulations in Ti. Temperatures ranged from 100 K to 500 K with incident primary knock-on-atom (PKA) energies between 0.1 and 5 keV, as shown in Figure 2(a); researchers noted the number of defects at various times. The team established the dependences of the number of defects produced on simulation time at various temperatures. As temperature increased, the maximum number of defects created increased. Since the only difference between these simulations was temperature, the results indicate that a thermal-activated process is taking place. As Figure 2(b) shows, PKA energy also has a significant effect on the number of defects created during the radiation process.

Mechanical Properties of a Polycrystalline HCP Metal. Researchers have investigated the mechanical properties of an HCP metal as described by an embedded-atom model potential. The primary slip system for magnesium, to which this potential was parameterized, is (0002) <11$\bar{2}$0>. Twinning usually takes place along {10$\bar{1}$2} <10$\bar{1}$1> at room temperature. The Mg-polycrystal structure was oriented to allow both slip and twinning to be observed. Figure 3 shows the effects of applying a 2-GPa tensile stress in the horizontal direction to a textured polycrystal containing four 2-nm grains. The originally hexagonal grain structure has, to a large degree, already broken down. The red lines represent stacking faults (i.e., fcc coordinated regions) which are, in many cases, terminated by partial dislocations (black).

Planned Activities

Researchers will elucidate the governing mechanism associated with clustering. In particular, they will clarify
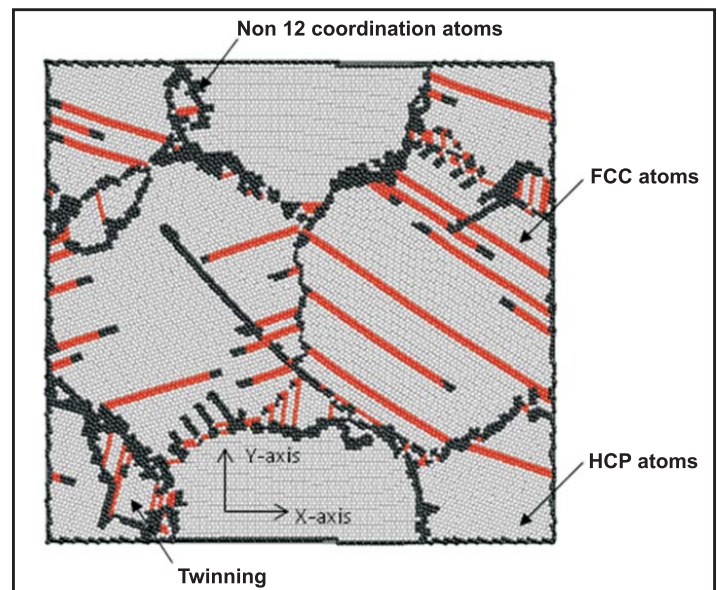
Figure 3. Structure after 9.58 percent tensile strain for an HCP polycrystal with 20-nm grain size under 2-GPa stress in the horizontal direction.

the role that immobile (at least on the time scale of these simulations) uranium defects have on the clustering mechanism. Researchers speculate that the uranium vacancies are responsible for clustering. A complete analysis of the clusters is also in progress.

Using the recently developed method for simulating radiation cascades, researchers will characterize defect clustering mechanisms in Ti. While initially researchers will simulate single-crystal materials, they will rapidly shift focus to polycrystalline materials, for which they will elucidate the coupling of radiation damage and microstructure.

Finally, researchers will fully characterize effects of stress, grain size, and microstructure on mechanical properties of HCP metals. In addition, the team will identify the plasticity mechanisms and effects of temperature.

NUCLEAR ENERGY RESEARCH INITIATIVE

Economic, Depository, and Proliferation Impacts of Advanced Nuclear Fuel Cycles

PI: K.B. Cady, Cornell University

Collaborators: University of Texas at Austin

Project Number: 07-051

Program Area: AFCI

Project Start Date: June 2007

Project End Date: May 2010

Research Objectives

The objective of this project is to compare two means of reducing actinide inventory: recycling actinides using fast burner reactors (FRs) and recycling actinides using inert matrix fuel (IMF) in light water reactors (LWRs). The project focuses on their economics and proliferation resistance. In addition to making use of the current LWR fleet, IMF can offer a four-fold increase in repository capacity when compared to direct disposal of an energy-equivalent quantity of spent LWR fuel, with over 98 percent destruction of plutonium (Pu)-239. Research also suggests that leaving IMF pins in the reactor after their reactivity has been depleted (effectively making them actinide targets) could offer a significant increase in actinide destruction. FRs can potentially increase repository capacity by more than an order of magnitude per kilowatt of electricity generated. However, FR spent fuel must be recycled many times in order to achieve this result, whereas the increase in repository capacity offered by IMF does not require reprocessing the IMF itself. Unlike previous studies that assumed continuous recycling of spent FR fuel, this project will analyze the impact of IMF and FR transmutation strategies over a finite period.

Research Progress

During this reporting period, burnup simulations have been run for IMF fuel with compositions as laid out in the proposal and for burnups extending to 650 MWd/kgIHM (for IMF with 12 elements without Pu+Np [neptunium] and 15 without Pu+MA) and 550 MWd/kgIHM (for IMF with 8 elements without Pu+Np and 8 without Pu+MA). The 15 IMF elements without Pu+MA have also been run to 850 MWd/kgIHM.

Researchers used ORIGEN 2.2 in conjunction with output data from these simulations to calculate the heat and radiological output from the spent IMF. A probabilistic model for the life-cycle cost of IMF and FR fuel cycles is under development. Unit costs are being assembled through Organisation for Economic Co-operation and Development/Nuclear Energy Agency (OECD/NEA) publications, published data from THORP, and the Advanced Fuel-Cycle Cost Basis report, which Idaho National Laboratory is assembling. A comparison of the total actinide inventory that would remain in the year 2100 for the two options was published in the article "A Practical Limit for Actinide Transmutation Using Inert Matrix Fuels" that appears in the Proceedings of the 2008 Physor Conference.

The project team undertook an assessment of best-case reprocessing costs assuming a system of government-owned reprocessing plants, each with a 40-year service life, that would reprocess spent nuclear fuel generated between the years 2010 and 2100. The results of this work appear in the article "Cost Analysis of the U.S. Spent Fuel Reprocessing Facility" that will appear in the *Energy Economics* journal. The team has also begun a literature survey to review previous work on high burnup IMF and FR fuel cycles applicable to the burn-down of transuranics (TRUs) from LWR-based fuel cycles and disposition Pu from dismantled weapons.

Planned Activities

The following are anticipated tasks for the coming year:

- Determine material balances (including proliferation-sensitive materials) for IMF and FR fuel cycles that operate over a finite time period; use the burnup/criticality codes—VBUDS, MCNPX/ MONTEBURNS, and REBUS-3—to determine isotopic balances for representative TRU vectors, typical LWR parameters, and FRs with different conversion ratios

- Determine the radiological and heat load to a repository for likely scenarios for each fuel cycle; use ORIGIN 2.2 and the spent-fuel composition for the respective IMF and FR cycles

- Determine fuel cycle cost in $/kWhr for each of the respective fuel cycles; apply probabilistic discount model unit cost data published by the OECD/NEA and investigate the effect of uncertainties in cost, discount rates, and time

NUCLEAR ENERGY RESEARCH INITIATIVE

Analysis of Advanced Fuel Assemblies and Core Designs for the Current and Next Generations of Light-Water Reactors

PI: Jean C. Ragusa, Texas A&M University

Collaborators: None

Project Number: 07-059

Program Area: AFCI

Project Start Date: September 2007

Project End Date: August 2010

Research Objectives

Existing light-water reactor (LWR) advanced fuel assembly designs could reduce the plutonium inventory of reprocessed fuel. Nevertheless, these designs are not effective in stabilizing or reducing the inventory of minor actinides (MAs). The objective of this project is to develop LWR fuel assemblies that can efficiently transmute plutonium and minimize MA inventories. The project will investigate and analyze advanced LWR assembly designs with improved thermal transmutation capability regarding transuranic elements and especially MAs. Researchers will study various fuel types, namely high burnup advanced mixed oxides (MOX) and inert matrix fuels, in various geometrical designs that are compliant with the core internals of current and future LWRs. The project team will analyze several fuel pin designs and fuel assembly designs while considering neutronics/thermal hydraulics effects.

The best-performing designs will be used in 3-D core-depletion methodology to determine overall transmutation performance in various fuel-cycle scenarios. The project will use transmutation efficiency and safety parameters to rank the various designs.

Research Progress

For fuel assembly neutronic designs, the project selected the DRAGON code (developed at the Ecole Polytechnique de Montreal, Canada). The code has outstanding geometric modeling capabilities and robust neutron transport solver features (such as self-shielding formalism and ray-tracing in general 2-D/3-D geometries, with solution procedures based on the method of characteristics and/or collision probabilities). This flexible geometric modeling capability allows for various pin configurations (cylindrical, annular, and cross-shaped). Several multigroup isotope libraries, based on a variety of evaluations, are available from 172 groups to 361 groups. The energy equivalence principle between standard uranium oxide (UOX) fuel assemblies and innovative fuel assemblies was derived and verified based on public domain data regarding the French experience with UOX- and MOX-loaded cores. Various advanced MOX (AMOX) fuel assemblies have been designed: 1) AMOX based on multiple recycling of previous-generation AMOX assemblies, with adequate U-235 enrichment to supplement reduction of fissile Pu content, and 2) standard UOX and AMOX assemblies with an $(Am,Zr)O_2$ coating. The first concept is similar to a design by the Commissariat à l'énergie atomique in France, but re-uses the penultimate AMOX generation rather than the first MOX generation to obtain the next generation. The second concept is novel and inspired by the integral fuel burnable absorber design by Westinghouse. Figure 1 presents the analysis related to the voiding of an AMOX assembly: as the moderator density increases, the neutron spectrum becomes harder and fission reactions from even-parity Pu isotopes lead to increased reactivity. Such designs, therefore, entail a maximum allowable loading of Pu. Depending upon the Pu vector isotopics, this limit is about 9 w/o to 12 w/o. Table 1 presents, in terms of net electricity production, the mass balances for various AMOX, americium (Am)-coated UOX, and Am-coated AMOX designs. The innovative design based on Am-coated pins is the most promising design, as this strategy could significantly decrease the Am inventory.

The research team is performing thermal hydraulic analysis of advanced PWR fuel assemblies with the VIPRE subchannel analysis code using neutronics data for various assembly design features. In particular, the radial and axial power profiles vary according to design characteristics. The maximum power peaking for the hottest rod is set at 2.5 herein, which is the same as for the reference Westinghouse PWR core. To confirm that the new designs maintain safety criteria, the team is conducting steady-state, single-pass hot-channel analyses using ⅛ core symmetry at 18 percent overpower.

Mass balance	Standard	Advanced MOX		
	UO$_2$	4 Pu	8% Pu	12% PU
ΔPu (kg/TWh-e)	26.54	-19.8	-48.3	-71.1
ΔNp (kg/TWh-e)	2.08	1.54	1.06	0.53
ΔCm (kg/TWh-e)	0.25	2	2.62	3
ΔAm (kg/TWh-e)	1.6	6.2	10.6	14.7
Am-Coated Pins	MOX		UOX	
Coating thickness	0.001cm	0.002cm	0.001cm	0.002cm
ΔPu (kg/TWh-e)	-47.5	-46	27.4	28.2
ΔNp (kg/TWh-e)	1.05	1.09	2.08	2.09
ΔCm (kg/TWh-e)	2.68	2.68	0.32	0.38
ΔAm (kg/TWh-e)	9.72	8.78	0.55	-0.51

Table 1. Mass balances.

Figure 2 on the right shows maximum fuel centerline temperatures in the core versus burnup for each of the following cases:

- Conventional 4.9 percent enriched UO$_2$ [Core Power = 3,120 MW$_t$]

- 4 percent Pu, 3.7 percent U-235 MOX [Core Power = 4,012 MW$_t$]

- 8 percent Pu, 2.3 percent U-235 MOX [Core Power = 4,012 MW$_t$]

- 12 percent Pu, 0.3 percent U-235 MOX [Core Power = 4,012 MW$_t$]

Fuel centerline temperatures for the UO$_2$ case differ substantially from those for the MOX cases; the difference is due to the UO$_2$ core's lower thermal power. The melting temperature for 12 percent Pu MOX illustrates the fuel melt thermal margin for these assembly designs. The plot covers the first cycle for the assembly. Since the assembly has its highest content of fissile material and is located in the hottest section of the core at this time, the plot shows the minimum thermal margin during the core lifetime.

Planned Activities

Following is a list of planned activities to be accomplished over the next year:

- Pursue development of advanced MOX and Am-coated UOX fuel pins

- Develop advanced ceramic fuel concepts

Figure 1. Moderator Voiding Effect.
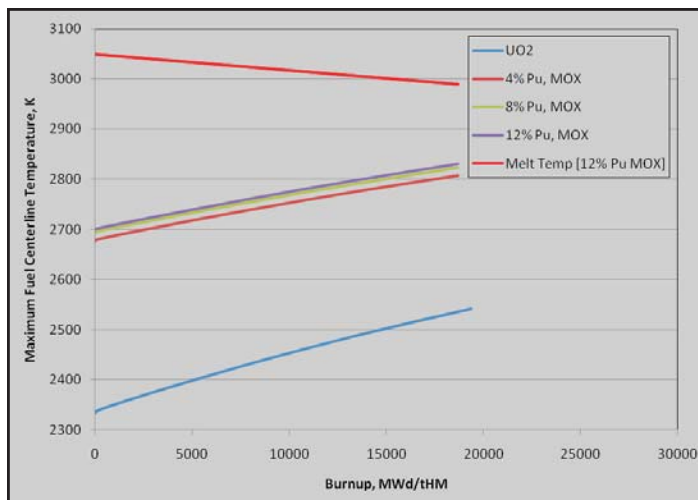
Figure 2. Maximum fuel centerline temperatures in the core versus burnup for each of the above cases.

- Continue modeling fuel pins and assembly concepts

- Develop linking methodology for passing information to and from neutronics and thermal hydraulic codes

- Enhance the iterative exchange of information between neutronics and subchannel codes

- Develop LWR-based fuel-cycle scenario (multiple recycles versus one recycle)

- Assess quantifiable metrics for fuel assembly designs (e.g., long-term radiotoxicity per TWe.h/yr, MA inventories per TWe.h/yr, safety parameters, etc.)

- Pursue evaluation of fuel assembly and core design safety margins

NUCLEAR ENERGY RESEARCH INITIATIVE

Powder Metallurgy of Uranium Alloy Fuels for Transuranic-Burning Fast Reactors

PI: Sean M. McDeavitt, Texas Engineering Experiment Station

Collaborators: None

Project Number: 07-060

Program Area: AFCI

Project Start Date: April 2007

Project End Date: March 2010

Research Objectives

This project is evaluating fast reactors to enable transmutation of transuranic (TRU) isotopes generated by nuclear energy systems. TRU isotopes have high radiotoxicity and relatively long half-lives, making them unattractive for disposal in a long-term geologic repository. Fast reactors are able to utilize TRU elements as fuel, thereby destroying those elements while releasing their valuable residual energy content. Using powder metallurgy methods, scientists can fabricate metallic fuel containing TRU isotopes.

The performance of U-10 wt. zirconium (Zr) and other uranium (U) alloy fuels was demonstrated at the Experimental Breeder Reactor-II between 1964 and 1994. This fuel was fabricated by injecting casting rods from a molten pool of U-Zr alloy. Even though this method is proven and effective, it was accompanied by high material losses due to chemical interactions with quartz casting molds. For the newer TRU-bearing fuel designs, direct melt casting is impractical since americium and, to a lesser extent, neptunium have especially high vapor pressures and cannot be contained in a molten alloy pool at 1,200°C to 1,500°C.

Research Progress

This project is developing powder metallurgical fabrication technologies to produce U-Zr-TRU alloys at relatively low processing temperatures (500°C to 600°C) using hot extrusion and/or alpha-phase sintering. The project team will quantify fundamental aspects of both processing methods. Surrogate metals will be used to simulate the TRU elements. For example, magnesium (Mg) will be used since it has not only a melting point close to that of plutonium but also vapor pressure properties comparable to those of americium. If successful, this process will produce novel solutions to some of the nagging issues related to metallic fuels, such as fuel-cladding chemical interactions and fuel swelling, volatility losses during casting, and casting mold material losses.

Two candidate processing pathways are being investigated: 1) hot extrusion between 500°C and 650°C, and 2) sintering of alpha uranium with liquid phase enhancements at approximately 650°C. The startup of these experimental activities involved the installation and shakedown of a large inert atmosphere glovebox (see Figure 1). This glovebox became fully operational in the fall of 2008. The glovebox is filled with approximately 120 ft^3 of argon gas, which is circulated and purified to contain less than 5 ppm H_2O and less than 30 ppm O_2. The box is equipped with an oxygen/moisture sensor, an overpressure safety system, and a furnace well (2-inch diameter by 15-inch depth) with a maximum temperature of 800°C. The box has two airlocks (one on each end); the right-hand airlock (visible in Figure 1) has been equipped with electrical and thermocouple feedthroughs for a small heater, enabling hydride-dehydride powder fabrication of high-purity finely divided uranium powder. The Texas Engineering Experiment Station's safety office has reviewed and approved the system's safety and operational procedures. Initial powder fabrication and sintering experiments are under way.

Figure 1. Glovebox installed at Texas A&M University for powder metallurgy of uranium alloys.

The Y-12 National Security Complex supplied depleted uranium metal slugs. The project team has installed and tested the equipment for the alpha-phase sintering experiments. The experiment will focus on low-temperature sintering of U-TRU-Zr alloy fuel, with Mg as a volatile surrogate for the TRUs. Previous work has indicated that some degree of sintering will occur near the α-β phase transition temperature of uranium (667°C). The key variables will be time, temperature, green density, powder morphology, and liquid metal enhancements. The planned procedure for the sintering experiments is as follows.

1) The research team will condition depleted uranium (DU) metal using a dilute nitric acid wash in an argon-filled glovebag to remove any contaminants on the surface, such as an oxide layer. (A glovebag will keep liquids out of the large stainless-steel process development glovebox.)

2) Using a sealed argon-filled plastic jar, the team will transfer the clean DU to the west airlock of the process development glovebox. The rest of the experiment will take place entirely inside of the large glovebox, except for post-test scanning electron microscopy (SEM) measurements, which will be made at the Texas A&M Microscopy Center.

3) The west airlock has a transformer and wiring installed in it so that a tube furnace can operate inside of the airlock. Inside this furnace, the DU metal slugs will be converted into powder through a hydride/dehydride process.

4) The team will measure a 3-gram sample of the DU-10 Zr (initial tests will not use Mg). The powder will then be placed in a double-action punch and die, then compacted using a hydraulic press.

5) The researchers will place the pressed pellet (diameter = .50 cm) in a furnace well in the middle of the glovebox (T_{max} = 1,073 K), then heat the pellet to a temperature close to the alpha-beta phase transition temperature. A linear variable differential transformer will be used to measure the pellet's sintering rate.

6) The researchers will examine the pellet with either a digital microscope (to be purchased) or the SEM.

The extrusion development activities will follow the approved uranium powder-generation procedure (Steps 1 to 3) noted above. The powder will be mixed with Zr and Mg powders and loaded into copper and vanadium sheaths to enable extrusion at temperatures between 500°C and 650°C. As in the fundamental sintering studies, Mg is to be used as a surrogate for plutonium and americium. This activity is still under review, but the project expects approval to proceed in January 2009.

Planned Activities

The following activities are planned for next year:

- Complete the alpha-phase sintering experiments and evaluate efficacy of liquid phase sintering

- Complete the initial hot extrusion experiments using copper sheaths and evaluate efficacy of bare extrusion and clad extrusion using vanadium metal sheaths

NUCLEAR ENERGY RESEARCH INITIATIVE

Neutronic and Thermal-Hydraulic Coupling Techniques for Sodium-Cooled Fast Reactor Simulations

PI: Jean C. Ragusa, Texas A&M University

Collaborators: University of Chicago, Commissariat à l'énergie atomique, Argonne National Laboratory (ANL)

Project Number: 07-063

Program Area: AFCI

Project Start Date: September 2007

Project End Date: August 2010

Research Objectives

The objective of this project is to develop and implement efficient neutronic-thermal-hydraulic coupling algorithms for sodium-cooled fast reactors. This project involves prototyping the following two methodologies: 1) coupling paradigms using an operator-split technique that can preserve the accuracy order of each physics component and 2) coupling paradigms using Jacobian-free formulations, with physics-based preconditioners. The research team will address different spatial and time scales found in sodium-cooled fast-reactor applications and will apply the team's methodology to demonstrate inherent safety features of sodium fast reactors with metallic fuel. In addition, the team will model typical anticipated transients without scram.

Research Progress

In order to assess inconsistencies of traditional coupling strategies, researchers are developing a test-bed code based on reduced physical models that includes the following physics components: multigroup neutron diffusion, monophasic conservation laws (mass, momentum, and energy) for the coolant, and nonlinear heat conduction. This code serves the following purposes:

- To demonstrate loss of accuracy order due to traditional operator-split techniques used in conventional coupling schemes
- To implement Jacobian-free, full resolution coupling schemes
- To develop adaptive preconditioning techniques
- To investigate high-order time discretizations and adaptive time-stepping strategies

The best-performing techniques will be proposed for implementation in the new neutronics/thermal-hydraulics code package simulation-based high-efficiency advanced reactor prototyping (SHARP) for advanced fast reactor analyses. SHARP is based on the UNIC code (neutronics) and the Nek-5000 code (computational fluid dynamics) developed at ANL.

The project team set up a fully implicit coupling paradigm, based on the Jacobian-Free Newton-Kylov (JFNK), for nonlinear physics multiphysics applications. The associated computer code developed serves as a test-bed code for methods development. The code contains the following features:

- State-of-the-art computer science toolbox and libraries for efficient spatial discretizations, handling and interfacing of the various physics components, and fast and robust linear algebra for parallel computing platforms. Some of the supporting libraries include PETSc (linear and nonlinear algebra), LibMesh (finite element spatial discretization), SLEPc and Arpack (eigensolvers), Gmsh (mesh generation), ParMetis (mesh partitioning), and VisIt (results visualization).

- Coarse grain physics models for rapid testing and verification. Finer grain models can replace the existing ones in a straightforward fashion through the common C++ interface.

Preliminary results for nonlinearly coupled neutron diffusion and heat conduction solved in the JFNK framework were obtained using third-order methods in space and time, yielding the theoretically expected convergence rate of three in space and time. This study

demonstrated that fully implicit multiphysics coupling schemes can preserve the theoretical convergence order, opening the way for more efficient multiphysics simulations in reactor analysis and design.

Planned Activities

Following is a list of anticipated tasks for the upcoming year:

- Complete development of the test-bed code for technique testing, which will include a flexible implementation in order to model both operator-split coupling and full-resolution coupling techniques; development of Jacobian-free techniques with adaptive preconditioners (i.e., a mechanism to switch between various degrees of representation for off-diagonal terms by recognizing that not all instants in a transient simulation need highly accurate preconditioners for the nonlinear terms); and adaptive time-stepping algorithms

- Develop a few transient scenarios representative of a sodium-cooled fast reactor (excluding, at first, the effect of moving meshes)

- Analyze the effect of multi-mesh coupled simulations on overall accuracy; address the effect of moving meshes. Such situations are typical of coupled simulations, where each physic component is solved on a specific mesh and can introduce inaccuracy.

- Perform a critical analysis of various techniques:
a) operator-split versus Jacobian-free,
b) preconditioners, and c) time-stepping strategies based on several transients runs

- Down-select and recommend methods to be implemented in the interface code of SHARP, which will drive the coupled neutronic/thermal-hydraulic simulations using UNIC/Nek

NUCLEAR ENERGY RESEARCH INITIATIVE

Fundamental Studies of Irradiation-Induced Defect Formation and Fission Product Dynamics in Oxide Fuels

PI: James Stubbins, University of Illinois

Collaborators: Argonne National Laboratory, Los Alamos National Laboratory (LANL), Oak Ridge National Laboratory (ORNL)

Project Number: 07-064

Program Area: AFCI

Project Start Date: May 2007

Project End Date: April 2010

Research Objectives

This project will address performance issues of oxide-type nuclear fuels in the proposed fast-spectrum reactors. Studying radiation effects and fission-product-transport processes in oxide-type nuclear fuels will establish a fundamental understanding of fuel performance. Researchers will model irradiation effects in cerium and uranium oxide (CeO_{2+x}, UO_{2+x}, and $[CeU]O_{2+x}$) surrogate fuels, comparing their performance with mixed oxide fuels. The irradiation effects will be induced by ion implantation over a range of energies and doses to simulate effects of fission-product damage. Researchers will also examine transport and trapping of simulated fission products. The team will use inert gas ions, such as krypton and xenon, for ion-implantation experiments to cause irradiation damage; the ions will also be used for dynamic transport studies to understand trapping and defect mobility processes in these fuel forms. Researchers will also examine ions that simulate fission products and can substitute for U or Ce atoms in the oxide structure.

To complement the experimental studies, the team will study defect dynamics through modeling, using molecular dynamics (MD) simulations of damage cascades in the oxide lattice, then employing kinetic Monte Carlo (kMC). The MD approach is useful in understanding the early stages of damage during energetic displacement cascades under irradiation. KMC is useful for using defect configuration energies from MD to examine defect and fission-product-transport mechanisms.

Research Progress

During the project's first year, the research effort focused on establishing modeling capabilities for molecular statics (MS)/MD determination of defect energy states and kMC modeling to determine defect transport and agglomeration characteristics. The team is using results of both the MD and kMC efforts as benchmarks against other data available in recent literature.

The research team utilized the GULP MD code for the molecular static and dynamics simulation for defect energies calculations (single-charged defect formation energies, neutral Frenkel defect energies, and Schottky defect energies) in UO_2 and CeO_2 lattices, as well as solution and migration energies of fission products in UO_2 and CeO_2 lattices with well-established pair potentials from earlier studies. Molecular static calculations were performed employing the energy minimizations with the Mott-Littleton approach. The team also employed the GULP code to model the preferred defect migration pathways and lattice configurations. Researchers then compared the calculated energetics data to models with two different potentials, as well as available experimental results; the modeling results were generally higher than the experimental data but consistent with other computational results.

The team will use the kMC approach to model fission-product migration in UO_2 and CeO_2, utilizing energies modeled using an MD code. This code, developed at LANL, has recently been modified to run on a different system; researchers are using the code to confirm earlier calculations of oxygen migration as a function of
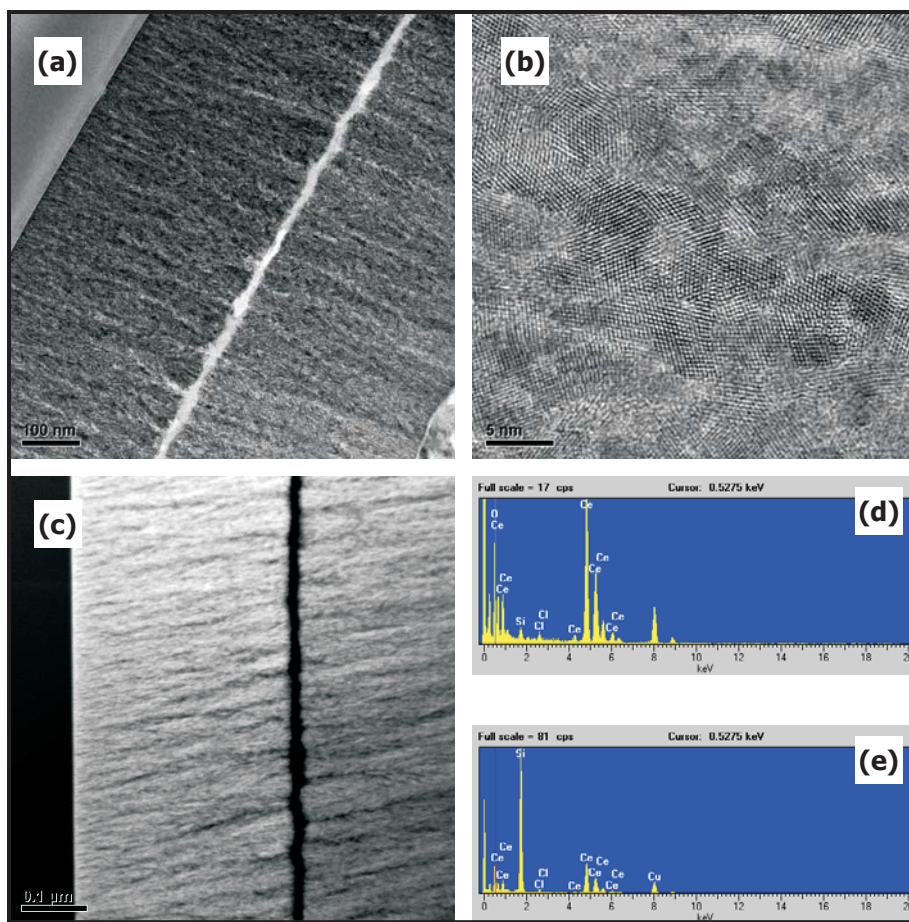
Figure 1. Transmission electron microscope (TEM) bright-field micrographs of 300 nm-thick CeO$_2$ film on Si substrate at TEM mode (a, b), dark-field micrograph of the same film in Scanning TEM mode (c), and energy disperse spectroscopy analysis on the film (d) as well as on the substrate (e).

these single crystals to experimentally determine defect transport and agglomeration processes.

To date, researchers have fabricated and examined several single-crystal thin films of CeO$_2$ grown on R-plane sapphire, silicon, or strontium titinate substrates. The team has been able to prepare films for both cross-section and plan-view examination. Figure 1 shows examples of these films, produced with transmission electron microscopy lattice-imaging techniques. The prepared films are 50 nm to 100 nm in thickness and single-crystal. They are suitable for ion implantation, which is the next step in the experimental program.

Planned Activities

During the next year, the project team will extend MS/MD and kMC modeling work to deal with various new atom and defect properties, including defect transport issues. The experimental program will start in full to examine ion-implanted CeO$_2$ and UO$_2$ single crystals (once UO$_2$ specimens are obtained). The team is well into construction of a molecular beam epitaxy system to produce individual thin-film single crystals; in the coming year, the system should be able to produce significant numbers of single-crystal CeO$_2$, UO$_2$, and doped versions of these structures.

stoichiometry in UO$_2$. Following this, the team will examine migration of multiple fission products. At present, the MD code can handle migration of only oxygen vacancies and interstitials, so researchers are reconstructing the code to handle other defect types and structures.

The project team is working to obtain various UO$_2$ single crystals, which are available through ORNL researchers. During the next program period, the team will ion-implant

NUCLEAR ENERGY RESEARCH INITIATIVE

Identification and Analysis of Critical Gaps in Nuclear Fuel Cycle Codes Required by the SINEMA Program

PI: Adrian Miron, University of Cincinnati (UC)

Collaborators: Idaho State University (ISU)

Project Number: 07-071

Program Area: AFCI

Project Start Date: July 2007

Project End Date: April 2009

Research Objectives

The research objectives of the project are to 1) carry out a detailed review of the existing codes describing aspects of the nuclear fuel cycle and 2) identify the research and development (R&D) needs required to develop a comprehensive model of a global nuclear energy infrastructure and associated nuclear fuel cycles. Researchers will also recommend appropriate computer codes for integrating into the Simulation Institute for Nuclear Enterprise Modeling and Analysis (SINEMA), the simulation network that will model the global nuclear energy infrastructure, associated fuel cycles, and components. SINEMA will provide an integrated toolbox to support the global and domestic assessment, development, and deployment of nuclear energy systems at various levels of detail. The plan is to implement SINEMA using interconnected and interactive pyramid architecture.

The project will accomplish the following three primary tasks:

1) Develop a detailed review of nuclear fuel cycle codes

   ➤ Develop appropriate questionnaires and typical letters to be submitted to code developers and their organizations

   ➤ Conduct a systematic and detailed review of domestic and international nuclear fuel cycle codes

   ➤ Develop a relational database

2) Identify R&D needs and gaps in nuclear fuel cycle computer codes

3) Identify best code packages to be linked within the SINEMA framework

Research Progress

The project team thoroughly reviewed several thousand codes included in the four databases available on the internet: the Radiation Safety Information Computational Center (RSICC); the Energy, Science, and Technology Software Center; the Nuclear Energy Agency Data Bank; and the International Atomic Energy Agency. As reported previously, the inherent problem is that none of these databases contain the code input and output parameters, which are paramount for this research. In the United States, RSICC can supply information on these codes once the registration, request, user software license, and export control agreement are cleared for export compliance by the U.S. Department of Energy (DOE). UC requested two such approvals, which DOE approved; UC also obtained user manuals for most of the codes of interest.

The team reviewed all DOE national laboratory websites. Team members identified several codes of interest that were not included in any of the above four databases. In order to obtain the necessary information to review these codes further, researchers are currently corresponding with the laboratories' persons of contact assigned to these codes.

In addition, codes currently used by the U.S. Nuclear Regulatory Commission (NRC) have been identified on the NRC website. The team obtained information on NRC codes of interest, as well as information on several nuclear fuel cycle codes developed by universities (e.g., Purdue University, Massachusetts Institute of Technology, University of Florida, and Georgia Institute of Technology).

Although not specified in the proposal workscope, UC researchers designed and developed a website for this project (http://www.min.uc.edu/nuclear/current_research/sinema-research). Visitors to the web page can fill in the UC code review questionnaire. The site includes other information about the project, including a project description, mini-survey, team contact information, progress reports, and some other useful links. The project webpage also includes a link to a current list of about 100 codes of interest. This list will be continuously updated as new information becomes available.

This website could help researchers achieve the required consistency for the nuclear fuel cycle code review and provide for a more professional, formal, secure, and fast communication with potential collaborators. Information in the code review questionnaire could be extracted and entered in UC's nuclear fuel cycle code relational database. Also, links to this database and various queries on its nuclear fuel cycle codes could be embedded in the web page in the future.

The project webpage includes a mini-survey that can be filled in online. The survey was used to gather information about nuclear fuel cycle codes used world-wide, along with problems for which these codes were used. The project team compiled a list of all nuclear engineering programs and departments at universities in the United States and Canada, and a team member sent an email to each faculty member at each university. The email directed faculty members to the mini-survey on the project website and requested help with the research. Initial responses were vague, but the team will continue sending requests to the academic community. In addition, similar emails will go to key persons at U.S. national laboratories.

The code review performed at UC and ISU included research on international and domestic nuclear fuel codes developed by the industry. The team acquired complete information for codes developed by Studvik and partial information for codes developed by Westinghouse. AREVA sent UC a list of codes they have used or developed in the United States and Europe, but declined to participate further in this research. GE declined to participate in this project altogether. Other U.S. companies reported that they run vendor codes and do not develop their own.

Literature research started at ISU with the review of the American Nuclear Society publication TRANSACTIONS, No. 97. In addition, team members have used standard databases to carry out the literature review on nuclear cycle codes going back as far as 1989. As a result of literature research, the team has added several potential codes of interest to the current list. Team members will obtain detailed information on these codes through direct contact with their authors.

The team repeatedly contacted several other international organizations but unfortunately received no information. Team members will pursue these attempts; however, the lack of response leaves little hope for future developments.

Team members intend to create a database containing all the information they have gathered. Based on current progress and an analysis of available information, team members concluded that this database can be designed ahead of the initial schedule. Since this is an important project milestone, the database design has been and will be carefully reviewed throughout this project.

The initial database design was also discussed with and evaluated by a UC professor who specializes in this field. Figure 1 shows the current database tables and their relationships.

Initially, development of the database was planned in Microsoft (MS) Access. The database expert suggested using MySQL RDMS, as implementing a MySQL database in a web environment is a relatively fluid process, especially compared to other database systems.

Currently, the database developed in MS Access is populated with a few codes to ensure the design is sound and properly working. The next immediate step will be to use MS Access's simple point-and-click interface and to design several queries to test the database. Afterwards, the project team will finalize development of the MySQL database, which will ultimately be populated with data on all acquired codes of interest.

Performing the database development in MySQL will also ease the process of creating a final deliverable. This will, in turn, allow other researchers to use this efficient tool remotely. Customized queries can be built into a PHP webpage—hosted on a web server, for example, or in a stand-alone package on a compact disk. The project team will examine ways of delivering the database during the next period.

Planned Activities

In the next period, efforts will focus on testing the database design and running several queries of interest. Once researchers are satisfied that the database produces expected results, they will populate the database with all the information obtained on the nuclear fuel cycle codes of interest identified so far.
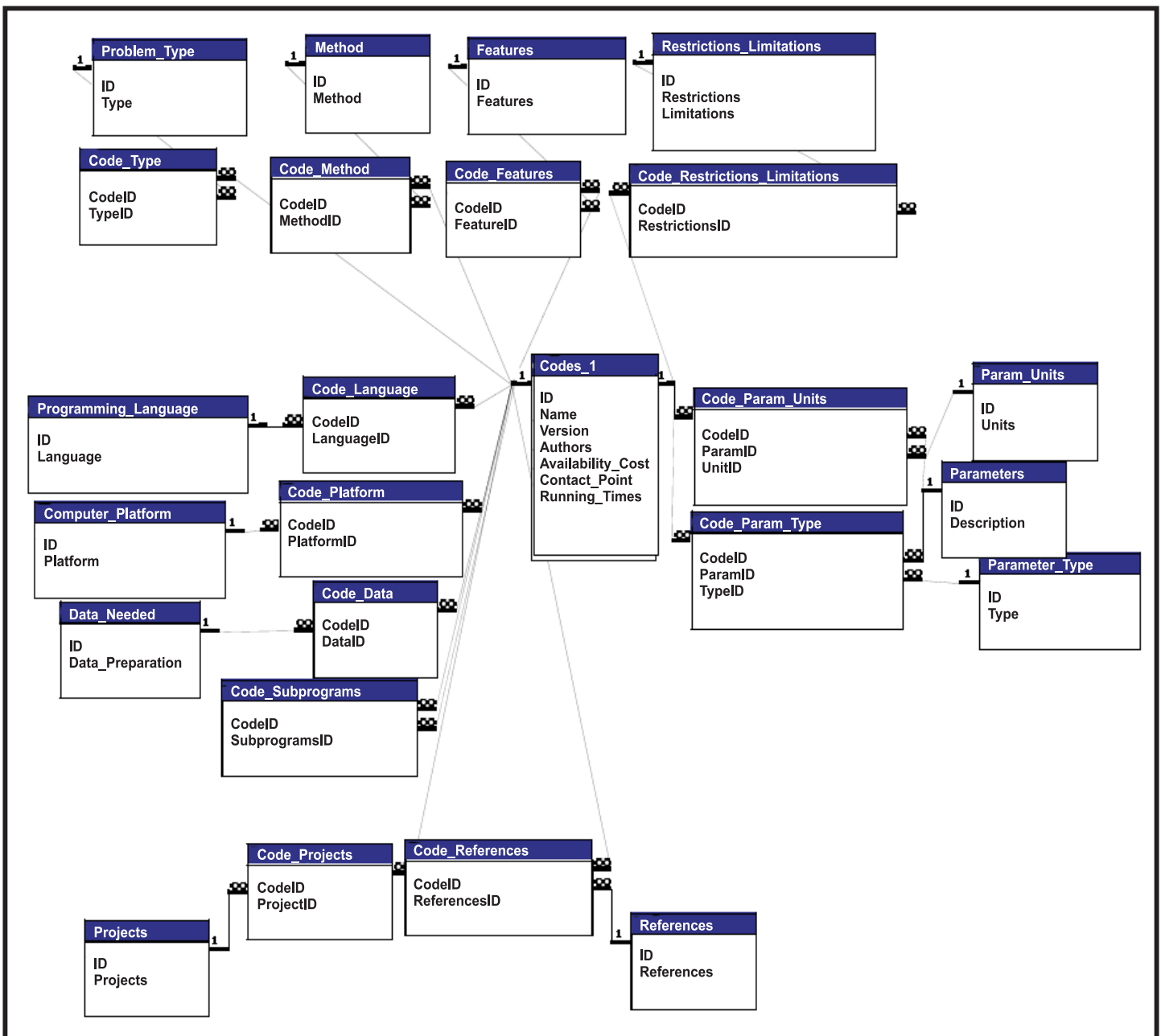
Figure 1. Project database (tables and relationships).

In parallel, ISU will fill in the UC questionnaire with information on the agreed-upon codes, and UC will then add this information to the database.

The research team will intensify efforts to get pertinent information on codes of interest developed by the U.S. national laboratories and include that information in the database.

The team will continue literature research and direct contact with the codes' authors.

Finally, several queries on the database will be designed to identify critical gaps in the nuclear fuel cycle codes and candidates for linkage in SINEMA's top-level code.

NUCLEAR ENERGY RESEARCH INITIATIVE

An Innovative Approach to Precision Fission Measurements Using a Time Projection Chamber

PI: Nolan Hertel, Georgia Institute of Technology

Collaborators: Abilene Christian University, California Polytechnic State University, Los Alamos National Laboratory (LANL), Lawrence Livermore National Laboratory, Idaho National Laboratory, Ohio University, Oregon State University

Project Number: 08-014

Program Area: AFCI

Project Start Date: October 2007

Project End Date: October 2010

Research Objectives

The principal objective of this project is to initiate a fission cross-section measurement program that will provide data with unprecedented accuracy needed for the Global Nuclear Energy Partnership (GNEP) initiative and Generation IV reactor designs. Reactor core calculations depend on the nuclear data to adequately predict the behavior of more advanced reactor systems. The research consortium will construct, install, and test a prototype of a three-dimensional time projection chamber (TPC) at the Los Alamos Neutron Science Center (LANSCE); the prototype will be used to perform the fission physics measurements. The TPC will be filled with hydrogen gas and will measure fission cross-sections using the H(n,n)H elastic scattering reaction as a reference standard. The TPC is the perfect tool for minimizing most of the systematic errors associated with previous fission cross-section measurements performed using other techniques. Initial studies indicate that the TPC can be used to obtain fission cross-sections with uncertainties of less than one percent. The project will establish the requisite infrastructure for a world-class fission measurement campaign that meets the nuclear data needs required for planning, modeling, designing, and executing the GNEP program.

In addition to providing high-quality fission cross-section data, the TPC will generate a rich, basic fission physics dataset as a function of neutron energy, including kinematics and angular distribution of fission products, ternary fission cross-sections for light isotopes, and fission product identification. As mentioned previously, a well-calibrated and tested TPC will reduce fission cross-section uncertainty measurements below one percent.

In addition to its data-generating ends, the project attains another goal: the work will train graduate students, undergraduate students, and post-doctoral researchers in experimental nuclear physics and radiation physics, thereby assisting in re-establishing the human resource required for a successful nuclear power renaissance. The effort funded under this project is carried out by a five-university research consortia and integrates with the efforts of three national laboratories funded by the GNEP program and the National Nuclear Security Administration.

Research Progress

Over the last 12 months, TPC project researchers have made significant progress. The collaboration has produced major components of the detector systems, including the physical detector, gas-handling system, and data-collection systems. Modeling and simulation efforts have optimized neutron beam characteristics at the LANSCE beam and provided some preliminary mock data. Online and offline software design has also progressed significantly. Specifically, the following list of tasks has been accomplished in the first year:

- Hardware construction
  - ➤ Built field cage
  - ➤ Built pressure vessel
  - ➤ Built micromegas gas amplification system
  - ➤ Designed data-acquisition cards
  - ➤ Designed slow control systems, which are now being constructed
  - ➤ Built gas-handling system

- ➤ Fabricated high-quality actinide targets and shipped them to LANL
- Modeling and simulation
    - ➤ Optimized models of the LANSCE beam line for TPC use
    - ➤ Fabricated GEANT models of the TPC detector
    - ➤ Simulated ionization tracks in the TPC gas volume
- Hydrogen standard
    - ➤ Made progress on the hydrogen scattering standard
    - ➤ Reviewed available H(n,n)H scattering data; designed a new neutron-scattering experiment
- Online and offline software
    - ➤ Built the neutron-induced fission fragment tracking experiment (NIFFTE) reconstructor
    - ➤ Constructed data input and output models to handle data flow through the TPC

Planned Activities

The planned activities for the project's second year are to complete the simulation effort ending in the mock data challenge. This effort includes creating isotope databases, data fitting, and minor actinide modeling. The first set of data should be available and ready for comparison to calculated results. The gas system will be installed at LANSCE and integrated into the safety system. Additionally, the project team will develop a gas-sampling system and temperature readout/control. Designing, testing, and assembling the data acquisition system will continue.
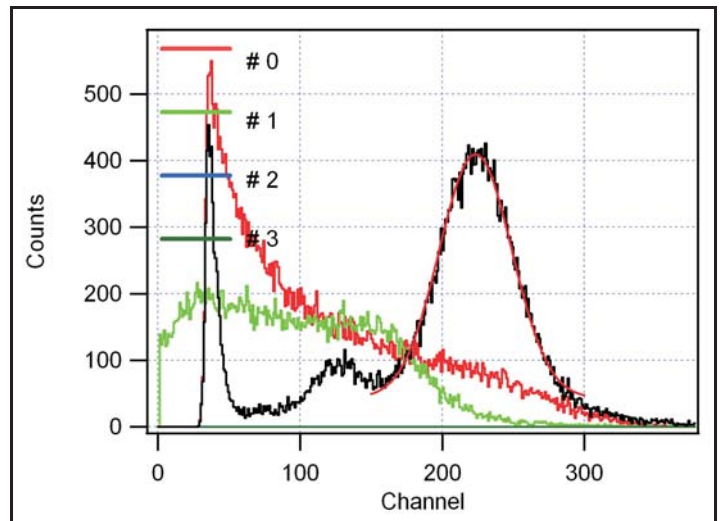
Figure 1. Gas amplification of micromegas.
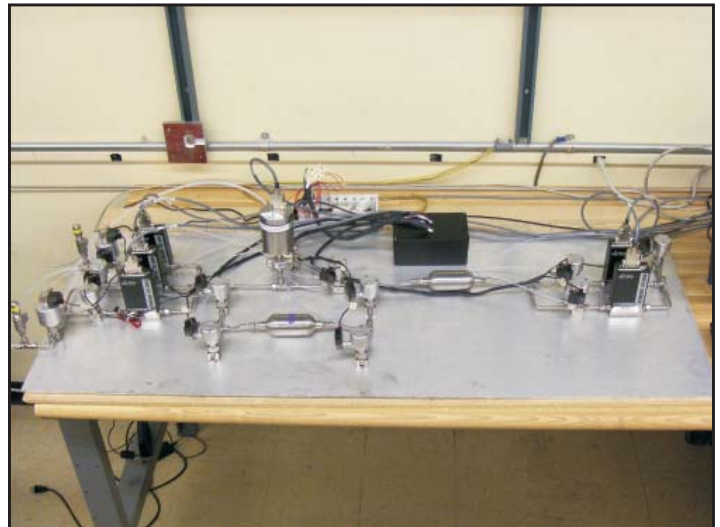
Figure 2. Gas-handling system for the TPC.

NUCLEAR ENERGY RESEARCH INITIATIVE

Risk-Informed Balancing of Safety, Non-Proliferation, and Economics for the Sodium-Cooled Fast Reactor

PI: George Apostolakis, Massachusetts Institute of Technology

Collaborators: Ohio State University, Idaho State University

Project Number: 08-020

Program Area: AFCI

Project Start Date: October 2007

Project End Date: October 2010

Research Objectives

The objective of this project is to develop risk-informed design and evaluation tools for the sodium-cooled fast reactor (SFR) that take into account safety, economics, licensability, and proliferation resistance. The research team will apply these tools to a number of design alternatives, identifying opportunities to reduce the SFR's cost while maintaining its high level of safety and proliferation resistance.

The proposed design variations, many of which incorporate passive safety features, include loop versus pool-type designs, differing fuel types, and sizes ranging from very large monolithic reactors to small modular ones. The resulting risk-informed methodology will help develop technical requirements for the industrial design organization, identify research needs, assess the technology risk of alternatives, and assist with planning. Industrial groups can use this methodology to perform design tradeoffs that would make the SFR economically competitive and licensable, yet still safe and proliferation-resistant.

Research Progress

Sodium-Cooled Fast Reactor Overview.
Researchers examined existing key SFR design considerations. The primary SFR designs examined were Argonne National Laboratory's advanced burner test reactor, General Electric's super-power reactor inherently safe module (S-PRISM), the Japan Atomic Energy Agency's SFR (JSFR), and the Russian BN1800. The S-PRISM reactor is unique among full-scale power reactors because of its emphasis on modularity. The S-PRISM chose a relatively small power/modular design to reduce construction time.

Historical Experience.
The project team has begun examining operating records from selected SFRs. Included in this review were EBR-II, Phenix, Superphenix, PFR, BN-350, BN-600, and Monju. In addition, project team members met in Idaho for a full day of discussion on design, operability, and maintainability with eight key staff members from EBR-II.

Power-generating sodium-cooled reactors generally have somewhat unreliable steam generators as a result of sodium-to-water or sodium-to-steam leaks and subsequent reactions. However, none of the EBR-II steam-generating components had such leaks, largely owing to the duplex tube design of the EBR-II evaporators and superheaters. One of the two superheaters (the mechanically bonded unit) was removed from service after about 17 years of operation because of a decline in heat-transfer efficiency. This superheater's performance declined because the pre-stress between duplex tubes relaxed. Destructive examination of the unit indicated that it was in otherwise excellent condition. Original fabrication "soap-stone" markings were still visible on the sodium side. Over the life of the plant, neither the other evaporators nor the metallurgically bonded superheater ever showed any indications of decreased performance.

Methodology Overview.
Figure 1 shows the overall methodology. The objective is to develop methods that will allow future groups to implement this general framework. These groups will perform design tradeoffs with the particular aim of making the SFR economically competitive and licensable, while maintaining safety and proliferation resistance.
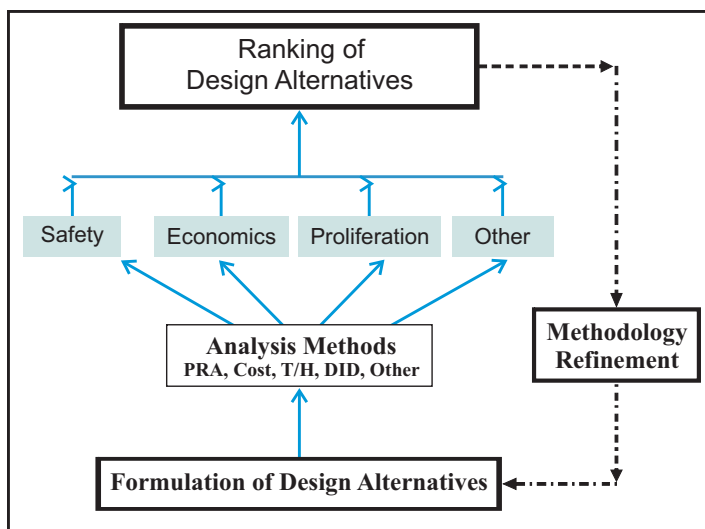
Figure 1. Methodology overview.

The project team formulates design alternatives using probabilistic risk assessment (PRA) methods and engineering knowledge. Team members then evaluate the alternative's impacts on safety, economics, and non-proliferation. Finally, the team ranks the design alternatives based on the combination of impacts.

Researchers are working on all aspects of this framework. The various tasks are discussed in the following paragraphs.

PRA Methodology. The U.S. Nuclear Regulatory Commission is developing a technology-neutral framework (TNF) to regulate plant designs that are substantially different from the current generation of light-water reactors (NUREG-1860). For the risk-cost tradeoff study, researchers are examining an approach to risk acceptance based in part on a concept developed for the TNF. Within this concept, an established risk-limit curve (frequency-consequence [F-C] curve, with C as doses) must envelop risk for the complete spectrum of conceivable accidents. Using this concept of acceptable risk, the designer's objective function would be to develop the minimum cost system that satisfies the risk-limit curve.

SFRs must account for energetic core disruptive accidents (ECDAs), which is an economic issue for these reactors. ECDA frequency is actually very low, and some design features being considered to deal with ECDAs are costly or reduce performance. Within the draft risk-informed TNF, researchers have been investigating the regulatory implications of the low frequency of these events.

A method for identifying candidate design alternatives for cost reduction is to employ importance measures such as the risk achievement worth (RAW). In a PRA, RAW of the ith basic event is the ratio of the end-state frequency (e.g., core-damage frequency), with the probability of basic event i set equal to unity (the event has occurred or the equipment has failed), to the base case end-state frequency. The PRISM PRA for RAW identified low-risk significant structures, systems, and components (SSCs). If these SSCs are expensive and the F-C curve of the TNF can be met with a more economical alternative, changing SSCs could save money.

Comparison of Core Disruptive Accident Responses for Metal and Oxide Fuels. Researchers have investigated the passive responses of metal- and oxide-fueled cores to a variety of unprotected accidents. While metal fuel generally provides a more desirable response because of its low operating temperature and small time constant (removing heat quicker than oxide fuel), SFR designs have successfully utilized both fuel options. Additionally, some emerging SFR designs, from the JSFR and the Westinghouse/Toshiba approach to the design of the actinide-recycling reactor, may soon incorporate a third independent scram system to significantly reduce scram failure probability.

Metal fuel is believed to perform favorably in ECDAs in which the vessel's integrity is threatened because of fuel vaporization. If these accidents can be ruled out for metal fuel, changing or simplifying systems that mitigate this hypothetical scenario would produce significant cost savings. Therefore, the project team conducted literature reviews of CDA overviews, CDA consequences, traditional CDA methodology and trends, mechanisms preventing metal fuels from experiencing ECDAs, and mechanisms preventing oxide fuels from experiencing ECDAs.

Impact of Design Choices on SFR Efficiency. Increasing plant thermal efficiency is the most effective way to reduce the SFR's per-megawatt cost. Every component of a nuclear reactor's busbar cost (capital, fuel, and operations and maintenance) is inversely proportional to the plant thermal efficiency. A 1 percent efficiency increase will result in a fractional efficiency increase of 2.5 percent.

Possible ex-core changes that can increase efficiency include changing the power cycle, removing the intermediate loop, and having a loop or a pool primary system layout. Possible in-core changes include fuel, diluent or TRU grading, and an assembly design that reduces intra-assembly peaking.

Dose Estimation. The TNF limit curve will specify the level of plant risk considered acceptable when performing economic tradeoff studies. Within this concept, a deterministic analysis is performed for the consequences of each licensing basis event (LBE) that represents a set of scenarios. The total frequency of the scenarios represented by the LBEs must fall below the limit curve. To apply the methodology, investigators must determine LBE's environmental source term. Then they must analyze environmental dispersion, starting at the point of release from containment and going to the receptor at the site boundary, or one mile from the site boundary. The project team has been developing and assembling tools to assess LBE consequences for the different plant design variations considered in this project. RELAP-5, ORIGEN, SAS4A, and MELCOR 2.0 are key safety analysis tools with which the team will examine the progression of accident scenarios.

Uncertainty Analysis. In the TNF approach to defining LBEs and determining their acceptability, the frequency and consequences of each LBE must fall within an acceptable zone defined by a limiting F-C curve. The TNF requires an uncertainty analysis demonstrating high confidence (e.g., 95 percent) in compliance with the criterion. In the SFR cost-risk tradeoff study, researchers must demonstrate that each major design variation satisfies the TNF risk criterion. Although this seems like a daunting task within such a limited study, the risk-limiting LBEs are likely to comprise only a few critical scenarios.

The ADAPT code will be applied to the integrated analysis of LBEs for the SFR. The starting point is an initiating event. System performance, which is traditionally determined by Level 1 PRA analyses, will undergo a time-dependent evaluation. This analysis will determine system failure probability as a function of time; researchers will use dynamic event trees and PRA tools like SAPHIRE to determine the branching probabilities. Human reliability analysis models will determine probabilities of operator actions based on the operators' observations of accident progression. The research team will assess system failure probabilities throughout the mission times, accounting for loads placed on those systems by the accident's progression.

Nonproliferation Analysis. The nonproliferation effort of the SFR project involves devising scenarios for diversion of weapons-usable materials (WUM) from the following:

- The SFR itself

- Transportation activities for moving fuel (new or used) between the SFR and the fuel-processing facility

- The fuel-processing facility (using either pyroprocessing or aqueous technologies)

The purpose of this work has been to identify realistic diversion scenarios, subject to current safeguards efforts, for evaluating probability of diverter success at the various facilities of interest. Researchers must do this within the project because such scenarios have not been identified in the available literature, and these scenarios are the basis for comparing the non-proliferation potential of alternative facilities and for improving that potential at individual facilities.

At all facilities, two fuel bundles may be sufficient for obtaining one significant quantity of WUM, so diversion of fuel bundles would be of interest. The research team assumes that all such scenarios would occur subject to International Atomic Energy Agency (IAEA) safeguards as are currently implemented at CANDU reactor facilities. (The relevant practices of such facilities are safeguards practice standards.)

Researchers have also investigated enhancing current IAEA practice with methods other than materials accounting-based safeguards assessments. The team's aim is to reduce proliferator success probability.

Planned Activities

In the first year, the project initiated the work summarized above, which is not yet complete. Research efforts will continue along these lines.

NUCLEAR ENERGY RESEARCH INITIATIVE

Deployment of a Suite of High-Performance Computational Tools for Multi-Scale Multi-Physics Simulation of Generation IV Reactors

PI: Michael Z. Podowski, Rensselaer Polytechnic Institute

Collaborators: Columbia University, State University of New York at Stony Brook, Brookhaven National Laboratory

Project Number: 08-033

Program Area: AFCI

Project Start Date: September 2007

Project End Date: September 2010

Research Objectives

The overall objective of this project is to deploy advanced simulation capabilities for next-generation reactor systems utilizing newly available, high-performance computing facilities.

The approach includes the following major components:

- Developing new simulation capabilities for state-of-the-art computer codes (FronTier, PHASTA, and NPHASE) coupled with molecular dynamics (MD)-type analysis

- Developing advanced numerical solvers for massive parallel computing

- Deploying a multiple-code computational platform for the Blue Gene supercomputer simulations of the sodium-cooled fast reactor (SFR) fuel performance during accidents

The planned deliverables of the project are listed below:

- Deploying high-performance computing tools for coupled thermal-hydraulic, neutronic, and materials multi-scale simulations of the SFR

- Applying the new computational methodology to study reactor fuel and core transient response under beyond-design and accident conditions

Research Progress

The research team has made progress on major project tasks, as described below.

Development of an MD-Based Model of Reactor Fuel Properties. The team has formulated an initial version of the MD model to investigate the reactor fuel

and cladding properties at a given temperature. Calculated parameters include atom positions, velocities, and forces. Parameters that can be derived from the simulations include diffusion constant, velocity correlation function, structure factor, and Van Hove function. The preliminary results of simulations are promising. Future work will include examining the effect of a nonuniform temperature distribution.

Model Development for Fuel Rod Failure Modes. The FronTier code has been used to verify consistency of normal operating conditions for both metallic and oxidic fuel rods, as well as to establish possible scenarios for fuel rod failure. New software modules for FronTier's phase transition algorithms are under development. The software modules improve accuracy of algorithms for the heat transfer problem in geometrically complex domains with discontinuous diffusion coefficients. Two-dimensional algorithms have been implemented, fully tested, and applied to axisymmetric simulations. The implementation of 3-D algorithms is currently under way. Furthermore, new computational software is under development to simulate the fracture of inhomogeneous brittle materials, as well as their interface to FronTier. The corresponding algorithms are based on energy minimization of the network of inelastic springs with critical tension that model solid walls. Such a description of solids makes it possible to avoid fast time scales associated with acoustic waves and to capture important features of the material fracture.

Development of a Model for Fission Gas Injection From Failed Fuel Element Into Reactor Coolant Channel. The team has formulated a PHASTA-based model for the direct numerical simulation of fission product gas jet injection into liquid sodium inside the coolant channel. The

major issue under investigation concerns properly capturing formation of gas bubbles and major characteristics of the jet inlet conditions.

Development of a Two-Fluid Model of Gas/Liquid Sodium Interaction in the Reactor Coolant Channel. The team has developed a preliminary two-fluid model of gas/liquid sodium flow and implemented this model in the NPHASE code. The major issues under investigation include formulating an appropriate computational grid, modeling the gas/liquid interfacial forces and two-phase flow turbulence, and numerical convergence. The test problem under investigation models the injection of the gas jet into liquid sodium turbulent flow. A low Reynolds number k-ε model is used for the liquid phase turbulence. The jet is modeled as multiple 50-micron diameter bubbles injected into the liquid sodium flow through a 0.1 mm wide opening. The gas-jet/liquid interfacial interactions include drag, turbulence dispersion, and virtual mass forces. The calculated parameters include the two-phase flow velocity field and gas concentration distribution. Sample results are shown in Figure 1. Work on model testing and validation is currently under way.

In addition to the above, the research team has begun conceptual work on developing an interface between PHASTA and NPHASE. Furthermore, researchers have investigated the development of improved computational algorithms for the individual codes.

Planned Activities

Following is a synopsis of the tasks the team plans to conduct over the next fiscal period:

- Implement the MD-based model of reactor fuel properties on the Blue Gene computer

- Perform numerical simulations to link molecular-scale phenomena to macroscopic physical properties of the SFR fuel

- Implement in the FronTier code 3-D algorithms of heat transfer in geometrically complex domains with discontinuous diffusion coefficients

- Develop a FronTier-based, stand-alone model of fuel rod failure modes

- Formulate a complete stand-alone model of fission gas injection into the reactor coolant channel following a cladding breach

- Perform numerical testing of the model using the PHASTA code

- Develop a parallel-processing version of the NPHASE code and load it on the Blue Gene computer

- Develop an interface between PHASTA and NPHASE

- Perform testing of the NPHASE-based fission product transport model using PHASTA's output as input to NPHASE

- Develop improved computational algorithms for FronTier, PHASTA, and NPHASE to enhance performance of the overall computational platform

- Present the new results of multiple code simulations at conferences and publish the results in conference proceedings and archival journals

Figure 1. NPHASE results of a gas jet injecting into turbulent flow: (a) computational grid and inlet conditions, (b) gas field volume fraction, and (c) stream-wise liquid velocity profile.

NUCLEAR ENERGY RESEARCH INITIATIVE

Real-Time Detection Methods to Monitor TRU Compositions in UREX+ Process Streams

PI: Sean M. McDeavitt, Texas Engineering Experiment Station (TEES)

Collaborators: Purdue University, University of Illinois-Chicago (UIC), Argonne National Laboratory (ANL)

Project Number: 08-039

Program Area: AFCI

Project Start Date: October 2008

Project End Date: September 2011

Research Objectives

The U.S. Department of Energy is developing advanced methods for reprocessing used nuclear fuel. The most prominent method under development is the uranium recovery by extraction (UREX+) family of processes that recovers uranium (U), selected fission products, and transuranic (TRU) isotopes for recycle or storage. As the UREX+ processes are implemented on a real scale over the next 20 years (e.g., more than 1,000 tons of fuel per day), safeguard strategies and materials control and accountability methods will become important issues to consider. Monitoring higher actinides during aqueous separations is a critical research area. A key deficiency in such monitoring is the lack of real-time assessments to detect diversion of TRU elements such as plutonium (Pu). Providing on-line materials accountability for the processes will make covert diversion of materials streams much more difficult.

The objective of this consortium is to develop real-time detection methods to monitor the UREX+ process and to safeguard separated TRUs against diversion from within a processing facility. The project team is implementing a comprehensive development strategy to incorporate an array of traditional detectors and advanced metastable fluid detectors into a novel assembly designed specifically for a UREX+ centrifugal contactor array. The development experiments range from laboratory benchmarks to hot-cell demonstrations with real UREX+ spent-fuel experiments. Consortium team members will also perform supporting research to develop safeguard strategies for the UREX+ process and to evaluate corrosion behavior of critical component materials in the UREX+ system.

Research Progress

Texas A&M University (TAMU) is the lead institution for this effort and is developing the detector assembly system and safeguards strategy. Purdue University is developing a suite of metastable fluid detectors that may be inserted into the assembly for neutron and alpha detection. UIC is performing critical corrosion tests and provides a local university/laboratory interface with ANL.

Texas A&M University

Detector Assembly Design. Figure 1 shows the detector assembly concept schematically. The concept involves diversion of the UREX+ process streams from
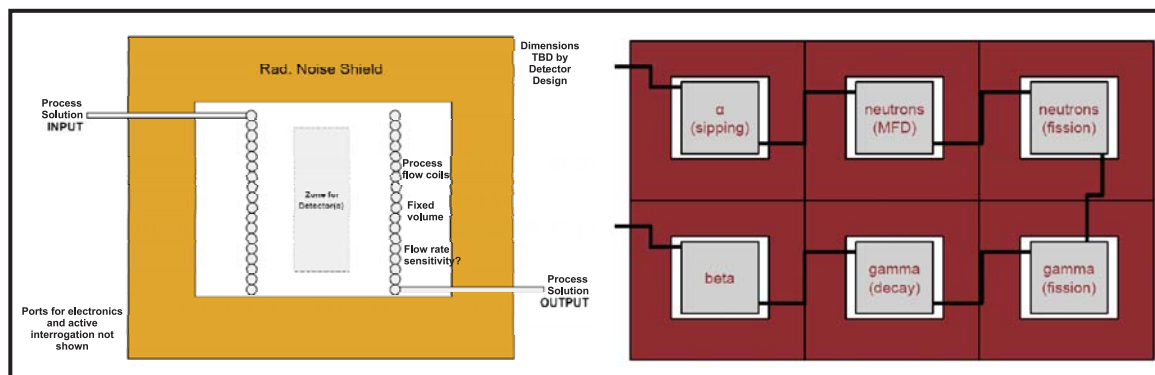
Figure 1. Detector assembly concept sketches.

the solvent extraction contactors through a series of shielded coils with radiation detection options sequentially installed to interrogate the process solution for selected radionuclides. For example, the raffinate of the UREX+ stream could be examined to verify that no transuranics were inadvertently diverted into the waste stream. The strawman concept (Figure 1) shows a detector inside a shielded coil, but the geometry of the system may vary dramatically depending on the point in the UREX+ process being examined. For example, the initial high-activity portions of the process stream may require collimation and long distances, and enabling alpha and neutron detection in the metastable fluid detectors (MFDs) may require special sipping protocols.

The engineering activities for this assembly currently comprise two projects: 1) modeling the detector assembly geometry and detector response and 2) the experimental demonstration of a prototype assembly to benchmark the model. In the first activity, a series of small samples taken from actual UREX+ stages have been obtained from ANL. The research team is measuring radioisotope spectra from these samples using various types of detectors and comparing those spectra with theoretical spectra derived using ORIGEN. The team is constructing a Monte Carlo N-Particle Transport Code (MCNP) model to enable theoretical insertion of various types of detectors into a UREX processing assembly. In addition, a demonstration test stand is under construction to enable system simulations with different detector styles. This system is designed to enable flow of a radioactive liquid through a simple stainless-steel coil with a central radiation detector. The Nuclear Science Center at TAMU (http://nscr.tamu.edu/) will use neutron activation to generate the initial isotopes. Once the system is operational, the researchers will quantify system performance and compare it with the MCNP model from the other project.

Safeguards Strategy Development. The safeguards strategy development began by looking at traditional safeguards methods, such as those implemented at the Rokkasho Reprocessing Plant in Japan, and new methods and detector systems, such as the tensioned MFD (TMFD), as well as methods being developed as part of the

coupled end-to-end demonstration (CETE). The team is investigating the TMFD for use of online alpha spectroscopy to quantify Pu in solution in real time. CETE uses coupled photon and neutron measurements to quantify Pu in spent nuclear fuel. The UREX+1a process was chosen to safeguard because the curium (Cm) is kept with the Pu product (see Figure 2 for a schematic). This makes for an interesting measurement because the number of neutrons from Cm will be several orders of magnitude more than the number of neutrons from Pu. The project team has identified material balance areas, key measurement points, and material balance periods for different detector schemes and scenarios for the UREX+1a reprocessing facility. Members are now investigating real-time plutonium measurement paired with process monitoring.
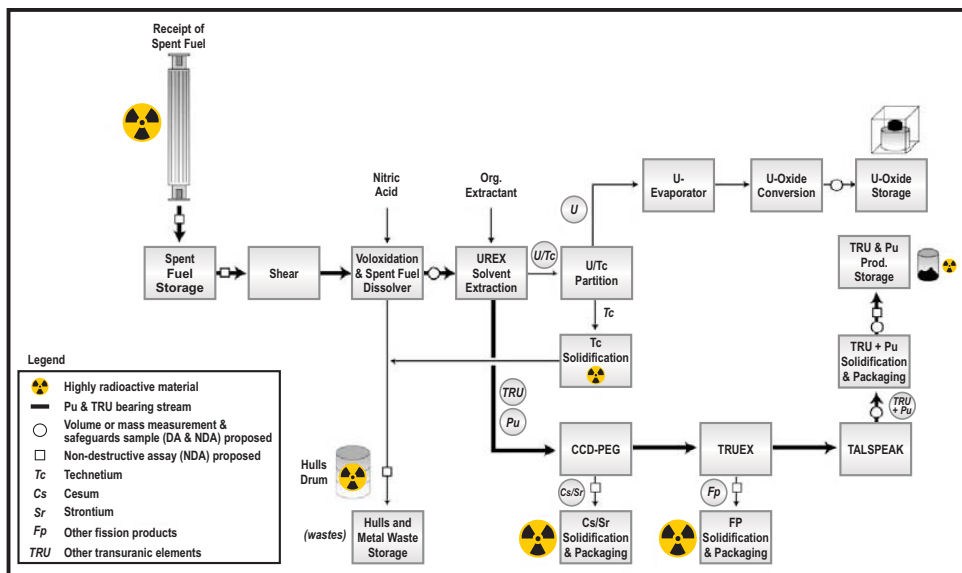
Figure 2. Schematic of the UREX+1a process.

Purdue University

Detection of Actinides from Mixtures of Various Isotopes of Uranium. The team utilized the TMFD system to detect trace (1 ppm level) quantities of uranium from dissolved uranyl nitrate (UN). Two forms of UN were tested. The first form was depleted uranium-based, whereas the second form was based on natural uranium. The team assessed different thresholds versus detection times for these two samples, which encompass different ratios of U-238, with U-234 (plus U-235) being a minor player for both natural and depleted forms of uranium. The energy of U-238 alpha emission differs from that of U-234; ability to detect the relative presence is a plus in deriving a real-time spectroscopy system for assessing streams in which other actinides, such as americium (Am), Cm, and Pu, may also be present. Team members are

cross-checking the quantity of alpha-emission activity, as deciphered using TMFD systems, with conventional liquid-scintillation spectroscopy systems at higher UN concentrations. (The experiments require higher concentrations because conventional spectroscopy systems do not function at the 1 ppm range.)

Active Monitoring for Fissile Content in the UREX+. In addition to alpha monitoring via sipping of nano quantities of the process streams, the team has also set up an active interrogation system based on using pulsed fast (14 MeV) neutrons to assess emission of fast fission-induced delayed neutrons from the various actinides. This method is different from traditional pulsed fast neutron activation analysis techniques, which interrogate objects with neutrons to then decipher the presence of various elements based on gamma spectroscopy. Various fissile elements such as U, Pu, and others will possess differing fission output from fast and thermal neutrons—in which the multiplicity of fission-induced delayed neutrons may then also provide a tell-tale signature from the neutron detectors employed. The team is assessing two forms of neutron detectors for this purpose: 1) the TMFD in acoustic mode, such that the compressive-tensile cycles at the microsecond scale are phase-locked with the interrogation neutron beam, and 2) a conventional fast-timing NE-213-type detector. To demonstrate this methodology's viability, team members are first testing for the presence of various uranium isotopes.

University of Illinois-Chicago

Corrosion Testing. In the corrosion studies, the first task was to develop a clear understanding of the corrosion atmospheres to which the internal contactor would be exposed. In the UREX process, two immiscible liquids of different densities are fed into the annulus of a centrifugal contactor. The aqueous solution is denser than the organic solution. The project team has concluded that the contactor materials may be exposed to diverse corrosion environments because of the type of acidic medium. Team members have identified nine different areas within the contactor, each with slightly different acidity. In considering these ambient environments and the UREX+ operational factors, the team is investigating the following parameters:

- Centrifugal contactor material: type and processing condition (e.g., as rolled, welded)
- Nitric acid (HNO_3) at concentrations in the range of 0.1M to 10M
- Hydrofluoric (HF) acid concentrations (0.1M max)
- Hydrodynamic regimes inside a centrifugal contactor

- Volume of acidic solutions flow in relation to centrifugal contactor throughput
- Operation temperature of centrifugal contactor
- Mechanical effect due to rotational speed

The interactions among the seven corrosion operational factors found in a UREX+ process centrifugal contactor can be summarized as follows: the 304 stainless steel forms a protective film of Cr_2O_3 in the presence of oxidizing acids like HNO_3; however, this protective layer—and the base metal as well—can be dissolved mainly by HF in HNO_3-HF solutions. Fresh aqueous HNO_3-HF solutions, along with organic (oil) solutions, are introduced into the centrifugal contactor continuously during its operation. These two solutions form dispersion in the mixing zone for a relatively short time as they are separated in the separation zone as part of the liquid-liquid extraction process. The centrifugal contactor's two main zones, mixing and separation, have different and specific turbulent flow patterns due to their specific complex geometries and operational parameters, such as flow rate and rotor speed.

Figure 3 shows data from the initial 14-day corrosion tests using 304SS. As expected, increased HNO_3-HF content and increased stirring create the most aggressive corrosion, but a modest temperature increase actually improved the corrosion resistance.
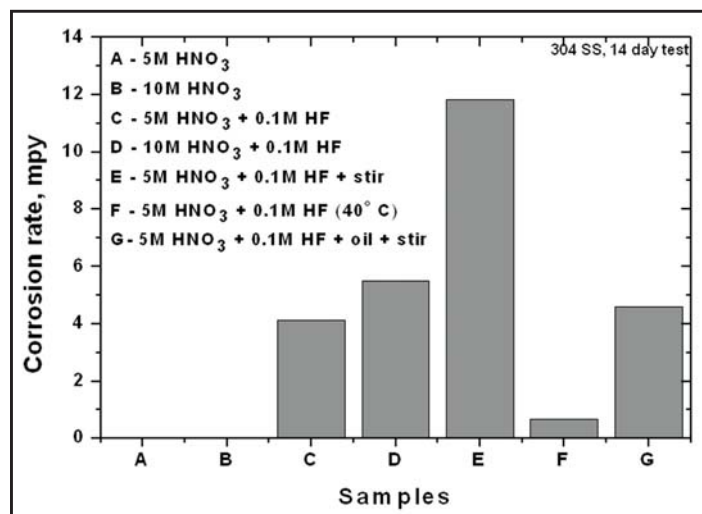
Figure 3. Corrosion rate of 304SS in various corrosive environments present in the UREX+ centrifugal contactor assembly.

Argonne National Laboratory

ANL has provided access to UREX+ development data and materials to enable the research described above. Team members have shipped samples from the UREX+ demonstration experiments to TAMU for analysis, and they are preparing a second set of samples for shipment to

Purdue University. In the following years, ANL will facilitate detector demonstrations in high-photon environments and with actual UREX materials.

Planned Activities

At the end of three years, the proposed detector assembly and detector arrays will be completed, benchmarked, and ready for full-scale application. Activities will include bench-scale testing with simulated and real UREX+ process fluids. In addition, a complete safeguards strategy will be in place to take advantage of the information stream enabled by this new detector system, and a corrosion database will be available to enable material selection for superior detector performance. In the coming year, the project team will continue the activities described above in order to advance this detector concept and to demonstrate the safeguards methodologies.

NUCLEAR ENERGY RESEARCH INITIATIVE

Performance of Actinide-Containing Fuel Matrices Under Extreme Radiation and Temperature Environments

PI: Brent J. Heuser, University of Illinois, Urbana-Champaign (UIUC)

Collaborators: University of Michigan, Georgia Institute of Technology (GT), South Carolina State University

Project Number: 08-041

Program Area: AFCI

Project Start Date: October 2007

Project End Date: September 2010

Research Objectives

The specific objectives for the first year of this project are listed below:

- Establish a growth facility at UIUC to fabricate thin-film fuel matrices containing actinide surrogates

- Characterize the thin-film samples to ensure that the desired film structure is obtained

- Perform ion bombardment/implantation experiments on thin-film samples

- Establish computational activities to study actinide surrogate and fission gas transport phenomena

These research objectives encompass the fabrication, modification via ion bombardment, and subsequent characterization of impurity (actinide surrogate/fission gas) segregation/precipitation in thin-film fuel matrices. The research is meant to address the need for improved understanding of the effects of radiation damage on actinide and fission gas transport in advanced burner reactor fuel matrices.

Research Progress

Thin-Film Growth Facility. Construction of a dedicated thin-film growth facility is nearly complete (see Figure 1). The all-metal facility will use three magnetron sputter guns to co-deposit one or two actinide surrogates, such as Ce or Nd, simultaneously with UO_2 (via reactive gas sputtering) to a heated substrate. Two DC and one RF power supplies are available to drive the sputter guns. Two mass-flow-control valves control gas flow of a high-purity Ar-plus-O_2 mixture. System pressure is maintained by a gate valve, which in turn is controlled via a feedback loop

with a Baratron capacitance manometer. This system will allow precise control of the sputter gas pressure and mixing ratio; such precision is necessary for thin-film deposition. Substrate temperature is controlled from 1°C up to 850°C. In addition, continuous substrate rotation and substrate biasing are both possible.

All of the above capabilities of this dedicated facility—an all-metal construction, high-purity process gas, high substrate temperature, substrate rotation, and substrate biasing—ensure the growth of high-purity, single-crystal films with control of the actinide surrogate concentration. Polycrystalline films can be grown as well by reducing the substrate temperature to near room temperature. Lower substrate temperatures lead to polycrystalline morphologies; lower surface diffusion of adsorbed atoms

Figure 1. Dedicated thin-film growth facility. The main processing chamber is to the left, load-lock (without transfer mechanism) to the right. The sample stage (not shown) mounts to the top of the main chamber.

results in higher-energy atomic configurations and incorporation of grain boundaries. This facility is in its initial commissioning phase.

Computation-Platform Acquisition. In addition to the thin-film growth facility, researchers have purchased three Xeon server computers with 16 CPU cores each at UIUC. The systems have been set up to perform parallel communication over shared memory only, avoiding expensive low-latency network equipment. A queuing system has been deployed to ensure 24-7 utilization. These machines allow the research team to run arbitrarily long simulations, with flexibility prioritizing job execution. For the given simulation demands, researchers' available computation resources have effectively tripled.

Actinide Surrogate-Containing CeO$_2$ Single-Crystal Films. CeO$_2$ single-crystal films have been grown on (2302) R-plane sapphire and strontium titanate (SrTiO$_3$) substrates under molecular beam epitaxy conditions. Figure 2 shows the relationship between the metal film and R-plane sapphire. A similar relationship exists for the SrTiO$_3$ substrate (not shown). Using x-ray diffraction, the research team has investigated the film quality of the CeO$_2$ matrix on R-plane sapphire and SrTiO$_3$. Generally, R-plane sapphire results in a slightly improved film quality, although SrTiO$_3$ is an adequate substrate for the team's purposes as well.
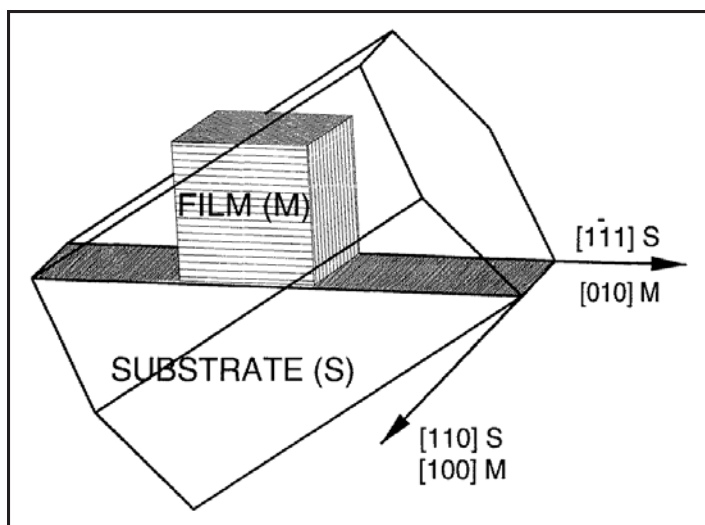
Figure 2. Structural relationship between CeO$_2$ and R-plane sapphire. An identical relationship exists for UO$_2$ and R-plane sapphire. Notice that the film cube edges are perpendicular to the substrate surface.

Computational Activities to Study Fission Gas Bubble and Actinide Stability in UO$_2$. The research goals are to develop a physics-based approach to assess fission gas bubbles and actinide stability in irradiated UO$_2$. To that effect, researchers have first identified possible UO$_2$ potentials from existing literature and have implemented

them in the molecular dynamics (MD) codes used at UIUC. These potentials have been evaluated for performance and applicability to UIUC's particular problem sets. The team has measured melting points, checked whether the Bredig transition is reproduced, and tested the damage build-up under irradiation.

In parallel, the team has developed binary collision model (BCM) software, expanding on the published TRIM algorithm using the ZBL universal potential. The software is designed to allow for arbitrary sample geometries and arbitrary irradiation conditions, as opposed to TRIM's fixed-layer geometry and external, monoenergetic, and monoisotopic irradiation. This BCM software is set up to simulate samples of UO$_2$ containing randomly dispersed spherical bubbles of Xe. Typical Xe bubble sizes (1 nm to 2 nm in diameter) and bubble density distributions (7×10^{-4} nm^{-3}) were applied.

Construction of Atomic Potentials for UO$_2$ and Other Related Actinides Using Ab Initio. Reliable interatomic potentials are the basic prerequisite for carrying out meaningful atomistic calculations and simulations of UO$_2$ and other related actinides and actinide oxides. So far, the interatomic potentials are available but with little justification for several critical issues, including a lack of long-range elastic energy contribution and the relatively simple treatment of many-body effects.

The first issue is more critical when interstitials form and when transport properties, e.g., diffusion, are concerned. The second issue has a general bearing on the quality of the potentials when bonding changes drastically, such as in irradiation. Current work at GT utilizes *ab initio* calculations (VASP and other *ab initio* codes) to obtain the needed energetic and related structural properties, in conjunction with the calculation of elastic interaction energies from elasticity theory. The results are used in a potential fitting program to obtain either parameters in analytical interatomic potential functions or coefficients of numerical interpretations of the potentials. The teams at UIUC and GT use the outcome of this effort.

Digital Microstructures and Grain Boundary Effects. To investigate how the presence of grain boundaries affects phase transitions and damage processes, researchers at GT performed atomistic (MD) simulations. To do so, the research team developed digital microstructures that mimic realistic microstructural topological properties (grain boundary area, triple junction length, and vertices) and statistical properties (distributions/moments of grain boundary area, triple junction length, and vertices). Using a newly developed inverse Monte-Carlo method, the team successfully created

the first digital microstructure model. They also developed methods to put atomic information in the model; these methods allow the team to set up different types of atoms, crystal structures, and detailed orientations of the crystals and boundaries.

Kinetics of Excess Oxygen Migration in Hyperstoichiometric Uranium Dioxide. Kinetic properties of point defects govern radiation tolerance, fission product accommodation, fission gas release, and microstructural evolution in-pile. The kinetics of this evolution will impact fuel stability during service. Modeling the defects and mobility of oxygen in oxide fuels opens a path to modeling the more complex phenomena of fission products' diffusion and their contribution to thermal conductivity. Researchers at GT have developed a kinetic Monte Carlo (kMC) model to study the point defect mobility and its interaction in UO_{2+x}.

Transmission Electron Microscopy (TEM) Analysis of CeO$_2$ Films. Researchers have used TEM to study the microstructure of CeO_2 thin films. The majority of the effort in the project's first year was to develop a specimen-preparation procedure. This procedure depends on the substrate used (sapphire and STO), as well as whether the team seeks plan view or cross-section view. A high-resolution TEM image of single-crystal CeO_2 on STO showed that the preparation procedure provides adequate thin area of the film in a cross-section orientation. Similar results have been obtained in plan view orientation.

Planned Activities

Experimental Activities. The following experiments are planned for the project's second year:

- High-energy, heavy ion bombardment of single-crystal CeO_2 and UO_2 films containing actinide surrogates. The purpose of these experiments is to study the effect of displacement damage without implanting bombardment ions into the film. Possible effects are enhanced transport and precipitation of the actinide surrogates. The experimental techniques employed will include transmission electron microscopy (TEM), electron energy loss spectroscopy, extended x-ray absorption fine structure, small angle x-ray scattering (SAXS), secondary ion mass spectrometry, and Rutherford backscattering spectrometry (RBS). The experimental parameter space will include sample temperature during bombardment, bombardment dose, actinide surrogate concentration, and oxygen stoichiometry.

- Fission gas bubble stability of single-crystal CeO_2 and UO_2 films with and without actinide surrogates under heavy ion bombardment. These experiments will help determine the influence of displacement damage on gas bubble stability, as well as the effect that the presence of actinide surrogates have on this stability. Bubbles will be created in the thin-film fuel matrix by surpassing the solubility of He and Xe during ion implantation. He/Xe implantation and heavy-ion bombardment represent separate experimental steps. The techniques employed will be post-irradiation TEM, *in situ* TEM, SAXS, and RBS. The experimental parameter space will include sample temperature during heavy ion bombardment, bombardment dose, actinide surrogate concentration, implantation dose, and oxygen stoichiometry.

Computational Activities. The following theoretical/computational activities are planned for the project's upcoming year:

- kMC simulations of fission-product migration and gas-bubble formation in the UO_2 matrix. The parameter space will include temperature and oxygen stoichiometry.

- *Ab initio* calculations of reliable interatomic potentials for development of the UO_2 microstructure. Along the path of the digital microstructure builder, researchers are close to finishing the effort and moving into actual MD simulation of the irradiation and defect process. Once the new interatomic potentials for UO_2 are available, the project team can perform simulations of irradiation and the defect process. Team members are currently testing the programs for irradiation effects using simple potentials.

- *Ab initio* atomistic simulations of irradiation effects on phase transitions and defect processes. The team has performed electronic structure calculations and hydrostatic pressure modeling of uranium and other metals, gaining data for the equation of state (EOS), which is crucial for potential fitting. The remaining work in the immediate future is to input these data into a potential fitting process to get the actual interatomic potentials for U-U, U-O, and O-O. In addition, researchers plan to continue using *ab initio* calculation to look into how the electronic structure change would affect the EOS, which is believed to be a minor effect but nonetheless requires a rigorous check.

- MD simulation of Xe bubble dissolution. To date, only the nuclear stopping (Rutherford scattering) of the fission fragments and its child-recoils has been taken under consideration. However, the fission fragments deposit a significant amount of energy along their trajectories due to their electronic energy loss, and it remains controversial as to whether these tracks can dissolve Xe bubbles. In the second year, the team will model this energy deposition along fission tracks through thermal spikes. These spikes have the potential to disrupt and even dissolve Xe bubbles close to the fission fragment trajectories.

NUCLEAR ENERGY RESEARCH INITIATIVE

Radiation Damage in Nuclear Fuel for Advanced Burner Reactors:
Modeling and Experimental Validation

PI: Niels Gronbech Jensen, University of California-Davis

Collaborators: California Institute of Technology, Northwestern University, University of California-Los Angeles

Project Number: 08-051

Program Area: AFCI

Project Start Date: October 2007

Project End Date: October 2010

Research Objectives

In this joint project, researchers are studying radiation damage of nuclear fuels through modeling, simulation, and experimental characterization. The project focuses on behavior, structure, and properties of fuel materials under conditions relevant to advanced burner reactor service.

Efficient predictive modeling requires the integration of a range of materials models and numerical methods, spanning multiple length and time scales. The project investigates the fundamental physical mechanisms that will aid new simulation tools for predicting active ion transport and damage evolution in nuclear materials. The investigation revolves around the electronic structure of nuclear oxide fuel materials with an aim toward equations of state, defect energies and migration probabilities, and interatomic force fields relevant for classical modeling of nuclear fuel's physical properties. For eventual validation of model results, the research team also conducts novel experimental characterization of damage and defect distributions in relevant materials and surrogates through (scanning) transmission electron microscopy (TEM). The tools and understanding developed through this research will provide specific prediction capabilities relevant for materials in nuclear fuel for a closed fuel cycle in a fast burner reactor, as well as new and validated computational techniques that can be applied for further research.

Research Progress

Following is a brief overview of progress in different project tasks.

Researchers have adapted the rare-event-enhanced-domain-following-molecular-dynamics (REED-MD) algorithm to oxide-fuel materials and have demonstrated its applicability by simulating the statistical ion tracks of relevant ions, from 85 keV recoil uranium (U) and 85 keV oxygen to 85 MeV fission products, such as barium and krypton. The code is based on full (local in space) MD using the Ziegler-Biersack-Littmark universal potential for atomic collisions. The code also represents energy dissipation through both a Brandt-Kitagawa electronic stopping mechanism for interacting with extended electrons and through a Firsov inelastic collision contribution that mimics energy transfer to localized electrons. The computational task of simulating ion tracks from very high initial energies until the ion comes to rest spans a large number of scales in both time and space; therefore, the procedure involves several key simulation techniques that allow for obtaining good statistical data. One is a domain-following scheme that applies well when the effective atomic interaction ranges are short-range. Another is the statistical oversampling (rare-event enhancement) of infrequent events, which allows for similar statistical quality of data that represent both frequent and infrequent events. Finally, an efficient parallel version of the algorithm has been developed and tested on a variety of computing cluster configurations.

Researchers have conducted several investigations to establish the usefulness of existing classical interatomic potentials for simulation of radiation-induced defect production and subsequent annealing using classical MD and Monte-Carlo techniques. The team has developed new codes to provide simulations of both thermodynamic and dynamic properties with fixed ionic potentials; investigations are ongoing.

The research team's effort in developing an improved interatomic potential for U oxides has been two-fold: 1) develop specific potentials for UO_2 and UO_3, and 2) rationalize and automate the process of interatomic potential development, employing databases derived from *ab initio* calculations. For UO_2, as well as the two most common phases of UO_3, the *ab initio* data comprises simulations where the unit cell was isometrically expanded and runs where each symmetrically distinct atom was perturbed along selected directions. For UO_2, researchers have also included *ab initio* results on stoichiometric defects formation energies, where they considered a 2x2x2 supercell (96 atoms). The fitting methodology that has been developed until now is summarized below:

- Specify which *ab initio* structures are to be included in the fit

- Compute "leave-three-out cross-validation" score for various models (as of now, only two models have been considered: the rigid-ion model and the shell model)

- Perform final fitting for the model having the best CV score

- Repeat the above task (this step is contingent on whether the fitted potential parameters lie in a physically plausible range)

For UO_2, a rigid-ion model was initially found to better fit the isometric expansion and perturbation data than a shell model. This result is surely anomalous (since a rigid-ion model is a special case of a shell model), and led researchers to suspect that the optimization package currently in use in the GULP software package is getting stuck in local minima. Given this problem, the research team has developed its own potential parameter optimization routines that are interfaced with GULP, which provides a reliable engine to calculate energies. In this fashion, the team has the option of using a variety of optimization schemes and has greater control over the fitting process, while still benefiting from GULP's well-tested and efficient energy calculation routines. For the δ phase of UO_3, the rigid-ion model seems to be performing well. For the γ phase of UO_3, the pair potentials do not seem to satisfactorily describe the structure's energetics. Researchers are exploring three-body potentials to alleviate this problem. Apart from continued emphasis on UO_2 and UO_3, researchers are now looking in detail into U_3O_8 in order to gather data regarding all possible oxidation states of U: U^{4+}, U^{5+}, and U^{6+}.

As radiation-induced defects migrate, more complex defects (such as gas impurities and bubbles) may form. With the aim of modeling such phenomena, the research team has used different levels of density functional theory (DFT) to approximate (neutral) defect energies in UO_2 with diifferent supercell geometries. Researchers have used the generalized gradient approach (GGA)+U and anti-ferromagnetism to explore convergence of defect energies with respect to size. The incorporation energy of a Schottky defect cluster is less than the incorporation energy of an interstitial xenon atom. Researchers hypothesize that incorporating a xenon atom into a Schottky defect cluster would be energetically favorable. $U_{32}O_{64}$ cells are currently under way to explore size convergence and incorporation energy of a noble gas atom in Schottky defects. With regard to the simulation tools available for these studies, the research team has encountered some problems with DFT+U, especially for larger simulation cells. DFT+U can give multiple self-consistent ground states, which are interpreted as resulting from different states of orbital occupancy and ordering.

To investigate orbital-ordering effects in more detail, researchers have studied the electronic structure in U oxides, with emphasis on the effects of *f* electrons. As UO_2 is nominally U4+ with 2 *f* electrons and UO_3 nominally U6+ with 0 *f* electrons, U oxides of intermediate concentration (UO_x [2<x<3] with 0 to 2 *f*-electrons) can generally exhibit charge and orbital ordering phenomena. The team has used GGA+U to calculate UO_2 in the fluorite structure, where U ions are eight-fold coordinated by oxygen. To see the effects of *f*-electron-orbital ordering more clearly, researchers have studied the charge density of the charged $(UO_2)+$ system with just one *f* electron. The single *f* electron can occupy different 5*f* orbitals, the degenerate atomic states in U that are split by the eight-fold oxygen crystal field. The oxygen coordination, therefore, is expected to have significant effects on the system's energy. Researchers expect a second challenge in the electronic structure of intermediate U oxides: oxygen defects (vacancy and/or interstitial) change U coordination, the crystal field, and therefore *f*-electron energy levels. The energy difference between low-energy orbitals is of the order of 50 meV to 200 meV in charged and neutral UO_2, an energy scale relevant to the thermodynamics of UO_{2+x}.

With high-resolution TEM, researchers can experimentally observe core electron energy loss spectra (EELS), which can help address the proper theoretical description of UO_2 and its defects. In particular, the oxygen k-edge near edge spectra in UO_2 that represents a 1s transition to an unoccupied p-state can be compared with the theoretically generated spectra. In work to date, researchers have used high-resolution TEM to study uranium dioxide oxygen k-edge and compared results with theoretical calculations. EELS can be generated using a variety of electronic structure codes; in particular, Wein2k is chosen for treating all of the electrons. In the calculations, the Hubbard U parameter for the correlated f states can be altered, and the effect on localization of electron density can be observed. In all cases, the electron density is well localized. The observation is consistent with published results: once the f states are treated with a minimal U value, the effect on the density of states is marginal. With this result, calculations performed with a reasonable U correlation factor agree favorably with measured EELS.

Planned Activities

In accordance with the project plan, next year's research will involve the following activities:

- An in-depth investigation of the equation of state for existing published fixed ionic potentials will accompany an investigation of the potential being developed within NERI-C. In particular, researchers are interested in learning whether the desired structure for uranium dioxide is the true ground state of the potential or merely a meta-stable configuration. Answering this question has important consequences for atomistic simulations of finite-temperature thermokinetic properties, and for large-scale MD simulations of radiation damage aimed at understanding the damage distribution after a collision cascade. This work will also address the more fundamental question of the practicality of variable charge potentials, which are necessary for accurate descriptions of oxide-fuel materials in which ionic flux has changed the local stoichiometry.

- With an improved understanding of damage and defects, the REED-MD code will be updated with an initial inclusion of a cumulative damage term, which mimics the material's defects as they arise from the material's history. This is the first step in arriving at a simulation model that can simulate the effect of an aging material. Such damage models include results from several other NERI-C components, such as noble gas bubble formation, migration energy calculations, and characterization of defect structure and stability through electronic structure calculations.

- Experimental work toward validation of theoretically calculated defect structures will begin through the EELS work initiated during FY 2008.

NUCLEAR ENERGY RESEARCH INITIATIVE

Advanced Instrumentation and Control Methods for Small and Medium Export Reactors with IRIS Demonstration

PI: J. Wesley Hines, University of Tennessee (UT)

Collaborators: North Carolina State University (NCSU), Pennsylvania State University, South Carolina State University (SCSU), Westinghouse

Project Number: 08-058

Program Area: AFCI

Project Start Date: October 2007

Project End Date: October 2010

Research Objectives

This research project will investigate, develop, and validate advanced methods for sensing, controlling, monitoring, and diagnosing small- and medium-sized export reactors (SMRs) and apply these techniques to the International Reactor Innovative and Secure (IRIS). The research focuses on three topical areas with the following objectives:

- Develop and apply simulation capabilities and sensitivity/uncertainty analysis methodologies to address sensor deployment analysis

- Develop and test an autonomous/hierarchical control architecture and apply it to the IRIS design

- Develop and test an integrated monitoring, diagnostic, and prognostic system for SMRs using the IRIS design as a test platform

The research tasks are focused on meeting the unique needs of reactors that may be deployed in developing countries with limited support infrastructure. These applications will require smaller, robust reactor designs with advanced technologies for sensors, instrumentation, and control. The methodologies developed can also be used for sensor deployment analysis, autonomous control, and monitoring/diagnosis/prognosis in other types of nuclear plant or hydrogen facilities, in addition to addressing two of the eight needs outlined in the recently published "Technology Roadmap on Instrumentation, Control, and Human-Machine Interface (ICHMI) to Support DOE Advanced Nuclear Energy Programs." The project will also help enhance scientific readiness of nuclear engineering students.

Project objectives will be fulfilled through an integration of the research collaborators' skills. NCSU will lead the modeling tasks through the development of an IRIS simulator. The simulator will be used by UT and Pennsylvania State University to develop autonomous and multivariate control strategies. These control strategies will utilize output from condition monitoring and prognostic methodologies, which UT will develop. When finalized, the control strategies will become the basis for automated contingency management through control system modification, redistribution, reconfiguration, and re-planning. Lastly, the instrumentation and control requirements will be written and will include optimal sensor identification and placement.

Research Progress

Research is well under way; all three research institutions have completed first-year goals and milestones. The research team had several consortium meetings in which all stakeholders reported on their research findings and planned for the future.

NCSU has developed a Fortran model of the IRIS reactor system to generate operational transients and fault conditions and to analyze IRIS interaction and sensitivity. Researchers completed several SIMULINK models of key IRIS components. The team is using these models to develop and verify control algorithms, optimal sensor placement strategies, and diagnostic/prognostic algorithms. Research at UT included the development of an adaptive condition-monitoring module, the development of a process test loop, initial analysis of an autonomous/hierarchical control architecture, and initial validation of the developed
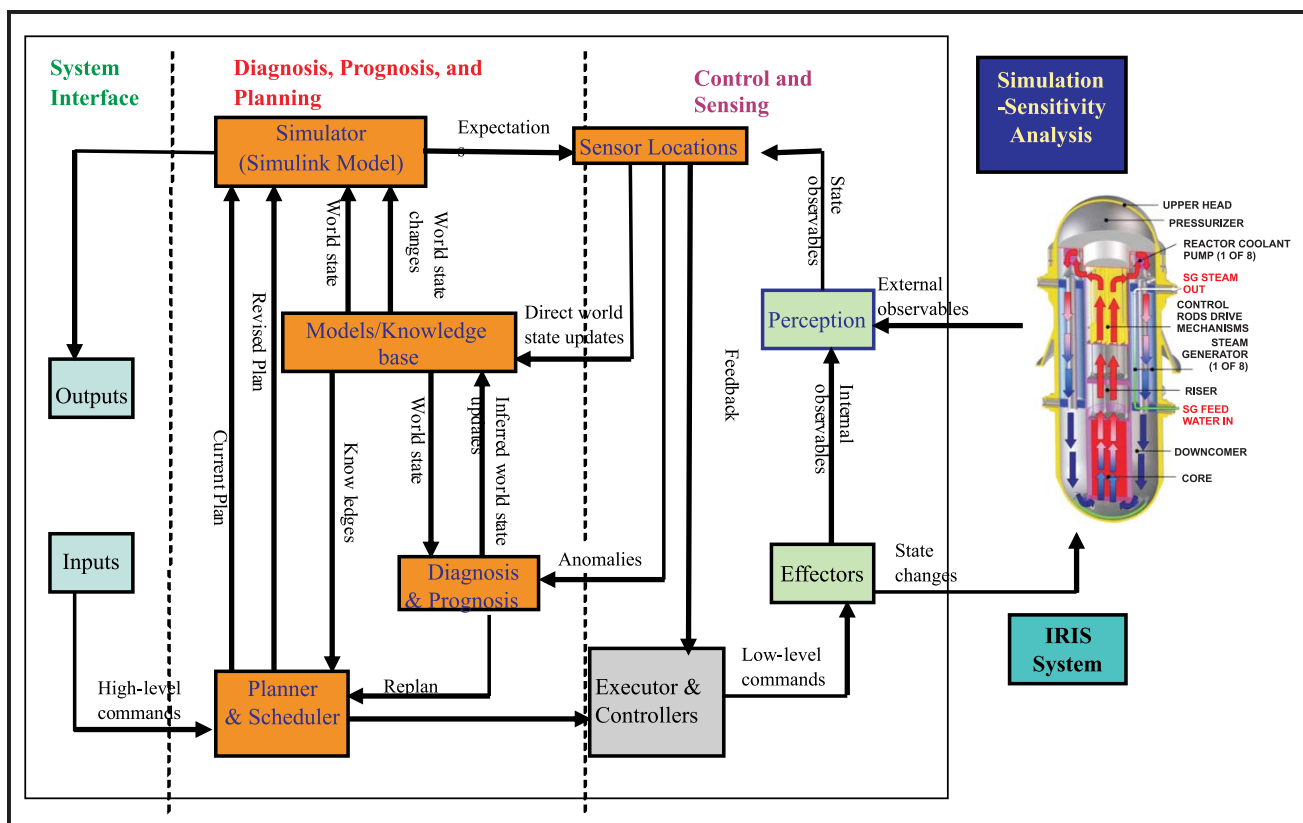
Figure 1. Integration of advanced instrumentation and controls for small and medium power reactors.

methods using simulated data. Pennsylvania State University has led the development of multivariate control algorithms.

The research team has also had participation from SCSU. Three undergraduate students worked with researchers at UT this summer, and one student worked with NCSU researchers. These students, along with the other consortia participants, are preparing papers to submit to conferences such as the American Nuclear Society's April 2009 conference on Nuclear Power Instrumentation, Controls, and Human Machine Interface Technology.

Planned Activities

The planned activities for the second year cover the three major topical areas:

- In the modeling and simulation development performed at NCSU, the tasks will focus on performing an uncertainty analysis for system model data inputs using linear and/or nonlinear approaches. Additionally, researchers will develop an optimum sensor deployment capability for improving predictive capability of system simulation models.

- In the topical area of multivariate autonomous control of modular reactors, the tasks will focus

on enhancing the multivariate controller under model uncertainty, developing a reconfigurable controller design using monitoring and diagnostics information from Topical Area 3, and demonstrating the digital controller implementation and the fault-tolerant controller in a laboratory multivariate flow control loop developed during the project's first year.

- In the topical area of monitoring, diagnostics, and prognostics, the tasks focus on developing and testing a case-based fault-identification module. Work includes simulating and running several fault states and using the collected data to develop a fault-identification module, applying the modeling and adaptation methods developed in the first year to the process loop (also developed in the first year), and developing a hybrid prognostic framework that combines Type I, II, and III prognostic models.

These three tasks are interconnected; results from one topical area will be used to complete tasks in other areas. SCSU students will continue to work with researchers at the prime universities and will complete summer internships working with students and faculty from NCSU, Pennsylvania State University, and UT.

NUCLEAR ENERGY RESEARCH INITIATIVE

Advanced Aqueous Separation Systems for Actinide Partitioning

PI: Ken Nash, Washington State University (WSU)

Collaborators: Hunter College (CUNY), Idaho National Laboratory (INL), Lawrence Berkeley National Laboratory (LBNL), Pacific Northwest National Laboratory (PNNL), Tennessee Technological University (TTU), University of New Mexico (UNM), University of North Carolina-Wilmington (UNC-W)

Project Number: 08-067

Program Area: AFCI

Project Start Date: October 2007

Project End Date: September 2010

Research Objectives

The objective of this project is to expand upon the results of earlier studies of partitioning americium (Am) from the lanthanides; these studies utilized synthesis of new separations materials integrated with radiochemical characterization of the complexes and separations systems. Multiple academic and national laboratory investigators contribute to this effort.

In the predominant trivalent oxidation state, the chemistries of lanthanides and actinides overlap substantially; thus, their mutual separation is quite challenging. Two fruitful approaches to efficient processes are 1) the application of complexing agents containing ligand donor atoms that are softer than oxygen (e.g., N, S, and Cl-) and 2) the oxidation of Am to the IV, V, or VI valence states to increase the essential differences in Am chemistry relative to the lanthanides. These approaches have two fundamental limitations: the softer donor atoms interact less strongly than oxygen with the hard acid lanthanide and actinide cations and the upper oxidation states of Am are all moderately strong oxidants in conventional media. The investigators are thus faced with the tasks of increasing the strength of actinide soft-donor interactions through subtle manipulation of conditions and of emphasizing materials and methods that accommodate the considerable redox instability of oxidized Am species in conventional aqueous separations systems. This program's essential feature is the creation of a synergistic network of experts: specialists in synthesis and characterization of new chelating agents and separations materials, with a complementary cadre of solution chemists experienced in coordination chemistry of f-elements relevant to biphasic separations. Each partner university has significant prior experience with 1) f-element chemistry (primarily lanthanides); 2) the design, synthesis, and characterization of chelating agents and functional polymers for separations; and 3) varying degrees of experience in separation science as it applies to either spent nuclear fuel processing or analysis of radioisotopes. The national laboratory partners have complementary facilities, the ability to conduct research with materials at higher levels of radioactivity, and the specific expertise of the laboratory co-investigators.

As scientific demands dictate, graduate students are sent to the national laboratories to conduct portions of their research, further advancing the project's educational objectives. To the same end, the project has been developing a network of predominantly undergraduate universities whose students and professors are invited to WSU for one-week tutorials on actinide science and the nuclear fuel cycle. During the first year of this project, this concept was tested on the partner universities and received rave reviews.

Research Progress

In this project, the principal facilities and expertise in academic actinide solution chemistry reside at WSU; investigators at WSU conduct most of the ligand/actinide complex characterization and separation activities (lanthanide studies are possible in several university

partner laboratories). The collaborating investigators bring specific expertise in 1) aromatic soft donor ligand design, characterization, and synthesis (UNC-W); 2) the ability to functionalize polymeric materials that will reduce reagent-phase partitioning issues in several extractant systems (CUNY); 3) the design of organophosphorus extractants based on pyridine derivatives, likely to exhibit improved radiation stability in harsh environments (UNM); 4) interactive in-house organic synthesis capabilities for creating soft-donor complexant molecules considered to be "targets of opportunity" that are complementary to materials being synthesized by external partners (WSU-Meier); and 5) extended radiochemical characterization capabilities (TTU). The roster of national laboratory partnering institutions includes LBNL, INL, and PNNL, all housing at least one experienced actinide scientist and separations specialist. As mentioned above, the project team has further established an initial network of predominantly (or exclusively) undergraduate institutions; students and faculty members will be invited to WSU for a one-week tutorial on actinide chemistry, nuclear science, chemical separations, and the nuclear fuel cycle. This tutorial will take place annually, including professors and students from different institutions each cycle. The purpose of this activity is to introduce this essential science to undergraduates who otherwise have minimal exposure to this field. The tutorials also provide training, orientation, and educational materials to faculty members, who can then incorporate this science into the curriculum at their home institutions.

For spent fuel separation applications, designing lipophilic chelating agents and developing processes for their use must equally emphasize complex stability (derived from creating a binding site compatible with a target's structural requirements), organic phase compatibility (derived from adjusting the attached alkyl groups' nature and positioning), and radiolytic/hydrolytic/redox stability. Fast ligand exchange/phase transfer kinetics is desirable. Because it is a continuous operation process, solvent extraction reagents are considered the prime targets of investigation, but polymeric materials also represent a viable and valuable tool in the separations toolbox. In some cases, the ultimate answer to difficulties with phase compatibility of selective receptors may well be their immobilization in a polymeric matrix and a shift from solvent extraction toward ion-exchange operations.

During the first year of this project, each external collaborator sent samples of separations-relevant materials to WSU team members, who are currently evaluating these samples. Characterization activities include homogeneous, single-phase solution chemistry investigations, liquid-liquid extraction studies, and studies of metal ion uptake onto resinous materials. Separation studies are providing guidance for improving material properties.

Following are the accomplished milestones for the project for this fiscal year:

- WSU has achieved success in preparing new pyridine and bipyridine derivatives of polyaza complexants: triazine rings are mated to the central core of 2,6-pyridyl or 2,9-bipyridyl core groups, creating tetraaza complexants analogous to those prepared in the European spent fuel processing program. The latest derivatives have incorporated normal alkane functional groups to improve lipophilicity of the moderately hydrophilic polyaza complexants. Metal ion uptake studies are also under way at WSU.

- UNC-W has completed metal complexation studies of many classes of metal ions with phenanthroline-2,9-dicarboxylic acid (PDA). Researchers have sent samples to WSU. PNNL and WSU have completed spectrophotometric titrations of complexes of PDA with Nd(III) and Am(III). Data analysis continues. The project team has evaluated PDA complexes' interaction with Am(III) and Nd(III) in aqueous solutions, which gives clear indications of metal-ligand interactions and of enhanced selectivity for Am over Nd. To complement the single-phase studies, WSU has begun characterization of the separation potential of PDA, phenanthroline, and the alcoholic derivative PDAM. The limited solubility of these compounds in typical solvent extraction media must be overcome for more complete assessment.

- Several samples of tetraethylhexyl-NOPOPO extractant have been sent to WSU for characterization of their Am/Eu extraction potential. As these ligands are seen as potential substitutes/replacements for CMPO in TRUEX, the focus is on their ability to extract both metal ions from nitric acid media. Investigators have also done some preliminary extraction studies on Pu(IV) and on Np(V) in this system. Samples of the tetraphenyl–NOPOPO derivative have been sent to TTU for extraction chromatographic studies, which have begun. UNM, WSU, and INL are involved in a separate project investigating radiation stability of NOPOPO compounds.

- CUNY has sent the first several 2-to-3 gram samples of resin-immobilized ligands to WSU. These materials contain 1 to 3 neutral phosphate esters bound to the polystyrene-divinylbenzene matrix via amine or amine/alcohol linkages. These carefully prepared metal-binding "environments" combine phosphoric acid or phosphate ester functional groups with a polyalcohol or polyamine microenvironment, enhancing the kinetics and, potentially, selectivity of the metal ion binding site. Previous work at CUNY has established that some of these materials exhibit high affinity for U(VI) from concentrated nitric acid media. Project team members have verified these observations at WSU and are making plans for additional actinide uptake studies. There are some indications that phosphate esters are too hydrolytically unstable for application in strong acid, but these same materials have exhibited exceptional affinity for uranyl from carbonate/bicarbonate media.

Planned Activities

During the next year, the project team will focus on expanding supplies of initial materials synthesized at partner institutions, and on continuing characterization of separations systems based on ligand supplies in hand at WSU. Some ligand design feedback has been derived from the metal ion uptake studies. The team will also address adjustments to increase solubility of the phenanthroline derivatives, hydrolytic stability of the phosphate resin materials, and purity of the NOPOPO compounds, based on characterization of metal complexes. Investigators are also preparing additional aliphatic polyaza compounds. They will continue to assist in characterization of resin materials and examine the separation potential of UNM organophosphorus extractions in extraction chromatography. PNNL has sent additional isotopes that will facilitate WSU-based characterization activities. Investigators are also working (in cooperation with Eichrom Industries) on developing a ^{234}Th radioisotope generator system that will further facilitate the radiotracer characterization process. Continued research flowing from the previous NERI projects will also persist for a time to bring those projects to a rational conclusion. Those results will complement the results expected from this study. Finally, initial contacts and planning for the first undergraduate tutorial session, to be conducted at the end of the next academic semester (May—June 2009), will begin in the next quarter. The team also expects to accomplish postings of graduate students and/or postdoctoral researchers working on this project to the laboratories of the national lab partners this year.

NUCLEAR ENERGY RESEARCH INITIATIVE

5.3   Nuclear Hydrogen Initiative

Nine NERI research projects are currently being performed that closely relate to the goals of the Nuclear Hydrogen Initiative, six of which were awarded in FY 2006 and three in FY 2007 (two NERI and one NERI-C).

The mission of NHI is to develop technologies to produce hydrogen with heat and/or electricity from next-generation nuclear energy systems at costs that are competitive with other transportation fuels. The goal is to demonstrate hydrogen production that is compatible with nuclear energy systems through scaled experiments, then to couple an engineering-scale demonstration plant with a Generation IV reactor concept.

NERI efforts related to this initiative involve the construction of integrated laboratory-scale experiments in support of the three primary NHI research areas:

- Hydrogen production with thermochemical cycles

- Hydrogen production with high-temperature electrolysis

- Support systems for the hydrogen production process

In FY 2008, NHI research projects focused on developing an efficient flowsheet for the sulfur-iodine (S-I) cycle, developing simulation tools, and conducting design/analysis of the S-I cycle. Research in high-temperature electrolysis is enhancing electrolyzer performance, developing improved cell materials, and creating new seal designs. Reactor/hydrogen support system research is creating new alloys and ceramics for heat exchangers, and optimizing heat exchanger design/performance.

Under the FY 2007 NERI-C project related to NHI, research efforts develop and model alternative thermochemical cycles for nuclear hydrogen production.

For more information about NHI, refer to this website: http://www.nuclear.energy.gov/NHI/neNHI.html.

This section provides an index of the research being performed under NHI and a summary of the ongoing projects.

NUCLEAR ENERGY RESEARCH INITIATIVE

Directory of Nuclear Hydrogen Intiative
Project Summaries and Abstracts

NUCLEAR ENERGY RESEARCH INITIATIVE

Nickel-Silicon Alloys for the Sulfur-Iodine Reactor—Hydrogen Production Process Interface

PI: Joseph W. Newkirk, University of Missouri-Rolla

Collaborators: Idaho National Laboratory (INL)

Project Number: 06-024

Program Area: NHI

Project Start Date: March 2006

Project End Date: March 2009

Research Objectives

The goal of this project is to develop materials suitable for use in the sulfuric acid decomposition loop of the sulfur-iodine thermochemical cycle for nuclear hydrogen production. Materials must have both acceptable corrosion resistance and sufficient ductility for component fabrication and avoidance of catastrophic failure. Nickel-silicon intermetallics show promise for such critical applications as the sulfuric acid vaporizer, vapor superheater, and decomposer. Past work indicates that adding minor alloying elements to nickel silicide (Ni_3Si) provides significant ductility at room temperature (7 percent to 10 percent elongation at failure), a unique property for normally brittle high-silicon materials. Ni_3Si can also be easily joined by traditional methods such as welding, and preliminary studies show this compound has excellent corrosion resistance.

In this work, the team will further develop Ni_3Si to maximize its ductility and corrosion resistance while reducing cost. Researchers will analyze the effects of adding elements such as niobium, boron, and iron. Microalloying may be used to improve resistance to corrosive impurities in the sulfuric acid-processing stream, such as iodine. Finally, the team will study the extent to which iron can be substituted for nickel in Ni_3Si without adversely affecting ductility or corrosion resistance.

Researchers will document mechanical properties of these new materials over a range of temperatures and strain rates. The team can then utilize these results to improve material properties and microstructure. As a final test, corrosion-resistant materials will be subjected to flowing sulfuric acid (H_2SO_4) at temperatures and pressures comparable to the actual sulfuric acid processing loop (120°C to 400°C at less then 10,000 psi) in order to measure corrosion rates. The research team will also form prototype plates, pipes, and forgings to demonstrate various fabrication techniques.

Research Progress

Efforts for this year focused on the corrosion protection mechanism and the alloy's behavior in conditions closer to those in the decomposition loop. The research team has also continued rolling studies, as well as casting and testing new alloy composition. Finally, researchers have gathered high-temperature mechanical properties data.

The team conducted intermittent corrosion testing in 70 percent sulfuric acid; the goal was to characterize the reaction kinetics and gain insight into the film formation mechanism. Plots of weight loss versus time show what appears to be a parabolic rate mechanism; however, log-log plots tell a different story. Figure 1 shows results of a comparison of two different rolled samples of the new composition. The mechanism goes through a change at about 90 minutes. Short-time data was not measured for these samples. At very short times (less than 10 minutes), the mechanism shows logarithmic behavior, which is usually seen in early film formation.

The second region (Figure 1) has a slope of one, indicating a nearly linear behavior. The final mechanism has a very low slope and very slow kinetics. This region does not fit a diffusion type of mechanism and could be due to interface reaction control. This rate of mass loss corresponds to values less than five mpy and would be considered sufficient for use in the decomposition loop.
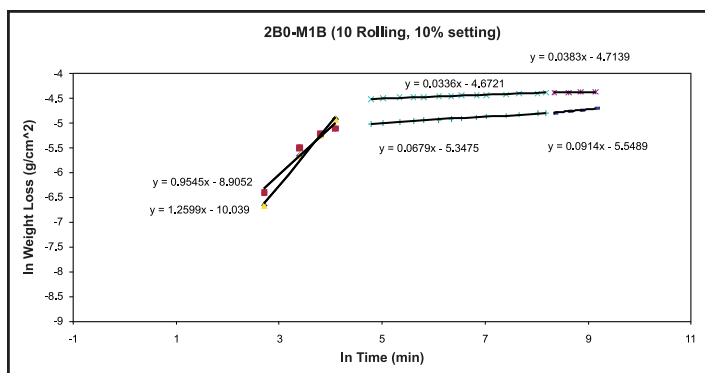
Figure 1. Results of two different samples of the new alloy composition.

Some additional test points extend the line of the third stage for a considerably longer time. This represents a stop in the testing in which the sample was removed, washed, and left out in the air for seven days (at which time the tests resumed). The continuation of the third-stage behavior illustrates the strength of the passive film and is very desirable for long-term survival of the alloy during service.

Testing at INL, under conditions closer to those potentially seen in the decomposition loop, shows promise. Figure 2 shows the results of tests carried out at 350°C and 500 psi in 96 percent sulfuric acid. The samples were of the same composition, but of two different heat treatment conditions. The sample 2B-B quickly passivated and dropped below five mpy.
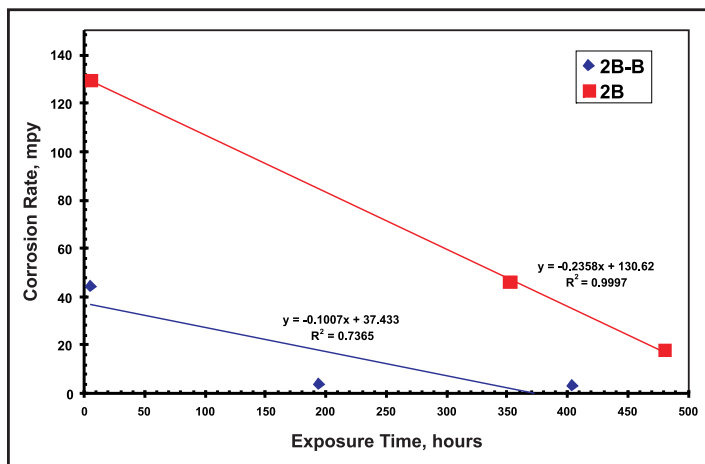
Figure 2. Results of tests carried out at 350°C and 500 psi in 96 percent sulfuric acid.

Figure 3 shows some of the difficulties still to be overcome. Testing in acid with less oxidizing potential has typically been problematic with commercial alloys. Tests show that samples with compositions similar to those shown above (Sample A-3) approach 10 mpy, which is excellent by most standards, but potentially insufficient for use in the decomposition loop. Kinetic studies of this

material show that it does not reach full passivation during high-temperature testing. The passivation time has been shown to be very important to the alloy's response, so more testing is being carried out with samples that have the best treatment combination to lead to early passivation.
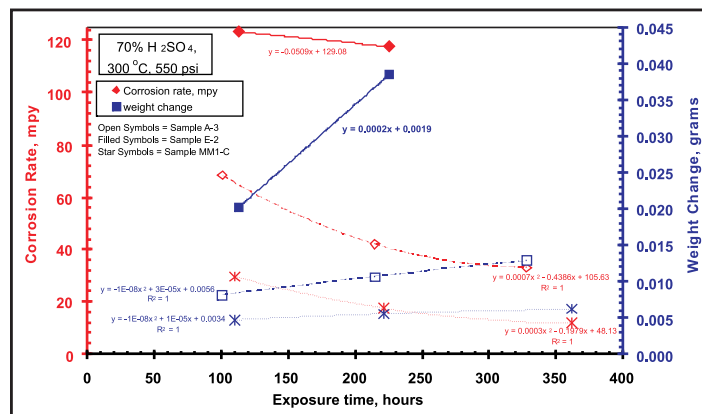
Figure 3. Results of tests carried out at 300°C and 550 psi in 70 percent sulfuric acid.

Gleeble studies performed at INL have yielded mechanical properties data over the temperature range expected for service. The alloys are very strong over the entire temperature range, actually increasing in strength with temperature peaking at around 600°C.

Researchers have studied iron-containing alloys, and the phases formed are complex. The team is sorting out these phases, which they will then use as guides for new alloys with iron. This work is not yet far enough along to produce a viable alloy for use. However, the data will be valuable in future work finding appropriate compositions to produce such an alloy.

Planned Activities

The project team plans passivation studies and long-term testing for the upcoming year. Alloys will be pre-passivated in the strongest acid and then tested. Also, the team will test the pre-passivated alloys under conditions more closely resembling those expected in service. Scratch tests will be performed as well to study re-passivation behavior.

Haynes Alloys has declined further involvement in the study. Several other companies have expressed interest; the project team will choose one to continue the collaboration. Better processing and higher-capacity rolling loads should yield further improvements in alloy performance.

The project will end in the early part of 2009. A proposal is planned for funding to continue alloy development and to apply the results in pilot plants.

NUCLEAR ENERGY RESEARCH INITIATIVE

Microstructure Sensitive Design and Processing in Solid Oxide Electrolyzer Cells

PI: Hamid Garmestani, Georgia Institute of Technology

Collaborators: Pacific Northwest National Laboratory

Project Number: 06-027

Program Area: NHI

Project Start Date: March 2006

Project End Date: March 2009

Research Objectives

This project focuses on improving properties of electrodes in solid oxide electrolyzer cells (SOECs) by optimizing the microstructure. Researchers developed a spray pyrolysis processing technique to synthesize large surface-area gradient porous fuel-cell electrodes. Synthesis of the porous lanthanide in an electric field produced an oriented structure.

Research Progress

During this fiscal year, the team modified process parameters for the spray pyrolysis and the electric field application. Using an in-house facility of their own design, the team examined high-temperature-conducting properties of the resulting microstructure. These results will be compared to the theoretical predictions on SOEC electrode properties. Based on the modeling efforts performed during the second year, the process parameters will be optimized to control the microstructure.

Fabrication of Gradient Porous SOEC Electrodes by Precise Process Design. The team achieved the goals proposed last year by selecting suitable precursors and experimental parameters to fabricate ideal gradient porous media. First, they investigated the influence of different solvents on the microstructure, comparing metal-organic precursors with organic solvents to an aqueous solution. The aqueous system achieved a coarse microstructure, but exhibited large cracks. On the other hand, organic systems gave the SOEC cathode a fine and homogenous deposition layer.

Deposition of Gradient Porous LSM Film. Researchers examined the effects of deposition parameters such as temperature and solution flow rate on the microstructure of lanthanum-strontium-magnetite (LSM) films. They achieved a gradient porous microstructure by applying a multiple-step spray deposition consisting of changes to the precursor solution concentration, deposition temperature, and solution flow rate. The overall results are summarized in Table 1. Optimal cathode properties consist of a fine layer close to the electrolyte's surface, with gradually coarser outer layers.

Researchers started by spraying a dilute 0.1 M solution at a flow rate of 0.73 ml/min onto a substrate at 520°C, which allowed sufficient time for surface reactions and deposition of particles in the proper arrangement to produce a uniform interlayer between the electrolyte and the porous electrode. By increasing the temperature to 540°C and the solution flow rate to 1.13 ml/min, gas-phase nucleation created smaller particles embedded in the initial layer, producing a more porous structure. A more highly concentrated 0.5 M solution allowed for more random particle deposition. In the third stage, the solution flow rate was kept constant at 1.13 ml/min; however, the temperature increased to 560°C to help increase the decomposition of precursors. In the fourth and last stage, researchers expect to have a layer with higher porosity in which particles may demonstrate slight growth. Increasing the temperature to 580°C, along with increasing solution flow rate to 1.58 ml/min, resulted in fast evaporation of highly concentrated solution, allowing little time for solute diffusion and particle densification and resulting in highly porous films.

Stage	Condition / Solvent	Precursors (mg)			Solvent (ml)	Temperature (ºC)	Solution flow rate (ml/min)	Pyrolysis process	LSM film composition	YSZ electrolyte
A	Aqueous	Lanthanum acetate	Strontium acetate	Manganese acetate	Water	480	0.73	Endothermic (vaporization)	Inhomogenous	Crack growth/YSZ failure
		110.6	30	86	25					
	Organic	Tris Lanthanum	Bis Strontium	Tirs Manganese	Ethylene glycol dimenthyl ether	480	0.73	Exothermic	Homogenous	No cracks
		80.3	22.7	100.7	25					
B	Organic	80.3	22.7	100.7	25	520, 540, 560, 580	0.73, 1.13, 1.58	Exothermic	Homogenous	No cracks
C	Organic	Tris Lanthanum	Bis Strontium	Tirs Manganese	1-2 Dimethoxyethane					
		180	60	160	100	520	0.73	Exothermic	Nanocrystaline fine interlayer	No cracks
		360	120	320	50	540	1.13		Gradient porous coarse layers	
		360	120	320	50	560	1.13			
		360	120	320	50	580	1.58			

Table 1. Spray conditions for three experimental stages.

Figure 1 depicts the plot of electrode thickness determined from scanning electron microscopy (SEM) cross-section micrographs as a function of time at each deposition step. The rate of deposition increased as a function of solution flow rate and deposition temperature.

Figure 2 reveals the effect of post heat treatment on the microstructure of gradient porous LSM film. The outer layer of the surface is formed by uniform deposition of submicron-sized spherical droplets, creating large pores with a narrow size distribution ranging from 1 µm to 5 µm. However, a large portion of the porosity is attributed to nano-sized pores. The annealing temperature of 700°C led to partial growth and agglomeration of the particles, resulting in a more uniform microstructure. If the particles undergo higher temperature sintering, fine pores will be filled and will no longer be available due to further grain growth.

Figure 1. The plot of the first gradient cathode film thickness as a function of deposition time.

Figure 2. SEM micrograph of the gradient porous LSM sample surface after 700°C heat treatment.

Figure 3(a) shows the gradient porous LSM cathode with an average thickness of about 20 µm. However, the SEM cross section of the heat-treated LSM film in Figure 3(b) shows that the film thickness has reached approximately 100 µm. Variation in film thickness is one of the drawbacks of the spray technique and is pronounced here due to the substrate's angular position with respect to spray direction.

Overall, the LSM film is compositionally homogeneous and crack-free with a semi-columnar porous structure. Scotch tape test results showed high cohesive strength of the film, with no peeling observed, and the LSM film demonstrated good adhesion to the yttria-stabilized zirconia (YSZ) substrate. At the interface layer, as the particles get smaller, a larger number of triple-phase boundaries (TPB) form at the three-dimensional sites between LSM particles, the YSZ electrolyte and gas-phase (O_2) or electrode surface sites. Higher porosity can be

developed, resulting in increased cathodic activity. Nanostructured electrodes dramatically reduce electrode/electrolyte interfacial polarization resistances and improve cell performance; this fact supports the theory that the microstructure close to the interface should be as fine as possible. However, smaller particles cannot always guarantee higher activity since they are more likely to grow and to be sintered at working temperatures in real cells and, thus, to fill the active sites. At the interface with YSZ, a thin uniform nanostructured active LSM interlayer with a crystallite size smaller than 100 nm is observed.

Crystallite Size Distribution.

Figure 4 shows the LSM average crystallite size of approximately 25 nm at 300°C, which changes to about 50 nm when increasing temperature to 900°C. Researchers achieved these results through x-ray diffraction line profile analysis. The relatively small variations in crystallite size of the LSM cathode heated to this range of operating temperatures confirms that the spray pyrolized gradient film fabricated at the temperature range of 520°C to 580°C comprises a highly crystalline LSM phase before undergoing further heat treatment. This is an advantage of the spray pyrolysis technique for processing stable optimal microstructures at much lower temperatures than conventional processes and without need for further heat treatment.

Electrical Conductivity of the Gradient Porous LSM Film.

High electrical conductivity of the LSM cathode at high temperatures results in lower ohmic polarization, while the porous microstructure provides a path for mass transfer through the cathode microstructure, thereby making low cathodic polarization possible. However, creating a balance between these two requirements is desirable in processing cathode microstructures for intermediate-temperature SOECs (IT-SOECs). Thus, it
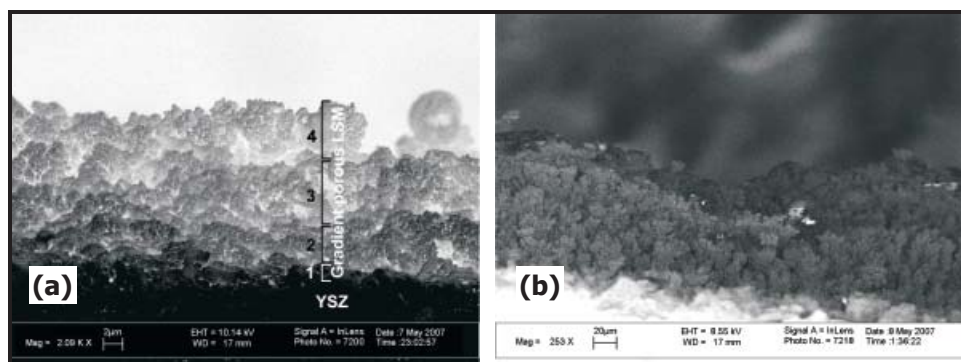
Figure 3. (a) SEM cross-section image of the gradient porous LSM made by multiple spray pyrolysis depositions; (b) SEM cross-section of the gradient porous LSM after heat treatment.
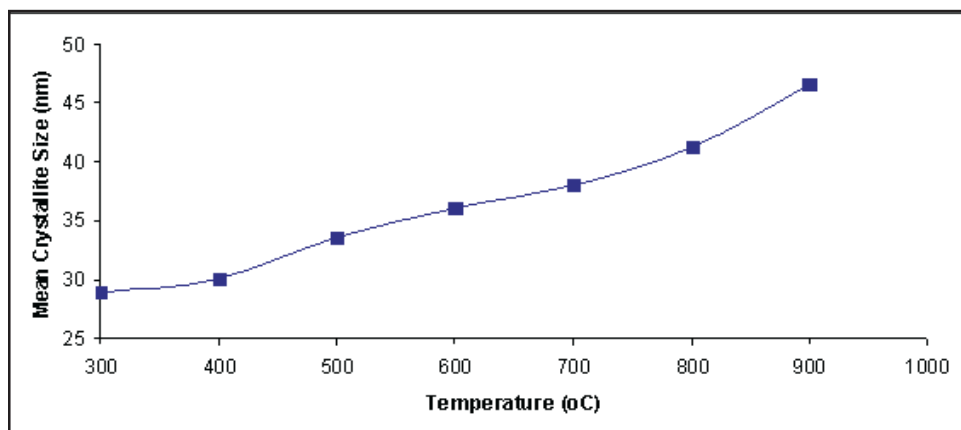
Figure 4. Relationship between LSM mean crystallite size and temperature.
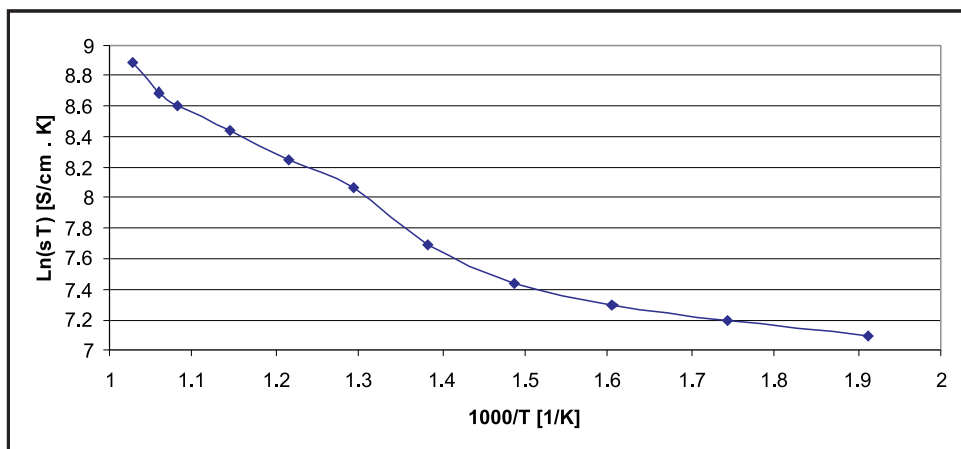
Figure 5. The electrical conductivity of gradient porous LSM film as a function of reciprocal absolute temperature.

is important to know that morphological changes in the microstructure have not resulted in a significant drop in the cathode film's electrical conductivity. To study the effect of gradient porous microstructure with columnar morphology on the charge transfer property, researchers measured the electrical conductivity of the gradient porous LSM cathode at an intermediate temperature range (500°C to 700°C), which is plotted over the reciprocal of temperature in Figure 5.

This plot suggests that conductivity of the gradient porous LSM film is in the acceptable range required for the SOEC cathode. Electrical conductivity increases with temperature, although at a lower rate between 250°C and 500°C (corresponding to 1.91 to 1.29) that changes drastically from 500°C to 700°C (1.29 to 1.03). This data shows the highest rate of charge transfer over the working temperature range for IT-SOECs. Researchers also observed another significant increase at 700°C. The deviation from a linear relationship can be attributed to the increased activation energy of the porous film for electron conduction with increase in temperature.

Planned Activities

The research team achieved a gradient porous microstructure, which is ideal for SOEC electrodes, in optimized and precisely controlled conditions. This work will be further optimized with an automated computer-controlled system that can produce the same result over a very large surface area where the deposition of each layer occurs through an x-y control system. After predicting thermal, electrical, and mechanical properties of SOEC porous electrodes based on previous research, the team will also apply statistical mechanics to predict transport and permeability properties.

NUCLEAR ENERGY RESEARCH INITIATIVE

Dynamic Simulation and Optimization of Nuclear Hydrogen Production Systems

PI: Paul Barton and Mujid Kazimi, Massachusetts Institute of Technology

Collaborators: None

Project Number: 06-041

Program Area: NHI

Project Start Date: March 2006

Project End Date: February 2009

Research Objectives

This project is part of a research effort to design a hydrogen plant interfaced with a nuclear reactor—a promising alternative to fossil-fuel-generated hydrogen. The objective is to build models for dynamic simulation and optimization of hydrogen production options using nuclear energy. There is a natural interdependence between design and operational decisions for integrated nuclear hydrogen production systems. This interdependence requires a modeling and simulation environment that can capture the physical design descriptions and map these to steady state and dynamic predictions of the hypothesized system's behavior. Simulating these systems can provide invaluable information for the next step, whether this step is an experiment or a design decision. The simulation environment must be adaptable, flexible, and expandable.

This project will develop a dynamic modeling, simulation, and optimization environment for nuclear hydrogen production systems. A hybrid discrete/continuous model will capture the continuous dynamics of the nuclear plant, the hydrogen plant, and their interface, along with discrete events such as major upsets. This hybrid model will make use of accurate thermodynamic sub-models for the description of phase and reaction equilibrium in the thermochemical reactors. Use of the detailed thermodynamic models will allow researchers to examine the process in detail and have confidence in the accuracy of the property package they use. The hybrid model will also allow researchers to study plant operations and accident scenarios. Researchers will be able to use it to conduct parameter estimation studies to identify possible improvements in materials, mechanical design, and safety issues. The seamless connection between modeling,

simulation, and optimization can help establish optimal control schemes. These schemes can then be tested in the model.

Research Progress

In this project, the research team analyzed system interface operation and conducted an overall process safety study. They performed the following seven tasks:

1) Created a prototype dynamic model for the heat-transfer loop and for representing the interaction of two heat loops

2) Developed a novel simplification of the gas dynamics equations, taking into account only the relevant time scales for simulated phenomena

3) Validated the simplified system of equations representing the heat transfer loop using the canonical form and RELAP (the reactor leak and power safety excursion code, shortened form)

4) Extended the electrolyte non-random two-liquid (NRTL) thermodynamic model for application to multi-electrolyte, mixed-solvent solutions

5) Developed detailed models for the thermodynamic representation of the aqueous acidic solutions in the sulfur iodine (SI) cycle (sulfuric acid and hydrogen iodide)

6) Developed a robust bilevel optimization formulation for parameter estimation in liquid-liquid and vapor-liquid-liquid equilibrium problems

7) Studied process flowsheets for the HI_x section of the SI thermochemical cycle

Descriptions of the work performed under each task follow:

Prototype Dynamic Model for the Heat-Transfer Loop. Researchers developed a model of an idealized heat-transfer loop. This loop consists of a compressor and a pipe with sections at different exterior temperatures. The compressor closes the loop and provides the pressure differential to make the gas flow inside the pipe. Dimensions and temperatures of this interface are in accordance with the Idaho National Laboratory (INL) design. The model equations constitute a system of quasi-linear hyperbolic partial differential algebraic equations in time and one spatial dimension on multiple coupled domains (each domain corresponding to an element of the overall heat transfer interface). Previous attempts to simulate similar systems involving a nuclear reactor have used numerical methods that introduce errors and produce unphysical numerical artifacts, such as oscillations. A particular challenge was to couple the model of the compressor with the explicit numerical method used to solve the gas dynamics equations.

Modeling the Interaction of the Two Heat Loops. A dynamic model was developed to represent the heat-transfer loop design from INL. This model represents the gas loop removing heat from the nuclear reactor and the gas loop taking that heat to transfer it to the hydrogen plant. The two heat-transfer loops are coupled through an intermediate heat exchanger. Each loop consists of a compressor and a pipe with sections at different external temperatures. The compressor closes the loop and provides the pressure differential to make the gas flow inside the

pipe. Loop 1 in Figure 1 represents the loop designed by INL, and it transfers the heat to the chemical plant. This loop receives 50 MW from Loop 2, and it uses helium to transfer heat from the intermediate heat exchanger to the process heat exchanger. The intermediate heat exchanger corresponds to a compact heat exchanger, such as the ones designed by Heatric. The process heat exchanger (represented by blue in Figure 1) corresponds to a tube-in-shell heat exchanger.
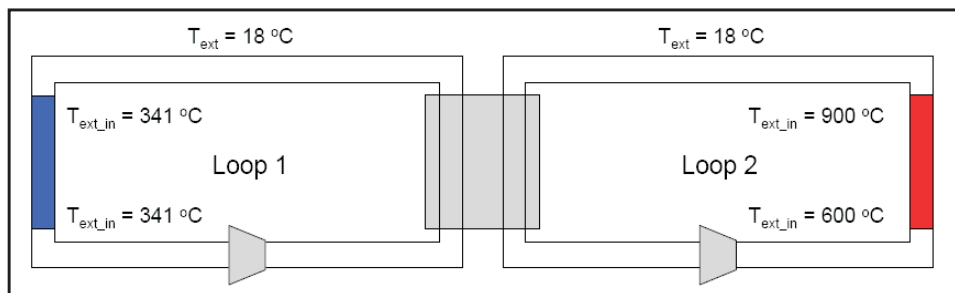
Figure 1. Loop 1 and Loop 2 coupled by a compact heat exchanger.

Researchers were able to simplify the model equations by taking into account only the relevant time scales for the simulated phenomena. In this case, simulation of the fast time scales is often not necessary because discrete disruptions in the flow of the gas are rare. As changes in pressure propagate with the speed of sound, the research team can make a quasi-steady-state approximation (singular perturbation) for the equations related to the fast dynamics. To validate the predictions from the new simplified system of equations, the research team compared its results with simulation results from the software RELAP, as shown in Figure 2. Hence, researchers are now able to use the simplified equations to represent gas dynamics. This simplification allows the use of implicit integrators; therefore, the team can implement bigger models and achieve faster simulation speeds.
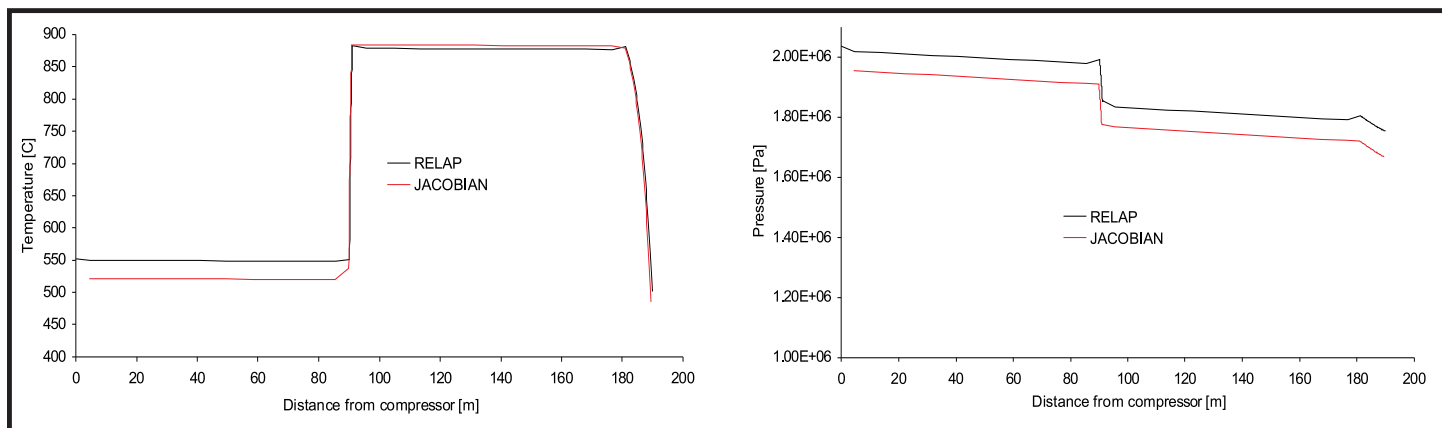
Figure 2. Comparison of modeling results using Jacobian® and RELAP.

Refinement of the Electrolyte-NRTL Model for Application to Multi-Electrolyte, Mixed-Solvent Systems. The research team developed an alternative formulation for the electrolyte-NRTL model. The changes can be summarized as the substitution of the Pitzer-Debye-Hückel equation with a detailed form of the original Debye-Hückel model, the inclusion of hydration chemistry in the model in a way that reflects the effect of hydration on the solution's structure, and re-derivation of the NRTL term for consistent extension of the model to multi-electrolyte solutions. The team applied the models with considerable success to an extensive database of univalent and bi and trivalent electrolytes, aqueous solutions of acids and bases, and multi-electrolyte solutions.

Modeling of the Thermodynamics of the SI Thermochemical Cycle. The team validated the majority of the thermodynamic models developed using a very large database of experimentally measured electrolyte systems; they needed to examine the new model in systems that are widely known and measured. After that, they applied the new models to simulate SI cycle thermodynamics. The description of the sulfuric acid system using the refined formulation of the electrolyte-NRTL model appears superior to the modeling efforts previously presented. More experimental data and a consistent database are needed for accurate representation of all sections of the SI cycle.

Bilevel Optimization Formulation for Parameter Estimation in Phase Equilibrium Problems. The research team developed a novel approach for parameter estimation in phase equilibria, demonstrating its importance with the example of the NRTL excess Gibbs free-energy model. They cast parameter estimation as a bilevel program with multiple lower-level programs corresponding to (generalized) semi-infinite constraints given by requirements for 1) stabilizing the predicted phase split, 2) excluding additional spurious phase splits, 3) predicting the correct number of phases in each phase split, and 4) predicting the correct number of azeotropes. Global optimization techniques are necessary for the lower-level program; otherwise, the model predictions might correspond to unstable phase splits. Additionally, global solution of the upper-level program gives a certificate of optimality, which is useful in the case of model-experiment mismatch. The formulation developed is independent of the thermodynamic model used for predicting phase equilibria.

Self-Consistent Database for Thermodynamic Properties of H_2SO_4 and HI. Overall, the majority of problems related to uncertainty in modeling of thermochemical cycles lie in predicting thermodynamic properties in various sections of the process. One major difficulty with modeling the SI cycle is inconsistency of experimental data at the conditions of interest. Hence, the team needs to develop a comprehensive framework that deals with all aspects of SI cycle thermodynamics. This framework starts with development of a self-consistent database of thermodynamic properties for the SI thermochemical cycle's various sections. For this objective, the team gathered in a database published thermodynamic data for the aqueous solutions of sulfuric acid and hydrogen iodide (i.e., *P-T-x-y* data, azeotropic data, heats of mixing, and mixture heat capacities). The team then evaluated the data critically for self-consistency, studying the data on the basis of a flexible functional form chosen for excess Gibbs free energy, describing the deviation from ideality of the liquid phase, while treating the gas phase as ideal.

Study of the Proposed Flowsheets for the HI_x Section of the SI Thermochemical Cycle. The HI_x section is the key section of the SI thermochemical cycle because of the high heat demands and the difficulty introduced by the complex azeotropic behavior of the HI-I_2-H_2O mixture. The main considerations include examining various flowsheet options (reactive distillation, extractive distillation, electrodialysis). In the reactive distillation option, the primary benefits are that the complete reaction occurs in one vessel and that H_2 production is higher and more efficient. A large heat load is required, but a large portion of it can be recovered and used in other places in the system. Also, the existing azeotrope that prevents high HI concentrations imposes serious operational constraints. Finally, the high pressures and temperatures, along with high concentration of very caustic substances, pose a problem when considering materials to be used in constructing the system. Many of these problems show up regardless of the type of column. In the extractive distillation option, the amount of H_3PO_3 requires a good deal of energy for separation. At this point, the optimum theoretical estimate suggests efficiencies below 50 percent. Several studies have suggested the use of electro-electrodialysis (EED) to concentrate the HI

solution in order to break the azeotrope, allowing for higher H_2 yields. The main problem this presents is that, without proper models, the method's potential efficacy is unclear. Researchers have estimated efficiencies up to 56.8 percent with use of EED. Currently, work is focused on the reactive distillation option.

Planned Activities

In the last phases of this work, researchers will finish building the different models for each unit operation and the overall system model. The research team will then integrate these models with the heat-transfer interface model and perform several case studies, including accident scenarios for analysis, involving the integrated systems.

NUCLEAR ENERGY RESEARCH INITIATIVE

High-Performance Electrolyzers for Hybrid Thermochemical Cycles

PI: John W. Weidner, University of South Carolina (USC)

Collaborators: Sandia National Laboratories (SNL), Savannah River National Laboratory (SRNL), Argonne National Laboratory (ANL)

Project Number: 06-054

Program Area: NHI

Program Start Date: March 2006

Program End Date: March 2009

Research Objectives

The objective of this project is to provide the scientific basis for developing high-performance electrolyzers for use in two candidate thermochemical cycles for producing hydrogen from nuclear power: 1) the hybrid sulfur process and 2) the modified calcium-bromine (Ca-Br) cycle. There are still a number of challenges in making these thermochemical cycles commercially viable, including 1) reducing the high cost of platinum and ruthenium catalysts, 2) minimizing sulfur dioxide (SO_2) crossover (a serious lifetime-limiting phenomenon), and 3) finding suitable operating conditions for optimal electrolyzer performance and cycle efficiency.

This work builds on the successful application of the proton exchange membrane (PEM) electrolyzer for producing hydrogen through the conversion of water and sulfur dioxide ($H_2O + SO_2 \rightarrow H_2SO_4 + H_2$) and the dissociation of hydrogen bromide ($HBr \rightarrow Br_2 + H_2$). Researchers will explore methods for improving the utilization of platinum and ruthenium in the cathodes and anodes, along with replacing them with other materials such as metal alloys, silicides, or mixed metal oxides. New membranes with low gas crossover, high conductivity, mechanical stability, and temperature resistance will enable operation at higher temperatures and pressures. The researchers will evaluate the most promising catalysts and membranes over a range of conditions (i.e., 30°C to 120°C, 1 atm to 10 atm, and 50 percent to 80 percent conversions) and will apply mathematical models to optimize cell and process performance.

Research Progress

During the initial part of this work, researchers established the viability of gas-phase electrolysis for both the hybrid sulfur and the modified Ca-Br cycles and showed that catalyst loading does not play a significant role in electrolyzer performance. They evaluated the effect of membrane thickness and concluded that thinner membranes exhibit better performance because of the increased water flux to the anode, which results in lower sulfuric acid concentration and a lower cell voltage. A new mathematical model determines water transport as a function of membrane thickness, current density, and membrane pressure differential. The team observed that increased pressure differential ($\Delta P = P_c - P_a$) leads to better performance, as shown in Figure 1.
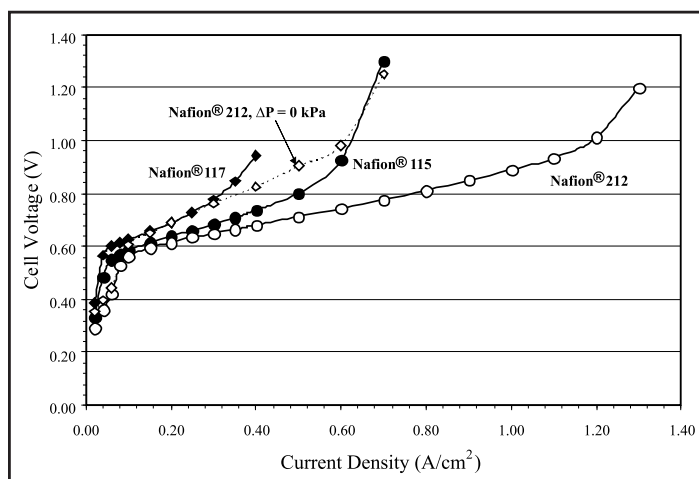
Figure 1. Polarization curves of the membranes tested in the hybrid sulfur electrolyzer (cell T = 80°C and ΔP = 600 kPa, unless otherwise noted).

Performance of the N212 membrane is significantly worse at a low pressure differential due to decreased water flux to the anode, which leads to increased sulfuric acid concentration. As shown in Figure 2, the cell voltage is dependent on sulfuric acid concentration and is not directly related to the membrane pressure differential; it is the sulfuric acid concentration that determines cell voltage. Because the acid concentration is affected by water transport, understanding and controlling this phenomenon is important in the operation of the electrolyzer.
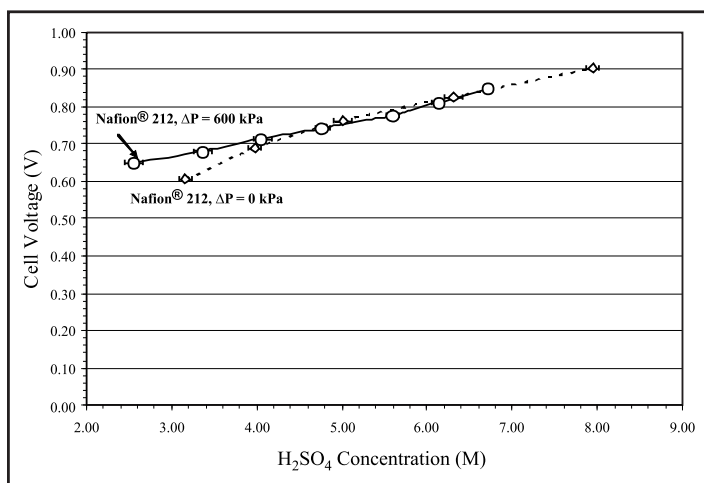
Figure 2. Cell voltage versus H_2SO_4 concentration for the N212 polarization curves shown in Figure 1 at two membrane pressure differentials.

Besides affecting sulfuric acid and cell voltage, water transport can affect the rate of SO_2 crossover to the cathode. Because SO_2 is soluble in water, increasing the water flux to the anode can prevent SO_2 crossover to the cathode. Researchers have already demonstrated the model's ability to predict water transport. The next step is to determine the mechanics of SO_2 crossover. Figure 3 shows the electrochemical monitoring technique in which the membrane pressure differential is held at 0 kPa. The electrolyzer is connected to a potentiostat such that the water side is the anode and the gas side is the cathode (i.e., reversed from normal operation). Nitrogen is initially sent to the gas side and a voltage step is applied. After the steady-state current is reached, the gas is switched to SO_2 and the current is measured. The limiting current corresponds to SO_2 crossover to the water side, which is oxidized to H_2SO_4. From the transient current between t* and t_f, researchers determined the solubility of SO_2 in Nafion and the diffusion coefficient. As expected, increasing the pressure differential decreased the SO_2 crossover current as a result of higher water flux in the opposite direction.
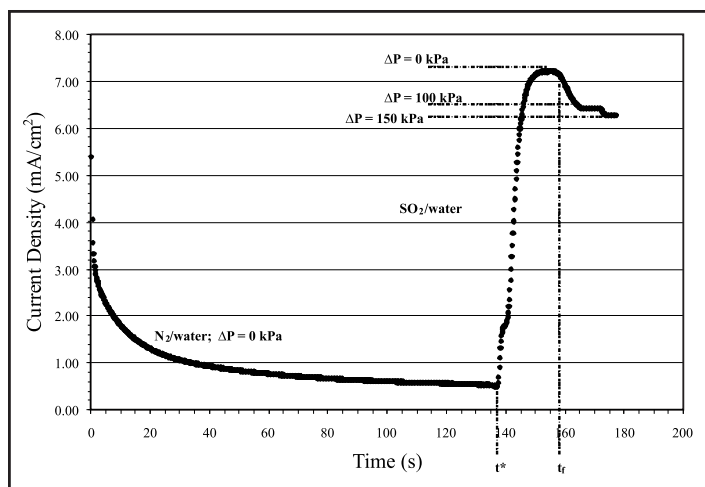
Figure 3. Electrochemical monitoring technique with membrane pressure differential increased in steps at a cell temperature of 80°C.

Although increasing the membrane pressure differential decreases SO_2 crossover, it is not the only way to prevent this phenomenon. Collaborators developed a sulfonated Diels-Alder poly(phenylene) (SDAPP) membrane with a high ion exchange capacity that limits gas crossover, giving significant improvement over Nafion at temperatures above 100°C, especially at higher current densities, as shown in Figure 4. Mechanical stability may also translate to longer lifetimes at elevated temperatures.
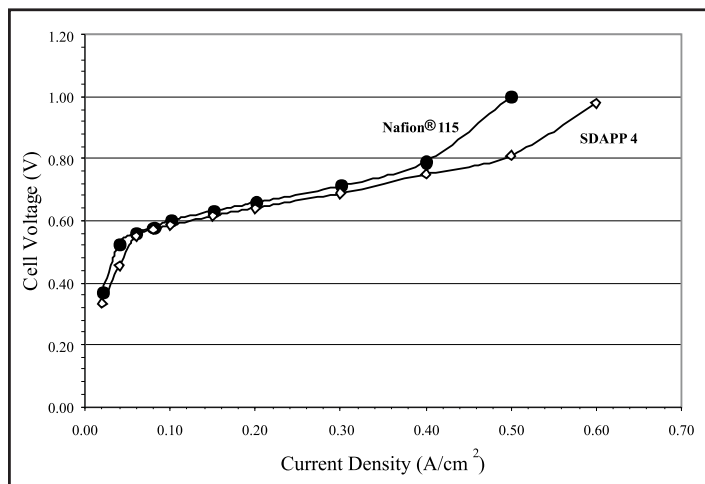
Figure 4. Comparison of N115 and 3.5 mil thick SDAPP 4 membrane at ΔP = 300 kPa and T = 120°C.

Figure 5 compares SO_2 crossover current of the SDAPP and Nafion membranes as a function of cell temperature. The SO_2 crossover current decreases as the temperature increases because of the lower solubility in Nafion at higher temperatures. The results indicate that at the same temperature and pressure differential, the SDAPP membrane, though thinner, allows for less SO_2 crossover than the Nafion membrane.
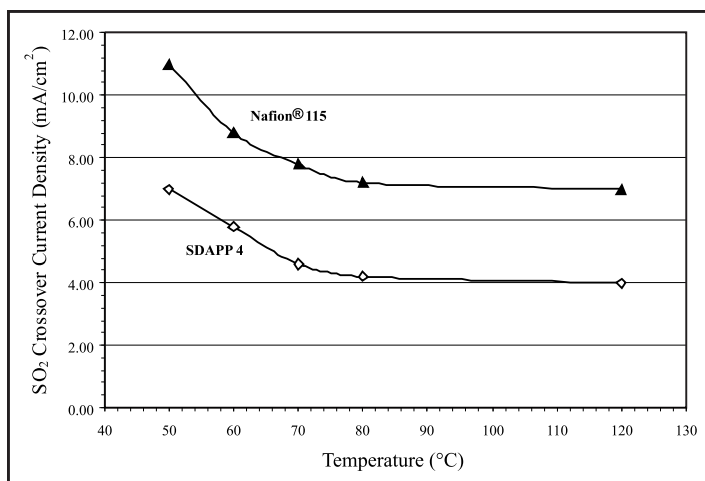
Figure 5. SO$_2$ crossover current as a function of temperature at zero ΔP.

Figure 6. SO$_2$ crossover current for N115 and SDAPP 4 as a function of current density at two pressure differentials and cell T = 80°C. The points are measured by electrochemical monitoring and the lines are the model predictions.

Finally, the effect of current density on SO$_2$ crossover was investigated for the different membranes (Figure 6). In addition to increasing the pressure differential, increasing the current density leads to increased water flux to the anode as a result of a lower activity of water; the increased current density leads to greater H$_2$SO$_4$ production at the anode, which lowers the water activity and leads to increased water flux due to diffusion. Model predictions indicate that increasing the current density leads to decreased SO$_2$ crossover, the same effect observed in the electrochemical monitoring technique (Figure 3) when the pressure differential was increased. Both actions lead to increased water flux to the anode, which limits SO$_2$ crossover to the cathode.

Planned Activities

These results indicate that water transport plays an important role in the elecrolyzer performance. It affects the sulfuric acid concentration at the anode, which determines

the cell voltage, and affects the rate at which SO$_2$ crossover occurs. Because the pressure differential has such a large effect on water transport, work is under way to reach high pressures (approximately 2,000 kPa) on the cell. Once completed, this work will allow for operation at very high-pressure differentials.

In addition, the platinum loading on the anode and cathode had negligible effects on electrolyzer performance. Therefore, there are opportunities to develop electrocatalysts that are less expensive, but still provide the requisite activity. Work is under way to evaluate a series of less expensive electrocatalysts that are active and durable under the conditions studied here.

NUCLEAR ENERGY RESEARCH INITIATIVE

Development of Efficient Flowsheet and Transient Modeling for Nuclear Heat Coupled Sulfur Iodine Cycle for Hydrogen Production

PI: Shripad T. Revankar, Purdue University

Collaborators: None

Project Number: 06-060

Program Area: NHI

Project Start Date: April 2006

Project End Date: March 2009

Research Objectives

The main goal of the proposed project is to develop a flowsheet for the closed-loop sulfur iodine (SI) cycle using current advances in acid decomposition and product gas separation for high thermal efficiency and to develop methods for transient analysis of the cycle. Specific objectives of the proposed project include the following: 1) to perform benchmark flowsheet analysis of the baseline General Atomics (GA) SI cycle, 2) to investigate and implement the membrane techniques to the hydrogen iodide (HI) and H_2SO_4 decomposition and separation processes, 3) to perform comparative flowsheet analysis of the modified cycles, 4) to develop component-wise models of the SI cycle to apply to the transient analysis, and 5) to perform a preliminary analysis of transient behavior of the closed-loop SI cycle. These objectives address the research and development needs of the Nuclear Hydrogen Initiative program elements, including thermochemical cycles and reactor-hydrogen production process interface.

Research Progress

The SI process consists of three chemical reactions expressed as the following equations:

Section I (Bunsen reaction):

$$I_2 + SO_2 + 2H_2O \rightarrow 2HI + H_2SO_4$$
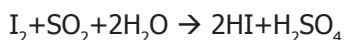
Section II (sulfuric acid decomposition):

$$H_2SO_4 \rightarrow H_2O + SO_2 + \frac{1}{2}O_2$$
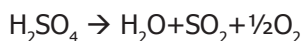
Section III (hydrogen iodide decomposition):

$$2HI \rightarrow H_2 + I_2$$
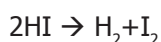
In the SI cycle, all process fluids are recycled and no greenhouse gases are emitted. The SI thermochemical cycle was simulated using ASPEN PLUS version 12. Researchers used the SI cycle flowsheet for Sections I, II, and III developed by GA as a reference. The present simulations followed the methodology applied to the GA flowsheet. The team performed a step-by-step simulation starting from the single-component simulation to the whole-section simulation. For the single-component simulation, the team obtained conversed solutions and the results were comparable to the GA result. For the whole-section simulation, the team obtained the converged solution for Section II and the results were also comparable to the GA result. The sensitivity analysis shows the same behavior as in the GA report. For the whole-section simulation, the team obtained converged solution for Sections I, II, and III, and the results were also comparable to the GA result. There have been various attempts to resolve the convergence issue in Sections I and III.

For HI decomposition, Section III, a reactive distillation column with seven stages and the condenser and reboiler were used as shown in Figure 1. The HI/I_2/ H_2O product of Section I is pumped up to 22 bar and heated to the feed temperature of the reactive

Flow rate: 126.164 kmol/h
H_2O: 51%
I_2: 39%
HI: 10%
H_2: 0%
Temperature: 262ºC
Pressure: 22bar
Phase: liquid
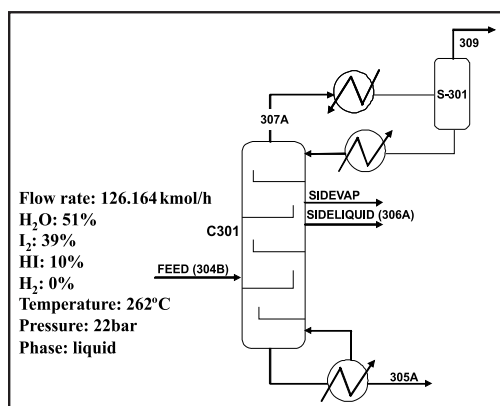
Figure 1. Simplified reactive distillation.

distillation column (C301) in a network of heat exchangers (type: shell and tubes) (E301/E302/ E303). This heat is recovered from the two liquid products of the distillation column, the bottom stream (305A) containing most of the iodine and the side outlet (306A) containing most of the water and undecomposed hydrogen iodine.

The vapor molar fractions and liquid molar fractions are presented in Figure 2. The results indicate that at the top of the column, water is predominant and no HI is present at Stage 1 in the vapor phase.

The present simulation results were compared with GA results. As shown in Figure 3, the results compare well with the GA results.

A simplified model of the SI-cycle for transient analysis was developed. Balance equations for the simplified model were presented and parameters for the model were introduced. Several transient calculations that have been performed rely on straightforward perturbations of the heat transfer through the heat exchanger, Q, such as temperature or flow rate on either side of the heat exchanger. In Figure 4, a 50 Kelvin ramp increase in the hot side of the heat exchanger loop (driving force) and in the cold side temperature (response) transient is shown. The driving force and response are indicated by regions on the plot.

Planned Activities

The remaining tasks for the third year of the project are to 1) implement the membrane separation techniques for the HI and H_2SO_4 decomposition processes and modify the flowsheet, 2) perform comparative flowsheet analysis of the modified cycles, 3) optimize the flowsheet for each section for process efficiency, and 4) perform detailed transient analysis of the simplified thermochemical process coupled to the nuclear reactor heat transport system for hydrogen generation using the SI cycle.
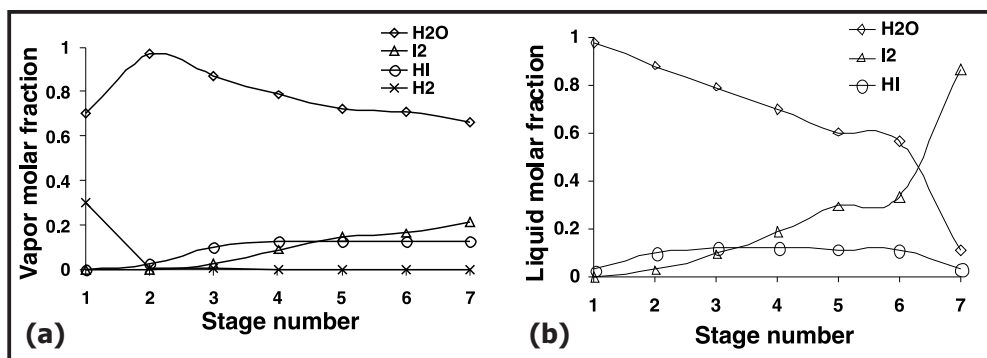
Figure 2. Vapor molar fraction (a) and liquid molar fraction (b) in the reactive distillation column when the hydrogen production rate is 1 kmol/h.
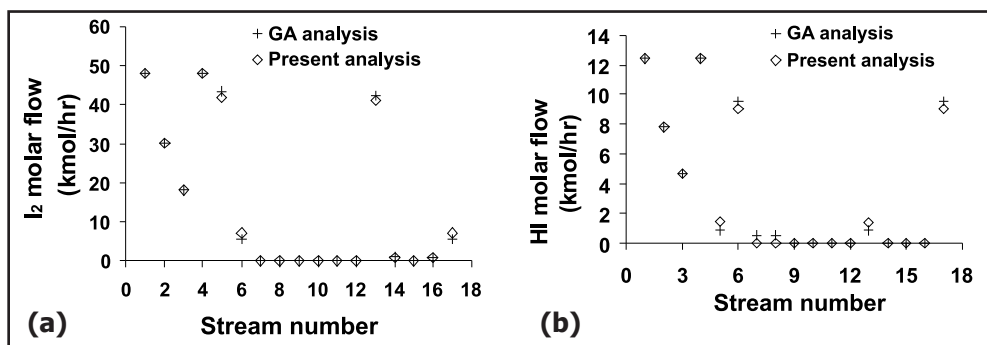
Figure 3. (a) I_2 flow rate and (b) HI flow rate in the flow sheet.
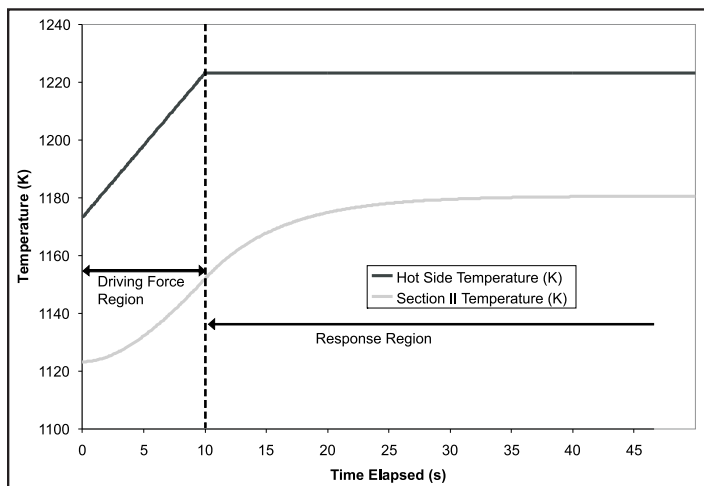
Figure 4. Two Section II driving and response regions with a 50 K ramp increase.

NUCLEAR ENERGY RESEARCH INITIATIVE

Gradient Meshed and Toughened Solid Oxide Electrolyzer Cell Composite Seal With Self-Healing Capabilities

PI: Kathy Lu, Virginia Polytechnic Institute and State University

Collaborators: Idaho National Laboratory

Project Number: 06-140

Program Area: NHI

Project Start Date: June 2006

Project End Date: May 2009

Research Objectives

High-temperature electrolysis of water steam is a promising approach for hydrogen production. The potential is even more promising when abundant heat from nuclear power reactors can be efficiently utilized. Hydrogen production through the above approach also allows for low electric consumption. Overall conversion efficiencies for high-temperature electrolysis are in the 45 percent to 50 percent range, compared to approximately 30 percent for conventional electrolysis. However, current solid oxide electrolyzer cell (SOEC) seals hinder this promising technology due to a mismatch in thermal expansion coefficients that cause seal cracking and gas leakage. Under such motivation, this research focuses on increasing SOEC operation time and high-temperature stability for splitting water into hydrogen. Specifically, researchers are focusing on improving SOEC seal thermal stability and performances by alleviating thermal stress and seal-cracking issues. They are also trying to understand the seal-interconnect interaction differences at different atmospheres for extended periods of time. This novel seal design will enable long-term SOEC operation by providing mechanisms for glass-matrix toughening and crack self-healing.

Researchers will conduct experiments to prove proposed thermal stress-release mechanisms and to predict long-term cell performance. They will assess the seals' overall stability, performance, and interaction with other cell components.

Research Progress

Researchers have successfully printed intricate 3-D mesh structures of 200 μm wire width from shape memory alloy (SMA) TiNiHf powders and have systematically studied the 3-D mesh structure integrity and width precision. The team studied SMA particle size effect on the 3-D printing. With the prerequisite that powder is flowable during roller spreading, smaller SMA particles are preferred for a stronger 3-D mesh structure. With a decrease in SMA particle size, binder-spreading time increases while spreading rate decreases, resulting in different binder-spreading profiles, as Figure 1 shows.

The team sintered the 3-D printed TiNiHf SMA meshes using a two-step sintering process. First, the team removed the binder from the 3-D printing process and pre-sintered the mesh structure in a vacuum furnace at 1,150°C. After that, they encapsulated the pre-sintered wire mesh in an Ar gas-filled quartz tube for sintering at 1,280°C. The wire mesh densification drastically improved while the wire mesh dimension decreased substantially.
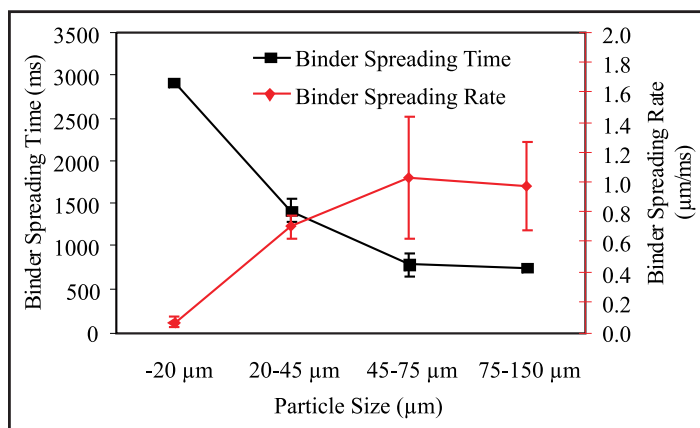
Figure 1. Binder spreading time and rate for different size TiNiHf powders.

The researchers have systematically studied novel glasses of different compositions based on the SrO-La$_2$O$_3$-

Al_2O_3-B_2O_3-SiO_2 system (SABS). The properties studied include glass transition temperature T_g, softening temperature T_d, thermal expansion coefficient CTE, and thermal stability after long-time thermal treatment at 800°C. These SABS glasses desirably have T_g from 635°C to 775°C, T_d from 670°C to 815°C, and thermal expansion coefficient CTE from 11.5-13.0 x 10-6/°C. Glasses of less than 5 mol% B_2O_3 content are thermally stable after being kept at 850°C for 200 hours (Figure 2). Ni addition into SABS glass can effectively lower glass transition temperature Tg and softening temperature Td while not substantially affecting the glass thermal expansion coefficient CTE and thermal stability. As the B_2O_3:SiO_2 ratio increases, the SrO-La_2O_3-Al_2O_3-B_2O_3-SiO_2 glass connectivity decreases and the amount of non-bridging oxygen atoms increases. The SABS-0 glass shows the highest glass structure connectivity and thermal stability.

Elements	Diffusion distance (µm)					
	0 hr	5 hr	10 hr	20 hr	50 hr	100 hr
Al	3.93	1.64	4.59	3.27	3.93	3.27
Cr	2.93	1.96	3.93	2.29	2.62	2.62
Fe	2.62	3.27	3.27	2.62	2.29	2.29
La	3.93	3.93	3.93	4.91	3.60	3.93
Mn	2.29	1.64	2.62	1.34	.982	2.62
O	2.95	2.62	3.93	2.62	2.62	2.62
Si	3.60	3.60	4.26	3.93	2.62	3.60
Sr	2.93	3.93	3.93	3.60	2.95	2.95
Ti	1.64	2.95	2.62	0.98	2.29	1.96

Table 1. Crofer 22 APU and SABS-0 glass diffusion couple interfacial layer thickness at different thermal treatment times in high-purity Ar atmosphere at 800°C.

Figure 2. XRD patterns of SABS-0 glass thermally treated at 850°C for different times.

The research team studied Crofer 22 APU-SABS-0 glass, Ni substrate-SABS-0 glass, and SMA-SABS-0 glass interfacial diffusion at 800°C in Ar atmosphere for up to 200 hours. During this study, the SABS-0 glass bonds well with the Crofer 22 APU interconnect and Ni substrate but not with the SMA substrate. Crofer 22 APU compositions show limited diffusion into the SABS-0 glass. Also, the SABS-0 glass shows limited diffusion into Crofer 22 APU. The Crofer 22 APU-SABS-0 glass interface zone thickness is almost constant, with thermal treatment time up to 100 hours in an Ar atmosphere at 800°C, approximately 2.0 µm to

3.0 µm. For the Ni-SABS-0 glass diffusion couple, the same observation holds true. Some composition spikes appear in the intermediate hours of diffusion couple thermal treatment, but such composition variation disappears after longer thermal treatment hours. La and Al show slightly higher concentration at the interfacial boundaries of the Ni-SABS-0 glass diffusion couples. Since the diffusion layer thicknesses are fairly small, they should not present detrimental effects to the SOECs.

The research team also studied TiNiHf-SABS-0 glass interfacial diffusion. This study showed substantial diffusion of Ni, Hf, and Ti into the SABS-0 glass. Also, there is substantial diffusion of O, La, Si, and Sr into TiNiHf alloy substrate. The TiNiHf-SABS-0 glass interfacial zone thickness is 15 µm to 30 µm, depending on the diffusion couple interface locations. Some composition spikes appear in the intermediate hours of the diffusion couple thermal treatment.

Planned Activities

Researchers plan to perform the following tasks over the next fiscal year:

- Continue to study the SABS glass seal systems and tailor their compositions to produce complementary thermal behaviors during SOEC operation

- Conduct comprehensive seal testing to demonstrate smooth thermal expansion coefficient transition, cracking resistance, and crack self-healing capabilities of the new composite seal

- Make seals using actual SOEC seal configurations and model the process to optimize cost and performance

NUCLEAR ENERGY RESEARCH INITIATIVE

Liquid Salts as Media for Process Heat Transfer from Very High-Temperature Reactors: Forced Convective Channel Flow Thermal Hydraulics, Materials, and Coatings

PI: Kumar Sridharan, University of Wisconsin-Madison

Collaborators: None

Project Number: 07-030

Program Area: NHI

Project Start Date: June 2007

Project End Date: May 2010

Research Objectives

This project investigates the use of liquid salts as heat transfer fluids to utilize process heat from very high-temperature reactors and other Generation IV reactors for hydrogen production. Favorable thermal properties of liquid salts (such as their lower melting point, high boiling point, high heat capacity, chemical stability, and low pumping power requirements) allow for efficient transport of high-temperature thermal energy. Successful implementation of a liquid salt reactor/hydrogen production process interface will require an accurate assessment of thermal hydraulics in small-diameter-channel, high-efficiency, compact heat exchangers. In the small channels, under high-flow velocity and high-temperature conditions, both thermal hydraulics and materials will be key operational issues. In particular, the project team will need information on corrosion/erosion resistance of materials and coatings for construction of intermediate heat exchanger (IHX) systems, along with operational experience to determine the minimum channel sizes to avoid clogging and to optimize heat transfer.

The specific objectives of the project are to 1) investigate materials' and coatings' corrosion performance in liquid salts by performing static corrosion tests in liquid FLiNaK and liquid 32%MgCl$_2$-68%KCl salts at 850°C for 500 hours, 2) fabricate a forced convection loop to study thermal hydraulics in small channels (including clogging effects) and particle transport and deposition issues, and 3) evaluate materials and coatings under prototypic velocity liquid salt flow conditions. Materials to be investigated include 1) Inconel alloys 800H, 600, and 617, and 2) carbon-carbon and silicon-carbide (SiC) composites. Coatings to be studied include optimized electroplated nickel (Ni), as well as hard carbon and pyrolytic carbon coatings.

Research Progress

Nickel Coatings on Incoloy 800H. Ni-201 (a nearly pure Ni alloy) displays excellent corrosion performance in molten FLiNaK salts at 850°C, so researchers have carefully investigated Ni electroplating for corrosion protection of alloys in a molten FLiNaK environment. Ni electroplating is a cost-effective industrially mature process, and its non-line-of-sight nature allows for Ni deposition on inside surfaces of long pipes. A commercial firm electroplated test samples of Incoloy 800H with Ni (80 µm and 120 µm thick), and then researchers tested the samples in FLiNaK at 850°C for 500 hours. As Figure 1 and Figure 2 show, this corrosion prevention method was largely successful. Compositional profiles across the Ni layer did indicate some diffusion of iron (Fe) and chromium (Cr) from the alloy through the Ni plating and into the salt. The research team is thoroughly studying mechanisms of diffusion, particularly of Cr through the Ni plating; the studies emphasize the role of grain boundaries and voids that formed in the Ni-electroplating during these diffusion processes. To this end, the team is heat-treating Ni-electroplated samples to densify and change the grain boundary character distribution.
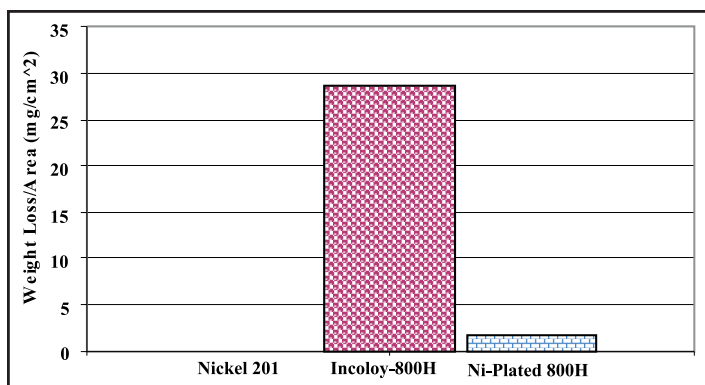
Figure 1. Weight-loss per area of Ni-201 (commercially pure NI), Incoloy-800H, and Ni-plated Incoloy-800H tested in FLiNaK for 500 hours at 850°C.
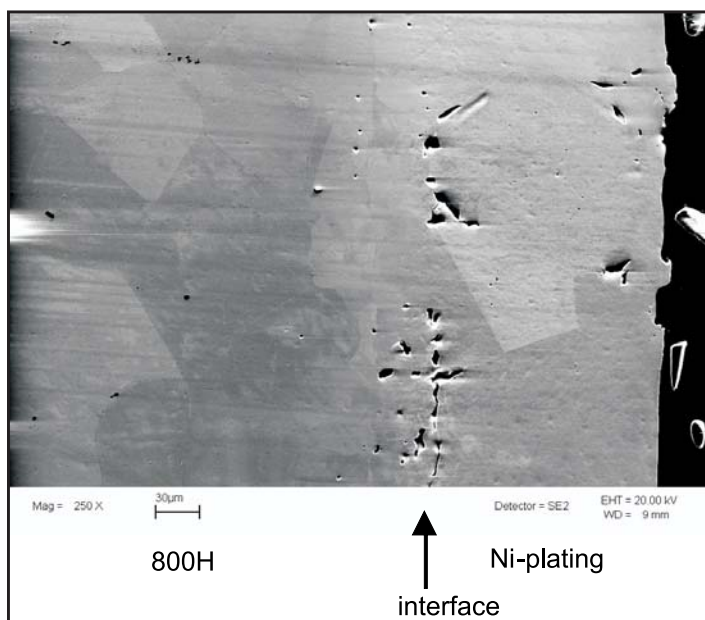
Figure 2. Cross-sectional scanning electron microscopy (SEM) image of Ni-electroplated Incoloy 800H after exposure to molten FLiNaK salt at 850°C for 500 hours.

Electrochemistry. Researchers have continued electrochemistry work. The latest study focuses on checking the viability of potentiometry as an alternative corrosion test to the longer-term molten-salt static corrosion cell tests. In the potentiometry tests, a voltage is measured between a sample made of the alloy under study, and a reference electrode. The smaller the voltage difference between any two materials, the more likely the materials would be compatible with each other in the relevant medium. Figure 3 shows the results from short-term potentiometry tests on four alloys. Several factors complicate data interpretation, such as oxide buildup on the alloy sample prior to immersion in the FLiNaK salt, and the gradual dissolution of elements and sample potential. Nevertheless, these electrochemistry experiments are providing an initial assessment of the propensity of various alloys for dissolution in molten FLiNaK salt.
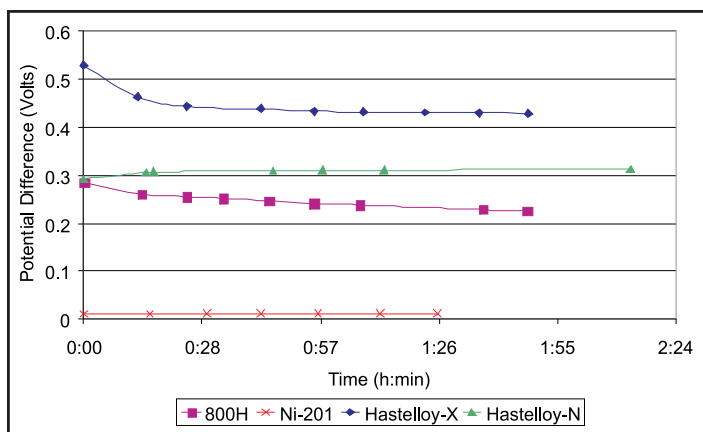
Figure 3. Short-term potentiometry results from four alloy samples showing the potential difference of the test alloys as a function of molten salt exposure time versus a 10 mol% NiF_2 reference electrode.

SiC and Pyrolytic Graphite-Coated SiC Composites Tested in FLiNaK. The project team is considering pyrolitic carbon-coated SiC composite for process heat exchanger material for an intermediate salt loop. The University of California, Berkeley, provided SiC composite samples, and the project team has completed the samples' initial pre-corrosion characterization and post-corrosion (in FLiNaK at 850°C for 500 hours). The German aerospace company DLR made the SiC composites, and Hyper-Therm High Temperature Composites, Inc. used the CVD process to deposit the pyrolytic carbon coating. The composite substrate itself consists of two distinct Si_aC_b phases, one phase that is very rich in carbon and the other that is leaner in carbon, approaching the composition of stoichiometric SiC.

Figure 4 shows the microstructure of the uncoated and coated SiC composites after corrosion testing in FLiNaK at 850°C for 500 hours. The uncoated sample shows drastic attack of the microstructure along the grain and interphase boundaries (see Figure 4(a)). However, for the coated composite sample, there was remarkably little attack on both the coating and the base composite after exposure to this aggressive environment (see Figure 4(b)).
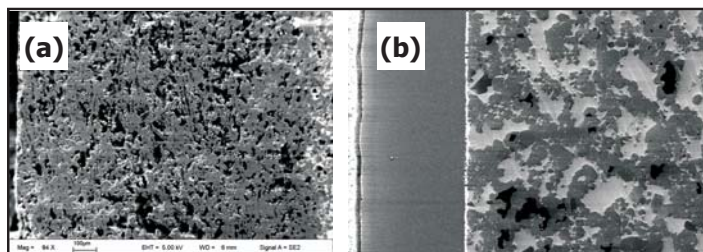
Figure 4. Cross-sectional SEM image of the SiC composite after exposure to molten FLiNaK 850°C for 500 hours: (a) uncoated composite and (b) coated composite.

Corrosion Testing of Alloys in KCl-MgCl₂. The U.S. Department of Energy Next Generation Nuclear Plant (DOE-NGNP) program is interested in several code-certified high-temperature alloys; therefore, the research team has selected these alloys for corrosion evaluation in chloride salts. The materials selected include Inconel 600, 617, 625, and 718; Incoloy 800H; Hastelloy N and X; Haynes 230; Ni-201; and SS-316. The team performed initial corrosion testing in molten KCl-MgCl₂ at 850°C for 100 hours in alumina crucibles.

The team initiated post-corrosion testing SEM analysis of the following alloys: Inconel 625, Hastelloy X, Incoloy 800H, and Ni-201 (see Figure 5). Incoloy 800H, Hastelloy X, and Ni-201 showed attack along the grain boundaries. The Inconel 625 showed attack in the vicinity of Nb- and Ti-rich precipitates, as evidenced by enrichment of these elements in certain regions of the microstructure. For Hastelloy X, darker regions in the microstructure showed enrichment of molybdenum (Mo), indicating that Mo is generally resistant to attack in molten chloride salt.
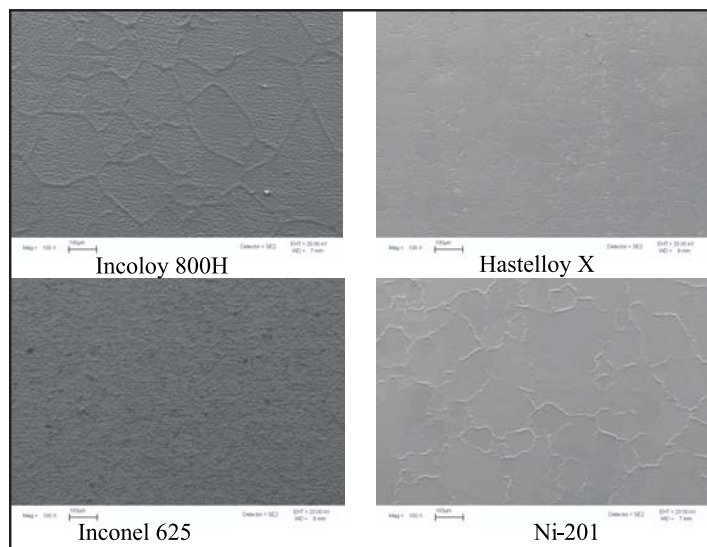
Figure 5. SEM plan view images of the Inconel 800H, Hastelloy X, Incoloy 625, and Ni-201 after corrosion testing in KCl-MgCl₂ salt at 850°C for 100 hours.

Molten Salt Loop Design and Construction. The team has nearly completed design and construction of a forced convective loop for examining mass and heat transfer issues in molten salts (see Figure 6). The team will first use the loop to examine KCl-MgCl₂ (68 mol % to 32 mol %) salt under conditions similar to those expected in the NGNP's IHX. Laminar flow (Re is approximately 150) through four different 316 stainless-steel test sections (run independently) will be investigated to determine convection coefficients, Cr removal and deposition, and pressure drop through the heated test section.

The project team has constructed a vertical-cantilever centrifugal pump for the loop that is expected to operate at temperatures up to 600°C. The pump is expected to pump up to six gallons per minute of salt at temperature. This flow rate is much higher than desired, so the team built a bypass section into the loop to keep flow through the test sections at prototypical conditions.

A manometer-type setup will measure pressure drop over the test sections. Two small reservoirs will be placed next to each other with a connected gas plenum. Each reservoir will connect to the loop with stainless steel tubing. The difference in salt height in each reservoir will be equivalent to the pressure drop of the test section. A laser displacement sensor will measure the height of salt in each reservoir. These sensors are capable of measuring a change in height of 50 μm, equivalent to a pressure drop of 1 Pa.

A thermal flow meter will measure salt flow. The project team will apply a heat source to the flowing salt over a six-inch region, then measure the thermal history of the wall and centerline temperatures downstream of the heat source. The wall and centerline temperatures are mainly dependent on the salt's heat capacity, thermal conductivity, and mass flow rate. If the numbers are nearly exact for the salt's heat capacity and the heat input, researchers can calculate the salt's mass flow rate to a high degree of certainty using thermal-hydraulic codes. All temperatures will be measured with K-type thermocouples.
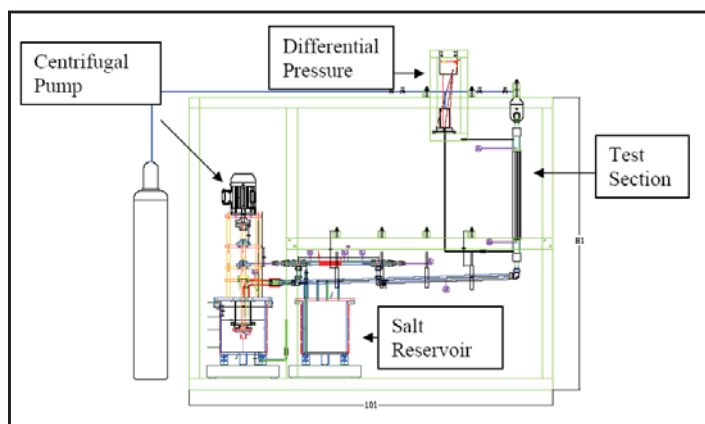
Figure 6. Schematic illustration of the molten salt flow loop that is being built for studying heat and mass transfer issues in flowing molten salts. The total height of the loop will be approximately 4.5 feet.

Planned Activities

Plans for the upcoming year include a detailed investigation of molten FLiNaK salt-driven diffusion of Cr through the Ni coating deposited on Incoloy 800H, as well as a model Fe-Cr-Ni ternary alloy with Fe, Ni, and Cr compositions identical to the Incoloy 800H. Additionally,

the project team will perform tests to study effects of a reducing agent such as zirconium on corrosion of alloys in molten FLiNaK salt. Studies on corrosion of candidate alloys in molten KCl-MgCl$_2$ will continue; the team will compare corrosion performance of materials in FLiNaK and KCl-MgCl$_2$ salts, and provide the assessment to the DOE-NGNP program. Other immediate planned activities include testing hard carbon coating using plasma-based technologies and testing carbon-carbon composites to be procured from Oak Ridge National Laboratory.

A major goal will be to have an operating molten salt forced convective loop, the construction of which is nearly complete. The team will use this loop to examine effects of liquid salt flow through small channels (1 mm to 10 mm), similar to channels for the IHX, and to investigate other thermal-hydraulics issues pertaining to high-temperature molten salt. These tests should produce experimental pressure-drop and heat-transfer data for small-channel flow of liquid salts in heating and cooling conditions. The team will also use the flow loop for dynamic corrosion tests with exposure times of up to 1,000 hours; the team will investigate products formed in the loop's hot section and plated out in the loop's cold section.

NUCLEAR ENERGY RESEARCH INITIATIVE

Optimization of Heat Exchangers

PI: Ivan Catton, University of California-Los Angeles (UCLA)

Collaborators: None

Project Number: 07-057

Program Area: NHI

Project Start Date: June 2007

Project End Date: June 2010

Research Objectives

The objective of this research is to develop tools to design and optimize heat exchangers (HEs) and compact heat exchangers (CHEs) for intermediate loop heat transport systems found in the very high-temperature reactor (VHTR) and other Generation IV designs by addressing heat transfer surface augmentation and conjugate modeling.

This research will be performed in two phases. During the first phase, the team will search for augmented heat transfer surface morphologies using a combination of experiment and modeling. For a particular type of surface augmentation, team members will conduct experiments to obtain closure of the model and then apply it to optimize the surface. A final experiment will confirm findings from the model. These surfaces will become candidates for the next research phase, when they will be integrated into an HE design. The objective is to develop and demonstrate a model that can be used to optimize HEs. The model equations are available but have not been used for a two-fluid-stream HE, nor has closure been fully developed. Researchers will also design and optimize a printed circuit heat exchanger (PCHE) for either a high-temperature Brayton cycle in support of the VHTR or for the reactor-hydrogen production process interface. This research will ultimately result in a validated computer program for HE design that maximizes heat transfer and minimizes pumping power.

The project's major technical objectives include the following:

- Develop a surface that increases surface heat removal effectiveness by a factor of four without a marked increase in pumping power

- Develop a new type of mathematical model capable of predicting flow and heat transfer in two-dimensional (2-D) and three-dimensional (3-D) spatial structures at different scales

- Design and carry out experiments to measure heat transfer augmentation and validate the HE and CHE models used for optimization

- Design and test a PCHE for a high-temperature inert gas cycle

Research Progress

In the first NERI annual reporting period, the research team completed Phase I of the proposed research. Phase I tasks included development of a theoretical and computational fluid dynamics (CFD) model predicting friction and heat transfer through porous media, construction of a database for augmented surfaces, and development of closure needed to model CHEs.

In Quarter I, researchers focused on developing a computer code capable of predicting friction and heat transfer over surfaces augmented with 2-D and 3-D roughness elements. The code is based on a rigorous spatial averaging technique used for heterogeneous media transport phenomena called the volume average theory (VAT). The research team applied VAT to the conjugate heat transfer problem of turbulent transport through HEs modeled as porous media.

Researchers have developed a code for solving the VAT transport equations for the case of fully developed turbulent flow in a channel with surfaces augmented with regular morphology consisting of 2-D and 3-D roughness elements. The code was validated against experimental data from literature for a variety of geometries and for channels augmented with ribs varying in geometry, size, and pitch. Figure 1 and Figure 2 show results of the friction factor for four geometries and the Nusselt number for three geometries, respectively.
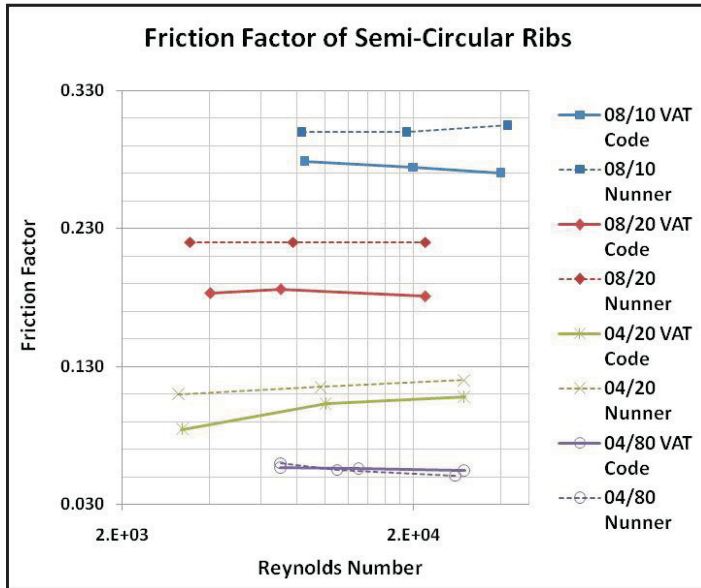
Figure 1. Friction factor experimental comparison.
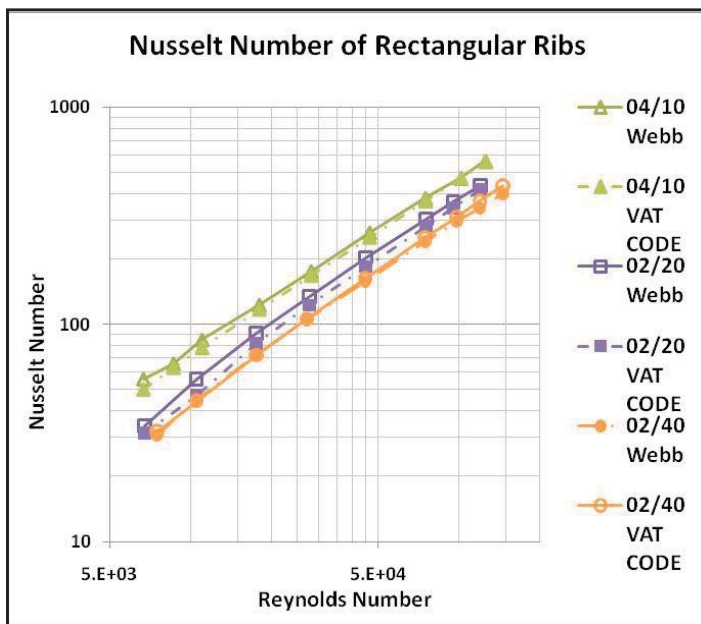
Figure 2. Nusselt number experimental comparison.

In Quarter 2, researchers focused on continued development of the VAT code to include more sophisticated and efficient numerical techniques. The alternating direction implicit (ADI) method was implemented, along with a single grid domain, in order to solve the two-temperature conjugate problem. Using the ADI method allows for an improved and efficient algorithm for solving the VAT-based transport equations. Researchers also added the capability to handle irregular surface morphologies, such as roughness elements, that change in height in the flow direction.

The ADI method required discretizing the VAT-based transport equations into three-point, stencil-yielding equations at each discreet point for direction in each half-time step, resulting in ADI Step 1 (sweep in the vertical direction):

$$A_{jTF}^s \tilde{\bar{T}}_{i,j-1}^{s+1/2} + B_{jTF}^s \tilde{\bar{T}}_{i,j}^{s+1/2} + C_{jTF}^s \tilde{\bar{T}}_{i,j+1}^{s+1/2} + D^s T_{S_{i,j}}^{s+1/2} = F_{iTF}^s$$

as well as ADI Step 2 (sweep in the horizontal direction):

$$A_{iTF}^s \tilde{\bar{T}}_{i-1,j}^{s+1} + B_{iTF}^s \tilde{\bar{T}}_{i,j}^{s+1} + C_{iTF}^s \tilde{\bar{T}}_{i+1,j}^{s+1} + D^s T_{S_{i,j}}^{s+1} = F_{jTF}^{s+1/2}$$

The conjugate nature of the problem involving the energy equations required a method for solving the solid and fluid temperatures simultaneously at each discreet point for both sweep directions. The three-point stencil equations were then formed into a block matrix form for each discrete point in each half-time step, resulting in ADI Step 1 (sweep in the vertical direction):

$$\begin{bmatrix} A_{jTS}^s & 0 \\ 0 & A_{jTF}^s \end{bmatrix} \begin{bmatrix} T_{S_{i,j-1}}^{s+1/2} \\ \tilde{\bar{T}}_{i,j-1}^{s+1/2} \end{bmatrix} + \begin{bmatrix} B_{jTS}^s & D^s \\ D^s & B_{jTF}^s \end{bmatrix} \begin{bmatrix} T_{S_{i,j}}^{s+1/2} \\ \tilde{\bar{T}}_{i,j}^{s+1/2} \end{bmatrix} + \begin{bmatrix} C_{jTS}^s & 0 \\ 0 & C_{jTF}^s \end{bmatrix} \begin{bmatrix} T_{S_{i,j+1}}^{s+1/2} \\ \tilde{\bar{T}}_{i,j+1}^{s+1/2} \end{bmatrix} = \begin{bmatrix} F_{iTS}^s \\ F_{iTF}^s \end{bmatrix}$$

and ADI Step 2 (sweep in the horizontal direction):

$$\begin{bmatrix} A_{iTS}^s & 0 \\ 0 & A_{iTF}^s \end{bmatrix} \begin{bmatrix} T_{S_{i-1,j}}^{s+1} \\ \tilde{\bar{T}}_{i-1,j}^{s+1} \end{bmatrix} + \begin{bmatrix} B_{iTS}^s & D^s \\ D^s & B_{iTF}^s \end{bmatrix} \begin{bmatrix} T_{S_{i,j}}^{s+1} \\ \tilde{\bar{T}}_{i,j}^{s+1} \end{bmatrix} + \begin{bmatrix} C_{iTS}^s & 0 \\ 0 & C_{iTF}^s \end{bmatrix} \begin{bmatrix} T_{S_{i+1,j}}^{s+1} \\ \tilde{\bar{T}}_{i+1,j}^{s+1} \end{bmatrix} = \begin{bmatrix} F_{jTS}^{s+1/2} \\ F_{jTF}^{s+1/2} \end{bmatrix}$$

For the project's experimental element, researchers have set up a wind tunnel, heating system, and data acquisition system. The wind tunnel will be used to measure heat transfer augmentation, obtain the necessary closure for particular types of surface augmentation, and validate the HE models used for optimization. A new heater and fan are being purchased for the wind tunnel.

In Quarter 3, researchers implemented a newly developed method for solving the two-temperature conjugate problems. This method used both ADI, as mentioned above, and a theoretical method to simplify closure of the VAT equations. The latter method examined proper scaling to work with friction factor and heat transfer coefficient data for multiple geometries, collapsing that data into a single general formulation. Applying the ADI method to each discrete point in a row or column results in the block tri-diagonal matrix of the form:

$$\begin{bmatrix} \begin{bmatrix} B^s_{jTS} & D^s \\ D^s & B^s_{jTF} \end{bmatrix} & \begin{bmatrix} C^s_{jTS} & 0 \\ 0 & C^s_{jTF} \end{bmatrix} & \begin{bmatrix} 0 & 0 \\ 0 & 0 \end{bmatrix} & \cdots & & \begin{bmatrix} 0 & 0 \\ 0 & 0 \end{bmatrix} \\ \begin{bmatrix} A^s_{jTS} & 0 \\ 0 & A^s_{jTF} \end{bmatrix} & \begin{bmatrix} B^s_{jTS} & D^s \\ D^s & B^s_{jTF} \end{bmatrix} & \begin{bmatrix} C^s_{jTS} & 0 \\ 0 & C^s_{jTF} \end{bmatrix} & & & \vdots \\ \begin{bmatrix} 0 & 0 \\ 0 & 0 \end{bmatrix} & \ddots & \ddots & \ddots & & \begin{bmatrix} 0 & 0 \\ 0 & 0 \end{bmatrix} \\ \vdots & & \begin{bmatrix} A^s_{jTS} & 0 \\ 0 & A^s_{jTF} \end{bmatrix} & \begin{bmatrix} B^s_{jTS} & D^s \\ D^s & B^s_{jTF} \end{bmatrix} & \begin{bmatrix} C^s_{jTS} & 0 \\ 0 & C^s_{jTF} \end{bmatrix} \\ \begin{bmatrix} 0 & 0 \\ 0 & 0 \end{bmatrix} & \cdots & & \begin{bmatrix} 0 & 0 \\ 0 & 0 \end{bmatrix} & \begin{bmatrix} A^s_{jTS} & 0 \\ 0 & A^s_{jTF} \end{bmatrix} & \begin{bmatrix} B^s_{jTS} & D^s \\ D^s & B^s_{jTF} \end{bmatrix} \end{bmatrix} \begin{bmatrix} T^{s+1/2}_{S,i,3} \\ \tilde{T}^{s+1/2}_{i,3} \\ \vdots \\ T^{s+1/2}_{S,i,N-1} \\ \tilde{T}^{s+1/2}_{i,N-1} \\ T^{s+1/2}_{S,i,N} \\ \tilde{T}^{s+1/2}_{i,N} \end{bmatrix} = \begin{bmatrix} F^s_{ITS} \\ F^s_{ITF} \\ F^s_{ITS} \\ F^s_{ITF} \\ \vdots \\ F^s_{ITS} \\ F^s_{ITF} \\ F^s_{ITS} \\ F^s_{ITF} \end{bmatrix}$$

To solve for the conjugate temperature solution in each ADI step, a block matrix is formed for each row in Step 1 and then solved for temperature using the Thompson Algorithm. Similarly, in Step 2, a block matrix is formed for each column and is solved for temperature, this time using the Thomas Algorithm. As the matrix is populated with block matrices, matrix algebra must be used in lieu of conventional mathematics to execute the Thomas Algorithm.

To simplify closure for the VAT-based equations, researchers hypothesized that proper scaling could collapse the multitude of data available to a general formulation for friction and heat transfer coefficients. The team carried out CFD-based numerical calculations of the friction factor, and then compared those calculations to established results and correlation. The resulting data is representative of various porous media morphology: different sizes of spheres, sand, and pulverized coke. Figure 3 shows the comparison, and the results show the validity of VAT calculations.
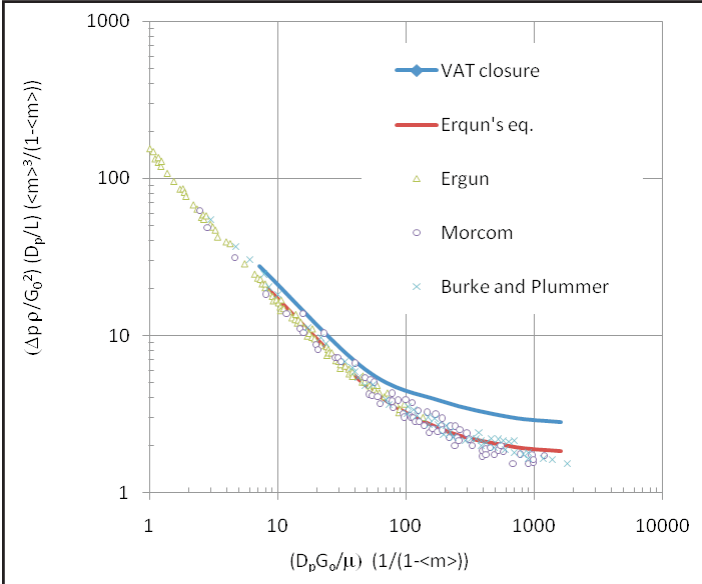

Figure 3. Comparison of VAT closure to the data.

In Quarter 4, researchers further developed the VAT-based model and CFD code, extending them to a three-temperature conjugate solution. Developments from Quarters 2 and 3 are the basis for the setup and method, with the addition of a third fluid temperature. This creates a three-by-three block matrix for each discrete point. The resulting block matrix for each row or column is shown below:

$$\begin{bmatrix} \begin{bmatrix} B^s_{jTH} & D^s_H & 0 \\ D^s_H & B^s_{jTS} & D^s_C \\ 0 & D^s_C & B^s_{jTC} \end{bmatrix} & \begin{bmatrix} C^s_{jTH} & 0 & 0 \\ 0 & C^s_{jTS} & 0 \\ 0 & 0 & C^s_{jTC} \end{bmatrix} & \begin{bmatrix} 0 & 0 & 0 \\ 0 & 0 & 0 \\ 0 & 0 & 0 \end{bmatrix} & \cdots & \begin{bmatrix} 0 & 0 & 0 \\ 0 & 0 & 0 \\ 0 & 0 & 0 \end{bmatrix} \\ \begin{bmatrix} A^s_{jTH} & 0 & 0 \\ 0 & A^s_{jTS} & 0 \\ 0 & 0 & A^s_{jTC} \end{bmatrix} & \begin{bmatrix} B^s_{jTH} & D^s_H & 0 \\ D^s_H & B^s_{jTS} & D^s_C \\ 0 & D^s_C & B^s_{jTC} \end{bmatrix} & \begin{bmatrix} C^s_{jTH} & 0 & 0 \\ 0 & C^s_{jTS} & 0 \\ 0 & 0 & C^s_{jTC} \end{bmatrix} & \ddots & \vdots \\ \begin{bmatrix} 0 & 0 & 0 \\ 0 & 0 & 0 \\ 0 & 0 & 0 \end{bmatrix} & \ddots & \ddots & \ddots & \begin{bmatrix} 0 & 0 & 0 \\ 0 & 0 & 0 \\ 0 & 0 & 0 \end{bmatrix} \\ \vdots & \ddots & \begin{bmatrix} A^s_{jTH} & 0 & 0 \\ 0 & A^s_{jTS} & 0 \\ 0 & 0 & A^s_{jTC} \end{bmatrix} & \begin{bmatrix} B^s_{jTH} & D^s_H & 0 \\ D^s_H & B^s_{jTS} & D^s_C \\ 0 & D^s_C & B^s_{jTC} \end{bmatrix} & \begin{bmatrix} C^s_{jTH} & 0 & 0 \\ 0 & C^s_{jTS} & 0 \\ 0 & 0 & C^s_{jTC} \end{bmatrix} \\ \begin{bmatrix} 0 & 0 & 0 \\ 0 & 0 & 0 \\ 0 & 0 & 0 \end{bmatrix} & \cdots & \begin{bmatrix} 0 & 0 & 0 \\ 0 & 0 & 0 \\ 0 & 0 & 0 \end{bmatrix} & \begin{bmatrix} A^s_{jTH} & 0 & 0 \\ 0 & A^s_{jTS} & 0 \\ 0 & 0 & A^s_{jTC} \end{bmatrix} & \begin{bmatrix} B^s_{jTH} & D^s_H & 0 \\ D^s_H & B^s_{jTS} & D^s_C \\ 0 & D^s_C & B^s_{jTC} \end{bmatrix} \end{bmatrix} \begin{bmatrix} \tilde{T}^{s+1/2}_{H,i,3} \\ T^s_{i,3} \\ \tilde{T}^{s+1/2}_{C,i,3} \\ \tilde{T}^{s+1/2}_{H,i,4} \\ T^{s+1/2}_{S,i,4} \\ T^{s+1/2}_{C,i,4} \\ \vdots \\ \tilde{T}^{s+1/2}_{H,i,N-1} \\ T^{s+1/2}_{S,i,N-1} \\ \tilde{T}^{s+1/2}_{C,i,N-1} \\ \tilde{T}^{s+1/2}_{H,i,N} \\ T^{s+1/2}_{S,i,N} \\ T^s_{CN} \end{bmatrix} = \begin{bmatrix} F^s_{ITS} \\ F^s_{ITS} \\ F^s_{ITC} \\ F^s_{ITS} \\ F^s_{ITS} \\ F^s_{ITC} \\ \vdots \\ F^s_{ITS} \\ F^s_{ITS} \\ F^s_{ITC} \\ F^s_{ITS} \\ F^s_{ITS} \\ F^s_{ITC} \end{bmatrix}$$

The research team began developing a new code to solve the ADI equations for one, two, and three temperatures. The new code includes a single domain that captures the porous layer, fluid layer, and base plate layer. With the addition of a single domain, calculations can be solved with a single pass instead of a brute-force method, which would compare the solutions at the interface, as was the case with the original CFD code. The ADI code was developed to be structured and object-oriented, making it readable and organized for future users.

In Quarter 4, the research team researched and ordered experimental equipment. An induction furnace will be used to develop heat transfer coefficients for various geometries. The team will design geometries in SolidWorks, then employ rapid prototyping to develop the physical geometries. Researchers will place each geometry in an inductive coil, then measure temperatures on either side of the geometry. Temperature responses are due to step changes in temperature within the geometry. The team will compare results to those calculated with a VAT-based CFD code, using those comparisons to determine heat transfer coefficients.

Planned Activities

The following are planned activities for the upcoming year:

- Complete development and validation of an augmented surface model

- Complete data sets needed for an augmented surface model by conducting experiments using a laboratory wind tunnel and CFD

- Conduct an optimization study of selected surfaces

- Develop a VAT-based HE model, implementing a 3-D ADI method to evaluate the full HE

- Validate the HE model

- Develop an initial design using VAT-based optimization code

- Select high-temperature conditions and materials for further study

- Propose some PCHE candidates for study

- Present three papers at the American Society of Mechanical Engineers summer heat transfer conference

NUCLEAR ENERGY RESEARCH INITIATIVE

Advanced Electrochemical Technologies for Hydrogen Production by Alternative Thermochemical Cycles

PI: Serguei N. Lvov, Pennsylvania State University (PSU)

Collaborators: University of South Carolina (USC), Tulane University, Argonne National Laboratory (ANL)

Project Number: 08-047

Program Area: NHI

Project Start Date: October 2007

Project End Date: September 2010

Research Objectives

The main objective of this project is to establish the most efficient technologies for hydrogen production that are compatible with next-generation nuclear-produced heat sources. The heat created by nuclear power plants can be utilized by moderate-temperature thermochemical cycles to convert water into hydrogen and oxygen. The consortium researchers are investigating several prospective thermochemical cycles. Key reactions are being studied via experimental and theoretical approaches. In addition, researchers are evaluating each cycle with respect to efficiency via process simulation and to viability for future sustainable energy infrastructure.

This project initially targeted several promising alternative thermochemical cycles: the calcium-bromide (Ca-Br), the copper-chloride (Cu-Cl), and the active metal alloy. Potential benefits of these cycles include medium temperature operation (below 675°C), high efficiency, simple unit operations, and relatively simple separations. These cycles include an electrochemical reaction and are therefore referred to as hybrid cycles. For the highest efficiency, it is critical that the electrochemical reaction be optimized to obtain good performance at the lowest possible cell potential.

Because of the importance of the electrochemical reactions, this project focuses on the development of advanced electrochemical technologies, which will lead to overall improvement in cycle performance. The following activities are under way: 1) development of electrolyzers; 2) development of new membranes, electrocatalysts, electrodes, and membrane-electrode assemblies (MEAs); 3) development of separation methods for handling incomplete electrochemical reactions; and 4) identification and modeling of the behavior of the electrochemically active species and electrochemical reactions involved in the electrolyzer processes. In addition, this project includes process simulation and flowsheet analyses to guide the experimental program towards higher efficiency and lower cost processes in the electrolyzer. The modeling and experimental work is iterative: as new experimental data are obtained, the models and flowsheets are updated and optimized to find opportunities for increasing efficiency and reducing costs.

While this project is primarily concerned with alternative thermochemical cycles, the technologies developed will be applicable to proton exchange membrane electrolyzers and other hydrogen production electrochemical processes.

Research Progress

Cu-Cl Cycle. A number of research groups at PSU, USC, and Tulane University have been working on different parts of the Cu-Cl electrolyzer. Some highlights of this collaborative research are given below.

The USC group has developed an analytical method for online analysis of copper compounds in highly
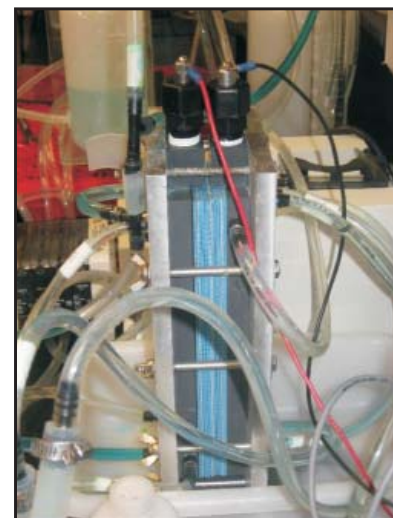
Figure 1. Electrodialysis stack developed at USC.

concentrated aqueous solutions. Researchers examined and experimentally confirmed the possibility of using UV-visible spectroscopy to determine the $CuCl_2$ concentration in solution. The absorbance of $CuCl_2$ solutions at particular visible wavelengths varies linearly with concentration and does not exhibit a maximum, as is the case with conductivity measurements. The developed approach was further used to monitor the concentration of $CuCl_2$ in electrodialysis experiments. The longest wavelength transmitted through the solutions is fairly independent of the presence of solids, and thus this wavelength can be used to monitor the concentration of $CuCl_2$ solutions even in the presence of small amounts of suspended solids.

The USC group designed and constructed an electrodialysis apparatus with detachable electrodes suitable for concentrating $CuCl_2$ solutions (Figure 1). The objective of this task was to determine the feasibility of using electrodialysis to concentrate solutions in thermochemical or hybrid cycles and to compare its energy requirements with other methods of concentrating solutions, such as evaporation. Neosepta AHA and CMB are suitable as the anion-exchange membrane and the cation-exchange membrane, respectively. This method can be used to isolate the electrodes from undesirable ions in Cu-Cl cycle reactions. More than 100 hours of operation have been logged, and in the best performance, the $CuCl_2$ of the feed solution was reduced from 1.26 percent to 0.15 percent while the $CuCl_2$ in the concentrated solution reached 23.13 percent.

The PSU group has been developing the synthesis of new membrane materials for the Cu-Cl electrolyzer. The focus was on new classes of chloride-conductive materials: 1) grafted polyolefin copolymers that contain both a crystalline hydrophobic phase and an amorphous hydrophilic phase with a co-continuous and clear phase separated morphology, and 2) poly(ethylene-co-hexenylamine) (PEHA) random copolymers. The goal is to develop a new polymer structure that has high chloride conductivity (with a high ion-exchange capacity [IEC] value) while maintaining good chlorine-exchange membrane stability (chemical, thermal, and water-swelling). For the first samples, researchers used crosslinking to improve the dimensional stability of the membranes and to control water swelling.

The PSU group also developed experimental tools for measuring ion conductivity, IEC, and water uptake of the chloride-conductive membranes. Researchers tested a range of commercial membranes—AHA, ACM, ACS, AMI, AAV, AHT, and ASV—and compared the properties to those of the newly developed materials. The newly synthesized PEHA materials with an IEC of 3.3 mmol/g indicate a chlorine-ion conductivity of approximately 5.6 mS/cm in 2 N HCl, which is comparable to some commercial membranes. The membrane structure is being further modified to increase the conductivity level and to upgrade mechanical properties.

In parallel, PSU researchers began developing new electrocatalysts for the Cu-Cl electrolyzer. To prepare PtRu, Pt, and Ru metal-based catalysts, the group used the incipient wetness method with ceramic materials BN and Al_2O_3, as well as carbon as a support. The researchers studied performance of a wide range of synthesized catalytic materials (PtRu, PdRu, PtRu/BN, PtRu/Al_2O_3, PtRu/C, Pt/BN, Ru/BN, TiO_2, RuO_2) in a 6 M HCl(aq) environment. Carbon was found to be the best support when compared with BN and Al_2O_3.

PSU initiated experimental tests with a newly developed Cu-Cl electrolyzer. The system is intended for extensive testing of the newly developed components involved in the Cu-Cl cycle process (Figure 2). Researchers conducted CuCl electrolysis tests at various flow rates and temperatures from 25°C to 65°C using MEAs prepared with commercial AHA and AMI membranes and ELAT
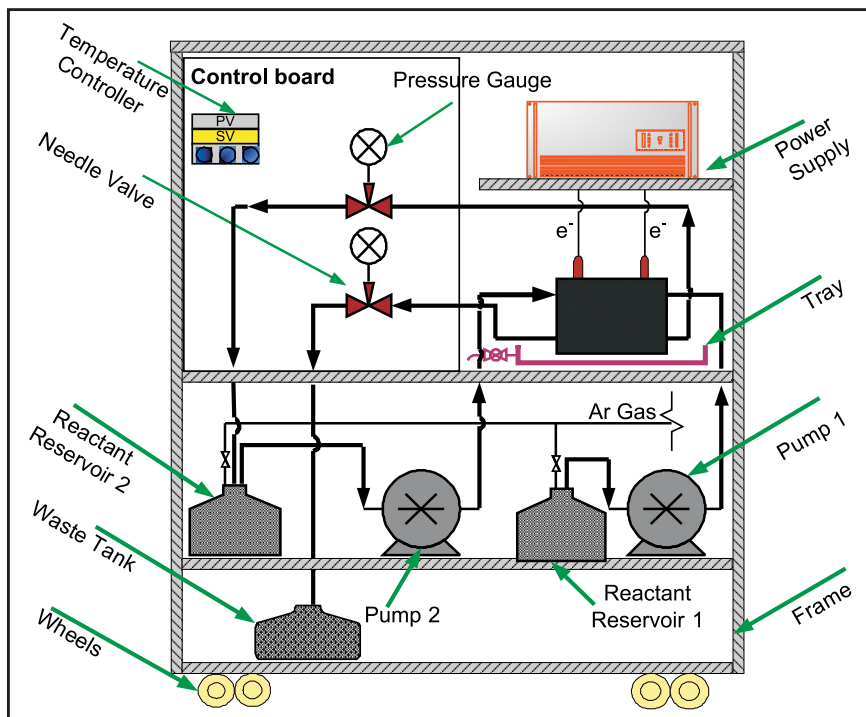
Figure 2. Cu-Cl electrolyzer developed at PSU.

electrodes. The electrodes were assembled on both sides of a membrane with the catalytic layer out. Linear sweep voltammetry measurements were carried out with a scanning range of 0.3 – 0.9 V. Faraday current efficiency was estimated for several membranes based on the ratio of the experimentally produced amount of hydrogen to the theoretical amount. The efficiency of the process at low currents (<100 mA) was approximately 98 percent; however, it dropped as the current increased. Copper crossover and precipitation on the cathode side is considered the main cause of the efficiency drop. These tests will guide synthesis of the new membranes toward decreased copper permeability.

The experiment provided two other findings: the effect of flow rate on electrolysis kinetics is insignificant, and a temperature increase from 24°C to 65°C boosted performance. Using the linear sweep voltammetry technique, researchers experimentally determined the single-cell decomposition potential to be 0.46 mV at 24°C and 0.41 mV at 45°C. Therefore, it was found that an elevated temperature can be beneficial for the electrolyzer operation.

The PSU group also developed an accurate thermodynamic model of the $Cu(I)-Cu(II)-Cl-H_2O$ in the temperature range of 0°C to 100°C for the anolyte of the Cu-Cl electrolyzer. Researchers developed a self-consistent thermodynamic database for the $Cu(I,II)-HCl-H_2O$ system applicable for 0°C to 100°C, 1 – 50 bar, 0 – 6 mol kg^{-1} of HCl, and 0 – 2 mol kg^{-1} $Cu(I,II)Cl(aq)$. It is now possible to accurately predict the solubility of $CuCl(s)$ and other thermodynamic properties of $Cu(I,II)Cl(aq)$ in concentrated $HCl(aq)$. It was found that the theoretically calculated decomposition potential is close to the measured value.

The group at Tulane University performed Aspen Plus modeling of the three-reaction version of the Cu-Cl thermochemical cycle. The modeling involved three stages: 1) with reactors being stoichiometric and all reactions going to completion, 2) including the $CuCl_2$ hydrolysis step as an equilibrium reactor, and 3) including a FORTRAN code for operating the electrolyzer. The third-generation Aspen flowsheet (see Figure 3) with the actual implementations has two significant advantages: 1) no compressors (only pumps and throttling valves) and 2) no solids transfer steps (with fluidized bed for O_2/HCl production section). The method of separating the water/HCl stream was considered to include two distillation columns in series. This provides satisfactory separation for the process. Researchers optimized the hydrolysis reaction conditions to minimize the amount of excess water required. In addition, the research

group verified specifications of the major units, including the oxychloride reactor and the two distillation columns.

Ca-Br Cycle. The USC group carried out experimental
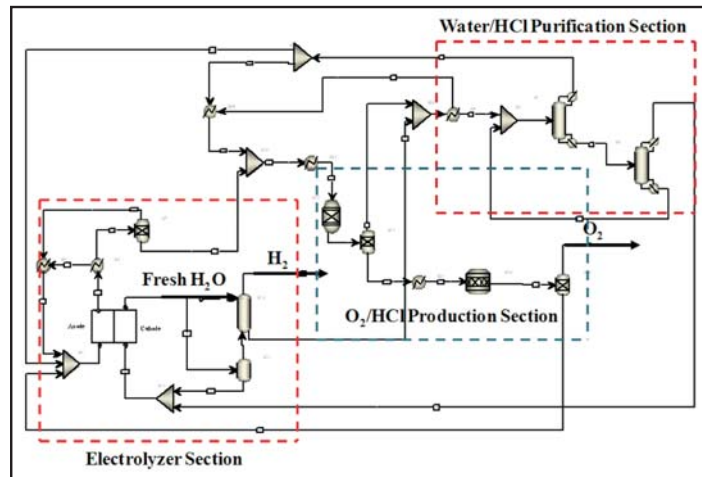
Figure 3. Third-generation Aspen Plus flowsheet developed at Tulane University.

research on the electrochemical reactions and systems involved in the Ca-Br alternative cycle. Researchers developed low-cost nanostructured electrocatalysts for the bromide ion's oxidation (anodic process) and for hydrogen-ion reduction and H_2 evolution (cathodic process) in the HBr electrolyzer. Using two sol-gel procedures, researchers synthesized niobium-doped titanium dioxide and then characterized the resulting product. Using cyclic voltammetry with a rotating disk electrode (RDE), the group studied the activity of the RuO_2 catalyst to be used for preparing new MEA, along with three other catalysts: Pt, Vulcan XC 72R carbon black, and the new niobium-doped titanium dioxide. Vulcan XC 72R carbon black and RuO_2 have comparable good intrinsic activity towards oxidation of the bromide ion. Pt has the highest intrinsic activity, while TiO_2-Nb has the lowest. Perhaps improving the conductivity of TiO_2-Nb will raise its activity.

Researchers determined steady-state polarization and kinetics parameters for the bromine evolution reaction on four catalysts: Pt, Vulcan XC 72R carbon black, RuO_2, and TiO_2-Nb. The surface of the anode side of the developed MEA was characterized using BET surface-area measurements and SEM imaging (Figure 4). The dew point curve of the $HBr-H_2O$ mixture
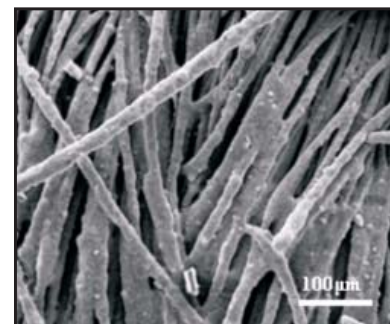
Figure 4. Nb-TiO_2 catalyst on ETEK carbon cloth developed at USC.

was plotted on Aspen Plus to determine the change in the amount of water condensing in the presence of bromine species in the anode region. HBr oxidation in the acid solution shows a steady-state V-I response, which supports the Volmer-Tafel mechanism with chemical recombination as the rate-determining step. The presence of HBr caused water condensation at lower mole fractions due to the thermodynamic non-idealities.

The USC researchers redesigned and built an HBr electrolyzer. They prepared MEAs with RuO_2 and the three other catalysts. The group then observed the electrolyzer's performance when the MEAs were made with the four catalysts at the anode (Pt in the cathode in all cases), and correlated that performance to the catalysts' kinetic parameters and the electrodes' surface morphology. To determine the charge transfer resistance of the electrolyzer cell's anode, researchers used Galvano electrochemical impedance spectroscopy while running the electrolyzer as a hydrogen pump. From the RDE, BET, SEM, and EIS results, the group concluded that performance of the HBr electrolyzer's anode is affected by both the catalyst's intrinsic activity and the electrode surface area. Both high-surface-area carbon black and TiO_2-Nb (10 mol %) have reasonably good activities and high surface areas; therefore, they hold promise as anode catalysts for HBr oxidation.

Active Metal Alloy Cycle. The PSU group conducted experimental studies on the K-Bi alternative thermochemical cycle. The main objectives were to find the optimal parameters for cycle operation and to evaluate reaction rates and degrees of completion. The K-Bi alternative cycle consists of two reactions: alloy hydrolysis and electrolysis. The group constructed an experimental system to study the high-temperature hydrolysis reaction. Researchers induced a reaction between the K-Bi active alloy and steam at 675°C, then used XRD, EDX, GC, and chemical analyses to identify the reaction products. Through the reaction with the molten K-Bi alloy, steam converts to hydrogen at rates that depend significantly on available reaction interface; the estimated rates will dictate design requirements for the reactor. The electrolysis reaction of the K-Bi cycle was studied at 580°C. The decomposition potential was determined to be about 1.65 V,

which is similar to that determined by thermodynamic calculations. The research group found that, owing to the anode's electrochemical oxidation, the electrode materials' stability is a serious issue in this cycle. In addition, oxidation and dissolution processes result in low currents and hamper the reaction kinetics.

Coordination Activities. Two NERI-C working group meetings (one in October 2007 at PSU and the other in April 2008 at Tulane University) have been held during the last year to share information and to exchange ideas. The Ontario Research Foundation workshop held in October 2008 and the Canadian Chemical Engineering annual meeting, also in October 2008, were attended. Unrestricted information from these meetings was distributed to the NERI-C members. The consortium has developed a website available at http://www.energy.psu.edu/neri-c/mission.html.

Planned Activities

Future research will be focused mainly on the processes and systems involved in the Cu-Cl thermochemical cycle, the most promising cycle of the ones considered earlier. Following DOE recommendations, the research activities were discontinued on both the Ca-Br and active metal-alloy cycles. In FY 2008 and FY 2009, the consortium participants will be working on the following fundamental tasks:

- Development of an advanced Cu-Cl electrolyzer (PSU, USC)
- Synthesis and characterization of new ion exchange membranes (PSU)
- Phase equilibria in the electrolyzer anolyte (PSU)
- Development of nanostructured electrocatalysts (USC)
- Electrolyzer modeling (USC, PSU, Tulane University)
- Use of electrodialysis for separation and purification of the spent anolyte and catholyte (USC)
- Development of an Aspen Plus model for the electrolyzer and the electrodialysis (Tulane University, USC)
- Coordination of activities related to the Cu-Cl thermochemical cycle (ANL)

Index of NERI Projects

FY 2007 NERI-C Projects